Effects of Stiffness and Polydispersity

on the Phase Behaviour of Block Copolymers

P.M. Jager

Effects of Stiffness and Polydispersity
on the Phase Behaviour of Block Copolymers
P.M. Jager
Ph.D. thesis
University of Twente
The Netherlands
July 2006

EFFECTS OF STIFFNESS AND POLYDISPERSITY
ON THE PHASE BEHAVIOUR OF BLOCK COPOLYMERS

PROEFSCHRIFT

ter verkrijging van

de graad van doctor aan de Universiteit Twente,

op gezag van de rector magnificus,

prof.dr. W.H.M. Zijm,

volgens besluit van het College van Promoties

in het openbaar te verdedigen

op vrijdag 14 juli om 13.15 uur

door

Pieter Menno Jager

geboren op 14 juni 1976

te Rotterdam, Nederland

Dit proefschrift is goedgekeurd door de promotor
Prof. dr. J.J.M. Slot

Contents

Chapter 1

Introduction

In the past decades much attention has been paid to the phase behaviour of different kinds of block copolymer systems both experimentally and theoretically [1]. This phase behaviour determines to a large extend the mechanical, optical and electrical properties of these materials. In a polymer chain a number of units are connected in a linear fashion. These units are referred to as segments, beads or simply as monomers. If all monomers are of the same kind a homopolymer is formed. In a block copolymer different kinds of homopolymers or blocks are connected to each other. For example a diblock copolymer consists of two different kinds of blocks A and B connected to each other.

Block copolymers are applied in thermoplastic elastomers which form an interesting class of synthetic materials. Their industrial interest primarily stems from the fact that they combine the mechanical properties of elastomers with the processability of thermoplastics, in other words they share their elasticity with rubbers but in contrast with the latter they can be re-processed simply by re-melting. At least one kind of block should be able to crystallize sufficiently above room temperature, while the non-crystalizable blocks provide the elasticity to the system. In these systems the crystalizable blocks form crosslinks between chains so that a network is formed. Without crosslinks the chains can move freely with respect to each other so that the system behaves as a liquid with a high viscosity. However due to the partial crystallization the freedom of each chain to move is restricted.

In a melt of block copolymers the chains are not moving independently of each other. Different kinds of interactions between chains are present that determine in part the phase behaviour. The Flory-Huggins interaction [2] describes the incompatibility

between chemically different kinds of blocks. In a melt of diblock copolymers A-rich and B-rich domains are formed if the Flory-Huggins interaction strength between A- and B-blocks is strong enough, because both blocks are connected to each other. This is called microphase separation. There are different kinds of microphase structures possible which are displayed in the left part of Fig. (1.1). These are the so-called classical structures which are formed close to the order-disorder phase transition. If the Flory-Huggins interaction strength becomes larger more complicated structures are possible such as the gyroid structure described in [3] and [4]. In [5] the classical
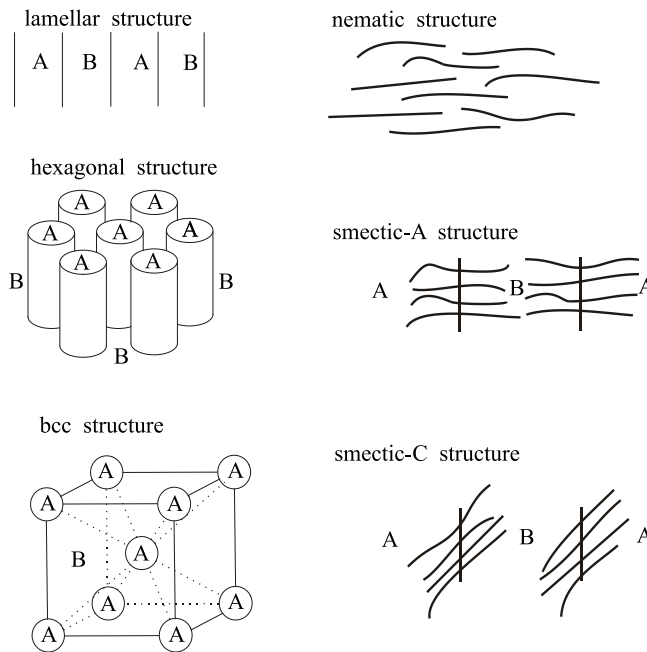
Figure 1.1: Possible phase structures

phases were determined in the phase diagram of a melt of diblock copolymers which are totally flexible. The system is monodisperse with respect to the chain length and chain composition. So the length of both the A- and B-block is identical for each chain in the melt.

In [5] and [6] totally flexible chains are described as Gaussian chains. In a Gaussian chain the bond between consecutive beads is modelled by a harmonic spring. The spring- or bond length is governed by a Gaussian distribution with a certain

width. The bonds can be rotated freely with respect to each other so that the chain behaves as a random walk.

In a homopolymer melt, polymer chains can be described as random walks if the chain length is long enough. This also holds for a copolymer melt if the incompatibility between different monomers or blocks is small enough. However, on smaller length scales the chain does not necessarily behave as a Gaussian chain. For example in DNA the helix structure restricts the possibility to bend the chain. To describe this effect the chains are considered to be semi-flexible. This is accomplished by adding a bending stiffness to the coarse grained description of the chain. Because of the excluded volume effect the semi-flexible chains tend to align. A Maier-Saupe interaction [7] between the semi-flexible blocks describes this alignment effect whose strength becomes larger when the stiffness increases. If this interaction is strong enough a nematic phase is formed in which semi-flexible blocks are oriented more or less parallel to each other. This phase is displayed on the right side of Fig. (1.1) in which the smectic-A and -C phase are also drawn. This smectic-A or -C phase is formed instead of the lamellar phase, because chains become oriented due to the semi-flexibility. In the hexagonal and bcc phase orientational ordering is also possible.

At high temperatures the diblock copolymers are in the disordered state which is both homogeneous and isotropic. Here the kinetic energy of the chains is dominating strongly over the Flory-Huggins and Maier-Saupe interaction between chains. When the temperature is lowered a phase transition takes place at a certain critical temperature. The disordered state is converted into a certain ordered structure which could be the nematic phase or a microphase structure. When the phase transition is second order or weakly first order the Landau theory can be applied in the neighbourhood of the phase transition point. In this thesis the phase behaviour is investigated in this so-called weak segregation regime. The concentration and orientation profile in a microphase structure can be approximated by a linear combination of harmonic functions with the same period and amplitude. This so-called first harmonics approximation makes further analysis possible. Further away from the phase transition at much lower temperatures the separation between A- and B-blocks becomes more markedly. Here the weak segregation approximation is not valid. Other approaches must be applied in the intermediate and strong segregation regime such as the self-consistent field theory by Matsen and Schick [8].

In this thesis much attention has been paid to the influence of stiffness on the phase behaviour of a melt of monodisperse diblock copolymers in the weak segrega-
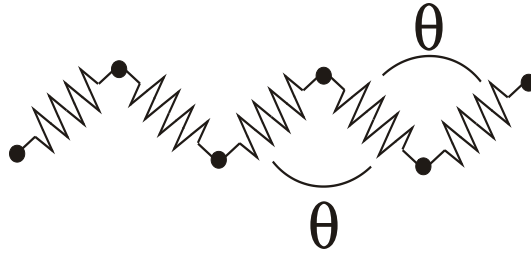
Figure 1.2: Bixon-Zwanzig model

tion regime. This problem was also investigated in [9], [10], [12] and [13]. In these papers the spinodal is calculated which is the stability limit of the Flory-Huggins or Maier-Saupe interaction parameter at which the order-disorder phase transition takes place. In [12] the freely jointed chain model is used to describe semi-flexible chains. In this discrete model rods are connected to each other which can be rotated freely with respect to the connection points between the rods. In the derivation of the Landau free energy both a scalar (density) and a tensorial (orientation) order-parameter were introduced. In [10] semi-flexible chains are described by the Kratky-Porod model. However, an orientational order-parameter tensor was not introduced. A melt of rod-coil diblocks has been investigated in [9] and [13] in which an orientational tensor for the rod part is included in the derivation. In [12] and [13] the orientational tensor varies spatially in a microphase structure, but in [9] only a global orientational tensor is considered. In [9] besides the spinodal also the complete phase diagram was calculated.

In this thesis another model is used to describe semi-flexibility which is the Bixon-Zwanzig model of [15]. In this discrete model in Fig. (1.2) the monomers are beads which are connected by springs. The springs are not completely free to rotate with respect to each other. The rotational freedom is restricted by a fixed angle θ between two subsequent springs. This angle θ determines the bending stiffness of the chain. If $\theta = 180°$ the chain behaves as a rigid rod and in the limit $\theta \to 0°$ it becomes totally flexible. The discrete model is further coarse grained to a continuous description by Bawendi and Freed [16]. In other models the total chain length is fixed which makes further analysis difficult in the weak segregation regime. However, in the Bawendi-Freed model the chain length is only on average constant due to the presence of the springs. This less restrictive condition makes it possible to derive an

monodisperse polydisperse
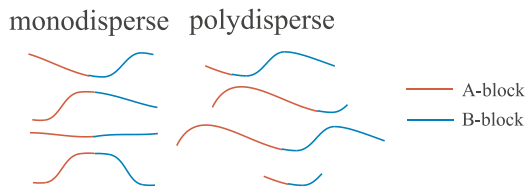
A-block

B-block

Figure 1.3: Monodisperse and polydisperse diblocks

exact expression for the Landau free energy.

The analysis in the papers [5], [9], [10], [12] and [13] is restricted to a melt of diblock copolymers which are monodisperse. In reality it is usually difficult to synthesize such a melt of identical diblocks displayed in the left part of Fig. (1.3). In the right part a polydisperse system is displayed. Here in some chains the A-block is longer than average and in other chains it is shorter. The length of the B-block is also variable and is assumed to be independent of the length of the A-block. Due to the polydispersity macrophase separation is possible instead of microphase separation [38]. A possible macrophase structure could be a melt with one big A-rich and one big B-rich domain on a macroscopic length scale. The A-rich domain is formed by collecting diblocks in which the A-block fraction is greater than average. The remaining diblocks form the B-rich domain.

The effect of polydispersity on the phase behaviour of diblock copolymers is considered in several papers. In [22] the spinodal and phase diagram are determined for a melt of polydisperse flexible diblock copolymers. The polydispersity is described by the Schultz-Zimm distribution [2]. The influence of both stiffness and polydispersity on the spinodal of a diblock melt is investigated in [23] which is an extension of the analysis in [10].

In [6] the Landau free energy as a functional of the density order-parameter profile is derived for a very general melt of flexible multi-block copolymers in the weak segregation limit. The length of each block and the number of blocks in a multi-block copolymer can be chosen arbitrary. The general melt is a mixture with an arbitrary composition of different kinds of multi-block copolymers. In chapter two of this thesis the theory has been extended by adding an arbitrary bending stiffness to each block which is described by the Bawendi-Freed model of [16] mentioned earlier. Due to the stiffness an orientational tensor must be introduced in the derivation of the Landau free energy. In chapter three this more general free energy has been applied to a simple system, namely a melt of monodisperse semi-flexible diblock copolymers.

The spinodal and complete phase diagram is calculated numerically for this simple system. First the theory of chapter two is used to derive a simplified expression of the Landau free energy as a function of only one variable. In the free energy of a microphase structure a possible space dependent orientational tensor is taken into account. It is explained how such a spatial orientation can be described and visualized in a smectic phase and in a more complicated microphase such as the hexagonal phase. In several phase diagrams structures of the melt are predicted as a function of the composition, persistence length and the strength of the Flory-Huggins and Maier-Saupe interaction. The influence of the Maier-Saupe interaction on the microphase structure is thoroughly discussed. In chapter four we study an example of a melt of polydisperse diblock copolymers. We use again the Schultz-Zimm distribution to describe the polydispersity in block length. The spinodal and corresponding period length scale are calculated as a function of polydispersity, stiffness and composition. In certain systems macrophase separation has been observed if the degree of polydispersity is large enough. Finally monodisperse triblocks are considered in the fifth chapter. In the same way as in chapter three the complete phase diagram has been calculated to predict structures of the melt as a function of composition, persistence length and the strength of the Flory-Huggins and Maier-Saupe interactions. Furthermore the spinodal and corresponding period length scale are calculated as a function of stiffness and chain composition. The theory and results of chapter two till five are currently being prepared for publication in both the Journal of Chemical Physics and Macromolecular Theory and Simulations.

Chapter 2

Theory

2.1 Introduction

In [6] the Landau free energy is derived for a general melt of flexible multi-block copolymers. In a multi-block copolymer chain different kinds of homopolymers or blocks are connected to each other. The length of each block and the number of blocks in a multi-block copolymer can be chosen arbitrary. The general melt is a mixture with an arbitrary composition of different kinds of multi-block chains. Each block consists of one kind of monomers or segments. The chemical incompatibility between two different kinds of monomers or blocks a and b is described by the Flory-Huggins interaction χ_{ab}. If χ_{ab} is strong enough microphase separation between a and b blocks occurs. The Landau free energy is expressed as a power series expansion of order-parameters Ψ^{α} belonging to different kinds of monomers $\alpha = a, b, \ldots$. Ψ^{α} is called the density order-parameter profile which we will call scalar order-parameter from now on in the rest of this thesis. The minimum of this free energy with respect to the scalar order-parameters Ψ^{α} describes the equilibrium phase behaviour of the melt. If at least one of the scalar order-parameters Ψ^{α} is nonzero then the melt is in a certain microphase, e.g. the bcc, hexagonal or lamellar phase. In [6] every block is considered to be totally flexible. In this chapter the theory is extended to a general melt of semi-flexible multi-block copolymers. Then a block of type a is in addition characterized by a persistence length λ_a. This makes the theory much more general. If $\lambda_a \rightarrow 0$ block a becomes totally flexible and if $\lambda_a \rightarrow \infty$ it can be regarded as a rigid rod. Because of the stiffness the blocks may become oriented when there is microphase separation. The theory is further extended by taking this orientation into

account by means of the tensor Q_{ij}^{α} with $i, j = x, y, z$ and $\alpha = a, b, ...$ This extension is realised by writing the Landau free energy as a power series expansion of both scalar order-parameters Ψ^{α} and orientation tensors Q_{ij}^{α}. Besides the Flory-Huggins interaction another interaction is included which is the Maier-Saupe interaction ω_{ab} between two different blocks or two blocks of the same kind . If this interaction is strong enough local or global nematic ordering arises of a and/or b-blocks. The nematic interaction ω_{ab} may also stimulate or counteract microphase separation. Conversely the Flory-Huggins interaction χ_{ab} may influence the alignment of blocks.

To describe the semi-flexible chains we apply the Bawendi-Freed version of the freely rotating chain model see [14], [15] and [16]. In this continuous chain model the chain length L may fluctuate and is only on average constant. Therefore we use a special parameter l to label the monomers. It is the average distance between a certain monomer and one of the chain ends measured along the contour. If l would be the actual contour length, then the tangent vector $\underline{u}(l) = \frac{d\underline{r}(l)}{dl}$ must be a unit vector. Because l is the average distance the squared length $u^2(l)$ is only on average equal to one, $\langle u^2(l) \rangle = 1$. This less restrictive condition makes the explicit derivation of the Landau free energy possible.

In the next chapter we want to apply the theory to investigate numerically the spinodals χ_s and ω_s of a melt of monodisperse semi-flexible diblock copolymers. If $\chi > \chi_s$ a microphase is formed and if $\omega > \omega_s$ nematic ordering occurs. For simplicity the three different parameters ω_{AA}, ω_{AB} and ω_{BB} have been taken equal so that there is only one parameter ω. The results will be compared with earlier results in [9], [10], [11], [12] and [13]. First the theoretical approach used in these papers is considered and compared to our theory.

In the paper of Friedel et. al. the Kratky-Porod model is used to describe semi-flexibility. The spinodal χ_s was calculated according to Eq.(5) of [10],

$$\chi_s = \frac{1}{2} \min_{\{q\}} \frac{S_{AA}^0(q) + S_{BB}^0(q) + 2S_{AB}^0(q)}{S_{AA}^0(q)S_{BB}^0(q) - S_{AB}^0(q)^2}, \tag{2.1}$$

a result obtained by Leibler in [5]. In that paper a possible orientation of A and B blocks in a certain microphase was not taken into account. This is justified if the diblocks are totally flexible, but if the chains are semi-flexible Eq. (2.1) is incomplete. In this expression the $S_{ab}^0(q)$ with indices $a, b = A, B$ are single-chain density-density correlation functions which could only be calculated approximately according to Eq. (7) in [10].

In [11] Matsen applied the self-consistent field theory to a melt of monodisperse

semi-flexible diblock chains. The semi-flexibility is described by means of the Saitô model introduced in [18]. The structure of the lamellar phase has been investigated not only at a χ close to χ_s but also when $\chi \gg \chi_s$. However, a possible orientation of A and B blocks is not taken into account in a microphase.

In Singh's paper [12] the freely jointed chain model is used to describe semi-flexible chains. In this discrete model rods are connected to each other which can be rotated freely with respect to the connection points between them. The rod length is a measure of the stiffness. This model is used to derive the Landau free energy of a melt of monodisperse semi-flexible diblock copolymers. The free energy here is written as a power series expansion of both the scalar order-parameters and orientation tensors of A and B monomers. This allows a more accurate calculation of the spinodals χ_s and ω_s. In Singh's paper both χ_s and ω_s are calculated as a function of the stiffness of the A- and B-block. It has also been investigated how χ_s depends on ω and ω_s on χ.

Holyst and Schick [13] considered a melt of monodisperse rod-coil diblocks. The spinodal χ_s is calculated in a similar manner as in this thesis. However, the orientation tensor $Q_{ij}^{\alpha}(\underline{q})$ here has the same form as in Singh's paper [12],

$$Q_{ij}^{\alpha}(\underline{q}) = (n_i^{\alpha} n_j^{\alpha} - \frac{1}{3}\delta_{ij})Q^{\alpha}(\underline{q}), \tag{2.2}$$

in which it has also been assumed that the orientation vectors $\underline{n}^A$ and $\underline{n}^B$ of the A- and B-block are equal, so $\underline{n}^A = \underline{n}^B = \underline{n}$. In the paper of Holyst [13] this form has not been used. The orientation tensor of the flexible part is neglected and tensor $Q_{ij}(\underline{q})$ of the rod is not further reduced to the form as given by Eq. (2.2). So the second order contribution to the free energy is written as a function of seven parameters $\Psi(\underline{q})$ and $Q_{ij}(\underline{q})$ with $ij = xx, yy, zz, xy, xz$ and yz. In this way a more general expression for the spinodal χ_s is obtained.

Reenders et. al. [9] calculated the complete phase diagram of a melt of monodisperse rod-coil diblocks. The phase diagrams they calculated displayed the various phases in which the melt can reside such as the bcc, hexagonal, lamellar, nematic and smectic-C state. Orientation of the flexible part was neglected. The orientation tensor of the rod part has the same form as Eq. (2.2). Reenders et. al. [9] made the ansatz that the wave vector $\underline{q}$ of the orientation tensor $Q_{ij}^{\alpha}(\underline{q})$ can only be zero, so that there is only global nematic ordering. A consequence of this ansatz is that a possible orientation is negligibly small if $\chi > \chi_s$ and $\omega = 0$. Therefore the tensor $Q_{ij}(\underline{q}) = Q_{ij}(\underline{0})$ is neglected in the part of the phase diagram in which $\omega < \omega_s$. In the

description of the smectic state a possible local orientation $Q_{ij}(\underline{q} \neq \underline{0})$ is not taken into account. However, in [12], [13] and this chapter a possible contribution of orientation tensors with nonzero $\underline{q}$ are not excluded if there is microphase separation. In a certain microphase structure the wave vectors in the orientation tensor $Q_{ij}^{\alpha}(\underline{q})$ must be the same as those in the scalar order-parameter $\Psi(\underline{q})$, because in that case the symmetry of the structure is conserved. In this way the orientation may play a more important role when $\chi > \chi_s$ and $\omega = 0$. However, in addition to the set of local orientations $Q_{ij}^{\alpha}(\underline{q})$ global orientations $Q_{ij}^{\alpha}(\underline{0})$ in the same direction are still possible in a certain microphase.

To describe a general melt of semi-flexible multi-block copolymers we will employ the typical *coarse graining* one usually encounters in polymer physics [21]. Consider a melt of n_c copolymer chains in a volume V. As these chains consist of arbitrary sequences (blocks) of up-to M chemically different types of monomers, the number of possible chains is astronomically large. To denote the various different species of chains present in the system, we will use the label s. Each chain belonging to species s, of which there are n_s present, will consist of $N_s + 1$ monomers also referred to as segments, connected by N_s deformable bonds of average length a having fixed bond angles between them. The idea being that each of the M chemically different blocks of segments will have their own fixed angle between subsequent bonds. We will label these M chemically different segments by Greek lowercase symbols α, β etc. running from 1 to M. In the sequal we will use a continuous notation, i.e. chains will be represented by continuous curves obtained via a proper continuum limit ($N_s \longrightarrow \infty$, $a \longrightarrow 0$ such that $L_s \equiv N_s a$ remains constant etc.). To specify a given chain species s, Ising-like variables $\sigma_s^{\alpha}(l)$ will be introduced with $\alpha = 1, ..., M$ and $l \in [0, L_s]$ in such a way that $\sigma_s^{\alpha}(l) \equiv 1$ when segment l is of type α and $\sigma_s^{\alpha}(l) \equiv 0$ otherwise. The conformations of the n_s chains belonging to species s will be specified by the positions of the corresponding segments that make up these chains and the set of tangent vectors along the chains, i.e. the set of curves $\{\underline{R}_m^s(l) \mid 0 \leqslant l \leqslant L_s\}_m$ with $m = 1, ..., n_s$ defined with respect to some origin O in V, and the set of tangent vectors to these curves $\{\underline{u}_m^s(l) \equiv \underline{\dot{R}}_m^s(l) \equiv \frac{\partial R_m^s(l)}{\partial l} \mid 0 \leqslant l \leqslant L_s\}_m$. As the bonds are deformable these tangent vectors will not be of unit-length at every point along the contours of the chains. Nevertheless, it will turn out that they will be unit vectors in an averaged sense, as will become clear later-on. The total set $\{\underline{R}_m^s(l), \underline{u}_m^s(l) \mid 0 \leqslant l \leqslant L_s\}_{sm}$ defines a configurational *micro-state* of the whole system. Such a micro-state will be denoted by γ. A variable G which is a function of these micro-states, i.e. a so-called *state-variable*, will be written as $\hat{G} \equiv G(\gamma)$. Examples of important state-variables

which we will need later-on are the *microscopic α-segment density $\hat{\rho}^\alpha(\underline{x})$*, defined for each $\underline{x} \in V$ by,

$$\hat{\rho}^\alpha(\underline{x}) \equiv \sum_{sm} \int_0^{L_s} dl \, \sigma_s^\alpha(l) \, \delta(\underline{x} - \underline{R}_m^s(l)) \tag{2.3}$$

and the *overall microscopic segment density $\hat{\rho}(\underline{x})$* through,

$$\hat{\rho}(\underline{x}) \equiv \sum_\alpha \hat{\rho}^\alpha(\underline{x}) = \sum_{sm} \int_0^{L_s} dl \, \delta(\underline{x} - \underline{R}_m^s(l)). \tag{2.4}$$

By integrating these densities over V we obtain respectively the total number of α-segments N^α and the overall number of segments N in the system. This last number can be either written as $\sum_\alpha N^\alpha$ or as $\sum_s n_s N_s$. Thus the fraction of α-segments is given by $f^\alpha \equiv \frac{N^\alpha}{N}$. Without loss of generality we will choose our length-scale in such a way that each segment has a unit volume and therefore that $N \equiv V$. In that case it follows that,

$$\frac{1}{V} \int_V d^3x \, \hat{\rho}(\underline{x}) \equiv 1 \tag{2.5}$$

and that f^α can be written as

$$f^\alpha \equiv \frac{1}{V} \int_V d^3x \, \hat{\rho}^\alpha(\underline{x}). \tag{2.6}$$

The description of semi-flexibility and the tendency to locally align will require the introduction of the *microscopic α-segment orientation-tensor density $\underline{\underline{\hat{S}}}^\alpha(\underline{x})$*, defined by,

$$\underline{\underline{\hat{S}}}^\alpha(\underline{x}) \equiv \sum_{sm} \int_0^{L_s} dl \, \sigma_s^\alpha(l) \, \underline{u}_m^s(l) \, \underline{u}_m^s(l) \, \delta(\underline{x} - \underline{R}_m^s(l)). \tag{2.7}$$

In order to account approximately for the effect of excluded volume due to the repulsive nature of the intra-chain and inter-chain potentials at short distances, we will assume that the system is *incompressible* , i.e. that the overall microscopic segment density is not only equal to 1 "globally", as in (2.5), but also "locally", that is $\hat{\rho}(\underline{x}) \equiv 1, \forall \underline{x} \in V$. As our aim is to derive a Landau free energy for this copolymer melt of *M quasi-components* [27], we need to define a set of 2*M order-parameters* or actually 2*M order- parameter fields* to describe the possible *inhomogeneous and anisotropic phases* of the system and to be able to calculate their free energy. These

order-parameter fields can be defined by coarse graining the following set of *micro-scopic order-parameter fields*,

$$\hat{\psi}^\alpha(\underline{x}) \equiv \hat{\rho}^\alpha(\underline{x}) - f^\alpha \qquad (\alpha = 1, ..., M) \tag{2.8}$$

and

$$\underline{\underline{\hat{Q}}}^\alpha(\underline{x}) \equiv \underline{\underline{\hat{S}}}^\alpha(\underline{x}) - \frac{1}{3}\hat{\rho}^\alpha(\underline{x})\underline{\underline{I}} \qquad (\alpha = 1, ..., M). \tag{2.9}$$

It is clear that due to the incompressibility assumption only $M - 1$ of the scalar fields will be independent, as it follows that,

$$\sum_\alpha \hat{\psi}^\alpha(\underline{x}) \equiv 0. \tag{2.10}$$

The interactions between the various segments in this copolymer melt can be described in terms of these microscopic order-parameter fields. This can be shown in the following way. Under the assumption that segment- segment interactions are pairwise additive, the total interaction energy $\hat{W}$ of the system will be of the form,

$$\hat{W} \equiv \frac{1}{2} \sum_{\alpha\beta} \sum_{sm} \sum_{s'm'} \int_0^{L_s} dl \int_0^{L_{s'}} dl' \, \sigma_s^\alpha(l) \, \sigma_{s'}^\beta(l') \times$$

$$\times w_{\alpha\beta}(\underline{R}_m^s(l) - \underline{R}_{m'}^{s'}(l') ; \underline{u}_m^s(l) \cdot \underline{u}_{m'}^{s'}(l')). \tag{2.11}$$

where $w_{\alpha\beta}(\underline{x}; \underline{u} \cdot \underline{u}')$ is the interaction potential between a segment of type α and a segment of type β, which is assumed to be short-ranged in space, i.e. $w_{\alpha\beta}(\underline{x}; \underline{u} \cdot \underline{u}') \simeq \widetilde{w}_{\alpha\beta}(\underline{u} \cdot \underline{u}') \, \delta(\underline{x})$ and $\widetilde{w}_{\alpha\beta}(\underline{u} \cdot \underline{u}')$ can be expanded in the following way,

$$\widetilde{w}_{\alpha\beta}(\underline{u} \cdot \underline{u}') = \varepsilon_{\alpha\beta} - \omega_{\alpha\beta} (\underline{u} \cdot \underline{u}')^2 + ... \tag{2.12}$$

This expansion does not contain the term $\underline{u} \cdot \underline{u}'$ or any odd power of it for that matter because of the fore-aft symmetry of the segments. Although formally $\hat{W}$ contains "self-energy" terms, i.e. terms with $\alpha = \beta$, $s = s'$, $m = m'$ and $l = l'$, we will not bother to explicitly exclude them in the notation used in (2.11). By substituting (2.12) into (2.11) it is easy to see that $\hat{W}$ can be written in terms of the specific microscopic segment densities $\hat{\rho}^\alpha(\underline{x})$ (2.3) and $\underline{\underline{\hat{S}}}^\alpha(\underline{x})$ (2.7) as,

$$\hat{W} \simeq \frac{1}{2} \sum_{\alpha\beta} \varepsilon_{\alpha\beta} \int_V d^3x \, \hat{\rho}^\alpha(\underline{x})\hat{\rho}^\beta(\underline{x}) - \frac{1}{2} \sum_{\alpha\beta} \omega_{\alpha\beta} \int_V d^3x \, \underline{\underline{\hat{S}}}^\alpha(\underline{x}) : \underline{\underline{\hat{S}}}^\beta(\underline{x}). \tag{2.13}$$

By eliminating one of the $\hat{\rho}$'s, say $\hat{\rho}^M$, from (2.13) using $\sum_\alpha \hat{\rho}^\alpha(\underline{x}) \equiv 1$ and substituting $\hat{\rho}^\alpha(\underline{x}) = \hat{\psi}^\alpha(\underline{x}) + f^\alpha$ and $\underline{\hat{S}}^\alpha(\underline{x}) = \underline{\hat{Q}}^\alpha(\underline{x}) + \frac{1}{3}\hat{\rho}^\alpha(\underline{x})\underline{I}$, one ends up with,

$$\hat{W} \simeq \frac{1}{2} \sum_{\alpha\beta}{}' E_{\alpha\beta} \int_V d^3x\, \hat{\psi}^\alpha(\underline{x})\hat{\psi}^\beta(\underline{x}) - \frac{1}{2} \sum_{\alpha\beta} \omega_{\alpha\beta} \int_V d^3x\, \underline{\hat{Q}}^\alpha(\underline{x}) : \underline{\hat{Q}}^\beta(\underline{x})$$

$$-\frac{1}{3} \sum_{\alpha\beta} \omega_{\alpha\beta} \int_V d^3x\, (\hat{\psi}^\alpha(\underline{x}) + f^\alpha) Tr \underline{\hat{Q}}^\beta(\underline{x}) \qquad (2.14)$$

with $E_{\alpha\beta} \equiv \varepsilon'_{\alpha\beta} - \varepsilon'_{\alpha M} - \varepsilon'_{\beta M} + \varepsilon'_{MM}$ and $\varepsilon'_{\alpha\beta} = \varepsilon_{\alpha\beta} - \frac{1}{3}\omega_{\alpha\beta}$. The accent in the first term of $\hat{W}$ implies that both sums run from 1 to $M-1$. In terms of the set of Flory χ-parameters [2] between the different segments, i.e.,

$$\chi_{\alpha\beta} \equiv \varepsilon_{\alpha\beta} - \frac{\varepsilon_{\alpha\alpha} + \varepsilon_{\beta\beta}}{2} \qquad \text{with} \qquad \chi_{\alpha\alpha} = 0 \quad , \forall \alpha, \qquad (2.15)$$

this $E_{\alpha\beta}$ can be written as,

$$E_{\alpha\beta} = \chi_{\alpha\beta} - \chi_{\alpha M} - \chi_{\beta M} \equiv -2\tilde{\chi}_{\alpha\beta} \qquad (2.16)$$

and therefore finally $\hat{W}$ becomes,

$$\hat{W} \simeq -\sum_{\alpha\beta}{}' \tilde{\chi}_{\alpha\beta} \int_V d^3x\, \hat{\psi}^\alpha(\underline{x})\hat{\psi}^\beta(\underline{x}) - \frac{1}{2} \sum_{\alpha\beta} \omega_{\alpha\beta} \int_V d^3x\, \underline{\hat{Q}}^\alpha(\underline{x}) : \underline{\hat{Q}}^\beta(\underline{x})$$

$$-\frac{1}{3} \sum_{\alpha\beta} \omega_{\alpha\beta} \int_V d^3x\, (\hat{\psi}^\alpha(\underline{x}) + f^\alpha) Tr \underline{\hat{Q}}^\beta(\underline{x}). \qquad (2.17)$$

For the binary case ($M = 2$), the only remaining $\tilde{\chi}$-parameter, $\tilde{\chi}_{11}$, reduces to the more familiar χ_{12}. With this interaction energy of the copolymer melt we can formulate the system's *partition function Z*, but for this it is necessary to specify the *unnormalized statistical weight* $e^{-\hat{H}_0}$ (we use units such that $k_B T = 1$) of the system in absence of these interactions. As we want to allow chains locally to have an arbitrary degree of flexibility, say ranging from fully flexible to rigid-rod like behaviour, we will describe the *unperturbed* semi-flexible melt by an ensemble of locally persistent Gaussian chains in the spirit of the Bawendi-Freed approach [15], [16]. The *unperturbed Hamiltonian* $\hat{H}_0$ in this approach is given by,

$$\hat{H}_0 \equiv \frac{3}{4} \sum_{sm} \left\{ \left[\underline{u}^s_m(0)\right]^2 + \left[\underline{u}^s_m(L_s)\right]^2 \right\} +$$

$$+ \frac{3}{4} \sum_{sm} \int_0^{L_s} dl \left\{ \frac{1}{\lambda_s(l)} \left[\underline{u}^s_m(l)\right]^2 + \lambda_s(l) \left[\underline{\dot{u}}^s_m(l)\right]^2 \right\}, \qquad (2.18)$$

where $\lambda_s(l)$ denotes the local *persistence length* of chains of type s. For a multiblock copolymer this $\lambda_s(l)$ will have the following form,

$$\lambda_s(l) \equiv \sum_{i=1}^{N_s^b} \lambda_s^{(i)} \left[\theta(l - \sum_{j=1}^{i-1} L_s^{(j)}) - \theta(l - \sum_{j=1}^{i} L_s^{(j)}) \right], \tag{2.19}$$

where $L_s^{(j)}$ and $\lambda_s^{(i)}$ respectively denote the block - and the persistence length of the j-th block in a chain of type s which consists of N_s^b blocks. The first term in (2.18) containing the orientation vectors of the endpoints of the chains and the particular choice of the coefficients in the second term of (2.18) ensure homogeneity of the chains and Porod-Kratky like behavior in an averaged sense, i.e. $\langle \left[\underline{u}_m^s(l) \right]^2 \rangle_0 = 1, \quad \forall l \in [0, L_s]$. $\langle \dots \rangle_0$ is an average over all possible chain configurations of one single free chain. It is defined in Eq. (2.35) in section 2.2.

The total Hamiltonian $\hat{H}$ for a certain melt configuration contains the unperturbed Hamiltonian $\hat{H}_0$ and the total interaction energy $\hat{W}$,

$$\hat{H} = \hat{H}_0 + \hat{W}. \tag{2.20}$$

Every configuration gives a contribution $\exp(-\hat{H})$ to the partition function Z. In section 2.2 a functional integral Z over all possible configurations is evaluated. From the partition function Z the Landau free energy F_L is derived by considering the most dominant contribution to Z. This contribution corresponds to the most probable i.e. equilibrium state of the melt. The final result (in units of $k_B T$) is given by,

$$\frac{F_L}{V} = \min_{\underline{\Psi}, \overline{\Upsilon}} \{ (\Gamma_{ab}^{(2)} - \widetilde{\chi}_{ab}) \Psi^a \Psi^b + 2\Gamma_{a\overline{b}}^{(2)} \Psi^a \Upsilon^{\overline{b}} +$$

$$(\Gamma_{\overline{ab}}^{(2)} - \frac{1}{2} \omega_{\overline{ab}}) \Upsilon^{\overline{a}} \Upsilon^{\overline{b}} - \frac{1}{3} \omega_{ab} \Upsilon^{a,ij} \delta_{ij} (\Psi^b + f^b) +$$

$$\Gamma_{abc}^{(3)} \Psi^a \Psi^b \Psi^c + 3\Gamma_{ab\overline{c}}^{(3)} \Psi^a \Psi^b \Upsilon^{\overline{c}} + 3\Gamma_{a\overline{bc}}^{(3)} \Psi^a \Upsilon^{\overline{b}} \Upsilon^{\overline{c}} + \Gamma_{\overline{abc}}^{(3)} \Upsilon^{\overline{a}} \Upsilon^{\overline{b}} \Upsilon^{\overline{c}} +$$

$$\Gamma_{abcd}^{(4)} \Psi^a \Psi^b \Psi^c \Psi^d + 4\Gamma_{abc\overline{d}}^{(4)} \Psi^a \Psi^b \Psi^c \Upsilon^{\overline{d}} + 6\Gamma_{ab\overline{c}\overline{d}}^{(4)} \Psi^a \Psi^b \Upsilon^{\overline{c}} \Upsilon^{\overline{d}} +$$

$$4\Gamma_{a\overline{bcd}}^{(4)} \Psi^a \Upsilon^{\overline{b}} \Upsilon^{\overline{c}} \Upsilon^{\overline{d}} + \Gamma_{\overline{abcd}}^{(4)} \Upsilon^{\overline{a}} \Upsilon^{\overline{b}} \Upsilon^{\overline{c}} \Upsilon^{\overline{d}} \} \tag{2.21}$$

with $\tilde{\chi}_{ab} \equiv \tilde{\chi}_{\alpha\beta} \delta(\underline{q}_1 + \underline{q}_2)$, $\omega_{\overline{ab}} \equiv \omega_{\alpha\beta} |2\delta_{ii'}\delta_{jj'} - \delta_{ij}\delta_{i'j'}| \delta(\underline{q}_1 + \underline{q}_2)$, $\Psi^a \equiv \frac{\psi^\alpha(-\underline{q}_1)}{V}$, $\Upsilon^{\overline{a}} \equiv \frac{Q_{ij}^\alpha(-\underline{q}_1)}{V}$ and $f^b = f^\beta \delta(\underline{q}_2)$. In this expression of the free energy we use the *composite*

labels $a \equiv (\underline{q}_1 \neq \underline{0}, \alpha)$, $b \equiv (\underline{q}_2 \neq \underline{0}, \beta)$ etc. and $\overline{a} \equiv (\underline{q}_1, ij, \alpha)$, $\overline{b} \equiv (\underline{q}_2, i'j', \beta)$. In the indices $\overline{a}$ and $\overline{b}$ the pairs ij and $i'j'$ are one of the six unique pairs xx, yy, zz, xy, xz and yz. The coefficient functions (Γ's) are called *vertices* and are defined by Eq. (2.76), (2.77) and (2.78) in section 2.2.

2.2   Derivation of a Landau free energy for a general semi-flexible block copolymer melt

In this section the Landau free energy given by Eq. (2.21) is derived. The starting point of the derivation is the partition function Z, i.e. the sum of the *Boltzmann weights* over all allowed states of the system. The set of all allowed states furnishes the so-called *state-space* or *configuration-space* Γ of the system, which in this case is given by,

$$\Gamma \equiv \{\{\underline{R}_m^s, \underline{u}_m^s\}_{sm} \mid \underline{u}_m^s \equiv \underline{\dot{R}}_m^s, \ \forall \, m, s \quad \& \quad \hat{\rho}(\underline{x}) = 1, \ \forall \underline{x} \in V\}. \tag{2.22}$$

As we are ultimately only interested in differences in free energy between possible inhomogeneous and/or anisotropic phases of the system, all combinatorial terms will be left out of this partition function since they only lead to constant terms in the free energy. With this in mind Z can be written as,

$$Z \equiv \prod_{sm} \int d^3 \widetilde{U}_m^s \int d^3 U_m^s G(\{\underline{U}_m^s, L_s\} \mid \{\widetilde{\underline{U}}_m^s, 0\}), \tag{2.23}$$

where the *orientational Green's function* $G(\{\underline{U}_m^s, L_s\} \mid \{\widetilde{\underline{U}}_m^s, 0\})$ is defined by,

$$G \equiv \prod_{sm} \int D\underline{R}_m^s \int_{(0,\widetilde{\underline{U}}_m^s)}^{(L_s, \underline{U}_m^s)} D\underline{u}_m^s \, \delta\left[\underline{R}_m^s - \int dl \, \underline{u}_m^s(l)\right] \delta\left[1 - \hat{\rho}\right] e^{-(\hat{H}_0 + \hat{W})} \tag{2.24}$$

which gives the probability that each chain has a certain initial and final orientation. In this coarse grained description incompressibility, which is due to interactions at the molecular level, has to be explicitly accounted for via the delta function $\delta\left[1 - \hat{\rho}\right]$. This partition function will be transformed in four steps into a form which is more amendable for further analysis. The first step involves a formal shift of the state-variable dependence of $e^{-\hat{W}}$ in (2.24). This is done by introducing the following two *functional decompositions of the identity* into G,

$$\prod_{\mu}{}' \int D\psi^{\mu}\, \delta\left[\psi^{\mu} - \hat{\psi}^{\mu}\right] = 1 \tag{2.25}$$

and

$$\prod_{\nu} \int D\underline{\underline{Q}}^{\nu}\, \delta\left[\underline{\underline{Q}}^{\nu} - \hat{\underline{\underline{Q}}}^{\nu}\right] = \underline{\underline{I}} \tag{2.26}$$

which yield,

$$
\begin{aligned}
G \;=\; & \prod_{\mu}{}' \int D\psi^{\mu} \prod_{\nu} \int D\underline{\underline{Q}}^{\nu}\, e^{-W} \times \\
& \times \prod_{sm} \int D\underline{R}^s_m \int_{(0,\widetilde{\underline{U}}^s_m)}^{(L_s,\underline{U}^s_m)} D\underline{u}^s_m\, e^{-\hat{H}_0}\, \delta\left[\underline{R}^s_m - \int dl\, \underline{u}^s_m(l)\right] \delta\left[1 - \hat{\rho}\right] \times \\
& \times \prod_{\lambda}{}' \prod_{\eta} \delta\left[\psi^{\lambda} - \hat{\psi}^{\lambda}\right] \delta\left[\underline{\underline{Q}}^{\eta} - \hat{\underline{\underline{Q}}}^{\eta}\right].
\end{aligned}
\tag{2.27}
$$

The elements Q^{ν}_{ij} and Q^{ν}_{ji} of the tensor $\underline{\underline{Q}}^{\nu}$ in which $i \neq j$ are identical, but in Eq. (2.27) they are treated as independent parameters. At a certain point this would obstruct the further derivation of the Landau free energy. This happens when we solve Eq. (2.63) and (2.64) iteratively, because then the matrix $A^{\overline{ab}}$ would not be invertible. In this matrix the rows and columns in which $ij = xy$, yz and xz would be identical to the rows and columns with reversed indices $ij = yx$, zy and zx. Such a matrix is not invertible. Therefore in the functional integral in Eq. (2.27) only the elements Q^{ν}_{ij} with unique pairs xx, yy, zz, xy, yz and xz may occur if we want to derive the desired expression of the Landau free energy. In the rest of the derivation we will ignore the other pairs yx, zy and zx. In the interaction energy W given by Eq. (2.17) the terms containing elements Q^{ν}_{ij} with $i \neq j$ are counted twice.

The second step involves substitution of the following *functional spectral representations* for the last $2M$ "delta-functions" in the above expression, i.e.,

$$\delta\left[1 - \hat{\rho}\right] \;\equiv\; \int Dh^0\, e^{i \int_V d^3x\, h^0(\underline{x})\{1 - \hat{\rho}(\underline{x})\}} \tag{2.28}$$

$$\delta\left[\psi^{\lambda} - \hat{\psi}^{\lambda}\right] \;\equiv\; \int Dh^{\lambda}\, e^{i \int_V d^3x\, h^{\lambda}(\underline{x})\, \{\psi^{\lambda}(\underline{x}) - \hat{\psi}^{\lambda}(\underline{x})\}} \quad (\lambda = 1, ..., M-1) \tag{2.29}$$

$$\delta\left[\underline{\underline{Q}}^{\eta} - \hat{\underline{\underline{Q}}}^{\eta}\right] \;\equiv\; \int D\underline{\underline{K}}^{\eta}\, e^{i \int_V d^3x\, \underline{\underline{K}}^{\eta}(\underline{x}) : \{\underline{\underline{Q}}^{\eta}(\underline{x}) - \hat{\underline{\underline{Q}}}^{\eta}(\underline{x})\}} \quad (\eta = 1, ..., M) \tag{2.30}$$

resulting in,

$$
\begin{aligned}
G \;=\; & \prod_{\mu}{}' \int D\psi^{\mu} \prod_{\nu} \int D\underline{\underline{Q}}^{\nu}\, e^{-W} \times \\
& \times \int Dh^0 \prod_{\lambda}{}' \int Dh^{\lambda} \prod_{\eta} \int D\underline{K}^{\eta}\, e^{\,i\int_V d^3x\,\{h^0(\underline{x})+\sum_{\alpha}{}'\,h^{\alpha}(\underline{x})\,\psi^{\alpha}(\underline{x})+\sum_{\beta}\underline{K}^{\beta}(\underline{x})\,:\,\underline{\underline{Q}}^{\beta}(\underline{x})\}} \times \\
& \times \prod_{sm} \int D\underline{R}^s_m \int_{(0,\widetilde{\underline{U}}^s_m)}^{(L_s,\underline{U}^s_m)} D\underline{u}^s_m\, e^{-\hat{H}_0}\, \delta\!\left[\underline{R}^s_m - \int dl\,\underline{u}^s_m(l)\right] \times \\
& \times e^{\,-\,i\int_V d^3x\,\{h^0(\underline{x})\,\hat{\rho}(\underline{x})+\sum_{\alpha}{}'\,h^{\alpha}(\underline{x})\,\hat{\psi}^{\alpha}(\underline{x})+\sum_{\beta}\underline{K}^{\beta}(\underline{x})\,:\,\hat{\underline{\underline{Q}}}^{\beta}(\underline{x})\}}.
\end{aligned}
\tag{2.31}
$$

In the third step the auxiliary integration fields $h^0(\underline{x}), h^1(\underline{x}), ..., h^{M-1}(\underline{x})$ are transformed to new fields $J^1(\underline{x}), ..., J^M(\underline{x})$, defined in the following way,

$$
\begin{aligned}
J^{\alpha}(\underline{x}) &\equiv h^{\alpha}(\underline{x}) + h^0(\underline{x}) \quad (\alpha = 1, ..., M-1) \\
J^M(\underline{x}) &\equiv h^0(\underline{x}).
\end{aligned}
\tag{2.32}
$$

Using this isometric transformation and (2.4), (2.8) and (2.10) it is easily verified that the following identities hold,

$$
h^0(\underline{x})\,\hat{\rho}(\underline{x}) + \sum_{\alpha}{}'\,h^{\alpha}(\underline{x})\,\hat{\psi}^{\alpha}(\underline{x}) \;=\; J^M(\underline{x}) + \sum_{\alpha}{}'\,J^{\alpha}(\underline{x})\,\hat{\rho}^{\alpha}(\underline{x}) - \sum_{\alpha} f^{\alpha}\, J^{\alpha}(\underline{x})
\tag{2.33a}
$$

$$
h^0(\underline{x}) + \sum_{\alpha}{}'\,h^{\alpha}(\underline{x})\,\psi^{\alpha}(\underline{x}) \;=\; J^M(\underline{x}) + \sum_{\alpha}\,J^{\alpha}(\underline{x})\,\psi^{\alpha}(\underline{x})
\tag{2.33b}
$$

and so by combining (2.31) with (2.23) Z can be written as,

$$
\begin{aligned}
Z \;=\; & \prod_{\mu}{}' \int D\psi^{\mu} \prod_{\nu} \int D\underline{\underline{Q}}^{\nu}\, e^{-W} \times \\
& \times \prod_{\lambda} \int DJ^{\lambda} \prod_{\eta} \int D\underline{K}^{\eta}\, e^{\,i\int_V d^3x\,\{\sum_{\alpha} J^{\alpha}(\underline{x})\,[\psi^{\alpha}(\underline{x})+f^{\alpha}]+\sum_{\beta}\underline{K}^{\beta}(\underline{x})\,:\,[\underline{\underline{Q}}^{\beta}(\underline{x})+\frac{1}{3}\rho^{\beta}(\underline{x})\,\underline{\underline{I}}]\}} \times \\
& \times \langle e^{\,-\,i\int_V d^3x\,\{\sum_{\alpha} J^{\alpha}(\underline{x})\,\hat{\rho}^{\alpha}(\underline{x})+\sum_{\beta}\underline{K}^{\beta}(\underline{x})\,:\,\hat{\underline{\underline{Q}}}^{\beta}(\underline{x})\}} \rangle_0.
\end{aligned}
\tag{2.34}
$$

In this expression $\langle ... \rangle_0$ denotes an average with respect to the *unperturbed ensemble*

of chain conformations defined by $\hat{H}_0$, i.e.,

$$\langle \hat{A} \rangle_0 \equiv \prod_{sm} \int d^3 \widetilde{U}_m^s \int d^3 U_m^s \int D\underline{R}_m^s \int_{(0,\underline{\widetilde{U}}_m^s)}^{(L_s,\underline{U}_m^s)} D\underline{u}_m^s \, e^{-\hat{H}_0} \times$$

$$\times \delta \left[\underline{R}_m^s - \int dl \, \underline{u}_m^s(l) \right] \hat{A}, \tag{2.35}$$

where the functional integrations over $\{\underline{R}_m^s\}$ and $\{\underline{u}_m^s\}$ are defined in such a way that $\langle 1 \rangle_0 \equiv 1$. The last step in the transformation of Z boils down to rewriting the integrand of (2.34) using the fields $\tilde{J}^1(\underline{x}), ..., \tilde{J}^M(\underline{x})$ in the spirit of [31],

$$\tilde{J}^\alpha(\underline{x}) \equiv J^\alpha(\underline{x}) - \frac{1}{V} \int_V d^3y \, J^\alpha(\underline{y}) \quad (\alpha = 1, ..., M). \tag{2.36}$$

It is easy to see that the use of these new fields in conjunction with (2.6) will eliminate the terms in (2.34) involving f^α. Thus we finally end up with,

$$Z = \prod_{\mu}' \int D\psi^\mu \prod_{\nu} \int D\underline{\underline{Q}}^\nu \, e^{-W} \times$$

$$\times \prod_{\lambda} \int DJ^\lambda \prod_{\eta} \int D\underline{\underline{K}}^\eta \, e^{i \int_V d^3x \{\sum_\alpha \tilde{J}^\alpha(\underline{x}) \psi^\alpha(\underline{x}) + \sum_\beta \underline{\underline{K}}^\beta(\underline{x}) : \underline{\underline{Q}}^\beta(\underline{x})\} + \Lambda} \tag{2.37}$$

with Λ defined by,

$$\Lambda \equiv \ln \langle e^{-i \int_V d^3x \{\sum_\alpha \tilde{J}^\alpha(\underline{x}) \hat{\rho}^\alpha(\underline{x}) + \sum_\beta \underline{\underline{K}}^\beta(\underline{x}) : \underline{\underline{\hat{Q}}}^\beta(\underline{x})\}} \rangle_0. \tag{2.38}$$

In order to be able to extract a Landau free energy from (2.37), we will need to rework Λ somewhat more. This, however, turns out to be the most essential step in the whole derivation of this free energy. Using the decompositions

$$\hat{\rho}^\alpha(\underline{x}) \equiv \sum_{sm} \hat{\rho}_{sm}^\alpha(\underline{x}) \quad \text{where} \quad \hat{\rho}_{sm}^\alpha(\underline{x}) \equiv \int_0^{L_s} dl \, \sigma_s^\alpha(l) \, \delta(\underline{x} - \underline{R}_m^s(l)) \tag{2.39}$$

$$\underline{\underline{\hat{S}}}^\beta(\underline{x}) \equiv \sum_{sm} \underline{\underline{\hat{S}}}_{sm}^\beta(\underline{x}) \quad \text{where}$$

$$\underline{\underline{\hat{S}}}_{sm}^\beta(\underline{x}) \equiv \int_0^{L_s} dl \, \sigma_s^\alpha(l) \, \underline{u}_m^s(l) \, \underline{u}_m^s(l) \, \delta(\underline{x} - \underline{R}_m^s(l)) \tag{2.40}$$

and

$$\hat{H}_0 \equiv \sum_{sm} \hat{H}_0^{sm} \quad \text{where}$$

$$\hat{H}_0^{sm} \equiv \frac{3}{4} \left\{ \left[\underline{u}_m^s(0) \right]^2 + \left[\underline{u}_m^s(L_s) \right]^2 \right\} +$$

$$+ \frac{3}{4} \int_0^{L_s} dl \left\{ \frac{1}{\lambda_s(l)} \left[\underline{u}_m^s(l) \right]^2 + \lambda_s(l) \left[\underline{\dot{u}}_m^s(l) \right]^2 \right\} \tag{2.41}$$

it follows that (2.38) can be written as,

$$\Lambda \equiv \sum_{sm} \ln \int d^3 \widetilde{U}_m^s \int d^3 U_m^s \int D\underline{R}_m^s \int D\underline{u}_m^s \delta(\underline{u}_m^s(0) - \widetilde{\underline{U}}_m^s) \, \delta(\underline{u}_m^s(L_s) - \underline{U}_m^s) \times$$

$$\times \delta \left[\underline{R}_m^s - \int dl \, \underline{u}_m^s(l) \right] e^{-\hat{H}_0^{sm} - i \int_V d^3 x \{ \sum_\alpha \tilde{J}^\alpha(\underline{x}) \hat{\rho}_{sm}^\alpha(\underline{x}) + \sum_\beta \underline{K}^\beta(\underline{x}) : \underline{\underline{\widetilde{Q}}}_{sm}^\beta(\underline{x}) \}}.$$

$$\tag{2.42}$$

From a closer inspection of this last expression, it becomes clear that each term in (2.42) in the sum over m for a given chain type s, i.e. each term in the sum over all chains of a given type in the system, gives the same contribution to Λ. Therefore Λ can be simplified to,

$$\Lambda = \sum_s n_s \ln \int d^3 \widetilde{U}^s \int d^3 U^s \int D\underline{R}^s \int D\underline{u}^s \delta(\underline{u}^s(0) - \widetilde{\underline{U}}^s) \, \delta(\underline{u}^s(L_s) - \underline{U}^s) \times$$

$$\times \delta \left[\underline{R}^s - \int dl \, \underline{u}^s(l) \right] e^{-\hat{H}_0^s - i \int_V d^3 x \{ \sum_\alpha \tilde{J}^\alpha(\underline{x}) \hat{\rho}_s^\alpha(\underline{x}) + \sum_\beta \underline{K}^\beta(\underline{x}) : \underline{\underline{\widetilde{Q}}}_s^\beta(\underline{x}) \}}. \tag{2.43}$$

Note that the dummy index m has been dropped in all quantities. By introducing the number density of chains of type s, i.e. $\rho_s \equiv \frac{n_s}{V}$, and defining

$$\hat{\Omega} \equiv -i \sum_\alpha \int_V d^3 x \, \{ \tilde{J}^\alpha(\underline{x}) \hat{\rho}_s^\alpha(\underline{x}) + \underline{K}^\alpha(\underline{x}) : \underline{\underline{\widetilde{Q}}}_s^\alpha(\underline{x}) \} \tag{2.44}$$

(2.43) can finally be written as,

$$\Lambda \equiv V \sum_s \rho_s \ln \langle e^{\hat{\Omega}_s} \rangle_0 \equiv V \langle \ln \langle e^{\hat{\Omega}} \rangle_0 \rangle_d. \tag{2.45}$$

In this last expression the second average with subscript d is a *disorder average, i.e.* an average over the quenched disorder in the copolymer chains. More important this quenched average involves the logarithm of a quantity proportional to the partition function, as can be seen from (2.37), and therefore it is the free energy that is being averaged over the disorder. To calculate the average of the logarithm of the partition function one can resort to the replica method [28], but this is not necessary for the kind of quenched disorder one encounters in statistical copolymer systems, as will be shown now.

As the Landau free energy for this system involves an expansion up-to fourth order in the order-parameter fields $\{\psi^\alpha(\underline{x})\}$ and $\{\underline{\underline{Q}}^\beta(\underline{x})\}$, the thing to do is to expand Λ up-to fourth order in $\hat{\Omega}$. The reason for this step will become clear in the process. The result is,

$$\frac{\Lambda}{V} \simeq \frac{1}{2} \langle\langle \hat{\Omega}^2 \rangle_0\rangle_d + \frac{1}{6} \langle\langle \hat{\Omega}^3 \rangle_0\rangle_d + \frac{1}{24} \langle\langle \hat{\Omega}^4 \rangle_0\rangle_d - \frac{1}{8} \langle\langle \hat{\Omega}^2 \rangle_0^2\rangle_d. \tag{2.46}$$

where we have used the fact that $\langle \hat{\Omega} \rangle_0 = 0$, a result that is easily obtained. Let's first consider the second-order term. By using (2.44) it follows that,

$$\frac{1}{2} \langle\langle \hat{\Omega}^2 \rangle_0\rangle_d \equiv \frac{(-i)^2}{2} \sum_{\alpha\beta} \int_V d^3x \int_V d^3y \, \{ \tilde{J}^\alpha(\underline{x}) \, \tilde{J}^\beta(\underline{y}) \sum_s \rho_s \langle \hat{\rho}_s^\alpha(\underline{x}) \hat{\rho}_s^\beta(\underline{y}) \rangle_0 +$$

$$+2 \sum_{ij} K_{ij}^\alpha(\underline{x}) \, \tilde{J}^\beta(\underline{y}) \sum_s \rho_s \langle \widehat{Q}_{s,ij}^\alpha(\underline{x}) \hat{\rho}_s^\beta(\underline{y}) \rangle_0 +$$

$$+ \sum_{ij} \sum_{i'j'} K_{ij}^\alpha(\underline{x}) \, K_{i'j'}^\beta(\underline{y}) \sum_s \rho_s \langle \widehat{Q}_{s,ij}^\alpha(\underline{x}) \, \widehat{Q}_{s,i'j'}^\beta(\underline{y}) \rangle_0 \}. \tag{2.47}$$

Now by invoking the Fourier-representations of both $\hat{\rho}_s^\alpha(\underline{x})$ and $\widehat{Q}_{s,ij}^\alpha(\underline{x})$, i.e.,

$$\hat{\rho}_\alpha^s(\underline{x}) \equiv \frac{1}{V} \sum_{\underline{q}} \int_0^{L_s} dl \, \sigma_s^\alpha(l) \, e^{i\underline{q}\cdot(\underline{x}-\underline{R}^s(l))} \tag{2.48}$$

and

$$\widehat{Q}_{s,ij}^\alpha(\underline{x}) \equiv \frac{1}{V} \sum_{\underline{q}} \int_0^{L_s} dl \, \sigma_s^\alpha(l) \, (\underline{u}^s(l) \, \underline{u}^s(l) \, - \frac{1}{3}\underline{\underline{I}}) e^{i\underline{q}\cdot(\underline{x}-\underline{R}^s(l))} \tag{2.49}$$

the four correlation functions appearing in (2.47) can be written as,

$$
\begin{aligned}
\langle\langle \hat{\rho}^\alpha(\underline{x})\,\hat{\rho}^\beta(\underline{y})\,\rangle_0\rangle_d &= \frac{1}{V^2}\sum_{\underline{q}\underline{q}'} e^{i(\underline{q}\cdot\underline{x}+\underline{q}'\cdot\underline{y})}\sum_s \rho_s \int_0^{L_s} dl \int_0^{L_s} dl'\,\sigma_s^\alpha(l)\,\sigma_s^\beta(l') \times \\
&\quad \times \langle\, e^{-i(\underline{q}\cdot\underline{R}^s(l)+\underline{q}'\cdot\underline{R}^s(l'))}\,\rangle_0 \\
&\equiv \frac{1}{V^2}\sum_{\underline{q}\underline{q}'} e^{i(\underline{q}\cdot\underline{x}+\underline{q}'\cdot\underline{y})}\sum_s \rho_s A_s^{JJ,\alpha\beta}(\underline{q},\underline{q}') \\
&\equiv \frac{1}{V^2}\sum_{\underline{q}\underline{q}'} e^{i(\underline{q}\cdot\underline{x}+\underline{q}'\cdot\underline{y})}\,A^{JJ,\alpha\beta}(\underline{q},\underline{q}'),
\end{aligned}
\tag{2.50}
$$

$$
\begin{aligned}
\langle\langle \widehat{Q}_{s,ij}^\alpha(\underline{x})\,\hat{\rho}_s^\beta(\underline{y})\,\rangle_0\rangle_d &= \frac{1}{V^2}\sum_{\underline{q}\underline{q}'} e^{i(\underline{q}\cdot\underline{x}+\underline{q}'\cdot\underline{y})}\sum_s \rho_s \int_0^{L_s} dl \int_0^{L_s} dl'\,\sigma_s^\alpha(l)\,\sigma_s^\beta(l') \times \\
&\quad \times \langle\, (u_i^s(l)\,u_j^s(l)-\tfrac{1}{3}\delta_{ij})\,e^{-i(\underline{q}\cdot\underline{R}^s(l)+\underline{q}'\cdot\underline{R}^s(l'))}\,\rangle_0 \\
&\equiv \frac{1}{V^2}\sum_{\underline{q}\underline{q}'} e^{i(\underline{q}\cdot\underline{x}+\underline{q}'\cdot\underline{y})}\sum_s \rho_s A_{s,ij}^{KJ,\alpha\beta}(\underline{q},\underline{q}') \\
&\equiv \frac{1}{V^2}\sum_{\underline{q}\underline{q}'} e^{i(\underline{q}\cdot\underline{x}+\underline{q}'\cdot\underline{y})}\,A_{ij}^{KJ,\alpha\beta}(\underline{q},\underline{q}')
\end{aligned}
\tag{2.51}
$$

and

$$
\begin{aligned}
\langle\langle \widehat{Q}_{s,ij}^\alpha(\underline{x})\,\widehat{Q}_{s,i'j'}^\beta(\underline{y})\,\rangle_0\rangle_d &= \frac{1}{V^2}\sum_{\underline{q}\underline{q}'} e^{i(\underline{q}\cdot\underline{x}+\underline{q}'\cdot\underline{y})}\sum_s \rho_s \int_0^{L_s} dl \int_0^{L_s} dl'\,\sigma_s^\alpha(l)\,\sigma_s^\beta(l') \times \\
&\quad \times \langle\, (u_i^s(l)\,u_j^s(l)-\tfrac{1}{3}\delta_{ij})\,(u_{i'}^s(l')\,u_{j'}^s(l')-\tfrac{1}{3}\delta_{i'j'})\,e^{-i(\underline{q}\cdot\underline{R}^s(l)+\underline{q}'\cdot\underline{R}^s(l'))}\,\rangle_0 \\
&\equiv \frac{1}{V^2}\sum_{\underline{q}\underline{q}'} e^{i(\underline{q}\cdot\underline{x}+\underline{q}'\cdot\underline{y})}\sum_s \rho_s A_{s,iji'j'}^{KK,\alpha\beta}(\underline{q},\underline{q}') \\
&\equiv \frac{1}{V^2}\sum_{\underline{q}\underline{q}'} e^{i(\underline{q}\cdot\underline{x}+\underline{q}'\cdot\underline{y})}\,A_{iji'j'}^{KK,\alpha\beta}(\underline{q},\underline{q}').
\end{aligned}
\tag{2.52}
$$

The functions $A^{JJ,\alpha\beta}(\underline{q},\underline{q}')$, $A_{ij}^{KJ,\alpha\beta}(\underline{q},\underline{q}')$ and $A_{iji'j'}^{KK,\alpha\beta}(\underline{q},\underline{q}')$ that appear in respectively (2.50), (2.51) and (2.52) will be calculated in appendix A. Now, with the help of these

last three expressions this second-order contribution to $\frac{\Lambda}{V}$ becomes,

$$
\begin{aligned}
\frac{1}{2} \langle\langle \hat{\Omega}^2 \rangle_0\rangle_d \;\equiv\; & \frac{(-i)^2}{2V^2} \sum_{\alpha\beta} \sum_{\underline{q}_1,\underline{q}_2} \{ A^{JJ,\alpha\beta}(\underline{q}_1,\underline{q}_2)\, \tilde{J}^\alpha(\underline{q}_1)\, \tilde{J}^\beta(\underline{q}_2) + \\
& + 2 \sum_{ij} A^{KJ,\alpha\beta}_{ij}(\underline{q}_1,\underline{q}_2)\, K^\alpha_{ij}(\underline{q}_1)\, \tilde{J}^\beta(\underline{q}_2) + \\
& + \sum_{i_1 j_1} \sum_{i_2 j_2} A^{KK,\alpha\beta}_{i_1 j_1 i_2 j_2}(\underline{q}_1,\underline{q}_2)\, K^\alpha_{i_1 j_1}(\underline{q}_1)\, K^\beta_{i_2 j_2}(\underline{q}_2) \}, \qquad (2.53)
\end{aligned}
$$

where $f(\underline{q})$ denotes the Fourier-transform of $f(\underline{x})$, i.e.,

$$
f(\underline{q}) \equiv \int_V d^3 x \, e^{i\,\underline{q}\cdot\underline{x}} f(\underline{x}). \qquad (2.54)
$$

As the orientational Green's function G (2.34) involves a functional integration over the J fields, while $\frac{1}{2}\langle\langle \hat{\Omega}^2 \rangle_0\rangle_d$ involves the $\tilde{J}$ fields, we need to transform $\frac{1}{2}\langle\langle \hat{\Omega}^2 \rangle_0\rangle_d$ to the former kind of fields. This is most easily done by recalling that from the definition of $\tilde{J}^\alpha(\underline{x})$ (2.36), it follows that,

$$
\tilde{J}^\alpha(\underline{q}) \equiv J^\alpha(\underline{q}) - J^\alpha(\underline{0})\,\delta(\underline{q}). \qquad (2.55)
$$

In other words $\tilde{J}^\alpha(\underline{q}) = J^\alpha(\underline{q})$ for $\underline{q} \neq \underline{0}$ and if $\underline{q} = 0$ then $\tilde{J}^\alpha(\underline{0}) = 0$. Therefore as the sums over the $\underline{q}$'s belonging to the fields $\tilde{J}^\alpha(\underline{q})$ in Eq. (2.53) are anyhow restricted to non-zero $\underline{q}$'s, we can simply change the $\tilde{J}$'s herein to J's. Symbolically we now can write the expression for $\frac{1}{2}\langle\langle \hat{\Omega}^2 \rangle_0\rangle_d$ as,

$$
\frac{1}{2} \langle\langle \hat{\Omega}^2 \rangle_0\rangle_d = -\frac{1}{2} [A^{ab} v_a v_b + 2 A^{\overline{a}b} w_{\overline{a}} v_b + A^{\overline{a}\overline{b}} w_{\overline{a}} w_{\overline{b}}], \qquad (2.56)
$$

where we have introduced two sets of *composite labels* $a \equiv (\underline{q} \neq \underline{0}, \alpha)$, $b \equiv (\underline{q} \neq \underline{0}, \beta)$ etc. and $\overline{a} \equiv (\underline{q}, ij, \alpha)$, $\overline{b} \equiv (\underline{q}', i'j', \beta)$ etc. and where $v_a \equiv \frac{J^\alpha(\underline{q})}{V}$ and $w_{\overline{a}} \equiv \frac{K^\alpha_{ij}(\underline{q})}{V}$. Furthermore the Einstein summation convention has been used. The third and fourth

order contributions of $\frac{\Lambda}{V}$ are given by,

$$\frac{1}{6} \langle\langle \hat{\Omega}^3 \rangle_0 \rangle_d = +\frac{i}{6} [B^{abc} v_a v_b v_c + 3 B^{\bar{a}bc} w_{\bar{a}} v_b v_c +$$

$$+3 B^{\bar{a}\bar{b}c} w_{\bar{a}} w_{\bar{b}} v_c + B^{\bar{a}\bar{b}\bar{c}} w_{\bar{a}} w_{\bar{b}} w_{\bar{c}}] \tag{2.57}$$

and

$$\frac{1}{24} \langle\langle \hat{\Omega}^4 \rangle_0 \rangle_d - \frac{1}{8} \langle\langle \hat{\Omega}^2 \rangle_0^2 \rangle_d = +\frac{1}{24} [C^{abcd} v_a v_b v_c v_d +$$

$$+4 C^{\bar{a}bcd} w_{\bar{a}} v_b v_c v_d + 6 C^{\bar{a}\bar{b}cd} w_{\bar{a}} w_{\bar{b}} v_c v_d +$$

$$+4 C^{\bar{a}\bar{b}\bar{c}d} w_{\bar{a}} w_{\bar{b}} w_{\bar{c}} v_d + C^{\bar{a}\bar{b}\bar{c}\bar{d}} w_{\bar{a}} w_{\bar{b}} w_{\bar{c}} w_{\bar{d}}]. \tag{2.58}$$

In the second order contribution (2.56) the A's are second order single-chain correlation functions. These are defined in Eq. (2.50), (2.51) and (2.52). In the third order term the B's are third order single-chain correlation functions defined in a similar way. The C's in Eq. (2.58) contain a regular and a non-local contribution, $C^{abcd} = C_{reg}^{abcd} - C_{nl}^{abcd}$, $C^{\bar{a}bcd} = C_{reg}^{\bar{a}bcd} - C_{nl}^{\bar{a}bcd}$, etc. The regular contributions are fourth order single-chain correlation functions which are similar to the A's and B's. The non-local correlation functions of a chain of kind s follow from the term $-\frac{1}{8} \langle\langle \hat{\Omega}^2 \rangle_0^2 \rangle_d$ and are given by,

$$C_{nl,s}^{abcd} = A_s^{ab} A_s^{cd} + A_s^{ac} A_s^{bd} + A_s^{ad} A_s^{bc},$$

$$C_{nl,s}^{\bar{a}bcd} = 4A_s^{\bar{a}b} A_s^{cd} + 4A_s^{\bar{a}c} A_s^{bd} + 4A_s^{\bar{a}d} A_s^{bc},$$

$$C_{nl,s}^{\bar{a}\bar{b}cd} = 6A_s^{\bar{a}\bar{b}} A_s^{cd} + 6A_s^{\bar{a}c} A_s^{\bar{b}d} + 6A_s^{\bar{a}d} A_s^{\bar{b}c},$$

$$C_{nl,s}^{\bar{a}\bar{b}\bar{c}d} = 4A_s^{\bar{a}\bar{b}} A_s^{\bar{c}d} + 4A_s^{\bar{a}\bar{c}} A_s^{\bar{b}d} + 4A_s^{\bar{a}d} A_s^{\bar{b}\bar{c}}$$

and

$$C_{nl,s}^{\bar{a}\bar{b}\bar{c}\bar{d}} = A_s^{\bar{a}\bar{b}} A_s^{\bar{c}\bar{d}} + A_s^{\bar{a}\bar{c}} A_s^{\bar{b}\bar{d}} + A_s^{\bar{a}\bar{d}} A_s^{\bar{b}\bar{c}}. \tag{2.59}$$

The quenched average is not taken over the A's separately, but over the terms in the non-local correlation functions, i.e. $\sum_s \rho_s A_s^{ab} A_s^{cd}$ etc. These contributions to the fourth-order coefficients are the so-called *non-local terms*, which are typical for polydisperse copolymer melts and which vanish once the number of segment types M exceeds the number of chain types in the system [27].

By Fourier-transforming all the integrals involving the ψ fields and the $\underline{Q}$ fields and making use of the fact that according to the definition of $\tilde{\chi}_{\alpha\beta}$ (see (2.16)) $\tilde{\tilde{\chi}}_{MM} \equiv$

0, the partition function Z (2.37) can be written as,

$$Z \equiv \prod_{c}{}' \prod_{\bar{d}} \int D\Psi^c \int D\Upsilon^{\bar{d}}\, e^{V\{\tilde{\chi}_{ab}\Psi^a\Psi^b + \frac{1}{2}\omega_{\bar{a}\bar{b}}\Upsilon^{\bar{a}}\Upsilon^{\bar{b}}\}}\, \widetilde{Z}[\underline{\Psi}, \overline{\Upsilon}] \tag{2.60}$$

with $\tilde{\chi}_{ab} \equiv \tilde{\chi}_{\alpha\beta}\,\delta(\underline{q}_1 + \underline{q}_2)$, $\omega_{\bar{a}\bar{b}} \equiv \omega_{\alpha\beta}\,|2\delta_{ii'}\delta_{jj'} - \delta_{ij}\delta_{i'j'}|\,\delta(\underline{q}_1 + \underline{q}_2)$, $\Psi^a \equiv \frac{\psi^\alpha(-\underline{q})}{V}$, $\Upsilon^{\bar{a}} \equiv \frac{Q_{ij}^{\alpha}(-\underline{q})}{V}$ and

$$\widetilde{Z}[\underline{\Psi}, \overline{\Upsilon}] \equiv \prod_g \prod_{\bar{h}} \int Dv_g \int Dw_{\bar{h}}\, e^{V\{i\,[v_a\Psi^a + w_{\bar{a}}\Upsilon^{\bar{a}}] + \frac{\Lambda[\underline{v},\overline{w}]}{V}\}}, \tag{2.61}$$

where $\underline{\Psi} \equiv \{\Psi^a\}_a$ and $\overline{\Upsilon} \equiv \{\Upsilon^{\bar{a}}\}_{\bar{a}}$. For large values of the system's volume V, $\widetilde{Z}[\underline{\Psi}, \overline{\Upsilon}]$ can be evaluated with the well-known *saddle-point method*, i.e. approximating $\widetilde{Z}[\underline{\Psi}, \overline{\Upsilon}]$ by,

$$\widetilde{Z}[\underline{\Psi}, \overline{\Upsilon}] \simeq e^{V\,\Phi[\underline{\Psi}, \overline{\Upsilon}]}, \tag{2.62}$$

where $\Phi[\underline{\Psi}, \overline{\Upsilon}]$ is the stationary value of $i\,[v_a\Psi^a + w_{\bar{a}}\Upsilon^{\bar{a}}] + \frac{\Lambda[\underline{v},\overline{w}]}{V}$ with respect to the set of v's and w's for which its absolute value is the smallest. This stationary point is a solution of the following set of equations,

$$
\begin{aligned}
i\,\Psi^a =~& A^{ab}\,v_b + A^{a\bar{b}}\,w_{\bar{b}} - \frac{i}{2}\,B^{abc}\,v_b v_c - i\,B^{a\bar{b}c}\,w_{\bar{b}}v_c - \frac{i}{2}\,B^{a\bar{b}\bar{c}}\,w_{\bar{b}}w_{\bar{c}} + \\
& -\frac{1}{6}\,C^{abcd}\,v_b v_c v_d - \frac{1}{2}\,C^{a\bar{b}cd}\,w_{\bar{b}}v_c v_d - \frac{1}{2}\,C^{a\bar{b}\bar{c}d}\,w_{\bar{b}}w_{\bar{c}}v_d - \frac{1}{6}\,C^{a\bar{b}\bar{c}\bar{d}}\,w_{\bar{b}}w_{\bar{c}}w_{\bar{d}} \\
& ,\forall a
\end{aligned}
\tag{2.63}
$$

and

$$
\begin{aligned}
i\,\Upsilon^{\bar{a}} =~& A^{\bar{a}\bar{b}}\,w_{\bar{b}} + A^{\bar{a}b}\,v_b - \frac{i}{2}\,B^{\bar{a}bc}\,v_b v_c - i\,B^{\bar{a}\bar{b}c}\,w_{\bar{b}}v_c - \frac{i}{2}\,B^{\bar{a}\bar{b}\bar{c}}\,w_{\bar{b}}w_{\bar{c}} + \\
& -\frac{1}{6}\,C^{\bar{a}bcd}\,v_b v_c v_d - \frac{1}{2}\,C^{\bar{a}\bar{b}cd}\,w_{\bar{b}}v_c v_d - \frac{1}{2}\,C^{\bar{a}\bar{b}\bar{c}d}\,w_{\bar{b}}w_{\bar{c}}v_d - \frac{1}{6}\,C^{\bar{a}\bar{b}\bar{c}\bar{d}}\,w_{\bar{b}}w_{\bar{c}}w_{\bar{d}} \\
& ,\forall\,\bar{a}.
\end{aligned}
\tag{2.64}
$$

As we ultimately want to arrive at a Landau free energy as an expansion up-to fourth order in the Ψ^a - and the $\Upsilon^{\bar{a}}$ fields, we only need to solve these last two vector-equations iteratively for v_a and $w_{\bar{a}}$ up-to third order in the Ψ's and the Υ's. Now, the set of equations (2.63) and (2.64) can be written in the following matrix form,

$$
\begin{bmatrix} I_a^b & A_{ac}^{-1}A^{c\bar{b}} \\ A_{\overline{ac}}^{-1}A^{\bar{c}b} & I_{\bar{a}}^{\bar{b}} \end{bmatrix} \begin{bmatrix} v_b \\ w_{\bar{b}} \end{bmatrix} = \begin{bmatrix} iA_{ab}^{-1}\Psi^b + ... \\ iA_{\overline{ab}}^{-1}\Upsilon^{\bar{b}} + ... \end{bmatrix}.
\tag{2.65}
$$

where I_a^b and $I_{\bar{a}}^{\bar{b}}$ are appropriate "unit" matrices. By defining the matrix $\mathbf{T}$ to be the inverse of the matrix on the lhs of this equation, i.e.,

$$
\mathbf{T} \equiv \begin{bmatrix} I_a^b & A_{ac}^{-1}A^{c\bar{b}} \\ A_{\overline{ac}}^{-1}A^{\bar{c}b} & I_{\bar{a}}^{\bar{b}} \end{bmatrix}^{-1}
\tag{2.66}
$$

it follows that the "first order" solution is given by,

$$
\begin{bmatrix} v_b \\ w_{\bar{b}} \end{bmatrix} = \mathbf{T} \begin{bmatrix} iA_{ab}^{-1}\Psi^b \\ iA_{\overline{ab}}^{-1}\Upsilon^{\bar{b}} \end{bmatrix}.
\tag{2.67}
$$

The contributions of terms second order in the Ψ's and the Υ's are then obtained by substitution of this first order result in the terms which are quadratic in the v's and the w's on the rhs of (2.65) and so on. The final result for v_a and $w_{\bar{a}}$ up-to third order in the Ψ's and the Υ's can then be written as,

$$
v_a \equiv M_{ae}^{(1)}\Psi^e + M_{a\bar{e}}^{(1)}\Upsilon^{\bar{e}} + \frac{i}{2}M_{aef}^{(2)}\Psi^e\Psi^f + iM_{ae\bar{f}}^{(2)}\Psi^e\Upsilon^{\bar{f}} + \frac{i}{2}M_{a\bar{e}\bar{f}}^{(2)}\Upsilon^{\bar{e}}\Upsilon^{\bar{f}} +
$$
$$
\frac{1}{6}M_{aefg}^{(3)}\Psi^e\Psi^f\Psi^g + \frac{1}{2}M_{aef\bar{g}}^{(3)}\Psi^e\Psi^f\Upsilon^{\bar{g}} + \frac{1}{2}M_{ae\bar{f}\bar{g}}^{(3)}\Psi^e\Upsilon^{\bar{f}}\Upsilon^{\bar{g}} + \frac{1}{6}M_{a\bar{e}\bar{f}\bar{g}}^{(3)}\Upsilon^{\bar{e}}\Upsilon^{\bar{f}}\Upsilon^{\bar{g}}
\tag{2.68}
$$

and

$$
w_{\bar{a}} \equiv M_{\bar{a}e}^{(1)}\Psi^e + M_{\bar{a}\bar{e}}^{(1)}\Upsilon^{\bar{e}} + \frac{i}{2}M_{\bar{a}ef}^{(2)}\Psi^e\Psi^f + iM_{\bar{a}e\bar{f}}^{(2)}\Psi^e\Upsilon^{\bar{f}} + \frac{i}{2}M_{\bar{a}\bar{e}\bar{f}}^{(2)}\Upsilon^{\bar{e}}\Upsilon^{\bar{f}} +
$$
$$
\frac{1}{6}M_{\bar{a}efg}^{(3)}\Psi^e\Psi^f\Psi^g + \frac{1}{2}M_{\bar{a}ef\bar{g}}^{(3)}\Psi^e\Psi^f\Upsilon^{\bar{g}} + \frac{1}{2}M_{\bar{a}e\bar{f}\bar{g}}^{(3)}\Psi^e\Upsilon^{\bar{f}}\Upsilon^{\bar{g}} + \frac{1}{6}M_{\bar{a}\bar{e}\bar{f}\bar{g}}^{(3)}\Upsilon^{\bar{e}}\Upsilon^{\bar{f}}\Upsilon^{\bar{g}}
\tag{2.69}
$$

with the various coefficients given by,

$$M_{ae}^{(1)} \equiv i\, T_a^b A_{be}^{-1} \tag{2.70a}$$

$$M_{\bar{a}e}^{(1)} \equiv i\, T_{\bar{a}}^b A_{be}^{-1} \tag{2.70b}$$

$$M_{a\bar{e}}^{(1)} \equiv i\, T_a^{\bar{b}} A_{\bar{b}\bar{e}}^{-1} \tag{2.70c}$$

$$M_{\bar{a}\bar{e}}^{(1)} \equiv i\, T_{\bar{a}}^{\bar{b}} A_{\bar{b}\bar{e}}^{-1} \tag{2.70d}$$

and

$$M_{\widetilde{ae}\widetilde{f}}^{(2)} \equiv -i\, M_{\widetilde{ad}}^{(1)} B^{\widetilde{dbc}} M_{\widetilde{be}}^{(1)} M_{\widetilde{cf}}^{(1)} \tag{2.71}$$

and

$$M_{\widetilde{ae}\widetilde{fg}}^{(3)} \equiv -i M_{\widetilde{ah}}^{(1)} \left[C^{\widetilde{hbcd}} + 3i\, B^{\widetilde{hbk}} M_{kl}^{(1)} B^{\widetilde{lcd}} \right] M_{\widetilde{be}}^{(1)} M_{\widetilde{cf}}^{(1)} M_{\widetilde{dg}}^{(1)}. \tag{2.72}$$

In these last two expressions a label such as $\widetilde{a}$ denotes both a and $\bar{a}$ and if $\widetilde{a}$ appears both as a subscript and a superscript, such as in $x_{\widetilde{a}} y^{\widetilde{a}}$, then the following summation convention is implied $x_{\widetilde{a}} y^{\widetilde{a}} \equiv x_a y^a + x_{\bar{a}} y^{\bar{a}}$.

If we now substitute the $\Psi - \Upsilon$ expansions for v_a (2.2) and w_a (2.69) into $i\,[v_a \Psi^a + w_{\bar{a}} \Upsilon^{\bar{a}}] + \frac{\Lambda[v,\overline{w}]}{V}$ we obtain $\Phi[\underline{\Psi}, \overline{\Upsilon}]$ and hence the partition function,

$$Z \simeq \prod_c{}' \prod_{\bar{d}} \int D\Psi^c \int D\Upsilon^{\bar{d}}\, e^{V\{\widetilde{\chi}_{ab}\Psi^a\Psi^b + \frac{1}{2}\omega_{\bar{a}\bar{b}}\Upsilon^{\bar{a}}\Upsilon^{\bar{b}} + \Phi[\underline{\Psi}, \overline{\Upsilon}]\}}. \tag{2.73}$$

The Landau free energy, that is the free energy of the system within the *mean field approximation*, can be obtained by again applying the saddle-point method, but now to approximately evaluate this last set of functional integrals. If we write the result as,

$$Z \simeq e^{-F_L}, \tag{2.74}$$

then this Landau free energy F_L (in units of $k_B T$) is given by,

$$\begin{aligned}
\frac{F_L}{V} = \min_{\underline{\Psi}, \overline{\Upsilon}} \{ & (\Gamma_{ab}^{(2)} - \widetilde{\chi}_{ab})\Psi^a\Psi^b + 2\Gamma_{a\bar{b}}^{(2)}\Psi^a\Upsilon^{\bar{b}} + (\Gamma_{\bar{a}\bar{b}}^{(2)} - \frac{1}{2}\omega_{\bar{a}\bar{b}})\Upsilon^{\bar{a}}\Upsilon^{\bar{b}} + \\
& + \Gamma_{abc}^{(3)} \Psi^a\Psi^b\Psi^c + 3\Gamma_{ab\bar{c}}^{(3)} \Psi^a\Psi^b\Upsilon^{\bar{c}} + 3\Gamma_{a\bar{b}\bar{c}}^{(3)} \Psi^a\Upsilon^{\bar{b}}\Upsilon^{\bar{c}} + \Gamma_{\bar{a}\bar{b}\bar{c}}^{(3)} \Upsilon^{\bar{a}}\Upsilon^{\bar{b}}\Upsilon^{\bar{c}} + \\
& + \Gamma_{abcd}^{(4)} \Psi^a\Psi^b\Psi^c\Psi^d + 4\Gamma_{abc\bar{d}}^{(4)} \Psi^a\Psi^b\Psi^c\Upsilon^{\bar{d}} + 6\Gamma_{ab\bar{c}\bar{d}}^{(4)} \Psi^a\Psi^b\Upsilon^{\bar{c}}\Upsilon^{\bar{d}} + \\
& + 4\Gamma_{a\bar{b}\bar{c}\bar{d}}^{(4)} \Psi^a\Upsilon^{\bar{b}}\Upsilon^{\bar{c}}\Upsilon^{\bar{d}} + \Gamma_{\bar{a}\bar{b}\bar{c}\bar{d}}^{(4)} \Upsilon^{\bar{a}}\Upsilon^{\bar{b}}\Upsilon^{\bar{c}}\Upsilon^{\bar{d}} \}.
\end{aligned} \tag{2.75}$$

The coefficient functions (Γ's) in this expression are called *vertices* and are defined by,

$$\Gamma^{(2)}_{\widetilde{ab}} \equiv \frac{1}{2} \sum_{perm(\widetilde{a},\widetilde{b})} [-iM^{(1)}_{\widetilde{ab}} + \frac{1}{2} A^{\widetilde{cd}} M^{(1)}_{\widetilde{ca}} M^{(1)}_{\widetilde{db}}] \tag{2.76}$$

and

$$\Gamma^{(3)}_{\widetilde{abc}} \equiv \frac{1}{6} \sum_{perm(\widetilde{a},\widetilde{b},\widetilde{c})} [\frac{1}{2} M^{(2)}_{\widetilde{abc}} + \frac{i}{2} A^{\widetilde{de}} M^{(2)}_{\widetilde{dab}} M^{(1)}_{\widetilde{ec}} - \frac{i}{6} B^{\widetilde{def}} M^{(1)}_{\widetilde{da}} M^{(1)}_{\widetilde{eb}} M^{(1)}_{\widetilde{fc}}] \tag{2.77}$$

and finally

$$\Gamma^{(4)}_{\widetilde{abcd}} \equiv \frac{1}{24} \sum_{perm(\widetilde{a},\widetilde{b},\widetilde{c},\widetilde{d})} [-\frac{i}{6} M^{(3)}_{\widetilde{abcd}} + \frac{1}{6} A^{\widetilde{ef}} M^{(3)}_{\widetilde{eabc}} M^{(1)}_{\widetilde{fd}} - \frac{1}{8} A^{\widetilde{ef}} M^{(2)}_{\widetilde{eab}} M^{(2)}_{\widetilde{fcd}} +$$
$$\frac{1}{4} B^{\widetilde{efg}} M^{(2)}_{\widetilde{eab}} M^{(1)}_{\widetilde{fc}} M^{(1)}_{\widetilde{gd}} - \frac{1}{24} C^{\widetilde{efgh}} M^{(1)}_{\widetilde{ea}} M^{(1)}_{\widetilde{fb}} M^{(1)}_{\widetilde{gc}} M^{(1)}_{\widetilde{hd}}]. \tag{2.78}$$

The fourth order vertex is symmetric with respect to a permutation of the indices $\widetilde{a}, \widetilde{b}, \widetilde{c}$ and $\widetilde{d}$. The second and third order vertex contain the same kind of symmetry. The terms in the vertices are not always permutational symmetric. For example if $\widetilde{a} = a$ and $\widetilde{b} = \overline{b}$ the vertex $\Gamma^{(2)}_{\underline{ab}}$ contains the terms $-iM^{(1)}_{\underline{ab}}$ and $-iM^{(1)}_{\underline{ba}}$. From Eq.(2.70b) and (2.70c) it is clear that in general $M^{(1)}_{\underline{ab}} \neq M^{(1)}_{\underline{ba}}$.

2.3 Concluding remarks

In this chapter we derived an expression of the Landau free energy of a general melt of semi-flexible multi-block copolymers. The Landau free energy is written as a power series expansion of the scalar order-parameter Ψ^a and the orientation tensor $\Upsilon^{\overline{a}}$. The orientation tensor $\Upsilon^{\overline{a}}$ has been taken into account, because the blocks have a certain persistence length λ_α. The stiffness of the chains is described by means of the Bawendi-Freed model [16].

Chapter 3

Phase behaviour of a melt of monodisperse semi-flexible diblock copolymers

3.1 Introduction

In the past decades much attention has been paid to the phase behaviour of melts of diblock copolymers and other kinds of block copolymers. This phase behaviour will be influenced by both the bending stiffness of blocks and the polydispersity in block length. In the literature these factors are not always included in the theoretical description of block copolymers, but in reality they may play an important role. In this chapter only the bending stiffness is considered.

In [23] a melt of diblock copolymers is investigated which is an extension of [10]. In [10] only semi-flexibility is taken into account, but in [23] polydispersity is also included. The polydispersity is described by the Schultz-Zimm distribution and other distributions. The structure factor and spinodal $\chi_s L$ are calculated for both a polydisperse and a monodisperse diblock melt to see the differences. It was found that the spinodal $\chi_s L$ increases if one or both blocks are polydisperse. So here polydispersity counteracts microphase separation.

In [9–13] a diblock melt is considered in which polydispersity is ignored. In [9, 13] a rod-coil system is investigated and in [10–12] the diblock is semi-flexible. In chapter 2 a general theory is developed which is applied to a monodisperse semi-flexible diblock melt in this chapter. The spinodals $\chi_s L$ and $\omega_s L$ are calculated in

section 3.5. The results in this section are compared to the results of [9–13].

The system described in chapter 2 is very general. Both polydispersity and semi-flexibility are included. In that chapter the Landau free energy is derived for a melt of semi-flexible multi-block copolymers. The incompatibility of chemically different blocks is described by the Flory-Huggins interaction. If this interaction is strong enough microphase separation occurs. Besides the Flory-Huggins interaction another interaction is included which is the Maier-Saupe interaction. If it is strong enough nematic ordering takes place, but it can also stimulate microphase separation. By means of the expression of the Landau free energy the spinodals $\chi_s L$ and $\omega_s L$ are calculated numerically for a melt of monodisperse semi-flexible diblock copolymers in section 3.5. In section 3.5 it has not been investigated which structures, for example the bcc phase, are formed when microphase separation has become possible. The complete phase diagram is calculated in section 3.6. This is a generalisation of the system investigated by Leibler in [5]. In that paper the phase diagram is calculated for a melt of monodisperse diblock copolymers which are totally flexible. The Landau free energy of this system is written as a power series expansion of only the scalar order-parameter. In our system besides a scalar order-parameter we also have to take into account an orientation tensor because of the persistence length of A- and B-blocks. The orientation of chains is induced by the Maier-Saupe interaction. Without this interaction local and global alignment may also be possible if there is microphase separation. In [5] it is justified to neglect a possible orientation, because the diblock chains are totally flexible.

In [32] the system of Leibler is extended by including corrections due to composition fluctuations. In this thesis these corrections are ignored. According to [32] the fluctuation corrections disappear when the chain length becomes infinite. In [22] the system is further extended by including polydispersity. In this paper the scattering function and spinodal $\chi_s L$ are calculated in which the polydispersity is modelled by the Schultz-Zimm distribution. In contrast to [23] the spinodal $\chi_s L$ is lowered in [22] when the degree of polydispersity increases. The phase diagram has also been determined for different degrees of polydispersity. If there is no polydispersity it appeared that the phase diagram is in agreement with the results calculated in [32].

In [9] Reenders calculated the complete phase diagram of a melt of monodisperse rod-coil diblocks. A possible orientation of the flexible part is neglected. Reenders made the ansatz that there is only global nematic ordering. A contribution of a local alignment is not taken into account. A consequence of this ansatz is that a possible orientation is negligibly small if $\chi > \chi_s$ and $\omega = 0$. Therefore the orientation tensor

is neglected in the part of the phase diagram in which $\omega < \omega_s$. If $\omega > \omega_s$ and $\chi > \chi_s$ the smectic state becomes possible in which only a global orientation is taken into account.

However, in [12, 13] and this thesis a possible local alignment has not been excluded. In this way the orientation plays a more important role in the phase behaviour. In the numerical results in section 3.6 a smectic A- and -C state is also found if there is no Maier-Saupe interaction. This interaction does not only influence the nematic and smectic part of the phase diagram but also changes the domain of the hexagonal and bcc phase. In section 3.3 it is explained how such a local orientation can be described in a smectic phase and in a more complicated microphase such as the hexagonal phase. In section 3.2 the general Landau free energy derived in chapter 2 is applied to a melt of monodisperse semi-flexible diblock copolymers. The minimum of the free energy with respect to the order-parameters is determined analytically.

3.2 Minimizing the Landau free energy of a melt of monodisperse semi-flexible diblock copolymers

For a melt of polydisperse multiblock copolymers the expression of the Landau free energy has been derived in the previous chapter. In this section the expression of a this general melt is applied to a melt of monodisperse diblocks. The minimum with respect to the order parameters is determined analytically. In the next section it is explained how the orientation of A- and B-blocks can be described in several classical microphase structures.

Below the spinodal $\chi < \chi_s$ the melt is in the isotropic state. When χ is increasing a phase transition is taking place at the the the spinodal. A certain microphase is formed when χ is further increased. In a microphase structure besides a scalar order-parameter there is also a certain amount of nematic ordering possible because of the bending stiffness of the chains. In the first harmonics approximation the Fourier transformed scalar order-parameter Ψ^a and the orientation tensor $\Upsilon^{\bar{a}} = \frac{Q_{\underline{\alpha}}^{\mu\nu}(-\underline{q})}{V}$ have the following form according to [12],

$$\Psi^a = \Psi^A(\underline{q}) = -\Psi^B(\underline{q}) = \Psi(\underline{q}) = \Psi \sum_{\underline{q}' \in H} \exp(i\varphi_{\underline{q}'}) \delta(\underline{q} - \underline{q}') \qquad (3.1)$$

and

$$\Upsilon^{\bar{a}} = \Upsilon^{\mu\nu}_\alpha(\underline{q}) = \Upsilon_\alpha(n^\mu_\alpha n^\nu_\alpha - \frac{1}{3}\delta^{\mu\nu}) \sum_{\underline{q}' \in H} \exp(i\varphi_{\underline{q}'})\delta(\underline{q} - \underline{q}') +$$

$$\Upsilon^0_\alpha(n^\mu_\alpha n^\nu_\alpha - \frac{1}{3}\delta^{\mu\nu})\delta(\underline{q}). \tag{3.2}$$

Besides a local orientation a possible contribution of a global orientation is also taken into account in Eq. (3.2). In $\Upsilon^{\bar{a}}$ the vector $\underline{n}^{\mu 1}$ is a unit vector which is the director of the orientation of block α. If the orientation of the A- and B-block are different each semi-flexible chain must be bent over a certain angle. In the derivation of the single-chain correlation function in Appendix A the tangent vectors of the A- and B-block at the connection point have been taken equal. So the A- and B-block cannot be rotated freely with respect to each other. Therefore it is energetically not favourable that there are two different orientations. It is then justified to assume that in Eq.(3.2) the directors n^μ_A and n^μ_B are equal, $n^\mu_A = n^\mu_B = n^\mu$.

In the nematic and smectic state the first harmonics approximation according to Eq. (3.2) can be applied, but it is not possible in the hexagonal and bcc structure. The orientation of nematic and smectic state is described by a constant director $\underline{n}_\alpha(\underline{x}) = \underline{n}$ in Eq. (3.18), but in the hexagonal and bcc state it must be spatially dependent. In the next section this spatially dependent director $\underline{n}_\alpha(\underline{x})$ is chosen such that the orientation tensors $\underline{\underline{Q}}^\alpha_{hex}(\underline{q})$ and $\underline{\underline{Q}}^\alpha_{bcc}(\underline{q})$ can be written as a linear combination of smectic-A states with different directors $\underline{n}_m$,

$$\underline{\underline{Q}}^\alpha_{hex}(\underline{q}) = \frac{1}{3}\sum_{m=1}^{3}\underline{\underline{Q}}^\alpha_{smecA}(\underline{q},\underline{n}_m) \tag{3.3}$$

and

$$\underline{\underline{Q}}^\alpha_{bcc}(\underline{q}) = \frac{1}{6}\sum_{m=1}^{6}\underline{\underline{Q}}^\alpha_{smecA}(\underline{q},\underline{n}_m), \tag{3.4}$$

in which $\Upsilon^{\bar{a}} = \frac{Q^{\mu\nu}_\alpha(-q)}{V}$. In this way the orientation tensor is invariant under the symmetry operations belonging to the corresponding microphase structure.

In the Landau free energy,

$$
\begin{aligned}
\frac{F_L}{V} = \min_{\underline{\Psi},\overline{\Upsilon}}\{ & (\Gamma^{(2)}_{ab} - \widetilde{\chi}_{ab})\Psi^a\Psi^b + 2\Gamma^{(2)}_{a\overline{b}}\Psi^a\Upsilon^{\overline{b}} + \\
& (\Gamma^{(2)}_{\overline{ab}} - \frac{1}{2}\omega_{\overline{ab}})\Upsilon^{\overline{a}}\Upsilon^{\overline{b}} - \frac{1}{3}\omega_{ab}\Upsilon^{a,ij}\delta_{ij}(\Psi^b + f^b) + \\
& \Gamma^{(3)}_{abc}\Psi^a\Psi^b\Psi^c + 3\Gamma^{(3)}_{ab\overline{c}}\Psi^a\Psi^b\Upsilon^{\overline{c}} + 3\Gamma^{(3)}_{a\overline{bc}}\Psi^a\Upsilon^{\overline{b}}\Upsilon^{\overline{c}} + \Gamma^{(3)}_{\overline{abc}}\Upsilon^{\overline{a}}\Upsilon^{\overline{b}}\Upsilon^{\overline{c}} + \\
& \Gamma^{(4)}_{abcd}\Psi^a\Psi^b\Psi^c\Psi^d + 4\Gamma^{(4)}_{abc\overline{d}}\Psi^a\Psi^b\Psi^c\Upsilon^{\overline{d}} + 6\Gamma^{(4)}_{ab\overline{cd}}\Psi^a\Psi^b\Upsilon^{\overline{c}}\Upsilon^{\overline{d}} + \\
& 4\Gamma^{(4)}_{a\overline{bcd}}\Psi^a\Upsilon^{\overline{b}}\Upsilon^{\overline{c}}\Upsilon^{\overline{d}} + \Gamma^{(4)}_{\overline{abcd}}\Upsilon^{\overline{a}}\Upsilon^{\overline{b}}\Upsilon^{\overline{c}}\Upsilon^{\overline{d}}\},
\end{aligned}
\tag{3.5}
$$

the first harmonics approximation according to Eq. (3.1) and (3.2) is applied to the order-parameters. The free energy is written as a power series expansion of the vector $(\Psi, \Upsilon_A, \Upsilon_B, \Upsilon_A^0, \Upsilon_B^0)$. In the second order term $\frac{F_L^{(2)}}{V}$ there is no coupling between the global and local order-parameters so that it can be written in the following form,

$$
\begin{aligned}
\frac{F_L^{(2)}}{V} = \begin{bmatrix} \Psi & \Upsilon_A & \Upsilon_B \end{bmatrix} & \begin{bmatrix} \widetilde{\Gamma}^{(2)} - \chi & \widetilde{\Gamma}^{(2)}_A & \widetilde{\Gamma}^{(2)}_B \\ \widetilde{\Gamma}^{(2)}_A & \widetilde{\Gamma}^{(2)}_{AA} - \frac{1}{3}\omega_{AA} & \widetilde{\Gamma}^{(2)}_{AB} - \frac{1}{3}\omega_{AB} \\ \widetilde{\Gamma}^{(2)}_B & \widetilde{\Gamma}^{(2)}_{AB} - \frac{1}{3}\omega_{AB} & \widetilde{\Gamma}^{(2)}_{BB} - \frac{1}{3}\omega_{BB} \end{bmatrix} \begin{bmatrix} \Psi \\ \Upsilon_A \\ \Upsilon_B \end{bmatrix} + \\
\begin{bmatrix} \Upsilon_A^0 & \Upsilon_B^0 \end{bmatrix} & \begin{bmatrix} \widetilde{\Gamma}^{(2)}_{AA,00} - \frac{1}{3}\omega_{AA} & \widetilde{\Gamma}^{(2)}_{AB,00} - \frac{1}{3}\omega_{AB} \\ \widetilde{\Gamma}^{(2)}_{AB,00} - \frac{1}{3}\omega_{AB} & \widetilde{\Gamma}^{(2)}_{BB,00} - \frac{1}{3}\omega_{BB} \end{bmatrix} \begin{bmatrix} \Upsilon_A^0 \\ \Upsilon_B^0 \end{bmatrix},
\end{aligned}
\tag{3.6}
$$

in which the following notation

$$
\widetilde{\Gamma}^{(2)} = \Gamma^{(2)}_{ab}S^a S^b, \ \widetilde{\Gamma}^{(2)}_\alpha = \Gamma^{(2)}_{a\overline{b}}S^a d_\alpha^{\overline{b}}
$$

$$
\widetilde{\Gamma}^{(2)}_{\alpha\beta} = \Gamma^{(2)}_{\overline{ab}}d_\alpha^{\overline{a}}d_\beta^{\overline{b}} \text{ and } \widetilde{\Gamma}^{(2)}_{\alpha\beta,00} = \Gamma^{(2)}_{\overline{ab}}d_{\alpha,0}^{\overline{a}}d_{\beta,0}^{\overline{b}},
\tag{3.7}
$$

$$
S^a \equiv (1 - 2\delta_{\alpha B})\exp(i\varphi_{\underline{q}}) = \pm\exp(i\varphi_{\underline{q}}) \text{ and } a = \underline{q}, \alpha
\tag{3.8}
$$

and

$$
d_\alpha^{\overline{b}} = d_{\alpha,0}^{\overline{b}} \equiv (n_\beta^{\mu_2}n_\beta^{\nu_2} - \frac{1}{3}\delta^{\mu_2\nu_2})\exp(i\varphi_{\underline{q}})\delta_{\alpha\beta} \text{ and } \overline{b} = \underline{q}, \beta, \mu_2\nu_2
\tag{3.9}
$$

is used.

The 3×3 matrix in the second order term is symmetric, so it has real eigenvalues. In general the eigenvalues λ_1, λ_2 and λ_3 of this matrix are different. λ_1 is the lowest

eigenvalue which becomes negative if $\chi > \chi_s(q_*)$ or $\omega_{\alpha\beta} > \omega_{\alpha\beta,s} = \omega_{\alpha\beta,s}(q_*)$ in which the wave number q_* is nonzero. The wave number q_* in the 2×2 matrix in Eq. (3.6) is zero and the two eigenvalues of this matrix are denoted as λ_{10} and λ_{20}. The smallest eigenvalue λ_{10} becomes negative if $\omega_{\alpha\beta} > \omega_{\alpha\beta,s} = \omega_{\alpha\beta,s}(q_* = 0)$. Exactly at $\chi = \chi_s$ the eigenvalue λ_1 is zero so that the determinant of 3×3 matrix in Eq. (3.6) is zero. From this determinant the spinodal χ_s can be easily derived which is given by,

$$\chi_s = \min_{q_*}\{\widetilde{\Gamma}^{(2)} - \frac{(\widetilde{\Gamma}_B^{(2)})^2(\widetilde{\Gamma}_{AA}^{(2)} - \frac{1}{3}\omega_{AA}) + (\widetilde{\Gamma}_A^{(2)})^2(\widetilde{\Gamma}_{BB}^{(2)} - \frac{1}{3}\omega_{BB}) - 2\widetilde{\Gamma}_A^{(2)}\widetilde{\Gamma}_B^{(2)}(\widetilde{\Gamma}_{AB}^{(2)} - \frac{1}{3}\omega_{AB})}{(\widetilde{\Gamma}_{AA}^{(2)} - \frac{1}{3}\omega_{AA})(\widetilde{\Gamma}_{BB}^{(2)} - \frac{1}{3}\omega_{BB}) - (\widetilde{\Gamma}_{AB}^{(2)} - \frac{1}{3}\omega_{AB})^2}\}.$$

(3.10)

This expression of χ_s can also be used to calculate the spinodals $\omega_{\alpha\beta,s}(q_*)$ in which the wave number q_* is the same as in $\chi_s = \chi_s(q_*)$. In the same way the 2×2 matrix in Eq. (3.6) is used to determine the spinodals $\omega_{\alpha\beta,s} = \omega_{\alpha\beta,s}(q_* = 0)$.

In this section we consider the free energy of a microphase in which λ_1 is negative and the other eigenvalues λ_2, λ_3, λ_{10} and λ_{20} are still positive. Then the primary eigenvector $\underline{x}_1$ which belongs to λ_1 is nonzero at the minimum of the free energy. The secondary eigenvectors $\underline{x}_2$, $\underline{x}_3$, $\underline{x}_{10}$ and $\underline{x}_{20}$ belonging to λ_2, λ_3, λ_{10} and λ_{20}, respectively, may also become nonzero. These vectors are induced by third and higher order terms in the free energy in which $\underline{x}_1$ is coupled to the secondary eigenvectors. The directions of the eigenvectors can be determined by the 3×3 matrix and 2×2 matrix in Eq. (3.6). If we know the directions of $\underline{x}_1$, $\underline{x}_2$, $\underline{x}_3$, $\underline{x}_{10}$ and $\underline{x}_{20}$ it is only necessary to write the Landau free energy as a power series expansion in $x_1 = \pm|\underline{x}_1|$, $x_2 = \pm|\underline{x}_2|$, $x_3 = \pm|\underline{x}_3|$, $x_{10} = \pm|\underline{x}_{10}|$ and $x_{20} = \pm|\underline{x}_{20}|$,

$$\frac{F_L}{V} = \min_{\{x_1,x_2,x_3,x_{10},x_{20}\}}\{\lambda_1 x_1^2 + \lambda_2 x_2^2 + \lambda_3 x_3^2 + \lambda_{10} x_{10}^2 + \lambda_{20} x_{20}^2 +$$
$$C_{111}^{(3)} x_1^3 + C_{112}^{(3)} x_1^2 x_2 + ... C_{1111}^{(4)} x_1^4 + ...\}.$$

(3.11)

In the power series expansion fifth and higher order terms are not taken into account. The normalized eigenvectors $\widehat{\underline{x}}_n = (\widehat{\Psi}_n, \widehat{\Upsilon}_n^A, \widehat{\Upsilon}_n^B)$ with $n = 1, 2, 3, 10$ or 20 are used to determine the C−coefficients in Eq. (3.11). For example $C_{112}^{(3)}$ and $C_{11,20}^{(3)}$ are given by

$$C_{112}^{(3)} = \widetilde{\Gamma}_{\alpha\beta\gamma}^{(3)} \widehat{\Upsilon}_1^\alpha \widehat{\Upsilon}_1^\beta \widehat{\Upsilon}_2^\gamma + \widetilde{\Gamma}_{\alpha\beta}^{(3)} \widehat{\Upsilon}_1^\alpha \widehat{\Upsilon}_1^\beta \widehat{\Psi}_2 + 2\widetilde{\Gamma}_{\alpha\beta}^{(3)} \widehat{\Upsilon}_1^\alpha \widehat{\Upsilon}_2^\beta \widehat{\Psi}_1 +$$
$$\widetilde{\Gamma}_\alpha^{(3)} \widehat{\Upsilon}_2^\alpha \widehat{\Psi}_1^2 + 2\widetilde{\Gamma}_\alpha^{(3)} \widehat{\Upsilon}_1^\alpha \widehat{\Psi}_1 \widehat{\Psi}_2 + \widetilde{\Gamma}^{(3)} \widehat{\Psi}_1^2 \widehat{\Psi}_2$$

(3.12a)

and

$$C_{11,20}^{(3)} = \widetilde{\Gamma}_{\alpha\beta\gamma}^{(3)} \widehat{\Upsilon}_1^\alpha \widehat{\Upsilon}_1^\beta \widehat{\Upsilon}_{20}^\gamma + 2\widetilde{\Gamma}_{\alpha\beta}^{(3)} \widehat{\Upsilon}_1^\alpha \widehat{\Upsilon}_{20}^\beta \widehat{\Psi}_1 + \widetilde{\Gamma}_\alpha^{(3)} \widehat{\Upsilon}_{20}^\alpha \widehat{\Psi}_1^2.$$

(3.12b)

The third order $\widetilde{\Gamma}$'s in this example are expressed in a similar way as the second order $\widetilde{\Gamma}$'s in Eq. (3.6). The free energy has to be minimized with respect to x_1, x_2, x_3, x_{10} and x_{20}. First the free energy is minimized with respect to the secondary parameters x_2, x_3, x_{10} and x_{20} at an arbitrary value of the primary parameter x_1. In this way the secondary parameters can be expressed as a power series expansion in x_1. Substituting these expressions in Eq. (3.11) yields the free energy as a function of only one parameter x_1. The first order partial derivative of F_L with respect to x_2, x_3, x_{10} and x_{20} must be equal to zero which yields four equations with four unknowns,

$$\frac{1}{V}\frac{\partial F_L}{\partial x_n} = 2\lambda_n x_n + C_{11n}^{(3)}x_1^2 + ... = 0 \quad \text{with} \quad n = 2, 3, 10 \text{ or } 20. \tag{3.13}$$

In the solutions the third and higher order terms in x_1 can be neglected, because when these are substituted in F_L this yields fifth and higher order terms. These terms are not taken into account. The solutions x_n with $n = 2, 3, 10$ or 20 does not contain linear terms and are given by,

$$x_n = \frac{-C_{11n}^{(3)}x_1^2}{2\lambda_n} + O(x_1^3). \tag{3.14}$$

When x_2, x_3, x_{10} and x_{20} are substituted, $\frac{F_L}{V}$ becomes,

$$\frac{F_L}{V} = \min_{x_1}\{\lambda_1 x_1^2 + C_{111}^{(3)}x_1^3 + (C_{1111}^{(4)} - \sum_{n\neq 1}\frac{(C_{11n}^{(3)})^2}{4\lambda_n})x_1^4\} =$$
$$\min_{x_1}\{\lambda_1 x_1^2 + C_{111}^{(3)}x_1^3 + \widetilde{C}_{1111}^{(4)}x_1^4\}. \tag{3.15}$$

At the minimum x_1 is

$$x_1 = \frac{-3C_{111}^{(3)} \pm \sqrt{9(C_{111}^{(3)})^2 - 32\lambda_1\widetilde{C}_{1111}^{(4)}}}{8\widetilde{C}_{1111}^{(4)}}. \tag{3.16}$$

3.3 Description of a spatially dependent orientation in a microphase

In the previous section besides a global orientation of A- and B-blocks a possible spatially dependent orientation is also taken into account in the Landau free energy.

Such a local orientation becomes possible in a microphase. The first harmonics approximation according to [12] given by Eq. (3.2) can only be applied to a nematic or smectic state. In this section it will be explained how an orientation tensor can be constructed such that it can also be applied to the hexagonal and bcc state. The orientation tensor is transformed back in real space and applied to the smectic-A and hexagonal state in Fig. (3.2) till (3.9). In these figures the orientation strength and direction of A- and B-blocks are displayed in a certain domain in the real space.

The definition of the microscopic orientation tensor $\widehat{\underline{\underline{Q}}}^{\alpha}(\underline{x})$ of block α is given by,

$$\widehat{\underline{\underline{Q}}}^{\alpha}(\underline{x}) \equiv \sum_{sm} \int_0^{L_s} dl\, \sigma_s^{\alpha}(l)\, (\underline{u}_m^s(l)\, \underline{u}_m^s(l) - \frac{1}{3}\underline{\underline{I}})\delta(\underline{x} - \underline{R}_m^s(l)). \qquad (3.17)$$

The macroscopic orientation tensor $\underline{\underline{Q}}^{\alpha}(\underline{x})$ in real space is written in the following form,

$$\underline{\underline{Q}}^{\alpha}(\underline{x}) = \left\langle \widehat{\underline{\underline{Q}}}^{\alpha}(\underline{x}) \right\rangle = Q^{\alpha}(\underline{x})(\underline{n}^{\alpha}(\underline{x})\underline{n}^{\alpha}(\underline{x}) - \frac{1}{3}\underline{\underline{I}}). \qquad (3.18)$$

In this form the unit vector $\underline{n}^{\alpha}(\underline{x})$ is the local director of block α. The scalar $Q^{\alpha}(\underline{x})$ can be regarded as the strength of the alignment of the α-monomers along the director $\underline{n}^{\alpha}(\underline{x})$. This becomes clear if we choose the coordinate system such that a certain monomer k of kind α is fixed at $\underline{R}_{k,\alpha}$. If ΔV is a volume element around $\underline{R}_{k,\alpha}$, then

$$Q^{\alpha}(\underline{R}_{k,\alpha}) = \lim_{\Delta V \to 0} \frac{1}{\Delta V} \int_{\Delta V} d^3x Q^{\alpha}(\underline{x}) = \frac{3}{2} \lim_{\Delta V \to 0} \frac{1}{\Delta V} \int_{\Delta V} d^3x n^{\alpha,\mu}(\underline{x}) n^{\alpha,\nu}(\underline{x}) \left\langle \widehat{Q}_{\mu\nu}^{\alpha}(\underline{x}) \right\rangle, \qquad (3.19)$$

according to Eq. (3.18). Inserting the definition of $\widehat{\underline{\underline{Q}}}(\underline{x})$ in Eq. (3.19) yields

$$Q^{\alpha}(\underline{R}_{k,\alpha}) = \frac{3}{2} \lim_{\Delta V \to 0} \frac{1}{\Delta V} \int_{\Delta V} d^3x \left\langle \sum_{sm} \int_0^{L_s} dl\, \sigma_s^{\alpha}(l) \left((\underline{n}^{\alpha}(\underline{x}) \cdot \underline{u}_m^s(l))^2 - \frac{1}{3} \right) \delta(\underline{x} - \underline{R}_m^s(l)) \right\rangle. \qquad (3.20)$$

The delta function cancels out all contributions of monomers which are outside ΔV. Because $\Delta V \to 0$, the number of monomers inside ΔV becomes smaller and if ΔV is small enough only the monomer k of kind α at $\underline{R}_{k,\alpha}$ remains. Then Eq. (3.20)

becomes,

$$
Q^\alpha(\underline{R}_{k,\alpha}) = \frac{3}{2} \lim_{\Delta V \to 0} \frac{1}{\Delta V} \int_{\Delta V} d^3x \left\langle \left((\underline{n}^\alpha(\underline{R}_{k,\alpha}) \cdot \underline{u}_{k,\alpha})^2 - \frac{1}{3} \right) \delta(\underline{x} - \underline{R}_{k,\alpha}) \right\rangle =
$$

$$
\frac{3}{2} \left\langle (\underline{n}^\alpha(\underline{R}_{k,\alpha}) \cdot \underline{u}_{k,\alpha})^2 - \frac{1}{3} \right\rangle \lim_{\Delta V \to 0} \frac{1}{\Delta V} \int_{\Delta V} d^3x \delta(\underline{x} - \underline{R}_{k,\alpha}) =
$$

$$
\frac{3}{2} \left\langle (\underline{n}^\alpha(\underline{R}_{k,\alpha}) \cdot \underline{u}_{k,\alpha})^2 - \frac{1}{3} \right\rangle \rho^\alpha(\underline{R}_{k,\alpha}). \tag{3.21}
$$

In this form we see that $Q^\alpha(\underline{R}_{k,\alpha})$ is zero if the direction of $\underline{u}_{k,\alpha}$ is completely arbitrary on average. A positive alignment strength $Q^\alpha(\underline{R}_{k,\alpha})$ means that the monomer prefers to be aligned parallel to the director. At the maximum alignment $Q^\alpha(\underline{R}_{k,\alpha}) = \rho^\alpha(\underline{R}_{k,\alpha})$ the monomer at $\underline{R}_{k,\alpha}$ is perfectly oriented parallel to the director. A negative alignment strength can be regarded as a stronger orientation perpendicular to $\underline{n}^\alpha(\underline{R}_{k,\alpha})$.

The orientation in the nematic and smectic state can be described by a space independent director $\underline{n}^\alpha(\underline{x}) = \underline{n}^\alpha$ in Eq. (3.18). Then the form of Eq. (3.18) is in agreement with Eq. (3.2) which is transformed back in real space. However, in the hexagonal and bcc state Eq. (3.2) cannot be applied, because there is more than one direction at which the A- and B-blocks prefer to be oriented. Therefore the orientation in these structures cannot be described by means of one constant director $\underline{n}^\alpha$. A simple way to express the director $\underline{n}^\alpha(\underline{x})$ of the hexagonal state is to divide the melt into domains at which $\underline{n}^\alpha(\underline{x})$ is locally constant. Such director field has been drawn in Fig. (3.1). In this figure the dots are the points at which the density of α-monomers is maximal. Each line connects a maximum with one of the six nearest points at which the density of α-monomers is minimal. Fig. (3.1) can be applied to both the hexagonal state with α-rich cylinders and the reverse state with an α-rich matrix. The local directors $\underline{n}_1$, $\underline{n}_2$ and $\underline{n}_3$ are chosen parallel to the set of wave vectors $H_{hex} = \{\pm\underline{q}_1, \pm\underline{q}_2, \pm\underline{q}_3\}$ in $\Psi(\underline{q})$ given by Eq. (3.1). The domains at which $\underline{n}^\alpha(\underline{x}) = \underline{n}_1$, $\underline{n}_2$ and $\underline{n}_3$ are denoted as V_{1k}, V_{2k} and V_{3k}, respectively. In this notation k is a certain integer. So $\underline{n}^\alpha(\underline{x})$ can be expressed as,

$$
\underline{n}^\alpha(\underline{x}) = \begin{cases} \underline{n}_1 \text{ if } \underline{x} \in V_{1k} \\ \underline{n}_2 \text{ if } \underline{x} \in V_{2k} \\ \underline{n}_3 \text{ if } \underline{x} \in V_{3k} \end{cases} . \tag{3.22}
$$

The orientation strength $Q^\alpha(\underline{x})$ in Eq. (3.18) can also be divided into the domains V_{1k}, V_{2k} and V_{3k},

$$
Q^\alpha(\underline{x}) = Q_j^\alpha(\underline{x}) \text{ if } \underline{x} \in V_{jk}, \tag{3.23}
$$
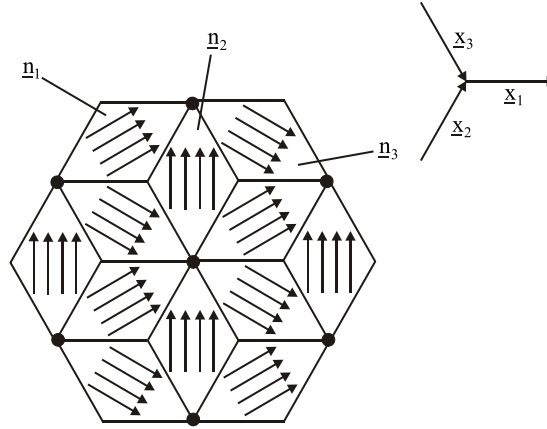
Figure 3.1: Director field in the hexagonal phase

in which $j = 1, 2$ or 3. The director and orientation strength given by Eq. (3.22) and (3.23) are inserted in Eq. (3.18) to calculate the Fourier transform of the orientation tensor $\underline{\underline{Q}}^\alpha(\underline{x})$. In the Fourier transform the integral over the whole space is written as a summation of integrals over the domains V_{jk},

$$
\underline{\underline{Q}}^\alpha(\underline{q}) = \frac{1}{V} \sum_{j,k} \int_{V_{jk}} d^3x \exp(i\underline{q} \cdot \underline{x}) \underline{\underline{Q}}^\alpha(\underline{x}) =
$$

$$
\frac{1}{V} \sum_{j,k} \int_{V_{jk}} d^3x \exp(i\underline{q} \cdot \underline{x}) Q^\alpha(\underline{x}) (\underline{n}^\alpha(\underline{x}) \underline{n}^\alpha(\underline{x}) - \frac{1}{3}\underline{\underline{I}}) =
$$

$$
\frac{1}{V} \sum_j (\underline{n}_j \underline{n}_j - \frac{1}{3}\underline{\underline{I}}) \sum_k \int_{V_{jk}} d^3x \exp(i\underline{q} \cdot \underline{x}) Q_j^\alpha(\underline{x}). \tag{3.24}
$$

The orientation strength $Q_j^\alpha(\underline{x})$ must be chosen such that the tensor $\underline{\underline{Q}}^\alpha(\underline{x})$ maintains the symmetry properties of the hexagonal structure. In each domain V_{jk} we may assume that there is a local smectic-A state with director $\underline{n}_j$. So a possible choice of $Q_j^\alpha(\underline{x})$ is,

$$
Q_j^\alpha(\underline{x}) = Q_{smecA}^\alpha(\underline{x}, \underline{n}_j) \quad \text{if } \underline{x} \in V_{jk}, \tag{3.25}
$$

which is inserted in Eq.(3.24). If $Q_{smecA}^\alpha(\underline{x}, \underline{n}_j)$ is written as a Fourier series, Eq.(3.24)

becomes,

$$\underline{\underline{Q}}^{\alpha}(\underline{q}) = \sum_j (\underline{n}_j \underline{n}_j - \frac{1}{3}\underline{\underline{I}}) \sum_{\underline{q}'} Q^{\alpha}_{smecA}(\underline{q}', \underline{n}_j) \frac{1}{V} \sum_k \int_{V_{jk}} d^3 x \exp(i(\underline{q} + \underline{q}') \cdot \underline{x}). \quad (3.26)$$

In Eq. (3.26) the integral,

$$I_j = \frac{1}{V} \sum_k \int_{V_{jk}} d^3 x \exp(i(\underline{q} + \underline{q}') \cdot \underline{x}) \quad (3.27)$$

is restricted to the domains V_{jk} belonging to the same director index j. These domains occupy $\frac{1}{3}$ of the whole space. In appendix C it has been proven that

$$I_j = \frac{1}{3}\delta(\underline{q} + \underline{q}'), \quad (3.28)$$

if $\underline{q}$ and $\underline{q}'$ are restricted to the set $H = H_{hex} \cup H_{nem}$ in which $H_{nem} = \{0\}$ and $H_{hex} = \{\pm q_* \underline{n}_1, \pm q_* \underline{n}_2, \pm q_* \underline{n}_3\}$. So if $\underline{q}$ and $\underline{q}' \in H$ Eq. (3.26) can be written as,

$$\underline{\underline{Q}}^{\alpha}(\underline{q}) = \frac{1}{3} \sum_j (\underline{n}_j \underline{n}_j - \frac{1}{3}\underline{\underline{I}}) \sum_{\underline{q}'} Q^{\alpha}_{smecA}(\underline{q}', \underline{n}_j)\delta(\underline{q} + \underline{q}'). \quad (3.29)$$

In the smectic-A state it is allowed to apply to first harmonics approximation according to Eq. (3.2) in which $\underline{q}'$ belongs to the set $H^j_{smecA} = \{\pm \underline{q}_{smecA}\} = \{\pm q_* \underline{n}_j\}$ at a certain j. In Eq. (3.29) we see that the orientation tensor of the hexagonal phase $\underline{\underline{Q}}^{\alpha}_{hex}(\underline{q})$ is the average of three smectic A phases,

$$\underline{\underline{Q}}^{\alpha}_{hex}(\underline{q}) = \frac{1}{3} \sum_{j=1}^3 \underline{\underline{Q}}^{\alpha}_{smecA}(\underline{q}, \underline{n}_j) \quad (3.30)$$

In the same way it can be derived that the orientation tensor $\underline{\underline{Q}}^{\alpha}_{bcc}(\underline{q})$ of the bcc phase can be expressed as the average of six smectic-A phases,

$$\underline{\underline{Q}}^{\alpha}_{bcc}(\underline{q}) = \frac{1}{6} \sum_{j=1}^6 \underline{\underline{Q}}^{\alpha}_{smecA}(\underline{q}, \underline{n}_j). \quad (3.31)$$

The phase factors $\exp(i\varphi_{\underline{q}'})$ in Eq. (3.2) and local directors $\underline{n}_j$ in the orientation tensors $\underline{\underline{Q}}^{\alpha}_{hex}(\underline{q})$ and $\underline{\underline{Q}}^{\alpha}_{bcc}(\underline{q})$ are chosen such that the symmetry properties of the microphase structure are maintained. The orientation tensors $\underline{\underline{Q}}^{\alpha}_{hex}(\underline{q})$ and $\underline{\underline{Q}}^{\alpha}_{bcc}(\underline{q})$ contain only contributions of smectic-A states. Contributions of smectic-C states could

also be possible, but these contributions are not taken into account. Very close to the spinodal χ_s nonzero angles θ are not possible, because then the lowest eigenvalue $\lambda_1 = \lambda_1(\theta)$ in the second order term of the Landau free energy becomes positive. Then it is less probable that a microphase contains contributions in which $\theta \neq 0$. Only at a greater χ negative eigenvalues $\lambda_1(\theta)$ with nonzero θ are possible. Maybe then a hexagonal or bcc state with a nonzero angle θ could be possible. This has not been investigated. The phase diagram is calculated in the neighbourhood of the phase transition point at which the mean field approximation is most reliable. Close to this point it is justified to assume that θ can only be zero in the hexagonal and bcc phase.

In this section the orientation of A- and B-blocks $\Upsilon_\alpha^{\mu\nu}(\underline{x}) = Q_\alpha^{\mu\nu}(\underline{x})/V$ in the smectic-A and hexagonal phase is calculated in real space to see how the chains are oriented. In the smectic-A phase the two wave vectors are chosen parallel to the x-axis,

$$\underline{q} = \pm q_* \begin{bmatrix} 1 \\ 0 \\ 0 \end{bmatrix}. \tag{3.32}$$

In this phase the elements of the tensor $\Upsilon_\alpha^{\mu\nu}(\underline{x})$ and the scalar order-parameter $\Psi(\underline{x})$ are,

$$\Upsilon_\alpha^{xx}(\underline{x}) = \frac{\Upsilon_\alpha}{V}\frac{4}{3}\cos(q_*x), \tag{3.33a}$$

$$\Upsilon_\alpha^{yy}(\underline{x}) = \Upsilon_\alpha^{zz}(\underline{x}) = -\frac{\Upsilon_\alpha}{V}\frac{2}{3}\cos(q_*x), \tag{3.33b}$$

$$\Upsilon_\alpha^{ij}(\underline{x}) = 0 \quad \text{if} \quad i \neq j \text{ and } i, j = x, y, z \tag{3.33c}$$

$$\text{and}$$

$$\Psi(\underline{x}) = 2\frac{\Psi}{V}\cos(q_*x). \tag{3.33d}$$

In the hexagonal phase the z-axis is chosen parallel to the cylinders. The wave vectors are in the xy-plane and are given by,

$$\underline{q} = \pm q_* \begin{bmatrix} 1 \\ 0 \\ 0 \end{bmatrix}, \pm \frac{1}{2}q_* \begin{bmatrix} 1 \\ -\sqrt{3} \\ 0 \end{bmatrix} \text{ and } \pm \frac{1}{2}q_* \begin{bmatrix} 1 \\ \sqrt{3} \\ 0 \end{bmatrix}. \tag{3.34}$$

In real space in the hexagonal phase the elements of the tensor $\Upsilon_\alpha^{\mu\nu}(\underline{x})$ and the scalar

order-parameter $\Psi(\underline{x})$ are,

$$\Upsilon_\alpha^{xx}(\underline{x}) = \frac{\Upsilon_\alpha}{V}\frac{4}{3}\cos(q_*x) - \frac{\Upsilon_\alpha}{V}\frac{1}{3}\cos(\frac{q_*}{2}x)\cos(\frac{q_*}{2}\sqrt{3}y), \qquad (3.35a)$$

$$\Upsilon_\alpha^{yy}(\underline{x}) = -\frac{\Upsilon_\alpha}{V}\frac{2}{3}\cos(q_*x) + \frac{\Upsilon_\alpha}{V}\frac{5}{3}\cos(\frac{q_*}{2}x)\cos(\frac{q_*}{2}\sqrt{3}y), \qquad (3.35b)$$

$$\Upsilon_\alpha^{zz}(\underline{x}) = -\frac{\Upsilon_\alpha}{V}\frac{2}{3}\cos(q_*x) - \frac{\Upsilon_\alpha}{V}\frac{4}{3}\cos(\frac{q_*}{2}x)\cos(\frac{q_*}{2}\sqrt{3}y), \qquad (3.35c)$$

$$\Upsilon_\alpha^{xy}(\underline{x}) = \Upsilon_\alpha^{yx}(\underline{x}) = -\frac{\Upsilon_\alpha}{V}\sqrt{3}\sin(\frac{q_*}{2}x)\sin(\frac{q_*}{2}\sqrt{3}y), \qquad (3.35d)$$

$$\Upsilon_\alpha^{yz}(\underline{x}) = \Upsilon_\alpha^{zy}(\underline{x}) = \Upsilon_\alpha^{xz}(\underline{x}) = \Upsilon_\alpha^{zx}(\underline{x}) = 0 \qquad (3.35e)$$

and

$$\Psi(\underline{x}) = 2\frac{\Psi}{V}\cos(q_*x) + 4\frac{\Psi}{V}\cos(\frac{q_*}{2}x)\cos(\frac{q_*}{2}\sqrt{3}y) \sim \Upsilon_\alpha^{zz}(\underline{x}). \qquad (3.35f)$$

The tensors Υ_α^{xx}, Υ_α^{yy}, Υ_α^{xy} and $\Upsilon_\alpha^{yx} = \Upsilon_\alpha^{xy}$ in the xy-plane form a symmetric matrix $\underline{\underline{M}}_\alpha$,

$$\underline{\underline{M}}_\alpha = \left[\begin{array}{cc} \Upsilon_\alpha^{xx} & \Upsilon_\alpha^{xy} \\ \Upsilon_\alpha^{xy} & \Upsilon_\alpha^{yy} \end{array} \right], \qquad (3.36)$$

which has two real eigenvalues and eigenvectors given by

$$\lambda_\alpha^\pm = \frac{1}{2}(\Upsilon_\alpha^{xx} + \Upsilon_\alpha^{yy}) \pm \frac{1}{2}\sqrt{(\Upsilon_\alpha^{xx} - \Upsilon_\alpha^{yy})^2 + 4(\Upsilon_\alpha^{xy})^2} \qquad (3.37)$$

and

$$\widehat{e}_\alpha^\pm = \frac{1}{\sqrt{(\Upsilon_\alpha^{xy})^2 + (\Upsilon_\alpha^{xx} - \lambda_\pm)^2}}\left[\begin{array}{c} -\Upsilon_\alpha^{xy} \\ \Upsilon_\alpha^{xx} - \lambda_\alpha^\pm \end{array} \right]. \qquad (3.38)$$

The eigenvectors $\widehat{e}_\alpha^+$ and $\widehat{e}_\alpha^-$ form an alternative coördinate system at every point (x, y) in the xy-plane. If $\widehat{e}_\alpha^+ = \widehat{e}_\alpha^{x'}$ and $\widehat{e}_\alpha^- = \widehat{e}_\alpha^{y'}$, then the eigenvalues λ_α^+ and λ_α^- are exactly equal to the orientation tensors $\Upsilon_\alpha^{x'x'}$ and $\Upsilon_\alpha^{y'y'}$, respectively. This can be easily verified by means of the definition of the microscopic orientation tensor $\widehat{\underline{\underline{Q}}}^\alpha(\underline{x})$ given by Eq. (3.17). So the eigenvalue is a measure of how strong the α-monomer is oriented along the corresponding eigenvector. If the eigenvalue is negative the orientation is weak in the corresponding direction. A positive eigenvalue means that the orientation is strong. If the eigenvalue is zero the orientation is the same as the orientation in an

isotropic melt. Because $\Upsilon_\alpha^{xx} + \Upsilon_\alpha^{yy} = -\Upsilon_\alpha^{zz}$, the eigenvalues of $\underline{\underline{M}}_\alpha$ can also be written as

$$\lambda_\alpha^\pm = -\frac{1}{2}\Upsilon_\alpha^{zz} \pm \frac{1}{2}\sqrt{(\Upsilon_\alpha^{zz})^2 - 4\det\underline{\underline{M}}_\alpha} = -\frac{1}{2}\Upsilon_\alpha^{zz} \pm \frac{1}{2}\sqrt{(\Upsilon_\alpha^{zz})^2 - 4\lambda_\alpha^+\lambda_\alpha^-}. \qquad (3.39)$$

In this form we see that,

$$\lambda_\alpha^+ - \lambda_\alpha^- = \sqrt{(\Upsilon_\alpha^{zz})^2 - 4\lambda_\alpha^+\lambda_\alpha^-} \geqq 0 \qquad (3.40)$$

$$\text{and}$$

$$\lambda_\alpha^+ + \lambda_\alpha^- + \Upsilon_\alpha^{zz} = 0. \qquad (3.41)$$

Because $\lambda_\alpha^+ \geqq \lambda_\alpha^-$, the α-monomers prefer to be oriented along $\widehat{e}_\alpha^+$ in the xy-plane.

In Fig. (3.2), (3.3) and (3.4) the density order-parameter $\Psi(\underline{x})$ and the eigenvectors $\widehat{e}_\alpha^+$ and $\widehat{e}_\alpha^-$ of the hexagonal phase are calculated in the xy-plane. These figures have been made universal such these can be applied to every A-block fraction f_A, chain length L and persistence lengths λ_A and λ_B. The figures corresponds to one of the eigenvectors $\widehat{\underline{x}}_n = (\widehat{\Psi}_n, \widehat{\Upsilon}_{A,n}, \widehat{\Upsilon}_{B,n})$ with $n = 1, 2$ and 3. The amplitude $\frac{\Psi}{V}$ of the scalar order-parameter in Eq. (3.35f) is taken equal to one. Along the horizontal and vertical axis q_*x and q_*y are plotted from 0 to 6π, respectively. x and y are multiplied by q_* to remove q_*-dependence. In this way the dependence of the parameters f_A, L, λ_A and λ_B have been removed. Only the signs of $\widehat{\Psi}_n$, $\widehat{\Upsilon}_{A,n}$ and $\widehat{\Upsilon}_{B,n}$ with respect to each other may become different if the fraction f_A or persistence length λ_A or λ_B is changed. In Fig. (3.3) and (3.4) $\widehat{e}_\alpha^+$ and $\widehat{e}_\alpha^-$ have been drawn, respectively, in which the amplitude $\frac{\Upsilon_\alpha}{V}$ in Eq. (3.35a) till (3.35e) has been taken equal to $+1$ or -1. If $\frac{\Upsilon_\alpha}{V} = +1$, the vector fields in Fig. (3.3) and (3.4) corresponds to $\widehat{e}_\alpha^+$ and $\widehat{e}_\alpha^-$, respectively and if $\frac{\Upsilon_\alpha}{V} = -1$ the fields $\widehat{e}_\alpha^+$ and $\widehat{e}_\alpha^-$ are reversed. In Fig. (3.2) in the darkest red parts there are maxima and the darkest blue parts are minima. The scalar order-parameter is chosen such that $\Psi(\underline{x}) = \Psi_A(\underline{x})$ and $\Psi(\underline{x}) = -\Psi_B(\underline{x})$. So the maxima and minima correspond to A-rich and B-rich domains, respectively. In the hexagonal phase displayed by Fig. (3.2) the cylinders are A-rich domains. In the reverse state there are more A-blocks outside the cylinders. This reverse state is completely analogeous to the state in Fig. (3.2) and need not to be considered separately.

In Eq. (3.35c) and (3.35f) we see that $\Psi(\underline{x})$ is proportional to $\Upsilon_\alpha^{zz}(\underline{x})$. The amplitudes $\frac{\Psi}{V}$ and $\frac{\Upsilon_\alpha}{V}$ in the expressions of $\Psi(\underline{x})$ and $\Upsilon_\alpha^{zz}(\underline{x})$ have either the same sign or different signs. According to Eq. (3.35c) and (3.35f) $\Psi(\underline{x})$ and $\Upsilon_\alpha^{zz}(\underline{x})$ have the same sign if $\frac{\Psi}{V}$ and $\frac{\Upsilon_\alpha}{V}$ have different signs. In that case if $\alpha = A$ the component $\Upsilon_A^{zz}(\underline{x})$
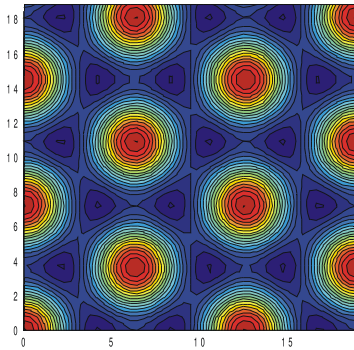
Figure 3.2: Scalar order-parameter $\Psi(\underline{x})$ in the hexagonal phase
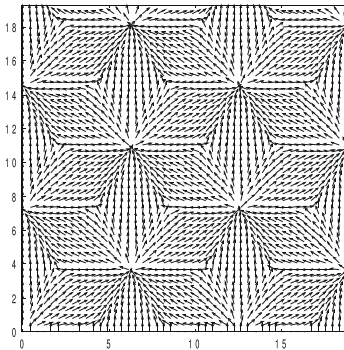
Figure 3.3: Field of eigenvector $\widehat{e_\alpha^+}$ of the hexagonal phase
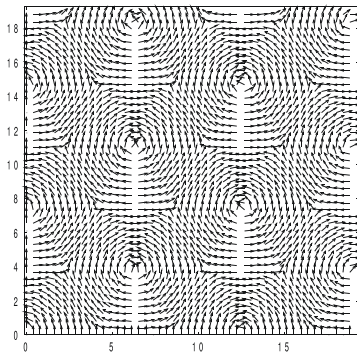
Figure 3.4: Field of eigenvector $\widehat{e_\alpha^-}$ of the hexagonal phase
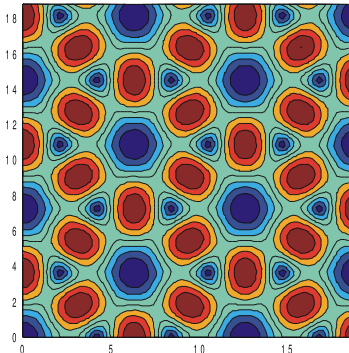
Figure 3.5: Eigenvalue difference $\lambda_\alpha^+ - \lambda_\alpha^-$ of the hexagonal phase

is positive in an A-rich cylinder which means that the A-blocks prefer to be oriented along the axis of the cylinder. In the B-rich matrix $\Upsilon_\alpha^{zz}(\underline{x})$ is negative so that the A-blocks are stronger oriented parallel to the xy−plane perpendicular to the cylinders. If the signs of $\frac{\Psi}{V}$ and $\frac{\Upsilon_\alpha}{V}$ are equal the reverse is taking place. Then the A-blocks are oriented along the z-axis outside the cylinders and inside the arrangement is parallel to the xy-plane.

The orientation in the xy-plane is measured with respect to the vectors $\widehat{e_\alpha^+}$ and $\widehat{e_\alpha^-}$ which are drawn in Fig. (3.3) and (3.4), respectively at the points (x, y). The ranging and scaling of the x- and y-axis is the same as in Fig. (3.2). In Fig. (3.3) we see that the vectors $\widehat{e_\alpha^+}$ are pointing towards or away from the closest axis of a cylinder. The vectors $\widehat{e_\alpha^-}$ are perpendicular to the vectors $\widehat{e_\alpha^+}$ and therefore in Fig. (3.4) the vectors $\widehat{e_\alpha^-}$ are pointing around the closest cylinder axis. The eigenvalues λ_α^+ and λ_α^- are a measure of orientation strength along $\widehat{e_\alpha^+}$ and $\widehat{e_\alpha^-}$. In Fig. (3.5) the difference $\lambda_\alpha^+ - \lambda_\alpha^-$ is plotted in the xy-plane in the same way as Fig. (3.2), (3.3) and (3.4). This difference is always positive or zero according to Eq. (3.40). In the most red parts in the figure $\lambda_\alpha^+ - \lambda_\alpha^-$ is maximum and in that domain the A-blocks prefer to be oriented along $\widehat{e_\alpha^+}$. The red parts are positioned between two cylinders. In the most blue domains the difference is very small and is zero in the centre. These blue parts are positioned exactly at an A- or B-rich domain. In the points at which $\Psi(\underline{x})$ is maximum or minimum different orientation directions in the xy-plane are crossing each other. So the orientation in the xy-plane is random at the maxima and minima. This explains why the difference $\lambda_\alpha^+ - \lambda_\alpha^-$ becomes zero. A small difference does not mean that the total orientation in the xy-plane is weak. In the centre of an A- or B-rich domain $\Upsilon_\alpha^{zz}(\underline{x})$ is negative which means that the alignment in the z-direction is weak. Because the tensor $\Upsilon_\alpha^{\mu\nu}$ is trace less, the total orientation $\Upsilon_\alpha^{xx}(\underline{x}) + \Upsilon_\alpha^{yy}(\underline{x})$ in the xy-plane must be positive. Exactly in the centre of an A- or B-rich domain $\lambda_\alpha^+ = \lambda_\alpha^-$ so that $\Upsilon_\alpha^{xx}(\underline{x}) = \Upsilon_\alpha^{yy}(\underline{x})$. In that point the orientation in the xy-plane is maximal, but there is no preferred direction.

From the numerical calculations it appears that in the neighbourhood of the phase transition point in the phase diagram the longest block has always the greatest persistence length. So if $L_A > L_B$, then $\lambda_A > \lambda_B$. At the same time in the primary eigenvector $\underline{x}_1 = (\Psi_1, \Upsilon_{A,1}, \Upsilon_{B,1})$ the signs of $\Upsilon_{A,1}$ and $\Upsilon_{B,1}$ are equal and Ψ_1 has a different sign, so

$$\underline{x}_1 = (\Psi_1, \Upsilon_{A,1}, \Upsilon_{B,1}) = (\pm|\Psi_1|, \mp|\Upsilon_{A,1}|, \mp|\Upsilon_{B,1}|). \tag{3.42}$$

In the neighbourhood of the phase transition point the total density and orientation parameters Ψ, Υ_A and Υ_B are mainly determined by the primary eigenvectors, $\Psi_1 \approx$

Ψ, $\Upsilon_{A,1} \approx \Upsilon_A$ and $\Upsilon_{B,1} \approx \Upsilon_B$. The contributions of the secondary eigenvectors can be neglected. In this way we can predict how the A- and B-blocks are oriented close to the phase transition point. For example in the hexagonal phase in Fig. (3.2) the amplitude Ψ have been chosen positive, so that the amplitudes Υ_A and Υ_B are negative according to Eq. (3.42). Therefore in the xy-plane the A- and B-blocks prefer to be oriented according to Fig. (3.3). Because $\Upsilon_A < 0$ and $\Upsilon_B < 0$ the orientation $\Upsilon_\alpha^{zz}(\underline{x})$ given by Eq.(3.35c) is positive in an A-rich cylinder in Fig. (3.2). Here the A- and B-blocks are stronger aligned along the axis of the cylinder. Outside the cylinders the orientation of diblocks is stronger parallel to the xy-plane. In the reverse state the B-blocks form cylinders in an A-rich matrix. Here the diblocks are aligned along the z-axis in the A-rich matrix and inside the cylinders the orientation is perpendicular to the z-axis. In the xy-plane the chains are still oriented according to Fig. (3.3).

In the limit $\lambda_A \downarrow \lambda_B$ the phase transition point in the phase diagram is reached when $L_A \downarrow L_B$ and the primary eigenvector $\underline{x}_1$ is not given by Eq. (3.42). The sign of Υ_1^B has changed, so that

$$\underline{x}_1 = (\Psi_1, \Upsilon_{A,1}, \Upsilon_{B,1}) = (\pm|\Psi_1|, \mp|\Upsilon_{A,1}|, \pm|\Upsilon_{B,1}|). \tag{3.43}$$

A consequence is that the A- and B-blocks are oriented perpendicular to each other. For example in the hexagonal phase the orientation of B-blocks in the xy-plane is displayed in Fig. (3.4) instead of Fig. (3.3). Additionally, when the B-blocks are aligned parallel to the z-axis, the A-blocks are always oriented in the xy-plane irrespective if $\lambda_A \downarrow \lambda_B$ or $\lambda_B \downarrow \lambda_A$.

The smectic-A state has been investigated in the same way. In Fig. (3.6), (3.7), (3.8) and (3.9) $\Psi(\underline{x})$, $\widehat{e_\alpha^+}$, $\widehat{e_\alpha^-}$ and the difference $\lambda_\alpha^+ - \lambda_\alpha^-$ are calculated in the xy-plane and $\frac{\Psi}{V} = -\frac{\Upsilon_\alpha}{V} = 1$ in Eq. (3.35a) till (3.35f). If $\frac{\Psi}{V} = \frac{\Upsilon_\alpha}{V} = 1$ the vector fields are reversed so that Fig. (3.7) and (3.8) correspond to $\widehat{e_\alpha^-}$ and $\widehat{e_\alpha^+}$, respectively. Because $\lambda_\alpha^+ \geqq \lambda_\alpha^-$ according to Eq. (3.40), the A- or B-blocks prefer to be aligned along $\widehat{e_\alpha^+}$. Close to the phase transition point if $\Psi > 0$, then according to Eq. (3.42) and (3.43) $\Upsilon_A < 0$. So in that case the A-blocks are oriented according to Fig. (3.7) with respect to the xy-plane. In this figure the A-blocks in the B-rich layers are a little bit stronger aligned parallel to the wave vector $\underline{q}$ but in the A-rich layers the alignment is some stronger in the direction perpendicular to $\underline{q}$. Such an orientation is possible if the block length L_A is longer than the size of a A-rich layer $\frac{1}{2}\lambda$. It has been verified numerically that if the A-block is stiffer than the B-block, $\lambda_A > \lambda_B$, or if $\lambda_A = \lambda_B$ it always follows that $L_A > \frac{1}{2}\lambda$ in the neighbourhood of the phase transition point.
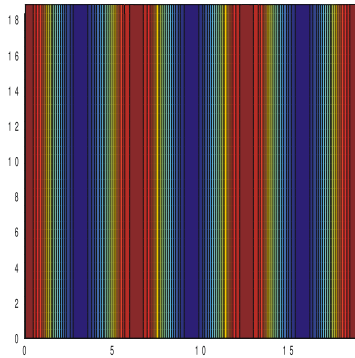
Figure 3.6: Scalar order-parameter $\Psi(\underline{x})$ in the smectic-A phase
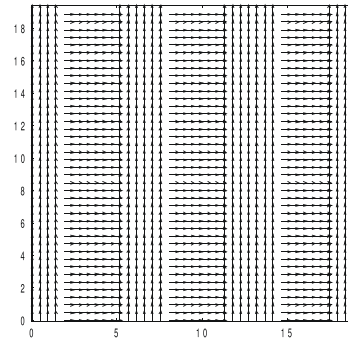
Figure 3.7: Field of eigenvector $\widehat{e_\alpha^+}$ of the smectic-A phase
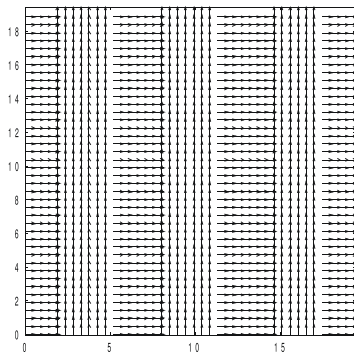
Figure 3.8: Field of eigenvector $\widehat{e_\alpha^-}$ of the smectic-A phase
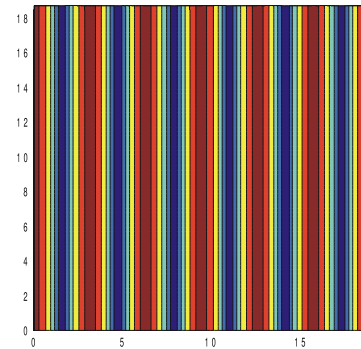
Figure 3.9: Eigenvalue difference $\lambda_\alpha^+ - \lambda_\alpha^-$ of the smectic-A phase

3.4 Determination of the phase diagram

In the phase diagram the Flory-Huggins parameter χ multiplied by the chain length L is plotted against the A-block fraction f. In each point $(f, \chi L)$ the most probable state of the melt is determined. First the spinodal $\chi_s L$ is calculated for which an expression is derived in this chapter. This expression depends on the second order vertices $\Gamma^{(2)}_{\widetilde{ab}}$ which are written down in detail in terms of the second order single-chain correlation functions $A_{\widetilde{ab}}$ in Appendix A. First the single-chain correlation functions $A_{\widetilde{ab}} = A_{\widetilde{ab}}(\underline{q}_1, \underline{q}_2)$ for the set $\underline{q}_1 = -\underline{q}_2 = \underline{q}$ are calculated. These correlation functions can be used to determine the vertices $\Gamma^{(2)}_{\widetilde{ab}} = \Gamma^{(2)}_{\widetilde{ab}}(\underline{q}, -\underline{q})$. The wave number $\underline{q}$ and director $\underline{n}$ are chosen as $\underline{q} = q_* \widehat{\underline{e}}_x$ and $\underline{n} = (\cos\theta, \sin\theta, 0)$ in the expression of the spinodal which is minimized with respect to q_* and θ. It has appeared that for every system of di- and triblocks the orientation θ is $\theta = 0°$.

In a point $(f, \chi L)$ in the phase diagram in which $\chi L > \chi_s L$ a microphase structure is possible. In each point the free energy is calculated for both the smectic-A, smectic-C, hexagonal and bcc phase by means of the expression,

$$\frac{F_L}{V} = \min_{x_1}\{\lambda_1 x_1^2 + C^{(3)}_{111} x_1^3 + (C^{(4)}_{1111} - \sum_{n\neq1}\frac{(C^{(3)}_{11n})^2}{4\lambda_n})x_1^4\} =$$
$$\min_{x_1}\{\lambda_1 x_1^2 + C^{(3)}_{111} x_1^3 + \widetilde{C}^{(4)}_{1111} x_1^4\}, \tag{3.44}$$

derived in section 3.2. At the minimum x_1 is

$$x_1 = \frac{-3C^{(3)}_{111} \pm \sqrt{9(C^{(3)}_{111})^2 - 32\lambda_1\widetilde{C}^{(4)}_{1111}}}{8\widetilde{C}^{(4)}_{1111}}. \tag{3.45}$$

In the first harmonics approximation each phase is described by a set H of wave vectors with the same magnitude q_*. These magnitude follows from minimization of the spinodal $\chi_s L$ with respect to q_*. The coefficient or eigenvalue λ_1 in the second order term in Eq. (3.44) depends on the vertices $\Gamma^{(2)}_{\widetilde{ab}} = \Gamma^{(2)}_{\widetilde{ab}}(\underline{q}_1, \underline{q}_2)$ in which $\underline{q}_1$ and $\underline{q}_2$ belong to the set H and $\underline{q}_1 + \underline{q}_2 = 0$. In the smectic-A and -C phase $H = \{\pm\underline{q}\} = \{\pm q_*\widehat{\underline{e}}_x\}$ and the two possible combinations $\underline{q}_1 = -\underline{q}_2 = +q_*\widehat{\underline{e}}_x$ and $\underline{q}_1 = -\underline{q}_2 = -q_*\widehat{\underline{e}}_x$ give the same contribution $c^{(2)}(\underline{q}, -\underline{q}, \theta)$ to λ_1 because of symmetry, so $\lambda_1 = 2c^{(2)}(\underline{q}, -\underline{q}, \theta)$. It can be easily explained that the same contribution $c^{(2)}(\underline{q}, -\underline{q}, \theta)$ can be used to determine λ_1 in the hexagonal and bcc phase which are $\lambda_1 = 6c^{(2)}(\underline{q}, -\underline{q}, \theta = 0°)$ and $12c^{(2)}(\underline{q}, -\underline{q}, \theta = 0°)$, respectively.

In the same way the third order coefficients $C^{(3)}_{111}$ in Eq. (3.44) depend on the vertices $\Gamma^{(3)}_{\widetilde{abc}} = \Gamma^{(3)}_{\widetilde{abc}}(\underline{q}_1, \underline{q}_2, \underline{q}_3)$ in which $\underline{q}_1$, $\underline{q}_2$ and $\underline{q}_3$ belong to the set H and $\underline{q}_1 + \underline{q}_2 + \underline{q}_3 = 0$. In the smectic-A and -C phase such triples are not possible so that $C^{(3)}_{111} = 0$. In the hexagonal phase each triple gives the same contribution $c^{(3)}$ and there are $2 \times 3! = 12$ combinations, so $C^{(3)}_{111} = 12c^{(3)}$. In the bcc phase $C^{(3)}_{111} = 48c^{(3)}$ in which the contribution $c^{(3)}$ is the same as the one in the hexagonal phase. The other third order coefficients $C^{(3)}_{11n}$ in Eq. (3.44) are calculated in a similar way.

The coefficient $C^{(4)}_{1111}$ in Eq. (3.44) contains contributions of sets of four wave vectors $\underline{q}_1$, $\underline{q}_2$, $\underline{q}_3$ and $\underline{q}_4$ belonging to the set H such that $\underline{q}_1 + \underline{q}_2 + \underline{q}_3 + \underline{q}_4 = 0$. In the smectic-A and -C phase six possible sets can be formed which are indicated by the label A,

$$A = \{\underline{q}_i \cdot \underline{q}_j = \pm q_*^2 \mid i, j = 1, 2, 3 \text{ or } 4\}. \tag{3.46}$$

So if $c^{(4)}_A = c^{(4)}_A(\theta)$ is a contribution of one combination then $C^{(4)}_{1111} = 6c^{(4)}_A(\theta)$ because of symmetry. In the hexagonal and bcc phase the contributions of set A to $C^{(4)}_{1111}$ are $18c^{(4)}_A(\theta = 0°)$ and $36c^{(4)}_A(\theta = 0°)$, respectively. Besides set A other sets B, C and D are possible which are,

$$B = \{\underline{q}_i \cdot \underline{q}_j = -q_*^2 \text{ or } \pm \frac{1}{2}q_*^2 \mid i, j = 1, 2, 3 \text{ or } 4\}, \tag{3.47}$$

$$C = \{\underline{q}_i \cdot \underline{q}_j = \pm q_*^2 \text{ or } 0 \mid i, j = 1, 2, 3 \text{ or } 4\} \tag{3.48}$$

and

$$D = \{\underline{q}_i \cdot \underline{q}_j = -\frac{1}{2}q_*^2 \text{ or } 0 \mid i, j = 1, 2, 3 \text{ or } 4\}. \tag{3.49}$$

If a contribution of one combination of set B, C or D is denoted by $c^{(4)}_B$, $c^{(4)}_C$ or $c^{(4)}_D$, respectively, then in the hexagonal phase $C^{(4)}_{1111}$ contains an additional term $72c^{(4)}_B$ and in the bcc phase $288c^{(4)}_B$, $72c^{(4)}_C$ and $144c^{(4)}_D$ must be added.

To limit calculation time the fourth order single-chain correlation functions $C_{\widetilde{abcd}}$ for only one combination of set A, B, C and D are calculated. These are applied to calculate the vertices $\Gamma^{(4)}_{\widetilde{abcd}}$ for each set separately. The vertices $\Gamma^{(4)}_{\widetilde{abcd}}$ belonging to a certain set are used to calculate $c^{(4)}_A(\theta)$, $c^{(4)}_B$, $c^{(4)}_C$ or $c^{(4)}_D$. The single-chain correlation functions $C_{\widetilde{abcd}}$ and vertices $\Gamma^{(4)}_{\widetilde{abcd}}$ of set A do not depend on the orientation angle θ of the director $\underline{n}$. A constant direction of the wave vector $\underline{q}$ is chosen and the direction of $\underline{n}$ is varied. So $C_{\widetilde{abcd}}$ and $\Gamma^{(4)}_{\widetilde{abcd}}$ do not have to be calculated for every orientation

angle θ if the free energy of the smectic-C phase has to be minimized with respect to θ.

The vertices $\Gamma^{(4)}_{\widetilde{abcd}}$ also contain terms with products of two third order single-chain correlation functions $B_{\widetilde{abc}}$. In these terms combinations are possible in which $B_{\widetilde{abc}} = B_{\widetilde{abc}}(\underline{q}_1, \underline{q}_2, \underline{q}_3) = B_{\widetilde{abc}}(\underline{q}, -\underline{q}, 0)$. Such combinations are ignored, because the matrices $M^{(1)}_{\widetilde{ab}} = M^{(1)}_{\widetilde{ab}}(\underline{q}_1, \underline{q}_2)$ are undefined when $\underline{q}_1 = \underline{q}_2 = 0$. In [6] similar terms are found in the final form of the free energy given by Eq. (A60) in Appendix A. This problem is also encountered when the spinodal $\omega_s L = \omega_{s,nem} L$ is calculated which is minimal at $q_* = 0$. To solve this problem the limit $q_* \to 0$ is taken so that $M^{(1)}_{\widetilde{ab}}$ is still defined. In Eq. (3.44) a summation is carried out over n which labels contributions of secondary eigenvectors with eigenvalues λ_n. In these terms when $n = 10$ or 20 the limits $\lim_{q_* \to 0} \lambda_n(q_*)$ and $\lim_{q_3 \to 0} C^{(3)}_{11n}(\underline{q}_1, \underline{q}_2, \underline{q}_3) = \lim_{q_3 \to 0} C^{(3)}_{11n}(\underline{q}, -\underline{q}, \underline{q}_3)$ are taken to avoid that in $M^{(1)}_{\widetilde{ab}}$ the wave vectors become exactly zero. In the same way the free energy of the nematic phase has been calculated in which it has appeared that the fourth order term is always negative in the neighbourhood of the phase transition point in both chapter 3 and 5. This follows from the fact that in both the bcc, hexagonal, smectic-A and -C phase the coefficient $\widetilde{C}^{(4)}_{1111}$ in Eq. (3.44) is always negative when the limit $q_* \to 0$ is taken.

The third order coefficients $C^{(3)}_{111}$ and $C^{(3)}_{11n}$ in Eq. (3.44) are also calculated by first calculating the single-chain correlation functions $B_{\widetilde{abc}}$ and vertices $\Gamma^{(3)}_{\widetilde{abc}}$ for one combination $\underline{q}$-vectors for which $\underline{q}_1 + \underline{q}_2 + \underline{q}_3 = 0$. Because of symmetry it is not necessary to calculate $B_{\widetilde{abc}}$ and $\Gamma^{(3)}_{\widetilde{abc}}$ for the other combinations.

To determine the phase diagram all vertices $\Gamma^{(2)}_{\widetilde{ab}}$, $\Gamma^{(3)}_{\widetilde{abc}}$ and $\Gamma^{(4)}_{\widetilde{abcd}}$ have to be calculated at every A-block fraction f. These vertices do not depend on the Flory-Huggins parameter χL, because q_* has been determined by minimizing the spinodal $\chi_s L$ with respect to q_*. The calculation of the vertices consumes most time due to the slowness of the numerical integration carried out for each single-chain correlation function. The implementation of the single-chain correlation functions in an algorithm is explained in detail in Appendix D. After the vertices at a certain f have been calculated the free energy as a function of χL can be calculated quickly for every microphase structure. At every point $(f, \chi L)$ the phase with lowest free energy is determined which is the most probable state of the melt. The lines at which one phase is converted into another phase are indicated in the phase diagram.

3.5 Spinodal analysis of a melt of monodisperse semi-flexible diblock copolymers

In this section we want to apply the theory in chapter 2 to investigate numerically the spinodals χ_s and ω_s of a simple melt of monodisperse semi-flexible diblock copolymers. For simplicity the three different parameters ω_{AA}, ω_{AB} and ω_{BB} have been taken equal so that there is only one parameter ω. In a melt of diblocks only the parameter $\tilde{\chi}_{AA}$ in Eq. (2.21) is nonzero and will be denoted as χ. The first harmonics approximation is applied to the scalar order-parameter Ψ^a and the orientation tensor $\Upsilon^{\bar{a}}$,

$$\Psi^a = \Psi^A(\underline{q}_1) = -\Psi^B(\underline{q}_1) = \Psi(\underline{q}_1) = \Psi \sum_{\underline{q} \in H} \exp(i\varphi_{\underline{q}})\delta(\underline{q}_1 - \underline{q}) \qquad (3.50)$$

and

$$\Upsilon^{\bar{a}} = \Upsilon_\alpha^{\mu_1 \nu_1}(\underline{q}_1) = \Upsilon_\alpha(n_\alpha^{\mu_1} n_\alpha^{\nu_1} - \frac{1}{3}\delta^{\mu_1 \nu_1}) \sum_{\underline{q} \in H} \exp(i\varphi_{\underline{q}})\delta(\underline{q}_1 - \underline{q}). \qquad (3.51)$$

If there is microphase separation the order-parameters Ψ^a and $\Upsilon^{\bar{a}}$ must contain the same set H of wave vectors with the same length q_*. Then the symmetry of the microphase structure is conserved. However, the orientation tensor $\Upsilon^{\bar{a}}$ may also contain additional contributions in which $q_* = 0$. These global terms must be chosen such that they do not break the symmetry. So $\Upsilon^{\bar{a}}$ must be written as

$$\Upsilon^{\bar{a}} = \Upsilon_\alpha^{\mu_1 \nu_1}(\underline{q}_1) = \Upsilon_\alpha(n_\alpha^{\mu_1} n_\alpha^{\nu_1} - \frac{1}{3}\delta^{\mu_1 \nu_1}) \sum_{\underline{q} \in H} \exp(i\varphi_{\underline{q}})\delta(\underline{q}_1 - \underline{q})+$$

$$\Upsilon_\alpha^0 (n_\alpha^{\mu_1} n_\alpha^{\nu_1} - \frac{1}{3}\delta^{\mu_1 \nu_1})\delta(\underline{q}_1). \qquad (3.52)$$

In $\Upsilon^{\bar{a}}$ the vector $\underline{n}^{\mu_1}$ is a unit vector which is the direction of the orientation of block α. If the orientation of the A and B block are different each semi-flexible chain will be bent. In the derivation of the single-chain correlation function in appendix A the tangent vectors of the A and B block at the connection point have been taken equal. So the A and B block cannot be bent freely with respect to each other. Therefore it is energetically not favourable that the two blocks have different orientations. So it is justified to assume that in Eq.(3.51) $n_A^\mu = n_B^\mu = n^\mu$. The orientation tensor expressed by Eq. (3.52) contains only one orientation direction $\underline{n}$. This form can

only be applied to the nematic state or a smectic phase. The scalar order-parameter Ψ^a and orientation tensor $\Upsilon^{\bar{a}}$ in the hexagonal or bcc phase can be described by a superposition of smectic phases with different directions $\frac{q}{q_*}$ and $\underline{n}$. The directions $\frac{q}{q_*}$ and $\underline{n}$ must be chosen such that the hexagonal or bcc phase maintains its symmetry.

The expressions of the spinodals χ_s and ω_s are derived by means of the second order term of the general expression of the Landau free energy given by Eq. (2.21). In the free energy both zero and nonzero modes q_* may contribute. First we consider contributions to the second order term in which $q_* \neq 0$. These contributions occur when there is microphase separation. A certain microphase can be described as a superposition of smectic phases. Because of symmetry each pair of modes $\{-\underline{q}, \underline{q}\}$ corresponding to a certain smectic phase gives the same contribution. Such a contribution can be written in the following matrix form,

$$
\frac{F_L^{(2)}(q_* \neq 0)}{V} = \begin{bmatrix} \Psi & \Upsilon_A & \Upsilon_B \end{bmatrix} \begin{bmatrix} \widetilde{\Gamma}^{(2)} - \chi & \widetilde{\Gamma}_A^{(2)} & \widetilde{\Gamma}_B^{(2)} \\ \widetilde{\Gamma}_A^{(2)} & \widetilde{\Gamma}_{AA}^{(2)} - \frac{1}{3}\omega & \widetilde{\Gamma}_{AB}^{(2)} - \frac{1}{3}\omega \\ \widetilde{\Gamma}_B^{(2)} & \widetilde{\Gamma}_{AB}^{(2)} - \frac{1}{3}\omega & \widetilde{\Gamma}_{BB}^{(2)} - \frac{1}{3}\omega \end{bmatrix} \begin{bmatrix} \Psi \\ \Upsilon_A \\ \Upsilon_B \end{bmatrix},
$$

$$(3.53)$$

using the first harmonics approximation of the order-parameters according to Eq. (3.50) and (3.52). At $\chi < \chi_s$ and $\omega < \omega_s$ the eigenvalues of the matrix are positive so that the isotropic state is stable. At $\chi = \chi_s$ or $\omega = \omega_s$ at least one of the eigenvalues is zero and becomes negative if χ or ω is further increased. Then the isotropic state becomes unstable. Because one of the eigenvalues is zero at $\chi = \chi_s$ or $\omega = \omega_s$, the determinant of the matrix must be zero. In this way χ_s and ω_s can easily be found,

$$
\chi_s = \min_{\{q_*, \underline{n}\}} \{ \widetilde{\Gamma}^{(2)} - \frac{(\widetilde{\Gamma}_B^{(2)})^2(\widetilde{\Gamma}_{AA}^{(2)} - \frac{1}{3}\omega) + (\widetilde{\Gamma}_A^{(2)})^2(\widetilde{\Gamma}_{BB}^{(2)} - \frac{1}{3}\omega) - 2\widetilde{\Gamma}_A^{(2)}\widetilde{\Gamma}_B^{(2)}(\widetilde{\Gamma}_{AB}^{(2)} - \frac{1}{3}\omega)}{(\widetilde{\Gamma}_{AA}^{(2)} - \frac{1}{3}\omega)(\widetilde{\Gamma}_{BB}^{(2)} - \frac{1}{3}\omega) - (\widetilde{\Gamma}_{AB}^{(2)} - \frac{1}{3}\omega)^2} \}
$$

$$(3.54)$$

and

$$
\omega_s = 3\min_{\{q_*, \underline{n}\}} \{ \frac{(\widetilde{\Gamma}^{(2)} - \chi)(\widetilde{\Gamma}_{AA}^{(2)}\widetilde{\Gamma}_{BB}^{(2)} - (\widetilde{\Gamma}_{AB}^{(2)})^2) - (\widetilde{\Gamma}_A^{(2)})^2\widetilde{\Gamma}_{BB}^{(2)} + 2\widetilde{\Gamma}_A^{(2)}\widetilde{\Gamma}_B^{(2)}\widetilde{\Gamma}_{AB}^{(2)} - (\widetilde{\Gamma}_B^{(2)})^2\widetilde{\Gamma}_{AA}^{(2)}}{(\widetilde{\Gamma}^{(2)} - \chi)(\widetilde{\Gamma}_{AA}^{(2)} + \widetilde{\Gamma}_{BB}^{(2)} - 2\widetilde{\Gamma}_{AB}^{(2)}) - (\widetilde{\Gamma}_A^{(2)} - \widetilde{\Gamma}_B^{(2)})^2} \}.
$$

$$(3.55)$$

In these equations χ_s and ω_s are minimized with respect to q_* and $\underline{n}$. From the numerical calculations it followed that the orientation direction $\underline{n}$ is always equal to the direction of the wave vector $\underline{q}$, so $\underline{n} = \frac{q}{q_*}$. In a certain microphase the mode

$q_* = 0$ may also contribute. In the smectic state this mode gives one contribution to the second order term which is given by,

$$\frac{F_L^{(2)}(q_* = 0)}{V} = \begin{bmatrix} \Upsilon_A^0 & \Upsilon_B^0 \end{bmatrix} \begin{bmatrix} \widetilde{\Gamma}_{AA}^{(2)} - \frac{1}{3}\omega & \widetilde{\Gamma}_{AB}^{(2)} - \frac{1}{3}\omega \\ \widetilde{\Gamma}_{AB}^{(2)} - \frac{1}{3}\omega & \widetilde{\Gamma}_{BB}^{(2)} - \frac{1}{3}\omega \end{bmatrix} \begin{bmatrix} \Upsilon_A^0 \\ \Upsilon_B^0 \end{bmatrix}. \tag{3.56}$$

In other microphases there are more contributions given by Eq. (3.56), because these are superpositions of smectic phases. Each contribution is the same because of symmetry. The eigenvalues of the matrix are positive if there is microphase phase separation. The third and fourth order terms in the Landau free energy may induce nonzero amplitudes Υ_A^0 and Υ_B^0. In that case the global part of the orientation tensor $\Upsilon^{\bar{a}}$ is a secondary order-parameter. This global part is a primary order-parameter in the nematic state. Then at least one of the eigenvalues is negative when ω is greater than the spinodal ω_s. In third and higher order terms of the free energy the amplitudes Υ_A^0 and Υ_B^0 may also induce secondary order parameters for which $q_* \neq 0$. The spinodal ω_s calculated from Eq. (3.56) is identical to the spinodal ω_s in Eq. (3.55) in the limit $q_* \to 0$.

In the following figures below $\chi_s L$ and $\omega_s L$ are investigated with the help of Eq. (3.54) and (3.55). In Fig. (3.10), (3.11) and (3.12) the spinodal $\chi_s L$ is plotted as a function of $f = L_A/L$. In Fig. (3.10) the effective persistence length of the A- and B-block are equal, $\lambda_A/L_A = \lambda_B/L_B$. If $\lambda_A/L_A = 10^{-4}$ the chain can be regarded as flexible and if $\lambda_A/L_A = 10^2$ the chain is very stiff such that it is approximately a rigid rod. We see that the spinodal decreases when the persistence length increases. This is expected because of a smaller entropy loss of stiff diblocks in the phase transition to an inhomogeneous state. In Fig. (3.11) the A- and B-blocks have a different effective persistence length so that the spinodal is asymmetric. The A-block is stiff and the B-block has different values for the bending stiffness. In Fig. (3.12) the B-block is flexible and the bending stiffness of the A-block is varied. In the left part of Fig. (3.12) we see that the spinodal has the lowest value at $\lambda_A/L_A = 10^{-4}$ and is first increasing for greater values of the bending stiffness. This is in contrast with Fig. (3.10). The wave number q_* at the left side of Fig. (3.12) has a larger value when $\lambda_A/L_A = 10^{-4}$. q_* becomes smaller when λ_A/L_A increases. So when the A-block is flexible the A-rich domains in the microphase are small. This is entropically favourable. If the A-block becomes stiffer, the density of the A rich domains decreases. The A-rich domains must become greater and therefore a greater repulsion χ is necessary. When the A-block is stiff enough this effect does not have a great influence on the spinodal any more. At a certain point the spinodal decreases a little

bit when the stiffness is further increased. A similar dependence of $\chi_s L$ on λ_A/L_A can be seen in Fig. (2) in [12].

In Fig. (3.13), (3.14), (3.15) and (3.16) the spinodal $\omega_s L$ has been investigated. In these figures $\omega_s L$ is always minimal at $q_* = 0$ so the melt is in the nematic state when $\omega > \omega_s$. In Fig. (3.13) the spinodal $\omega_s L$ is plotted as a function of λ_A/L_A on logarithmic scale. In this figure $\lambda_A/L_A = \lambda_B/L_B$ and $f = 0.5$. In the left part we see that $\omega_s L$ increases exponentially if the diblock becomes more and more flexible. So in a melt of totally flexible chains nematic ordering is not possible, because $\omega_s L \to \infty$. When the diblock becomes stiffer, in the right part of the figure $\omega_s L$ converges to a lower constant value. We expect this, because stiff diblocks loose a smaller amount of entropy at the transition to the nematic state.

In Fig. (3.14) the spinodal $\omega_s L$ is calculated as a function of f for different values of the bending stiffness of the A-block. The bending stiffness of the A- and B-block is again the same. Below the spinodal line at which $\lambda_A/L_A = 10^{-1}$ there are other lines of stiffer diblock chains. The lines are converging quickly to the line where $\lambda_A/L_A = 10^2$. The spinodal lines are not constant with respect to f. Each line has a maximum at $f = 0.5$. This can be explained by means of the intrinsic mixing entropy of A- and B-monomers of each chain. At $f = 0.5$ each chain has a greater intrinsic mixing entropy in the isotropic state. In the nematic state each chain has become more straight so that the A- and B-monomers are more separated. This lowers the intrinsic mixing entropy and therefore $\omega_s L$ must be greater. In Fig. (3.15) $\omega_s L$ is also calculated as a function of f, but now the A-block is always stiff and the bending stiffness of the B-block is varied. At $f < 0.5$ the B-block is longer and the B-block has a smaller bending stiffness. This explains why the maxima of the spinodals are shifted to the left. In Fig. (3.16) the spinodal $\omega_s L$ has been plotted as a function of χL in which the parameters of the diblock are $f = 0.5$, $\lambda_A/L_A = 10^2$ and $\lambda_B/L_B = 10^{-4}$. The line is truncated at $\chi L = \chi_s L$, because at greater χL a microphase is formed when $\omega = 0$. At lower χL the minimum of $\omega_s L$ is reached at $q_* = 0$. This means that the melt is in the nematic state when $\omega > \omega_s$. $\omega_s L$ does not depend on χ if $q_* = 0$, because the scalar order-parameter Ψ is zero. Therefore $\omega_s L$ is constant at lower χ in the figure. When χ becomes greater a second minimum of $\omega_s L$ arises at $q_* \neq 0$. It becomes lower when χ is increased and a certain χ close to χ_s the two minima are equal. In the right part of the figure in which $\omega_s L$ is not constant the second minimum is the lowest minimum. Then the melt is in the smectic-A state if $\omega > \omega_s$. $\omega_s L$ is decreasing strongly because at a greater χ it is easier to form the smectic-A state. It is not necessary to investigate $\chi_s L$ as a function of ωL. The
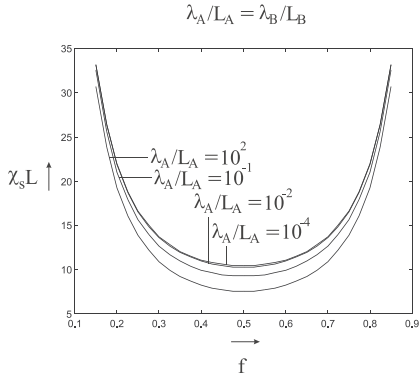
Figure 3.10: The spinodal $\chi_s L$ as a function of f calculated for different λ_A/L_A in which $\lambda_A/L_A = \lambda_B/L_B$.
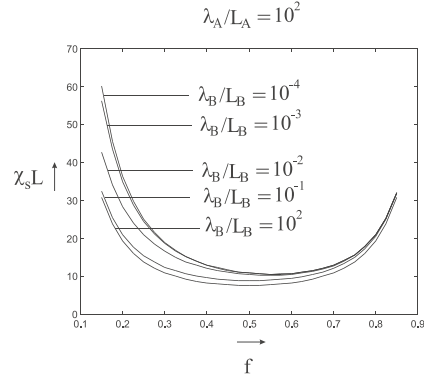
Figure 3.11: The spinodal $\chi_s L$ as a function of f calculated for different λ_B/L_B in which $\lambda_A/L_A = 10^2$.
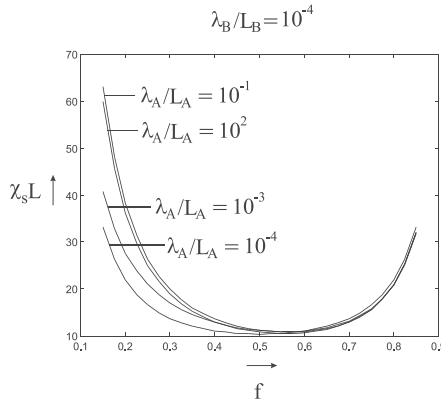
Figure 3.12: The spinodal $\chi_s L$ as a function of f calculated for different λ_A/L_A in which $\lambda_B/L_B = 10^{-4}$.
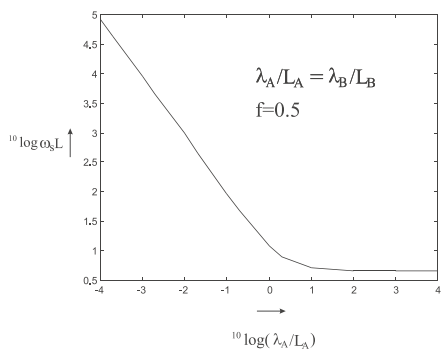
Figure 3.13: The spinodal $\omega_s L$ as a function of λ_A/L_A on logarithmic scale in which $\lambda_A/L_A = \lambda_B/L_B$ and $f = 0.5$.
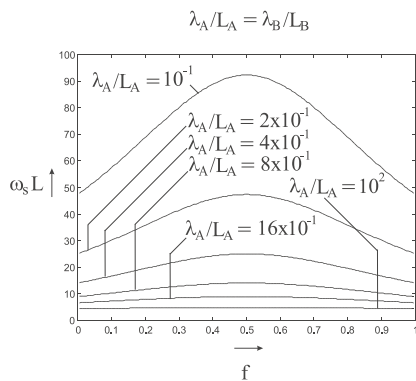
Figure 3.14: The spinodal $\omega_s L$ as a function of f calculated for different λ_A/L_A in which $\lambda_A/L_A = \lambda_B/L_B$.
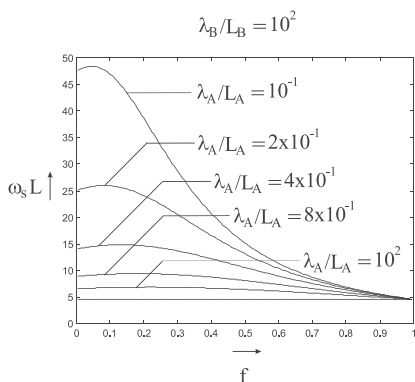
Figure 3.15: The spinodal $\omega_s L$ as a function of f calculated for different λ_A/L_A in which $\lambda_B/L_B = 10^2$.
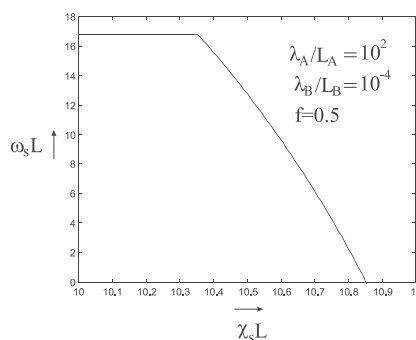
Figure 3.16: The spinodal $\omega_s L$ as a function of $\chi_s L$ in which $\lambda_A/L_A = 10^2$, $\lambda_B/L_B = 10^{-4}$ and $f = 0.5$.

function $\chi_s(\omega)$ appeared to be the inverse function of $\omega_s(\chi)$, because Eq. (3.54) and (3.55) are mathematically equivalent. The dependence of $\omega_s L$ on χL and $\chi_s L$ on ωL also occurs in the results in [12] and in very less degree in [13]. This dependence is caused by the great difference in bending stiffness of the A- and B-block. The nematic interaction ω has a stronger effect on the stiff part which causes a separation of rods and coils. If there is no difference in bending stiffness the nematic interaction ω does not distinguish between A- and B-blocks. Then the dependence of $\omega_s L$ on χL or $\chi_s L$ on ωL does not occur.

In the following table the spinodal $\chi_s L$ has been calculated for rod-rod, coil-coil and rod-coil diblocks with $f = 0.5$. These spinodals are results of our work and from [9–13] to show differences and similarities.

	this thesis	Reenders	Friedel	Matsen	Singh	Holyst-Schick
		[9]	[10]	[11]	[12]	[13]
rod-rod	7.55	–	7.55	6.14	8.30	–
coil-coil	10.49	–	10.49	10.49	10.49	–
rod-coil	10.85	9.09	10.40	–	8.71	9.00

The results according to our theory are in agreement with Friedel's results. Only in the spinodal of the rod-coil diblock there is a difference of 1%. In Matsen [11] the self-consistent field theory is applied which is a different theory compared to the Landau theory applied in this thesis and in [9, 10, 12, 13]. Maybe this has led to a lower $\chi_s L$ for a rod-rod diblock. In Singh's paper the spinodal of a rod-rod chain is greater than in our calculation. In Singh the connected A- and B-rod can still rotate freely with respect to each other while in our calculation the tangent vectors of the A- and B-part are always taken equal at the connection point. This extra degree of freedom gives a greater entropy so a greater $\chi_s L$ is necessary to form a microphase. In the calculation according to Singh, Holyst-Schick and Reenders there are no great differences in the spinodal of a rod-coil diblock, but the spinodal in our and also Friedel's calculation is significantly greater. In our and Friedel's calculation the chain is approximately described by the Bawendi-Freed model [16] which gives additional potentials $\frac{3}{4}u^2(l = 0)$ and $\frac{3}{4}u^2(l = L)$ at the begin- and end point of the chain. In the other papers these terms are missing in the Hamiltonian. Maybe this has led to different results. Such a difference also occurs if our spinodal $\omega_s L$ is compared to the one calculated by Holyst and Schick. For a rigid rod which contains only one kind of monomer $\omega_s L = 5.0$ according to Eq. (5.2) in [13]. The same value can also be read from Fig. (7) in Singh's paper. We find that $\omega_s L = 4.53$.

3.6   Results and discussion of the phase diagram

The theory in the previous sections is applied to calculate the phase diagram of a melt of semi-flexible diblock copolymers. In this section the influence of the stiffness on the phase behaviour is investigated in different systems. In each system the stiffness of the A- and B-block is fixed. We have considered and compared the following possibilities: (a) rod-coil ($\lambda_A/L_A = 10^2 \gg \lambda_B/L_B = 10^{-4}$); (b) semi-coil ($\lambda_A/L_A = 10^{-1} \gg \lambda_B/L_B = 10^{-4}$); (c) semi-semi ($\lambda_A/L_A = 10^{-1} = \lambda_B/L_B$); (d) coil-coil ($\lambda_A/L_A = 10^{-4} = \lambda_B/L_B$). The latter one is selected to compare it with the well-know system investigated by Leibler in [5]. The phase diagram is reproduced correctly.

Before presenting the results one important point has to be clarified. In our model the Maier-Saupe interaction and bending stiffness are described by independent parameters $\omega_{\alpha\beta}$ and λ_α/L_α in which $\alpha, \beta = A$ or B. However, in reality these parameters are related. The Maier-Saupe interaction between two blocks becomes stronger if the blocks become stiffer. In a rod-rod system in which $\lambda_A/L_A \gg 1$ and $\lambda_B/L_B \gg 1$ the parameters $\omega_{\alpha\beta}$ cannot be chosen small, because such a melt would be an unphysical system according to [29] and [30]. In these papers the Onsager model is applied to investigate a solution or melt of liquid-crystalline polymers. According to the Onsager model the isotropic state is not possible in a melt of rigid rods. Due to the excluded volume effect the rods will always align in a melt. In our theory the steric interaction is described by assuming that the melt is incompressible. Due to steric interactions the chains tend to align. The contribution of this alignment force is included in the Maier-Saupe parameters $\omega_{\alpha\beta}$. These parameters also contain contributions of attractive van der Waals forces. According to our theory the isotropic state is possible for every stiffness λ_A/L_A and λ_B/L_B if the parameters $\omega_{\alpha\beta}$ are zero. This means that there is no alignment force which is not possible. Due the excluded volume effect there is always an alignment force so that $\omega_{\alpha\beta} > 0$. If the A- or B-block becomes stiffer and stiffer a lower force is necessary to induce nematic ordering. Then at least one of the parameters $\omega_{\alpha\beta}$ may become greater than the spinodal $\omega_{\alpha\beta,s} = \omega_{\alpha\beta,s}(q_* = 0)$, so that the melt is always in the nematic state. In that case our theory cannot be used to make further predictions of the phase behaviour. Our expression of the Landau free energy can only be applied in the neighbourhood of a phase transition at which the isotropic state is converted into an ordered state. However, according to [29] and [30] in a melt of semi-flexible chains the isotropic state becomes possible if the persistence length λ of the chain is small enough. λ must satisfy the condition $\frac{\lambda}{d} < 50$ in which d is the diameter of the chain. In our theory the length-scale is chosen such that one

monomer occupies one unit of volume, so that the order of magnitude of d is one, $d \approx 1$. In system (c) in which ($\lambda_A/L_A = 10^{-1} = \lambda_B/L_B$) this condition is satisfied, because the diblock length L can be chosen such that $\lambda_A, \lambda_B \leq 10^{-1}L < 50$. Then it is allowed to choose the parameters $\omega_{\alpha\beta}$ such that each $\omega_{\alpha\beta}$ is smaller than the spinodal $\omega_{\alpha\beta,s} = \omega_{\alpha\beta,s}(q_* = 0)$.

In Fig. (3.17), (3.18) and (3.19) the phase diagram of a melt of monodisperse diblock copolymers has been calculated in which the persistence length of the A-block λ_A is much greater than the persistence length of the B-block, $\lambda_A \gg \lambda_B$. λ_B/L_B is taken equal to $\lambda_B/L_B = 10^{-4}$ so that the B-block can be regarded as totally flexible. The A-block is made very stiff, $\lambda_A/L_A = 10^2$, and behaves as a rigid rod. Because the B-block is very flexible the orientation Υ_B has been neglected in the calculation, $\Upsilon_B \approx 0$. Also the influence of the Maier-Saupe parameters ω_{BB} and ω_{AB} is neglected. Only the interaction $\omega_{AA} = \omega$ between stiff A-blocks is taken into account. In Fig. (3.17), (3.18) and (3.19) the ratio $r = \frac{\omega_{AA}}{\chi} = \frac{\omega}{\chi}$ is taken equal to 0, 0.4 and 0.7, respectively. In these figures we can clearly see that the phase behaviour is influenced in different ways by the strength of the nematic interaction ω with respect to χ. The domain of the bcc phase is a very narrow line when $r = 0$. The bcc line becomes broader at a greater r. The domains of the hexagonal and smectic-A phase also become greater. The smectic-C domain is shifted to a greater χ.

To explain the influence of r on the phase behaviour the components $|\Psi_1|$ and $|\Upsilon_1^A|$ in the primary eigenvector $\underline{x}_1 = (\Psi_1, \Upsilon_1^A, \Upsilon_1^B)$ are investigated in Fig. (3.21) in both the smectic-C, smectic-A, hexagonal and bcc phase. In this figure at $f = 0.6$ $|\Psi_1|$ and $|\Upsilon_1^A|$ are calculated as a function of χL at $r = 0, 0.4$ and 0.7 in the different microphase structures. The orientation θ of the smectic-C phase is found by minimizing the Landau free energy with respect to θ. At a lower χL close to the spinodal $\chi_s L$ the minimum is found at $\theta = 0°$ so that the smectic-C line coincides with the smectic-A line in Fig. (3.21). In this figure we see that the density parameter $|\Psi_1|$ in the different microphase structures is ordered according to the sequence,

$$|\Psi_{1,smecC}| \geq |\Psi_{1,smecA}| \geq |\Psi_{1,hex}| \geq |\Psi_{1,bcc}|, \tag{3.57}$$

in which $|\Psi_{1,smecC}|$, $|\Psi_{1,smecA}|$, $|\Psi_{1,hex}|$ and $|\Psi_{1,bcc}|$ denote the density parameters in the smectic-C, smectic-A, hexagonal and bcc phase, respectively. In the same way the orientation strength $|\Upsilon_1^A|$ is ordered by,

$$|\Upsilon_{1,smecC}^A| \geq |\Upsilon_{1,smecA}^A| \geq |\Upsilon_{1,hex}^A| \geq |\Upsilon_{1,bcc}^A|. \tag{3.58}$$

In Fig. (3.21) when r increases both $|\Psi_1|$ and $|\Upsilon_1^A|$ becomes lower in each microphase structure. So the Maier-Saupe interaction counteracts microphase separation. This
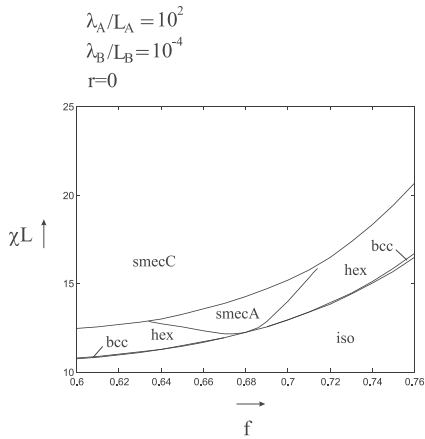
Figure 3.17: Phase diagram of a rod-coil diblock in which $r = 0$.
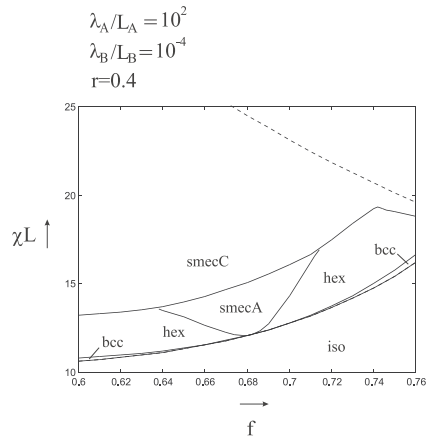
Figure 3.18: Phase diagram of a rod-coil diblock in which $r = 0.4$.
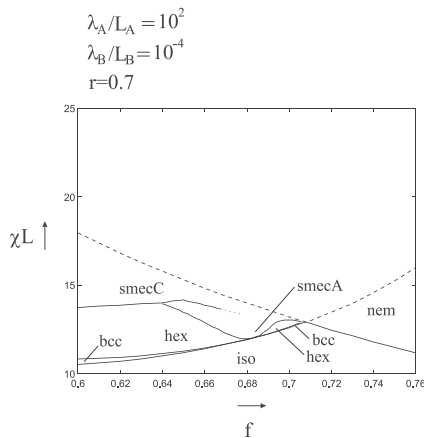
Figure 3.19: Phase diagram of a rod-coil diblock in which $r = 0.7$.

effect is also observed in the phase diagrams in Fig. (3.17), (3.18) and (3.19). The bcc and hexagonal domain become greater at a greater r and the domain of smectic-A and smectic-C phase are shifted to a greater χL. By means of Eq. (3.57) and (3.58) it can be concluded that the melt prefers a microphase with a lower $|\Psi_1|$ and $|\Upsilon_1^A|$ when r increases. The decrement of $|\Upsilon_1^A|$ is contrary to what we would expect, because a

strong Maier-Saupe interaction will induce a nematic state. The parameter $|\Upsilon_1^A|$ is the strength of a space dependent orientation. In the nematic state there is global alignment of stiff A-blocks with strength $|\Upsilon_{10}^A|$. A nonzero $|\Upsilon_{10}^A|$ is also induced in a microphase, but is very weak. The secondary eigenvector $\underline{x}_{10} = (\Upsilon_{10}^A, \Upsilon_{10}^B) \approx (\Upsilon_{10}^A, 0)$ contains a global orientation Υ_{10}^A. The secondary parameter $x_{10} = \pm|\underline{x}_{10}| \approx \pm|\Upsilon_{10}^A|$ is given by Eq. (3.14) in which $n = 10$,

$$x_{10} = \frac{-C_{11,10}^{(3)} x_1^2}{2\lambda_{10}} + O(x_1^3). \tag{3.59}$$

If the Maier-Saupe interaction increases the positive eigenvalue λ_{10} becomes lower which enhances the global orientation $|\Upsilon_{10}^A|$. This parameter increases strongly if $\omega_{\alpha\beta}$ reaches the spinodal $\omega_{\alpha\beta,s}(q_* = 0)$, because then $\lambda_{10} \downarrow 0$. In the bcc phase a global nematic ordering cannot be induced so that $|\Upsilon_{10,bcc}^A| = 0$.

In Fig. (3.18) and (3.19) there is a dashed line at which $\omega_{AA} = \omega = \omega_s(q_* = 0)$ or $\chi = \chi_s(q_* \neq 0)$. In Fig. (3.19) at $f = 0.71$ both $\omega = \omega_s(q_* = 0)$ and $\chi = \chi_s(q_* \neq 0)$ in the dashed line. At that point the eigenvalues λ_1 and λ_{10} in Eq. (3.11) are zero so that both microphase separation and nematic ordering become possible. Then the final form given by Eq. (3.15) cannot be applied at a greater χ. Here only the eigenvalue λ_1 is negative which makes it possible to write the free energy in a power series expansion of only one primary parameter x_1. If both eigenvalues λ_1 and λ_{10} are negative there are two primary parameters x_1 and x_{10}. Then the final form of the free energy becomes,

$$\begin{aligned}
\frac{F_L}{V} = \min_{\{x_1, x_{10}\}} \{ &\lambda_1 x_1^2 + \lambda_{10} x_{10}^2 + C_{111}^{(3)} x_1^3 + C_{11,10}^{(3)} x_1^2 x_{10} + C_{10,10,10}^{(3)} x_{10}^3 + \\
&\widetilde{C}_{1111}^{(4)} x_1^4 + \widetilde{C}_{111,10}^{(4)} x_1^3 x_{10} + \widetilde{C}_{11,10,10}^{(4)} x_1^2 x_{10}^2 + \widetilde{C}_{10,10,10,10}^{(4)} x_{10}^4 \},
\end{aligned} \tag{3.60}$$

in which the coefficients of the fourth order terms contain contributions from sec-

ondary eigenvectors $\underline{x}_2$, $\underline{x}_3$ and $\underline{x}_{20}$,

$$\widetilde{C}_{1111}^{(4)} = C_{1111}^{(4)} - \sum_{n \neq 1,10} \frac{(C_{11n}^{(3)})^2}{4\lambda_n}, \tag{3.61a}$$

$$\widetilde{C}_{111,10}^{(4)} = C_{111,10}^{(4)} - \frac{C_{11,2}^{(3)} C_{1,10,2}^{(3)}}{2\lambda_2} - \frac{C_{11,3}^{(3)} C_{1,10,3}^{(3)}}{2\lambda_3}, \tag{3.61b}$$

$$\widetilde{C}_{11,10,10}^{(4)} = C_{11,10,10}^{(4)} - \frac{(C_{1,10,2}^{(3)})^2}{4\lambda_2} - \frac{(C_{1,10,3}^{(3)})^2}{4\lambda_3} - \frac{C_{11,20}^{(3)} C_{10,10,20}^{(3)}}{2\lambda_{20}}, \tag{3.61c}$$

and

$$\widetilde{C}_{10,10,10,10}^{(4)} = C_{10,10,10,10}^{(4)} - \frac{(C_{10,10,20}^{(3)})^2}{4\lambda_{20}}. \tag{3.61d}$$

Numerically it appears that in each kind of microphase structure the coefficient $C_{1111}^{(4)}$ in Eq. (3.15) and (3.61a) becomes negative if χ becomes too great. $C_{1111}^{(4)}$ is always positive if χ is close enough to χ_s. Here the mean field approximation is more reliable. However, the coefficient $C_{10,10,10,10}^{(4)}$ in Eq. (3.61d) is always negative so that in Eq. (3.60) $\widetilde{C}_{10,10,10,10}^{(4)} x_{10}^4 < 0$. In that case the free energy given by Eq. (3.60) cannot have a finite minimum. Higher order terms would be necessary to compensate the negative contribution. These terms are very complicated and will not be calculated. So above the dashed line in Fig. (3.18) and (3.19) the phase behaviour cannot be predicted by means of Eq. (3.60). Because below the dashed line a smectic-C state is found, we also expect a layered structure above that line. In this structure the orientation tensor $\underline{\underline{Q}}_\alpha(\underline{x})$ is spatially dependent, but contains a stronger global component $\underline{\underline{Q}}_\alpha^0$, because $\lambda_{10} < 0$. In this way the spatial average $\left\langle \underline{\underline{Q}}_\alpha(\underline{x}) \right\rangle$,

$$\left\langle \underline{\underline{Q}}_\alpha(\underline{x}) \right\rangle = \frac{1}{V} \int_V d^3x \underline{\underline{Q}}_\alpha(\underline{x}) = \underline{\underline{Q}}_\alpha^0, \tag{3.62}$$

is nonzero. If $\omega < \omega_s(q_* = 0)$ there is also global nematic ordering possible in addition to the spatially dependent orientation. In that part of the phase diagram the global orientation x_{10} is a secondary parameter which is expressed by Eq. (3.59),

$$x_{10} = \frac{-C_{11,10}^{(3)} x_1^2}{2\lambda_{10}} + O(x_1^3). \tag{3.63}$$

$$\lambda_A/L_A = 10^2$$
$$\lambda_B/L_B = 10^{-4}$$
$$f = 0.6$$
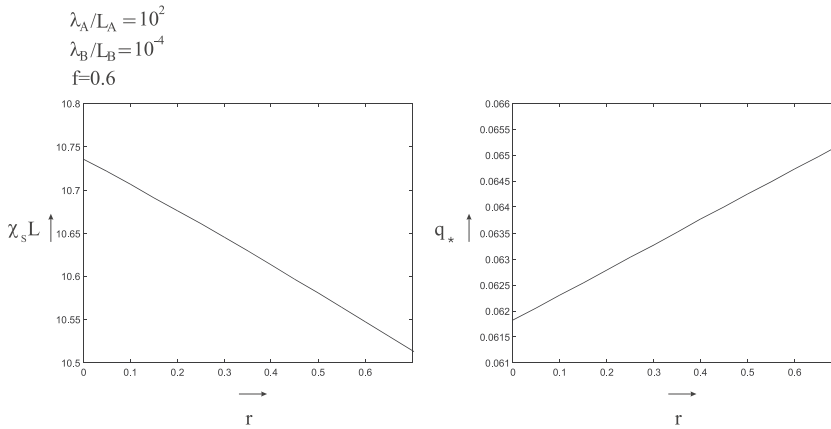
Figure 3.20: The wave mode q_* and the spinodal $\chi_s L$ as a function of r in a rod-coil diblock melt in which $f = 0.6$.

If $\lambda_{10} \gg 0$ this orientation is very weak, but when $\lambda_{10} \downarrow 0$ it becomes stronger. If it is too strong the expression of the Landau free energy given by Eq. (3.15) is not reliable.

In the right part of Fig. (3.18) the boundary line between the smectic-C and hexagonal domain has a nod at $f = 0.74$. At this point the angle θ at the boundary changes discontinuously from $12.9°$ to $89.9°$ when f is increasing. In the right part of Fig. (3.18) the smectic-C domain is close to the dashed line. Here the induced global nematic ordering given by Eq. (3.63) becomes stronger, because $\lambda_{10} \downarrow 0$. In the fourth order term in Eq. (3.15) this nematic ordering gives a great contribution. Due to this effect the minimum at $\theta = 89.9°$ has become the lowest minimum. In Fig. (3.19) at $f = 0.65$ such a nod is also found at which θ changes discontinuously. At this nod when f is increasing θ jumps from $13°$ to $89.9°$. At $f = 0.67$ the boundary line has been stopped and is extended by a dotted line. At $f > 0.67$ the eigenvalue λ_{10} in Eq. (3.11) is too close to zero so that the fourth order term has become negative. Here the phase behaviour cannot be predicted. However, reliable predictions can also not be made if the fourth order term is still positive but close to zero. Then Eq. (3.15) is also not reliable.

In Fig. (3.20) the spinodal $\chi_s L$ and the corresponding wave mode q_* are plotted as a function of the ratio r at $f = 0.6$ for a rod-coil diblock. When r increases $\chi_s L$ becomes lower due to the stronger Maier-Saupe interaction. This effect has also

been observed in section 3.5. It is caused by the great difference in bending stiffness between the A- and B-block. If the A- and B-block have the same bending stiffness the influence of the Maier-Saupe interaction on the spinodal $\chi_s L$ and the wave mode q_* is negligible. When r becomes greater q_* is increasing which means that the size of the A- and B-rich domains becomes smaller. A smaller domain size increases the total contact area between A- and B-blocks in the whole melt. This could explain why in Fig. (3.21) $|\Psi_1|$ and $|\Upsilon_1^A|$ are lowered when r increases. A weaker microphase separation increases the mixing entropy, but the enthalpic contribution $\widetilde{\chi}_{ab} \Psi^a \Psi^b$ in Eq. (3.5) becomes lower. At $r = 0$ the wave length $\frac{2\pi}{q_*}$ is maximal and a microphase cannot be formed at a smaller wave length. If the domain size becomes smaller the enthalpic contribution $\widetilde{\chi}_{ab} \Psi^a \Psi^b$ becomes too weak and cannot be compensated by an increment of the mixing entropy. However, when the Maier-Saupe interaction is switched on the enthalpic contribution $\frac{1}{2}\omega_{\overline{ab}} \Upsilon^{\overline{a}} \Upsilon^{\overline{b}}$ in Eq. (3.5) gives an additional compensation. This additional compensation could make it possible to form a microphase with a smaller domain size. Therefore in Fig. (3.20) q_* increases when r becomes greater. In the same way it can be explained why $\chi_s L$ is lowered by a stronger Maier-Saupe interaction.

In Fig. (3.22) the angle θ in degrees is calculated as a function of χL at $r = 0$ and 0.4 when $f = 0.68$. If $r = 0.7$ the angle θ of the smectic-C state cannot be investigated, because the fourth order term in Eq. (3.11) is negative for certain angles θ. At the phase transition point at $f = 0.68$ just above the spinodal the smectic-A state is formed. When χ becomes greater at a certain point the smectic-A state is converted into the smectic-C state. At the transition we see in Fig. (3.22) that the angle θ changes discontinuously from $\theta = 0°$ to a nonzero θ. After the transition when χ is further increased the angle θ increases and converges to a constant value. At a greater χ the function $\theta(\chi L)$ cannot be further drawn, because the coefficient $C_{1111}^{(4)}$ in Eq. (3.11) becomes negative. From Fig. (3.17), (3.18), (3.19), (3.20) and (3.21) it has been concluded that the Maier-Saupe interaction counteracts microphase separation. This may also explain the influence of ω in the smectic structure observed in Fig. (3.22). When the nematic interaction ω is switched on the transition from smectic-A to smectic-C takes place at a greater χ. At the same time the angle θ in the smectic-C state has become smaller.

In Fig. (3.24), (3.25) and (3.26) the phase diagram is calculated in which the persistence length of the A-block λ_A is again much greater than the persistence length of the B-block, $\lambda_A \gg \lambda_B$. In the previous phase diagrams the A-block is made very stiff such that it can be regarded as a rigid rod. In Fig. (3.24), (3.25) and (3.26)

$\lambda_A/L_A = 10^2$
$\lambda_B/L_B = 10^{-4}$
$f = 0.6$
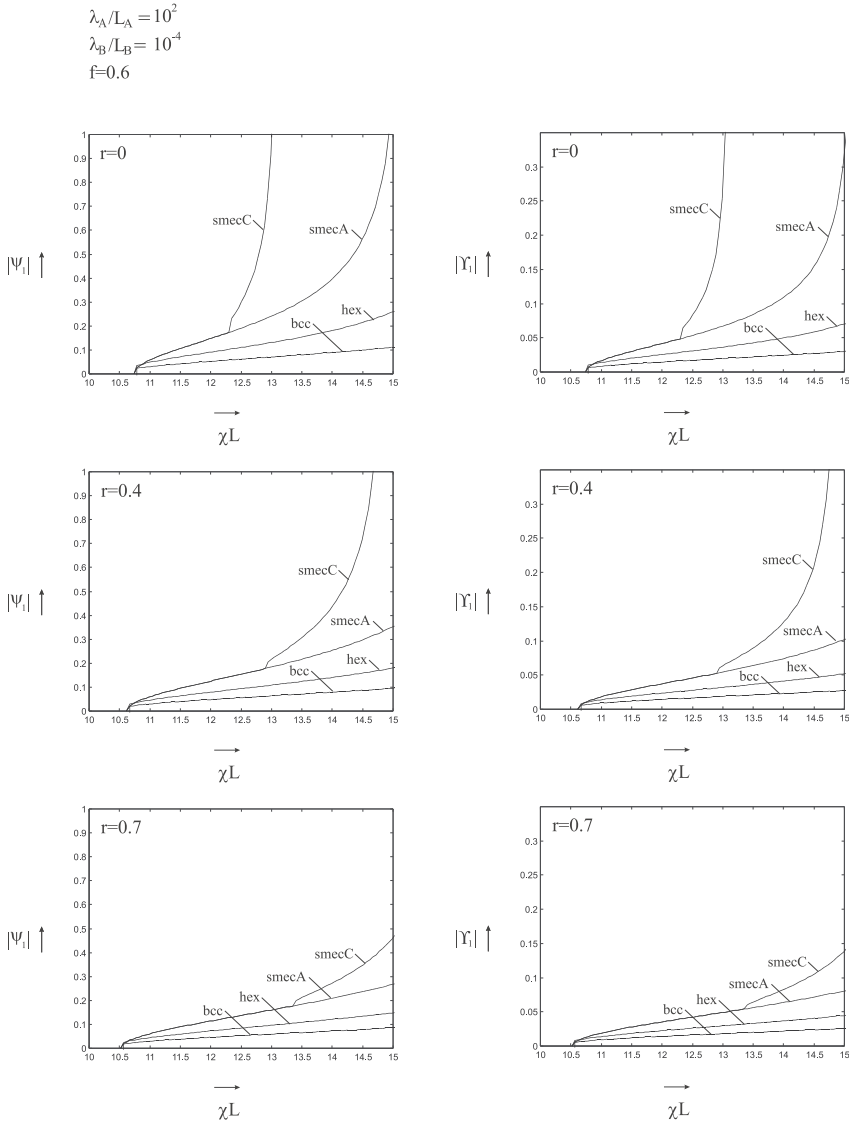
Figure 3.21: Components $|\Psi_1|$ and $|\Upsilon_1^A|$ calculated as a function of χL at $f = 0.6$ and $r = 0$, 0.4 and 0.7 in different microphase structures for a rod-coil diblock melt.
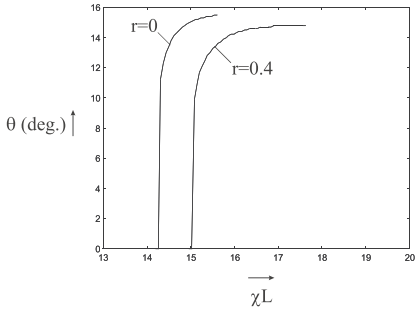
Figure 3.22: The orientation angle θ in the smectic-C phase as a function of χL of a rod-coil diblock at $f = 0.68$.
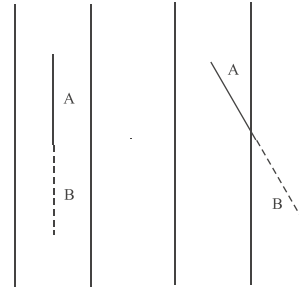
Figure 3.23: Orientation of an A-block in the middle of an A-rich layer in the smectic-A and smectic-C phase.

the stiffness of the A-block is made lower, $\lambda_A/L_A = 10^{-1}$. Here the A-block is called semi-flexible. The stiffness is such that it does not behave as a rigid rod or a Gaussian chain. The B-block is again totally flexible, $\lambda_B/L_B = 10^{-4}$. Therefore the orientation Υ_B has been neglected in the calculation, $\Upsilon_B \approx 0$, so that the Maier-Saupe parameters ω_{BB} and ω_{AB} are excluded. In Fig. (3.24), (3.25) and (3.26) the ratio $r = \frac{\omega_{AA}}{\chi} = \frac{\omega}{\chi}$ is taken equal to 0, 3 and 5, respectively. In the dashed line $\omega = \omega_s(q_* = 0)$ or $\chi = \chi_s(q_* \neq 0)$. If the parameter r is increased we see that the bcc region becomes broader which is also observed in Fig. (3.17), (3.18) and (3.19). The smectic-C phase is not formed at $r = 0$ when $f > 0.706$. The dotted line is an extension of the calculated solid line. When r increases the smectic-C domain is shifted to a lower χ which makes the hexagonal and smectic-A part smaller. Only very close to the phase transition point the size of the hexagonal part increases a little bit. Here the influence of r on the phase behaviour is the same as in the previous phase diagrams and can be explained in the same way. However, the influence of r on the smectic-C domain is different. The angle θ in the previous phase diagrams is within the interval $8° < \theta < 18°$ and depends on the parameters χ, r and f. In Fig. (3.24), (3.25) and (3.26) in the smectic-C phase the angle θ is constant, $\theta = 54.7°$. Exactly at $\theta = 54.7°$ the director $\underline{n}$ is such that $n_x^2 - \frac{1}{3} = \cos^2\theta - \frac{1}{3} = 0$. Then in the smectic-C state the tensor component $\Upsilon_A^{xx}(\underline{x})$ vanishes, $\Upsilon_A^{xx}(\underline{x}) = 0$. This means that orientation of A-blocks is random in the x-direction. Because $\Upsilon_A^{xx}(\underline{x}) = 0$ the components $\Upsilon_A^{zz}(\underline{x})$ and $\Upsilon_A^{yy}(\underline{x})$ are compensating each other, $\Upsilon_A^{zz}(\underline{x}) = -\Upsilon_A^{yy}(\underline{x})$. So if $\theta = 54.7°$ the orientation direction in an A-rich layer is perpendicular to the orientation in a B-

$\lambda_A/L_A = 10^{-1}$
$\lambda_B/L_B = 10^{-4}$
r=0

$\lambda_A/L_A = 10^{-1}$
$\lambda_B/L_B = 10^{-4}$
r=3
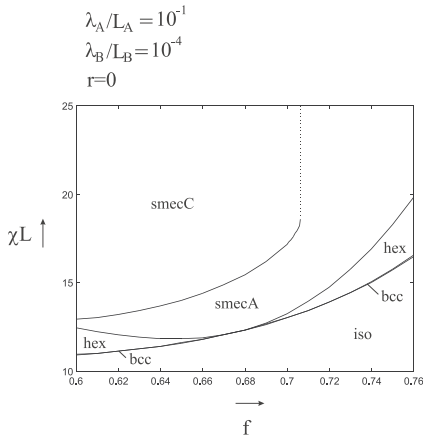
Figure 3.24: Phase diagram of a semi-coil diblock in which $r = 0$.
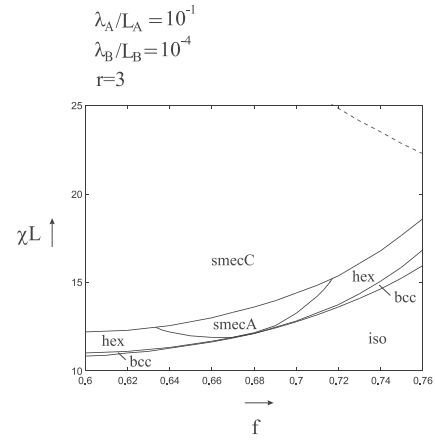
Figure 3.25: Phase diagram of a semi-coil diblock in which $r = 3$.

$\lambda_A/L_A = 10^{-1}$
$\lambda_B/L_B = 10^{-4}$
r=5
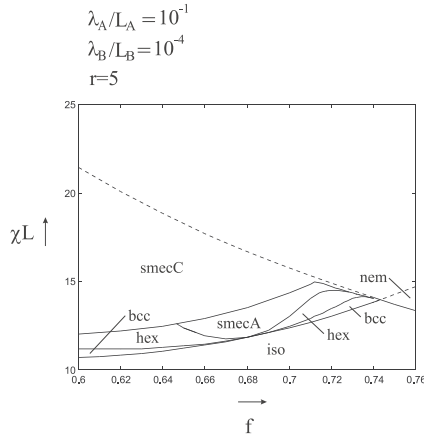
Figure 3.26: Phase diagram of a semi-coil diblock in which $r = 5$.

rich layer. From numerical calculations it appears that such a state is not formed. If $\theta = 54.7°$ it appears that in the primary eigenvector $\underline{x}_1 = (\Psi_1, \Upsilon_1^A, \Upsilon_1^B)$ the component Υ_1^A becomes zero, so that $\underline{x}_1 = (\Psi_1, 0, 0)$. Only in the secondary eigenvectors a nonzero orientation of A-blocks is possible. The contribution of these vectors is negligibly small so if $\theta = 54.7°$ the smectic-C state can be regarded as a lamellar

state with only a nonzero scalar order-parameter.

This effect does not only occur in Fig. (3.24), (3.25) and (3.26). In other kinds of diblocks it also appears that when $\theta = 54.7°$ the primary eigenvector is $\underline{x}_1 = (\Psi_1, 0, 0)$ for each χ and $\omega_{\alpha\beta}$. If $\theta \neq 54.7°$ there is always some orientation Υ_1^A or Υ_1^B if the persistence length of the A- or B-block is great enough. The alignment is such that the A-B contact is as small as possible. Without orientation the A- and B-blocks may have more contact which is enthalpically less favourable. However, the entropy of the melt is higher without orientation. Maybe the enthalpy gain due to the alignment has a greater effect and compensates the entropy loss.

To explain the influence of r on the phase behaviour the parameters $|\Psi_1|$ and $|\Upsilon_1^A|$ are calculated again as a function of χ at $f = 0.6$ and $r = 0, 2.5$ and 5 in Fig. (3.27). In this figure in the smectic-C phase the orientation θ is taken equal to $\theta = 54.7°$. The orientation strength $|\Upsilon_1^A|$ of the smectic-C phase is not drawn in Fig. (3.27), because in this state $|\Upsilon_1^A| = 0$ when $\theta = 54.7°$. In Fig. (3.27) we see that the density parameter $|\Psi_1|$ in the different microphase structures is also ordered according to Eq. (3.57),

$$|\Psi_{1,smecC}| \geq |\Psi_{1,smecA}| \geq |\Psi_{1,hex}| \geq |\Psi_{1,bcc}|, \qquad (3.64)$$

but the orientation strength $|\Upsilon_1^A|$ is ordered differently,

$$|\Upsilon_{1,smecA}^A| \geq |\Upsilon_{1,hex}^A| \geq |\Upsilon_{1,bcc}^A| \geq |\Upsilon_{1,smecC}^A| = 0. \qquad (3.65)$$

Here the orientation strength $|\Upsilon_{1,smecC}^A|$ in the smectic-C phase is zero. Therefore in Fig. (3.27) the density parameter $|\Psi_{1,smecC}|$ does not change very much when r increases. $|\Psi_{1,smecA}|$, $|\Psi_{1,hex}|$ and $|\Psi_{1,bcc}|$ become lower at a greater r. The influence of the Maier-Saupe interaction on $|\Upsilon_1^A|$ in the different microphase structures is not very great. From Eq. (3.64) and Fig. (3.24), (3.25) and (3.26) it can be concluded that close to the spinodal $\chi_s L$ the melt prefers a microphase with a lower $|\Psi_1|$ when r increases. Here microphase separation is counteracted by the Maier-Saupe interaction. However, at a greater χL the smectic-C phase is formed in which $|\Psi_1|$ is maximal according to Eq. (3.64). In this phase the Maier-Saupe interaction cannot have much influence on the microphase separation because there is no space dependent orientation, $|\Upsilon_{1,smecC}^A| = 0$. Only a very weak global orientation $|\Upsilon_{10}^A| = |x_{10}|$ given by Eq. (3.59) is possible which increases at a greater r. In the other microphases $|\Psi_1|$ is lowered by r. Then the smectic-C phase becomes more favourable because of the separation enthalpy. This could explain why the smectic-C domain is shifted to a lower χL when r becomes greater. So further away from the spinodal $\chi_s L$ the Maier-Saupe interaction enhances microphase separation by forming a smectic-C state with a greater density parameter $|\Psi_1|$.

$\lambda_A/L_A = 10^{-1}$
$\lambda_B/L_B = 10^{-4}$
$f=0.6$
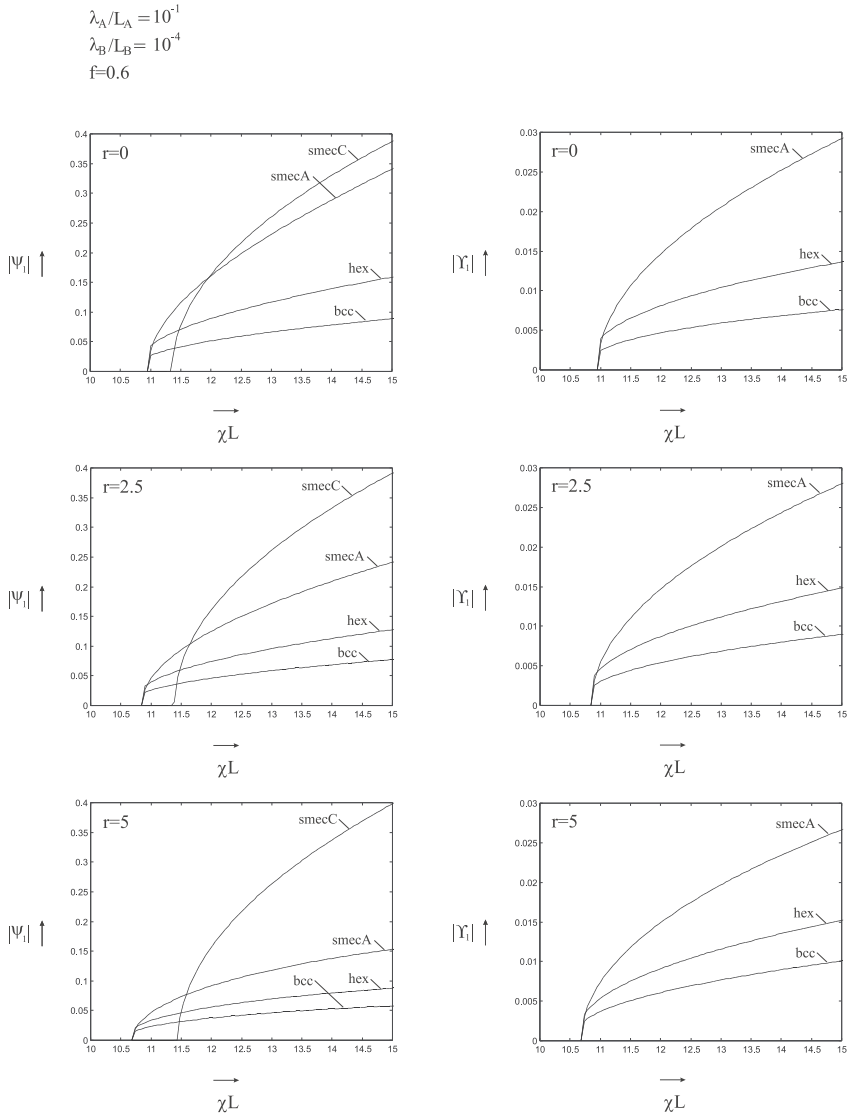
Figure 3.27: Components $|\Psi_1|$ and $|\Upsilon_1^A|$ calculated as a function of χL at $f = 0.6$ and $r = 0$, 2.5 and 5 in different microphase structures for a semi-coil diblock melt.
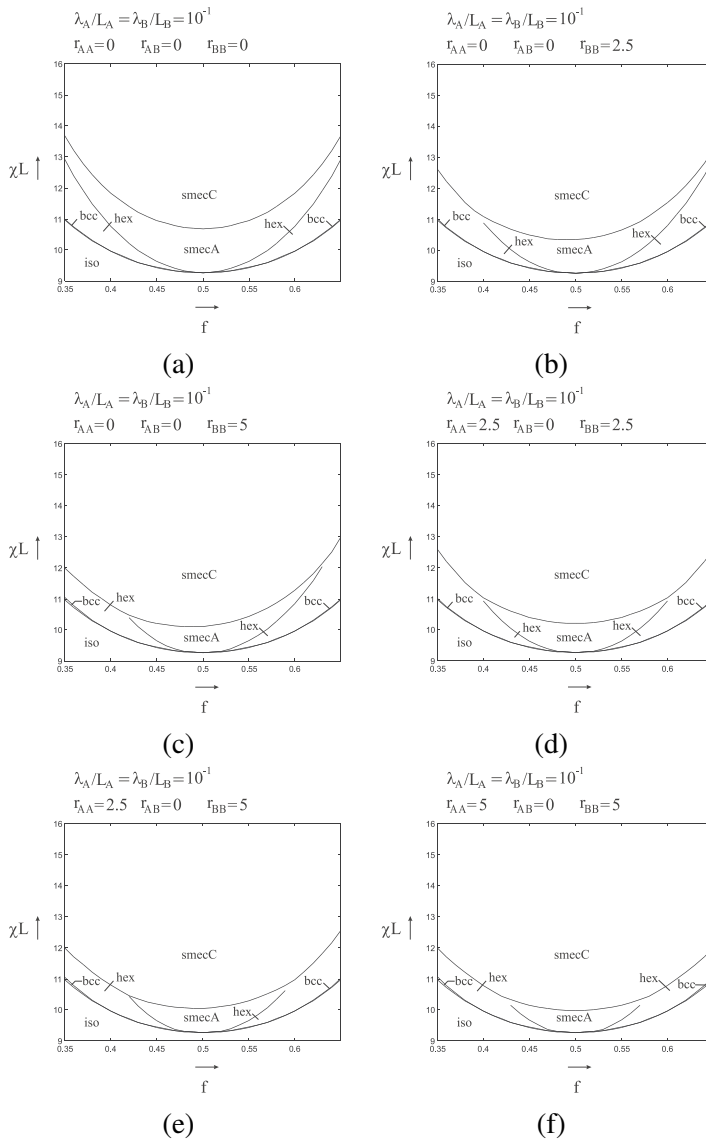
Figure 3.28: Phase diagrams of a semi-semi diblock in which $r_{AB} = 0$ and the other parameters r_{AA} and r_{BB} are varied
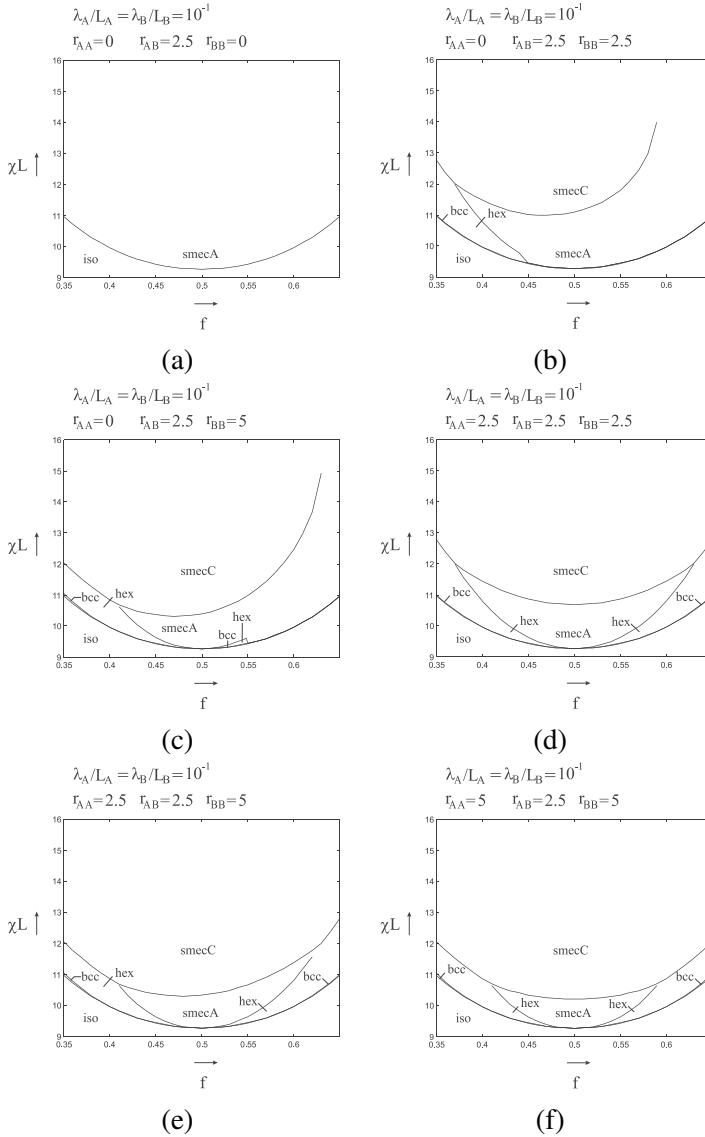
Figure 3.29: Phase diagrams of a semi-semi diblock in which $r_{AB} = 2.5$ and the other parameters r_{AA} and r_{BB} are varied.
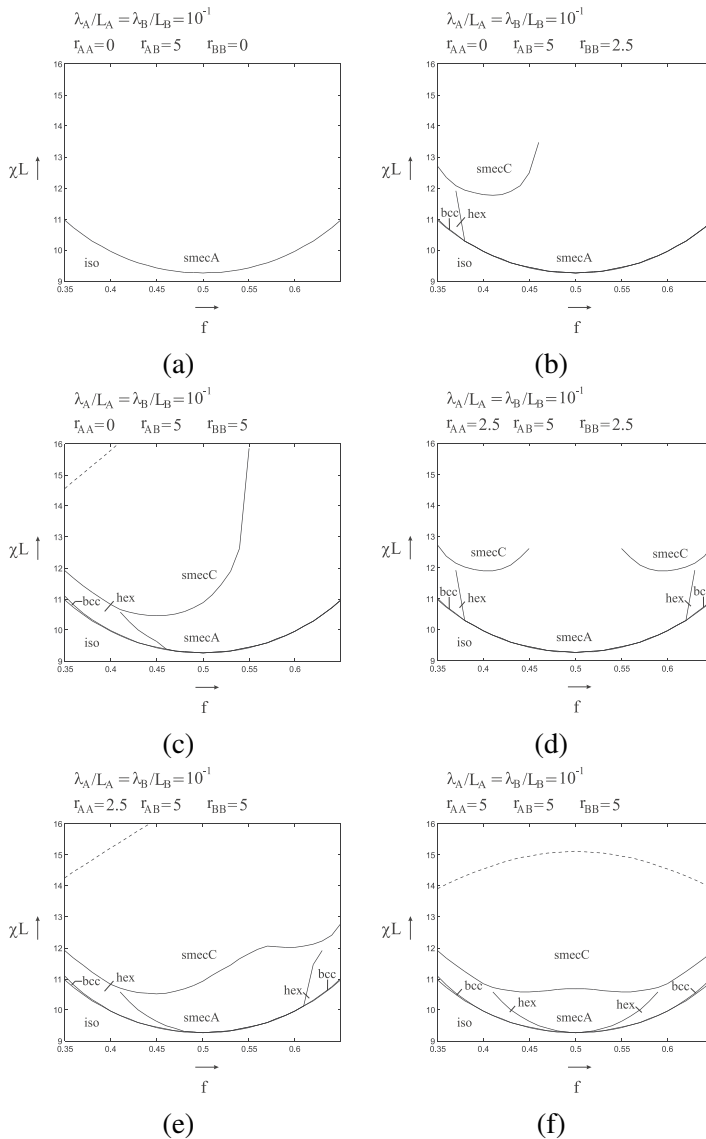
Figure 3.30: Phase diagrams of a semi-semi diblock in which $r_{AB} = 5$ and the other parameters r_{AA} and r_{BB} are varied.

In Fig. (3.28a) till (3.30f) the phase diagram has been determined in which both the A- and B-block are semi-flexible, $\frac{\lambda_A}{L_A} = \frac{\lambda_B}{L_B} = 10^{-1}$. In the previous phase diagrams it was justified to neglect the orientation of the B-block Υ_B, because the B-block is totally flexible. However in Fig. (3.28a) till (3.30f) both the A- and B-block are semi-flexible so that both orientations Υ_A and Υ_B have to be taken into account. Not only the Maier-Saupe parameter ω_{AA} influences the phase behaviour, but also the other parameters ω_{AB} and ω_{BB} may change the structure of the melt. In Fig. (3.28a) till (3.30f) it has been investigated how the phase behaviour is influenced by the three parameters ω_{AA}, ω_{AB} and ω_{BB}. In these figures the Maier-Saupe parameters are coupled to the Flory-Huggins interaction χ by choosing each ratio $r_{\alpha\beta} = \frac{\omega_{\alpha\beta}}{\chi}$ constant. In Fig. (3.28a) till (3.30f) the three parameters $r_{\alpha\beta}$ can have three different values 0, 2.5 and 5 which gives 18 different combinations if we choose $r_{AA} \leq r_{BB}$. Because of symmetry it is not necessary to consider combinations in which $r_{AA} > r_{BB}$. In the first six figures the interaction r_{AB} is always zero and the other parameters r_{AA} and r_{BB} are varied. In the second and third set of six figures $r_{AB} = 2.5$ and 5, respectively, and r_{AA} and r_{BB} are varied in the same way. In the dashed line in Fig. (3.30f) and other figures at least one of the parameters $\omega_{\alpha\beta}$ is equal to the spinodal $\omega_{\alpha\beta}(q_* = 0)$. Above the dashed line the phase behaviour cannot be predicted. If we compare Fig. (3.28a) and (3.28b) we see in Fig. (3.28b) that the smectic-C domain is shifted to a lower χ. The parameter has also a very small influence on the bcc line and the hexagonal domain which cannot be seen in Fig. (3.28b). The bcc line becomes broader and in the neigbourhood of the phase transition point the size of the hexagonal domain increases. In Fig. (3.28c) r_{BB} is greater which gives a greater change in the phase behaviour. The influence of r_{BB} is greater in the left part of the phase diagram, because here the B-block is longer. In the same way the parameter r_{AA} influences the phase behaviour in the right part of the phase diagram which can be seen in Fig. (3.28d) till (3.28f). In the figures in which $r_{AB} \neq 0$ we see the same effect if r_{AA} and r_{BB} are changed. The parameter r_{AB} has the contrary effect. If r_{AB} is increased the size of the bcc and hexagonal domain becomes smaller and the smectic-A part becomes greater. The smectic-C part is shifted to a greater χL. The influence of r_{AB} is stronger in the neighbourhood of $f = 0.5$, because here more interaction between A- and B-blocks is possible. In Fig. (3.29a) and (3.30a) $r_{AA} = r_{BB} = 0$ so that the influence of r_{AB} is very strong. Here the bcc, hexagonal and smectic-C phase have even disappeared and only the smectic-A phase is formed when $\chi L > \chi_s L$. In the other phase diagrams in Fig. (3.28a) till (3.30f) the effect of r_{AB} is compensated by the contrary effect of r_{AA} or r_{BB}. This can be illustrated by means of Fig. (3.28a), (3.29d) and (3.30f) in
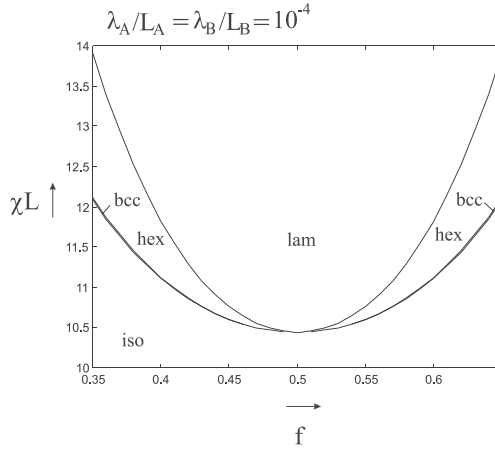
Figure 3.31: Phase diagram of a coil-coil diblock.

which the three r-parameters are equal, $r_{AA} = r_{AB} = r_{BB}$. In each of these figures at $f = 0.5$ the smectic-C state is formed at exactly the same Flory-Huggins strength $\chi L = 10.69$. Here the influence of r_{AB} is exactly compensated by r_{AA} and r_{BB}.

In the smectic-C state in Fig. (3.28a) till (3.30f) the orientation θ is $\theta = 54.7°$ which is the same as in Fig. (3.24), (3.25) and (3.26). Then in the primary eigenvector $\underline{x}_1 = (\Psi_1, \Upsilon_1^A, \Upsilon_1^B)$ the orientation parameters Υ_1^A and Υ_1^B are zero, $\Upsilon_1^A = \Upsilon_1^B = 0$. The influence of r_{AA} and r_{BB} on the phase behaviour is the same as the influence of r observed in Fig. (3.24), (3.25) and (3.26) and can be explained in the same way. The parameter r_{AB} has a contrary effect on the microphase structure of the melt which is rather obvious.

In Fig. (3.31) the phase diagram has been determined in which both the A- and B-block have a persistence length close to zero, $\frac{\lambda_A}{L_A} = \frac{\lambda_B}{L_B} = 10^{-4}$. Here the diblock chain can be regarded as totally flexible. In the general expression of the Landau free energy given by Eq. (3.5) the terms which contain an orientation tensor $\Upsilon^{\bar{a}}$ will disappear if the persistence length of each block approaches zero. Therefore it is justified to neglect the orientation and write the Landau free energy as a function of only the scalar order-parameter Ψ^a. In this way the phase diagram in Fig. (3.31) is calculated which is in agreement with Leibler's result in [5].

In Fig. (3.28a) till (3.30f) and (3.31) the phase transition point in the phase diagram is found at $f = f_c = 0.5$, but in Fig. (3.17), (3.18), (3.19), (3.24), (3.25) and

(3.26) f_c has been shifted to $f_c = 0.68$. If $f < f_c$ the bcc and hexagonal phase are formed by A-rich domains which prefer to be embedded by a B-rich matrix. The size of the embedded A-rich domains increases when the length L_A becomes greater. At $f > f_c$ the size is too great and therefore the melt prefers the reverse state in which the B-blocks are embedded by a matrix of A-blocks. Exactly at the phase transition point the probability that an A-block is inside the matrix is the same as the probability to be outside the matrix. Then a nonzero density order-parameter Ψ is not possible. Only the smectic-A or C state can be formed at the phase transition point. In Fig. (3.28a) till (3.30f) and (3.31) the A- and B-block have the same ratio λ_α/L_α, so that at $f = 0.5$ the A- and B-block are mathematically identical. This explains why the phase transition point is reached at $f = 0.5$. The phase transition point in Fig. (3.17), (3.18), (3.19), (3.24), (3.25) and (3.26) is shifted to $f = 0.68$ at which the stiffer A-block is longer than the flexible B-block. So the stiffer A-block prefers to be embedded by a matrix of flexible B-blocks in a greater domain of the phase diagram. The stiffness of the A-block makes it difficult to form an A-rich matrix. The number of possible melt configurations could be greater if a matrix of flexible B-blocks is formed. Even if the B-block is shorter than the A-block more melt configurations could still be possible because of the great flexibility of the B-blocks. Only if the B-block becomes too short the melt prefers to form the reverse state.

In each phase diagram in this section the smectic-A state is formed prior to the smectic-C state when χ is increasing. By means of Fig. (3.23) it is explained why the A- and B-blocks could be separated easier in the smectic-C state. In Fig. (3.23) an A-block in the the middle of an A-rich layer is drawn in the smectic-A and C state. In the smectic-A phase in the middle of a B-rich layer the A-blocks are stronger aligned along the wave vector q, but in the middle of an A-rich layer there are on average some more A-blocks which are oriented perpendicular to q. This will also bring some more B-blocks to the middle of the A-rich layer which will make the separation between A- and B-blocks weaker. So in the smectic-A phase only a weak separation is possible. In the smectic-C phase in Fig. (3.23) the A-block is rotated which will remove the B-block from the middle of the A-rich layer. Then a stronger separation becomes possible. Additionally the smectic-A state is rotational symmetric with respect to an arbitrary axis perpendicular to the layers. The smectic-C state does not have this symmetry and is therefore entropically less favourable. This entropy loss must also be compensated by a greater χ. This also may explain why the smectic-C phase is always formed at a greater χ.

Close to the order-disorder phase transition just above the spinodal χ_s the bcc

phase is always formed prior to the hexagonal phase when χ is increasing and the hexagonal phase appears prior to a smectic-A or -C state. These sequence of microphase structures in the phase diagram is strongly determined by total contact area between A-rich and B-rich domains in the whole melt. The contact areas A_{bcc}, A_{hex} and A_{smec} of the bcc, hexagonal and smectic phase are related as $A_{bcc} : A_{hex} : A_{smec} = 3 : 2 : 1$. At a lower χ the melt prefers a microphase with a greater contact area so that the mixing entropy is greater. At a greater χ a state with a smaller contact area is formed which is favourable because of the separation enthalpy.

3.7 Concluding remarks

The general theory in chapter 2 is applied to a melt of monodisperse semi-flexible diblock copolymers. The spinodals $\chi_s L$ and $\omega_s L$ have been calculated numerically for different kinds of diblocks. The numerical results are compared to results in [9–13]. In each of these papers a different model or approach is applied to calculate the spinodals $\chi_s L$ and $\omega_s L$. This could explain why there are quantitatively differences. However, qualitatively there are no great differences. $\chi_s L$ and $\omega_s L$ depend on the parameters λ_A, λ_B and $f = L_A/L$ in the same way. The dependence of $\chi_s L$ on ωL and $\omega_s L$ on χL is also similar.

In this chapter an expression of the Landau free energy of a melt of monodisperse semi-flexible diblock copolymers is derived using the general theory in chapter 2. This expression is written in terms of eigenvalues and eigenvectors of the matrices in Eq. (3.6). In this way the minimum of the Landau free energy with respect to the order-parameters is determined analytically. Besides a scalar order-parameter also the orientation tensors of the A- and B-block are taken into account. These orientation tensors contain a global and a local contribution. The local contribution is described and visualized in the smectic-A phase and in more complicated structures such as the hexagonal phase. This description of the orientation tensors is applied in the expression of the Landau free energy. By means of the Landau theory the phase structure can be predicted as a function of the composition, persistence length and the strength of the Flory-Huggins and Maier-Saupe interaction. In several phase diagrams the bcc, hexagonal, smectic-A, smectic-C and nematic phase are observed. First a diblock melt has been investigated in which the A-block is a rigid rod and the B-block is a totally flexible. In such a rod-coil diblock melt it has appeared that the Maier-Saupe interaction ω_{AA} between stiff A-blocks weakens microphase separation. At a greater χL a smectic-C phase is found in which $8° < \theta < 18°$.

If the stiff A-block is replaced by a semi-flexible block a different phase behaviour is observed. Here the Maier-Saupe interaction ω_{AA} weakens microphase separation only close to the spinodal $\chi_s L$. At a greater χL a smectic-C phase is found in which θ is always $\theta = 54.7°$. In this smectic-C phase the separation between A- and B-blocks is stronger than in other microphase structures which are found in the phase diagram. However, the orientation tensor of both the A- and B-block is negligible small. So this smectic-C phase can be regarded as a lamellar phase with only a nonzero scalar order-parameter. This smectic-C phase is shifted to a lower χL when ω_{AA} increases. Then microphase separation is enhanced by ω_{AA} if the melt is converted into the smectic-C phase with $\theta = 54.7°$. The phase diagram is also calculated if both the A- and B-block are semi-flexible. Then not only the Maier-Saupe interaction ω_{AA} between A-blocks, but also the parameters ω_{AB} and ω_{BB} may influence the phase behaviour. The Maier-Saupe interaction ω_{AA} and ω_{BB} weakens microphase separation close to the spinodal $\chi_s L$. At a greater χL a smectic-C with again $\theta = 54.7°$ is found which is shifted to a lower χL when ω_{AA} or ω_{BB} increases. This smectic-C phase can also be regarded as a lamellar phase without any alignment of A- or B-blocks. The effect of the parameter ω_{AB} on the phase behaviour appeared to be the reverse of that of ω_{AA} and ω_{BB}.

Chapter 4

Phase behaviour of a melt of polydisperse semi-flexible diblock copolymers

4.1 Introduction

In chapter 3 the phase behaviour of a melt of monodisperse semi-flexible diblock copolymers is investigated. In the general theory of multi-block copolymers in chapter 2 an arbitrary bending stiffness is added to the chains to make the description more realistic. However, it is not always possible to synthesize a melt in which all chains are perfectly monodisperse. There is often a certain degree of polydispersity. To approach reality closer, polydispersity is added which is described by the by the Schultz-Zimm distribution. In this chapter the influence of both polydispersity and bending stiffness on the spinodals $\chi_s \langle L \rangle$ and $\omega_s \langle L \rangle$ is investigated.

The same system has also been investigated in [23] in a different way. The spinodal χ_s has been derived in the framework of the random phase approximation which yields,

$$\chi_s = \frac{1}{2} \min_{\{q\}} \frac{S^0_{AA}(q) + S^0_{BB}(q) + 2S^0_{AB}(q)}{S^0_{AA}(q)S^0_{BB}(q) - S^0_{AB}(q)^2} \tag{4.1}$$

In this expression $S^0_{ab}(q)$ with indices $a, b = A, B$ are single-chain density-density correlation functions. In the derivation of χ_s a possible orientation of A and B blocks in a certain microphase structure has not been taken into account. In this thesis pos-

77

sible orientation tensors are not ignored because of the bending stiffness. Eq. (4.1) corresponds the the spinodal of a monodisperse system. Polydispersity is included by applying a certain distribution $p(L_\alpha)$ with $\alpha = A, B$ to the A- and B-block. L_α is the block length and $p(L_\alpha)$ is the probability to find a block of kind α with length L_α. The Schultz-Zimm and other distributions are used for $p(L_\alpha)$. The spinodal $\langle \chi_s \rangle$ of a polydisperse melt is determined by averaging Eq. (4.1) over $p(L_A)$ and $p(L_B)$,

$$\langle \chi_s \rangle = \int dL_A \int dL_B p(L_A) p(L_B) \chi_s. \tag{4.2}$$

In this chapter the averaging over $p(L_A)$ and $p(L_B)$ is carried out in a different way when calculating the spinodal of a melt of polydisperse diblock copolymers. Here the single-chain correlation functions are averaged and are inserted in the spinodal expressions given by Eq. (4.10) and (4.11). This will be further explained in detail in the next section. The influence of the polydispersity on the spinodal investigated in [23] appears to be contrary to the effect observed in the results of this chapter. In [23] the spinodal is increasing when the degree of polydispersity becomes greater, but according to our results the spinodal is decreasing when the system is made more polydisperse. This difference could be a consequence of the different way of averaging over $p(L_A)$ and $p(L_B)$.

In [22] and [35] a melt of polydisperse Gaussian diblock copolymers is investigated. The averaging is carried out by means of the Schultz-Zimm distribution in the same way as our paper. Here the the spinodal $\chi_s \langle L \rangle$ is also lowered when the degree of polydispersity is increasing. In [22] the A- and B-block have the same degree of polydispersity. Besides the spinodal and scattering function the phase diagram is also determined in which it is investigated whether the bcc, hexagonal, lamellar or disordered phase is formed at a certain point $(f, \chi \langle L \rangle)$. In general the transition lines between the different phase domains are lowered when the polydispersity becomes stronger. In the calculation of the phase diagram fluctuation corrections are taken into account according to the theory in [32]. According to [35] in the synthesis of a diblock melt the polydispersity of one kind of block in the chain can be often better controlled than the polydispersity of the other kind of block. In that paper the A-block has a fixed length and the polydispersity of the B-block is varied. The self-consistent field theory is applied to describe the system. The spinodal $\chi_s \langle L \rangle$ is calculated in the random phase approximation and confirmed by the results of the self-consistent field theory.

4.2 Theory

In chapter 2 an expression of the Landau free energy is derived for a general melt of semi-flexible multi-block copolymers. In this chapter this expression is applied to a melt of polydisperse semi-flexible diblock copolymers. Interactions of two types are incorporated into the free energy. The first one, Flory-Huggins interaction, unfavours contacts between different blocks and in the case of a diblock is described by a single parameter χ. The other interaction, Maier-Saupe, is responsible for the uniaxial alignment in the system and, in our case of an AB-diblock, is characterized by three parameters ω_{AA}, ω_{AB} and ω_{BB}. In what follows, for simplicity, we assume them all be equal to ω. Both χ and ω are generally assumed to be inversely proportional to temperature. Hence, describing the phase equilibrium in terms of χ and ω, one, in fact, describes the behaviour of the system as a function of temperature T. Apparently, for low enough χ and ω, i.e. at high T, the melt finds itself in a spatially homogeneous isotropic state. However, upon increase in χ (or ω) above certain values χ_s (or ω_s), this state becomes unstable against spatial arrangement of different blocks (or their axial alignment). E.g. a melt of monodisperse diblock copolymers becomes unstable against microphase separation if $\chi > \chi_s$. If polydispersity with respect to the length of the A- and B-block is included into the picture, both macrophase and microphase separation become possible at $\chi > \chi_s$. In the same way nematic ordering becomes possible when $\omega > \omega_s$. Micro- and macrophase separation may also be induced.

A possible macrophase structure could be a melt with one big A-rich and one big B-rich domain on a macroscopic length scale. The A-rich domain is formed by collecting diblocks in which the A-block fraction is greater than average. The remaining diblocks form the B-rich domain. In a melt of monodisperse chains it is not possible to form a such a macroscopic structure, because the composition and chain length are identical in each diblock. A greater degree of polydispersity makes a stronger separation possible on macroscopic length scale. Within the macroscopic A-rich and B-rich domain local microphase separation is possible which is called phase coexistence.

In this chapter only the spinodal analysis of a polydisperse melt of semi-flexible diblock copolymers is performed. For this purpose one needs the Landau free energy expansion only up to the second order in the density and orientational order-parameters. The microscopic order-parameters are defined in detail by Eq. (2.3) till (2.9). The final form of the Landau free energy given by Eq. (2.75) is written in terms of the coarse grained order-parameters which are Fourier transformed. In this form

the second order term is,

$$\frac{F_L^{(2)}}{V} = (\Gamma_{ab}^{(2)} - \widetilde{\chi}_{ab})\Psi^a\Psi^b + 2\Gamma_{a\overline{b}}^{(2)}\Psi^a\Upsilon^{\overline{b}} +$$

$$(\Gamma_{\overline{a}\overline{b}}^{(2)} - \frac{1}{2}\omega_{\overline{a}\overline{b}})\Upsilon^{\overline{a}}\Upsilon^{\overline{b}} - \frac{1}{3}\omega_{ab}\Upsilon^{a,ij}\delta_{ij}(\Psi^b + f^b). \tag{4.3}$$

Because of the polydispersity in the first harmonics approximation a global contribution must be taken into account in both the density and orientational order-parameters Ψ^a and $\Upsilon^{\overline{a}}$,

$$\Psi^a = \Psi^A(\underline{q}) = -\Psi^B(\underline{q}) = \Psi(\underline{q}) \equiv \Psi \sum_{\underline{q}' \in H} \exp(i\varphi_{\underline{q}'})\delta(\underline{q} - \underline{q}') + \Psi^0\delta(\underline{q}) \tag{4.4}$$

and

$$\Upsilon^{\overline{a}} = \Upsilon_\alpha^{\mu\nu}(\underline{q}) \equiv \Upsilon_\alpha(n_\alpha^\mu n_\alpha^\nu - \frac{1}{3}\delta^{\mu\nu}) \sum_{\underline{q}' \in H} \exp(i\varphi_{\underline{q}'})\delta(\underline{q} - \underline{q}') +$$

$$\Upsilon_\alpha^0(n_\alpha^\mu n_\alpha^\nu - \frac{1}{3}\delta^{\mu\nu})\delta(\underline{q}). \tag{4.5}$$

The set H in Eq. (4.4) and (4.5) is a set of wave vectors with equal length q_* describing a certain symmetrical structure, for example the smectic-A or -C phase in which $H = \{-\underline{q}, \underline{q}\}$. According to the Landau theory q_* is the wave number at which the disordered phase is instable and is converted into an ordered structure. The vector $\underline{n}^\mu$ is the director of the orientation of A- or B-blocks. In chapter 3 it has been explained that it is justified to assume that $\underline{n}_A^\mu = \underline{n}_B^\mu = \underline{n}^\mu$. In the nematic, smectic-A and smectic-C phase the director $\underline{n}^\mu$ is spatially independent, but in more complicated structures such as the bcc and hexagonal phase a spatially dependent director $\underline{n}^\mu(\underline{x})$ is necessary to describe the orientational structure. In section 3.3 the director $\underline{n}^\mu(\underline{x})$ is chosen such that the bcc and hexagonal phase can be expressed as a linear combination of smectic-A phases. In this way the second order term of the Landau free

energy according to Eq. (4.3) can always be written in the following matrix form,

$$
\frac{F_L^{(2)}}{V} = \begin{bmatrix} \Psi & \Upsilon_A & \Upsilon_B \end{bmatrix} \begin{bmatrix} \widetilde{\Gamma}^{(2)} - \chi & \widetilde{\Gamma}_A^{(2)} & \widetilde{\Gamma}_B^{(2)} \\ \widetilde{\Gamma}_A^{(2)} & \widetilde{\Gamma}_{AA}^{(2)} - \frac{1}{3}\omega_{AA} & \widetilde{\Gamma}_{AB}^{(2)} - \frac{1}{3}\omega_{AB} \\ \widetilde{\Gamma}_B^{(2)} & \widetilde{\Gamma}_{AB}^{(2)} - \frac{1}{3}\omega_{AB} & \widetilde{\Gamma}_{BB}^{(2)} - \frac{1}{3}\omega_{BB} \end{bmatrix} \begin{bmatrix} \Psi \\ \Upsilon_A \\ \Upsilon_B \end{bmatrix} +
$$

$$
\begin{bmatrix} \Psi^0 & \Upsilon_A^0 & \Upsilon_B^0 \end{bmatrix} \begin{bmatrix} \widetilde{\Gamma}_{00}^{(2)} - \chi & \widetilde{\Gamma}_{A,00}^{(2)} & \widetilde{\Gamma}_{B,00}^{(2)} \\ \widetilde{\Gamma}_{A,00}^{(2)} & \widetilde{\Gamma}_{AA,00}^{(2)} - \frac{1}{3}\omega_{AA} & \widetilde{\Gamma}_{AB,00}^{(2)} - \frac{1}{3}\omega_{AB} \\ \widetilde{\Gamma}_{B,00}^{(2)} & \widetilde{\Gamma}_{AB,00}^{(2)} - \frac{1}{3}\omega_{AB} & \widetilde{\Gamma}_{BB,00}^{(2)} - \frac{1}{3}\omega_{BB} \end{bmatrix} \begin{bmatrix} \Psi^0 \\ \Upsilon_A^0 \\ \Upsilon_B^0 \end{bmatrix},
$$

$$
\tag{4.6}
$$

after inserting the first harmonics approximation. In the first matrix the length q_* of the set H of wave vectors has a nonzero value and in the second matrix q_* is zero. The $\widetilde{\Gamma}$'s in the first matrix are given by

$$
\widetilde{\Gamma}^{(2)} = \Gamma_{ab}^{(2)} S^a S^b, \quad \widetilde{\Gamma}_\alpha^{(2)} = \Gamma_{a\bar{b}}^{(2)} S^a d_\alpha^{\bar{b}} \text{ and } \widetilde{\Gamma}_{\alpha\beta}^{(2)} = \Gamma_{\bar{a}\bar{b}}^{(2)} d_\alpha^{\bar{a}} d_\beta^{\bar{b}} \text{ in which } \alpha, \beta = A, B, \tag{4.7}
$$

and S^a and $d_\alpha^{\bar{b}}$ are defined as,

$$
S^a \equiv (1 - 2\delta_{\alpha B}) \exp(i\varphi_{\underline{q}}) = \pm \exp(i\varphi_{\underline{q}}) \text{ in which } a = \underline{q}, \alpha \tag{4.8}
$$

$$
\text{and}
$$

$$
d_\alpha^{\bar{b}} \equiv (n_\beta^{\mu_2} n_\beta^{\nu_2} - \frac{1}{3}\delta^{\mu_2\nu_2}) \exp(i\varphi_{\underline{q}})\delta_{\alpha\beta} \text{ in which } \bar{b} = \underline{q}, \beta, \mu_2\nu_2. \tag{4.9}
$$

The $\widetilde{\Gamma}$'s in the second matrix in Eq. (4.6) can be written in the same way. The eigenvalues of both matrices in Eq. (4.6) are positive if $\chi < \chi_s$ and $\omega < \omega_s$. In that case the Landau free energy has a minimum when the order-parameters are zero so that the melt is in the disordered state. When $\chi = \chi_s$ or $\omega = \omega_s$ at least one of the eigenvalues is zero and becomes negative if χ or ω is further increased. Then the order-parameters are nonzero at the minimum and the melt is converted into a certain ordered state. If one of the eigenvalues is zero the determinant of the first or second

matrix is zero. In this way the expressions of the spinodals χ_s and ω_s can be derived,

$$\chi_s = \min_{\{q_*, \underline{n}^\mu\}} \{\widetilde{\Gamma}^{(2)} - \frac{(\widetilde{\Gamma}_B^{(2)})^2(\widetilde{\Gamma}_{AA}^{(2)} - \frac{1}{3}\omega) + (\widetilde{\Gamma}_A^{(2)})^2(\widetilde{\Gamma}_{BB}^{(2)} - \frac{1}{3}\omega) - 2\widetilde{\Gamma}_A^{(2)}\widetilde{\Gamma}_B^{(2)}(\widetilde{\Gamma}_{AB}^{(2)} - \frac{1}{3}\omega)}{(\widetilde{\Gamma}_{AA}^{(2)} - \frac{1}{3}\omega)(\widetilde{\Gamma}_{BB}^{(2)} - \frac{1}{3}\omega) - (\widetilde{\Gamma}_{AB}^{(2)} - \frac{1}{3}\omega)^2}\}$$

(4.10)

and

$$\omega_s = 3 \min_{\{q_*, \underline{n}^\mu\}} \{\frac{(\widetilde{\Gamma}^{(2)} - \chi)(\widetilde{\Gamma}_{AA}^{(2)}\widetilde{\Gamma}_{BB}^{(2)} - (\widetilde{\Gamma}_{AB}^{(2)})^2) - (\widetilde{\Gamma}_A^{(2)})^2\widetilde{\Gamma}_{BB}^{(2)} + 2\widetilde{\Gamma}_A^{(2)}\widetilde{\Gamma}_B^{(2)}\widetilde{\Gamma}_{AB}^{(2)} - (\widetilde{\Gamma}_B^{(2)})^2\widetilde{\Gamma}_{AA}^{(2)}}{(\widetilde{\Gamma}^{(2)} - \chi)(\widetilde{\Gamma}_{AA}^{(2)} + \widetilde{\Gamma}_{BB}^{(2)} - 2\widetilde{\Gamma}_{AB}^{(2)}) - (\widetilde{\Gamma}_A^{(2)} - \widetilde{\Gamma}_B^{(2)})^2}\},$$

(4.11)

in which a minimization is carried out over q_* and the director vector $\underline{n}^\mu$. These expressions can be applied for both $q_* = 0$ and $q_* \neq 0$. The $\widetilde{\Gamma}$'s given by Eq. (4.7) depend on the coefficients $\Gamma_{ab}^{(2)}$, $\Gamma_{a\bar{b}}^{(2)}$ and $\Gamma_{\bar{a}\bar{b}}^{(2)}$ in the second order term of the Landau free energy. These coefficients are related to the second order single-chain correlation functions A_{ab}, $A_{a\bar{b}}$ and $A_{\bar{a}\bar{b}}$ in a quite complicated way which is written down in detail in section 2.2. In a melt of polydisperse chains A_{ab}, $A_{a\bar{b}}$ and $A_{\bar{a}\bar{b}}$ are average single-chain correlation functions,

$$A_{\widetilde{a}\widetilde{b}} = \sum_s \rho_s A_{s,\widetilde{a}\widetilde{b}},$$

(4.12)

in which $\widetilde{a} = a$ or $\bar{a}$ and $\widetilde{b} = b$ or $\bar{b}$. The parameter s in Eq. (4.12) labels the type of a chain and $\rho_s \equiv \frac{n_s}{V}$ is the number density of chains of type s. For a monodisperse melt $\rho_s = \frac{1}{\langle L \rangle} = \frac{1}{L}$, but if the melt is polydisperse ρ_s becomes,

$$\rho_s = \rho(L_A, L_B) = \frac{p(L_A)p(L_B)}{\langle L \rangle},$$

(4.13)

in which $p(L_\alpha)$ is the probability to find a block of kind α with a length L_α and the parameter s is replaced by a continuous set of block lengths $\{L_A, L_B\}$. For $p(L_\alpha)$ the Schultz-Zimm distribution is applied given by,

$$p(L_\alpha) = \frac{k_\alpha^{k_\alpha} \exp(\frac{-k_\alpha L_\alpha}{\langle L_\alpha \rangle})(L_\alpha)^{k_\alpha - 1}}{\Gamma(k_\alpha)\langle L_\alpha \rangle^{k_\alpha}}.$$

(4.14)

In this distribution $\langle L_\alpha \rangle$ is the average length and $\Gamma(k_\alpha)$ is the Gamma function. k_α is a dimensionless number which is a measure of polydispersity. If $k_\alpha \to \infty$ block α becomes monodisperse and if $k_\alpha = 1$ Eq. (4.14) is equal to the Flory distribution. This distribution corresponds to a broad polydisperse system.

4.3 Results and discussion

The spinodal χ_s given by Eq. (4.10) is a complicated function which depends on the composition $f = \langle L_A \rangle / \langle L \rangle$, Maier-Saupe parameter ω, average chain length $\langle L \rangle$, persistence length λ_α and polydispersity parameter k_α,

$$\chi_s = \chi_s(f, \omega, \langle L \rangle, \lambda_\alpha, k_\alpha) \ \text{ with } \ \alpha = A, B. \tag{4.15}$$

If we choose constant ratio's $\lambda_A / \langle L_A \rangle$ and $\lambda_B / \langle L_B \rangle$ it can be easily verified that $\chi_s \sim 1 / \langle L \rangle$. In that case $\chi_s \langle L \rangle$ is a function of only f, ω, $\lambda_\alpha / \langle L_\alpha \rangle$ and k_α,

$$\chi_s \langle L \rangle = \chi_s \langle L \rangle (f, \omega, \lambda_\alpha / \langle L_\alpha \rangle, k_\alpha) \ \text{ with } \ \alpha = A, B. \tag{4.16}$$

The corresponding wave number q_* multiplied by $\langle L \rangle$ is also a function of only f, ω, $\lambda_\alpha / \langle L_\alpha \rangle$ and k_α. In the same way the spinodal $\omega_s \langle L \rangle$ and corresponding $q_* \langle L \rangle$ depend only on f, χ, $\lambda_\alpha / \langle L_\alpha \rangle$ and k_α.

In Eq. (4.10) and (4.11) a minimization is carried out over the director vector $\underline{n} = (\cos \theta, \sin \theta, 0)$. It has been verified that the angle θ is always zero. So if a microphase structure is found at the spinodal $\chi_s \langle L \rangle$ or $\omega_s \langle L \rangle$, it is always a smectic-A phase or a superposition of smectic-A phases in different directions.

For the ratio's $\lambda_A / \langle L_A \rangle$ and $\lambda_B / \langle L_B \rangle$ we have chosen the following possibilities: (a) coil-coil ($\lambda_A / \langle L_A \rangle = 10^{-4} = \lambda_B / \langle L_B \rangle$); (b) semi-semi ($\lambda_A / \langle L_A \rangle = 10^{-1} = \lambda_B / \langle L_B \rangle$); (c) rod-coil ($\lambda_A / \langle L_A \rangle = 10^2 \gg \lambda_B / \langle L_B \rangle = 10^{-4}$); (d) semi-coil ($\lambda_A / \langle L_A \rangle = 10^{-1} \gg \lambda_B / \langle L_B \rangle = 10^{-4}$). In Fig. (4.1) till (4.4) $\chi_s \langle L \rangle$ and the corresponding wave number $q_* \langle L \rangle$ are calculated as a function of f for system (a), (b), (c) and (d). In these figures the parameters k_A and k_B are chosen such that $k_A = k_B = k$ and $\omega = 0$. In each figure the lines belonging to $k = 1, 2, 5, 10$ and $k \to \infty$ are displayed. In the same way $\omega_s \langle L \rangle$ is calculated as a function of f in Fig. (4.5) till (4.7) for system (b), (c) and (d). In these figures $\chi = 0$ and the corresponding wave number $q_* \langle L \rangle$ is always zero when Eq. (4.11) is minimized with respect to $q_* \langle L \rangle$. Hence, above ω_s the system always becomes unstable against nematic ordering if the Flory-Huggins parameter is chosen to be negligibly small. In Fig. (4.8), (4.9) and (4.10) $\chi_s \langle L \rangle$ and $q_* \langle L \rangle$ are calculated as a function of $\omega \langle L \rangle = \omega_s \langle L \rangle$ for system (b). The line is truncated at the spinodal $\omega_s \langle L \rangle = \omega_{s,nem} \langle L \rangle$ at which $\omega \langle L \rangle$ is large enough to form a nematic phase. In Fig. (4.8) and (4.9) the indices k are $k \to \infty$ and $k = 1$, respectively, and the composition is $f = 0.85$. In Fig. (4.10) $f = 0.5$ and $k \to \infty$. Here the dependence of $\chi_s \langle L \rangle$ and $q_* \langle L \rangle$ on $\omega \langle L \rangle$ is the same as in Fig. (4.8) and (4.9).

However, if $f = 0.5$ and $k = 1$ the wave number $q_* \langle L \rangle$ is always zero and does not depend on $\omega \langle L \rangle$. The spinodal $\chi_s \langle L \rangle$ is also independent of $\omega \langle L \rangle$.

In Fig. (4.1) till (4.10) the A- and B-block have the same degree of polydispersity. It is also interesting to investigate a diblock melt in the same way as in [35] in which the polydispersity of only one block is varied while the other block is always monodisperse. This is done in Fig. (4.11) till (4.17). In Fig. (4.11) till (4.13) $\chi_s \langle L \rangle$ and the corresponding wave number $q_* \langle L \rangle$ are calculated as a function of f for system (a) and (c) when $\omega = 0$. In each figure the lines belonging to the parameters $k_A = 1, 2, 5, 10$ and $k_A \to \infty$ are displayed and for k_B the limit $k_B \to \infty$ is always taken. In Fig. (4.12) the polydispersity of the rod-part is varied and the coil-part remains monodisperse. The reverse is done in Fig. (4.13) in which k_A and k_B are interchanged. In the same way in Fig. (4.14) and (4.15) $\omega_s \langle L \rangle$ is calculated for system (c) when $\omega = 0$. In these figures the minimum of $\omega_s \langle L \rangle$ is always reached when $q_* \langle L \rangle$ is zero. In Fig. (4.16) and (4.17) $\chi_s \langle L \rangle$ and $q_* \langle L \rangle$ are calculated as a function of $\omega \langle L \rangle = \omega_s \langle L \rangle$ for system (c) at $f = 0.5$. The line is again truncated at the spinodal $\omega_s \langle L \rangle = \omega_{s,nem} \langle L \rangle$. In Fig. (4.16) $k_A = 1$ and $k_B \to \infty$ and in Fig. (4.17) the parameters k_A and k_B are interchanged.

In general the spinodal $\chi_s \langle L \rangle$ and wave number $q_* \langle L \rangle$ are lowered when the polydispersity becomes stronger. So microphase separation takes place at a lower χ and the size of the A-rich and B-rich domains increases. For certain kinds of diblocks $q_* \langle L \rangle$ has even become zero which means that macrophase separation has become possible.

This phenomenon can be explained in the following way. In a monodisperse melt all diblocks have the same composition $f = \frac{\langle L_A \rangle}{\langle L \rangle} = \frac{L_A}{L}$. Then only small A-rich and B-rich domains can be formed at the spinodal $\chi_s \langle L \rangle$. However, in a polydisperse melt there are diblock chains possible whose composition deviates strongly from the average composition f. Some diblocks have a relatively long A- or B-block such that these diblocks can be considered as homopolymers. These chains prefer to be in the centre of A-rich and B-rich domains. If the polydispersity increases the number of homopolymer-like diblocks increases. Then more chains of this kind assemble to the centre of A-rich and B-rich domains which will make these domains greater. If the amount of homopolymer-like diblocks is great enough macrophase separation becomes possible at the spinodal $\chi_s \langle L \rangle$. In a monodisperse melt only a microphase structure can be formed with a small domain size. Due to the smaller domain size an A-block in an A-rich domain has to travel a shorter distance to reach a B-rich domain. This makes it easier to mix A- and B-blocks so that a stronger χ is necessary to keep
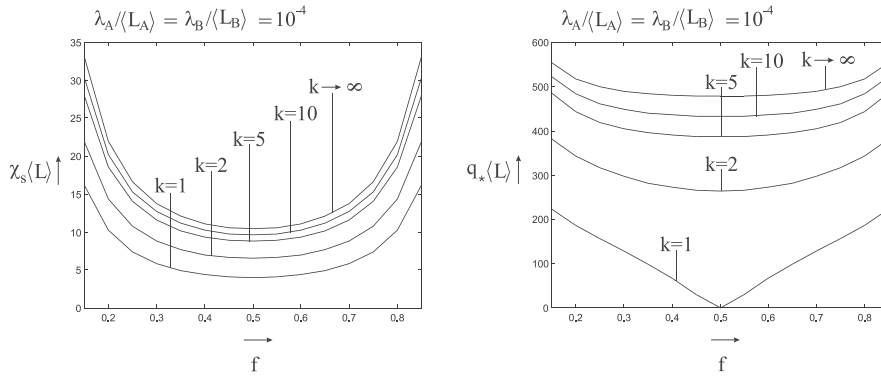
Figure 4.1: The spinodal $\chi_s \langle L \rangle$ and the corresponding wave number $q_* \langle L \rangle$ as a function of f calculated for different k in system (a).
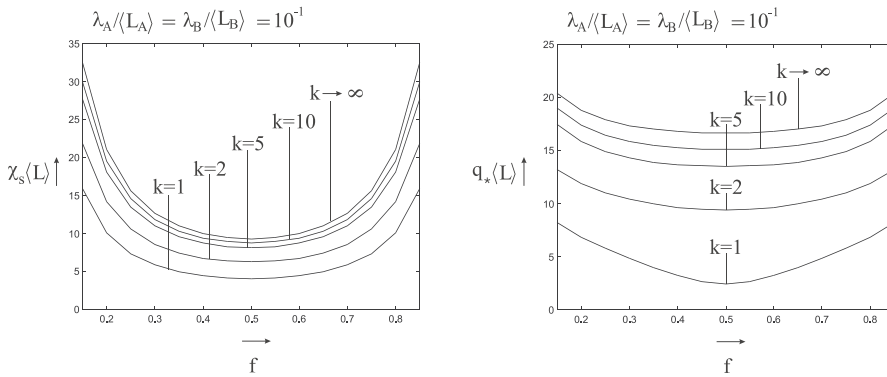
Figure 4.2: The spinodal $\chi_s \langle L \rangle$ and the corresponding wave number $q_* \langle L \rangle$ as a function of f calculated for different k in system (b).

the A- and B-blocks separated from each other. So if the polydispersity increases separation is stimulated, because the domain size increases. This could explain why $\chi_s \langle L \rangle$ is lowered when the polydispersity increases.

The spinodal $\omega_s \langle L \rangle$ calculated at $\chi = 0$ is also lowered by the polydispersity. In a polydisperse melt there is always a small amount of homopolymer-like diblocks with a much longer A- or B-block. If $\lambda_A / \langle L_A \rangle \gg \lambda_B / \langle L_B \rangle$ the diblocks with a much longer and stiffer A-block will align easier. These chains could make it possible to form a nematic phase at a lower ω. The chains are considered as semi-flexible if
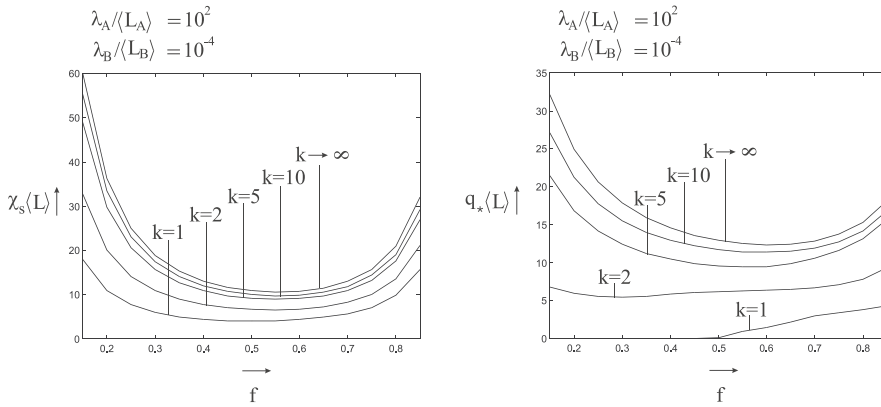
Figure 4.3: The spinodal $\chi_s \langle L \rangle$ and the corresponding wave number $q_* \langle L \rangle$ as a function of f calculated for different k in system (c).
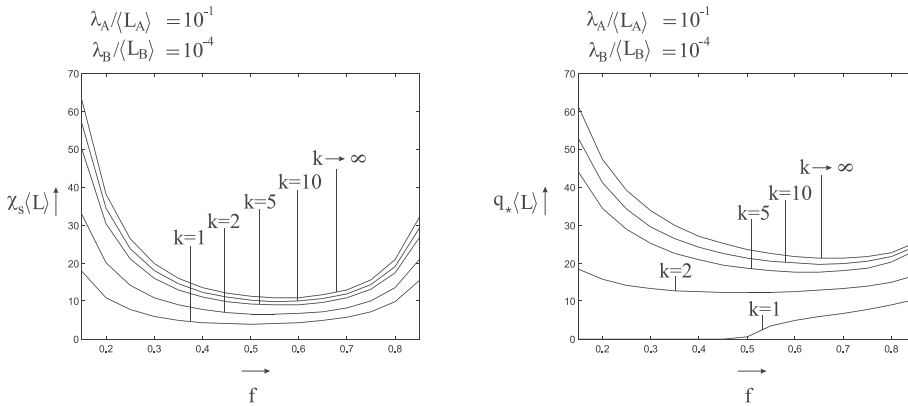
Figure 4.4: The spinodal $\chi_s \langle L \rangle$ and the corresponding wave number $q_* \langle L \rangle$ as a function of f calculated for different k in system (d).

$\lambda_A / \langle L_A \rangle = \lambda_B / \langle L_B \rangle = 10^{-1}$. In such a melt nematic ordering is also induced at a lower ω when the chains are polydisperse. This can be explained by means of the intrinsic mixing entropy of A- and B-blocks within one chain. In the disordered state the semi-flexible chains are curved a little bit. This increases the entropy, but too much curvature is energetically unfavourable. The curvature will also mix A- and B-blocks within one chain. To form a nematic phase each chain must be straightened.
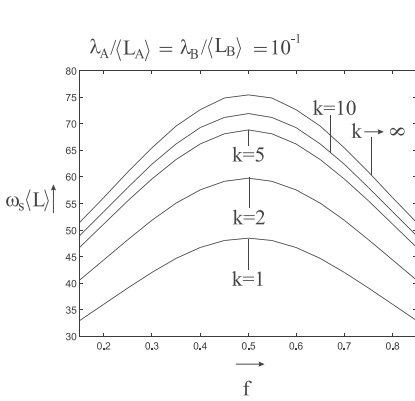
Figure 4.5: The spinodal $\omega_s \langle L \rangle$ as a function of f calculated for different k in system (b).
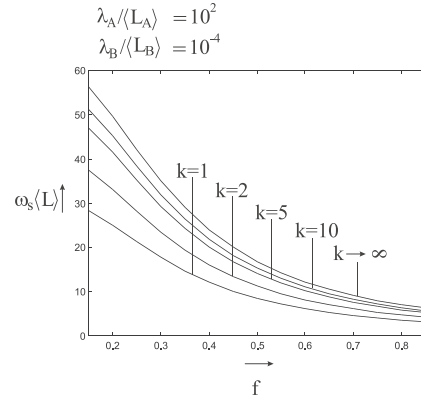
Figure 4.6: The spinodal $\omega_s \langle L \rangle$ as a function of f calculated for different k in system (c).
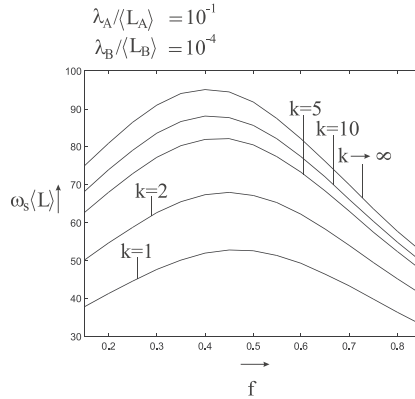
Figure 4.7: The spinodal $\omega_s \langle L \rangle$ as a function of f calculated for different k in system (d).

This will separate the A- and B-monomers within one chain which lowers the intrinsic mixing entropy. This effect is small for the homopolymer-like diblocks so that these chains will align easier. A monodisperse melt does not contain homopolymer-like diblocks which could explain the greater spinodal $\omega_s \langle L \rangle$.

The spinodal $\chi_s \langle L \rangle$ and corresponding wave number $q_* \langle L \rangle$ depend on $\omega \langle L \rangle$ as

$$\lambda_A/\langle L_A\rangle = 10^2$$
$$\lambda_B/\langle L_B\rangle = 10^{-4}$$

f=0.85
$k \rightarrow \infty$

$\chi_s\langle L\rangle \uparrow$

$\overrightarrow{\omega_s\langle L\rangle}$

$$\lambda_A/\langle L_A\rangle = 10^2$$
$$\lambda_B/\langle L_B\rangle = 10^{-4}$$

f=0.85
$k \rightarrow \infty$

$q_*\langle L\rangle \uparrow$

$\overrightarrow{\omega_s\langle L\rangle}$
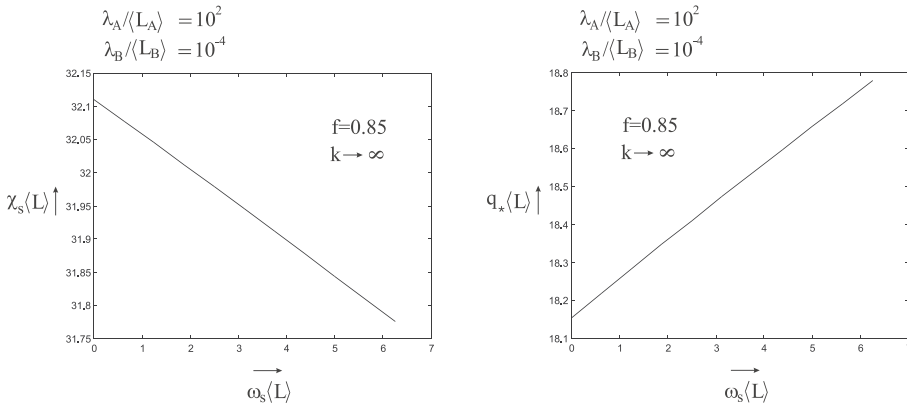
Figure 4.8: The spinodal $\chi_s\langle L\rangle$ and the corresponding wave number $q_*\langle L\rangle$ as a function of $\omega\langle L\rangle = \omega_s\langle L\rangle$ calculated for $f = 0.85$ and $k \rightarrow \infty$ in system (c).

$$\lambda_A/\langle L_A\rangle = 10^2$$
$$\lambda_B/\langle L_B\rangle = 10^{-4}$$

f=0.85
k=1

$\chi_s\langle L\rangle \uparrow$

$\overrightarrow{\omega_s\langle L\rangle}$

$$\lambda_A/\langle L_A\rangle = 10^2$$
$$\lambda_B/\langle L_B\rangle = 10^{-4}$$

f=0.85
k=1

$q_*\langle L\rangle \uparrow$

$\overrightarrow{\omega_s\langle L\rangle}$
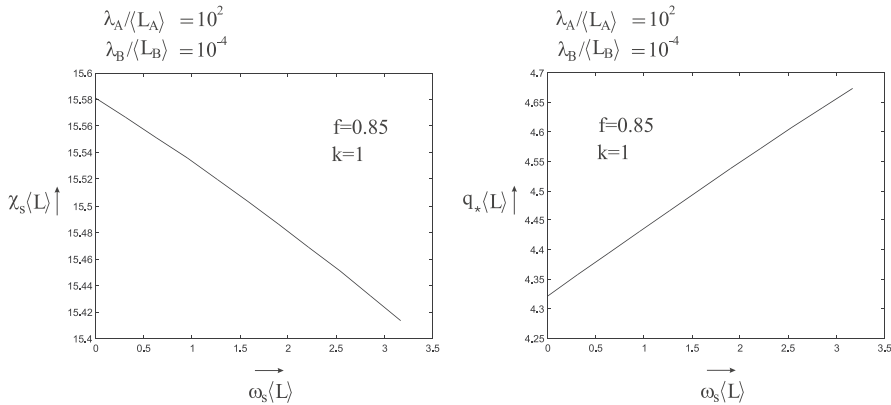
Figure 4.9: The spinodal $\chi_s\langle L\rangle$ and the corresponding wave number $q_*\langle L\rangle$ as a function of $\omega\langle L\rangle = \omega_s\langle L\rangle$ calculated for $f = 0.85$ and $k = 1$ in system (c).

long as $q_*\langle L\rangle \neq 0$. $\chi_s\langle L\rangle$ is lowered and $q_*\langle L\rangle$ is increased when $\omega\langle L\rangle$ increases and $\omega\langle L\rangle < \omega_{s,nem}\langle L\rangle$. This behaviour is also observed and explained in chapter 3 in which a melt of monodisperse diblock copolymers is investigated. If $q_*\langle L\rangle = 0$ at the spinodal $\chi_s\langle L\rangle$ not only macrophase separation, but also global nematic order
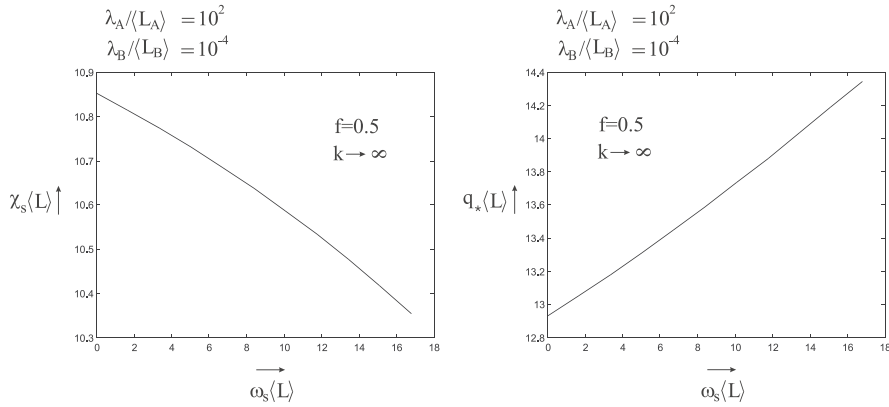
Figure 4.10: The spinodal $\chi_s \langle L \rangle$ and the corresponding wave number $q_* \langle L \rangle$ as a function of $\omega \langle L \rangle = \omega_s \langle L \rangle$ calculated for $f = 0.5$ and $k \to \infty$ in system (c).
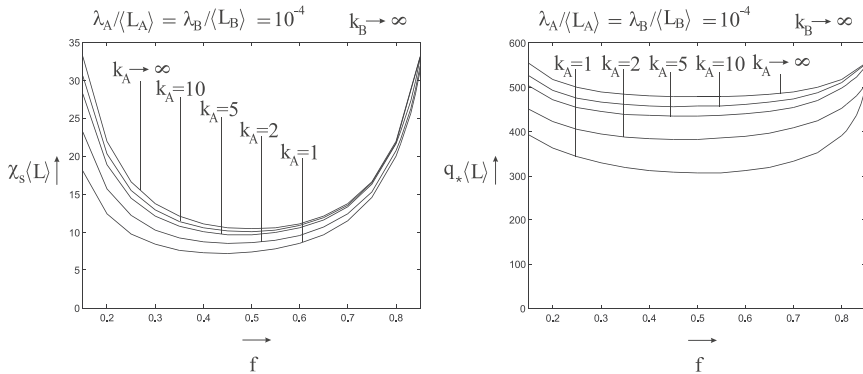
Figure 4.11: The spinodal $\chi_s \langle L \rangle$ and the corresponding wave number $q_* \langle L \rangle$ as a function of f calculated for different k_A in system (a).

may become possible. This can be investigated by determining the normalized eigenvectors $\widehat{x_i} = (\widehat{\Psi}_i, \widehat{\Upsilon}_i^A, \widehat{\Upsilon}_i^B)$ of the second matrix in Eq. (4.6) belonging to the smallest eigenvalue $\lambda = 0$. In this matrix in which $q_* \langle L \rangle = 0$ it has been verified that the coefficients $\widetilde{\Gamma}_{A,00}^{(2)}$ and $\widetilde{\Gamma}_{B,00}^{(2)}$ are zero for all possible parameters f, $\lambda_\alpha / \langle L_\alpha \rangle$ and k_α with $\alpha = A, B$. Consequently the scalar order-parameter is decoupled from the orientation tensors. Therefore at $\chi \langle L \rangle = \chi_s \langle L \rangle$ the eigenvector is $\widehat{x}_1 = (1, 0, 0)$. This eigenvector
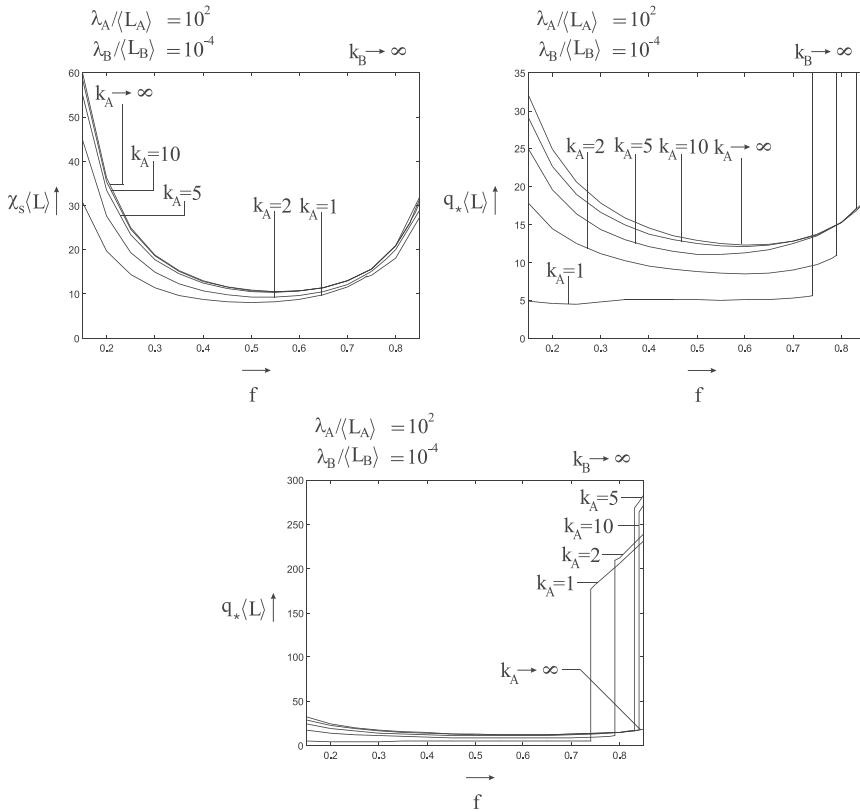
Figure 4.12: The spinodal $\chi_s \langle L \rangle$ and the corresponding wave number $q_* \langle L \rangle$ as a function of f calculated for different k_A in system (c).

does not change when $\omega \langle L \rangle$ is varied between zero and $\omega_{s,nem}$. As long as $\omega \langle L \rangle$ is not too great only macrophase separation is possible and global nematic order is not stimulated by the Flory-Huggins interaction χ. When $\omega \langle L \rangle \geq \omega_{s,nem} \langle L \rangle$ global nematic order takes place. Reversibly, when $\chi \langle L \rangle \leq \chi_s \langle L \rangle$ and $\omega \langle L \rangle = \omega_s \langle L \rangle$ the density components of the eigenvectors at $\lambda = 0$ are zero. These eigenvectors are independent of $\chi \langle L \rangle$. So the Maier-Saupe interaction ω does not stimulate macrophase separation. When both $\chi \langle L \rangle = \chi_s \langle L \rangle$ and $\omega \langle L \rangle = \omega_{s,nem} \langle L \rangle$ the eigenvalue $\lambda = 0$ is two or three fold degenerate. Then one eigenvector is $\widehat{x_1} = (1, 0, 0)$ and other eigenvectors $\widehat{x_2}$ and $\widehat{x_3}$ must contain nonzero orientational components.

In chapter 3 the influence of the bending stiffness on the spinodals $\chi_s L$ and $\omega_s L$
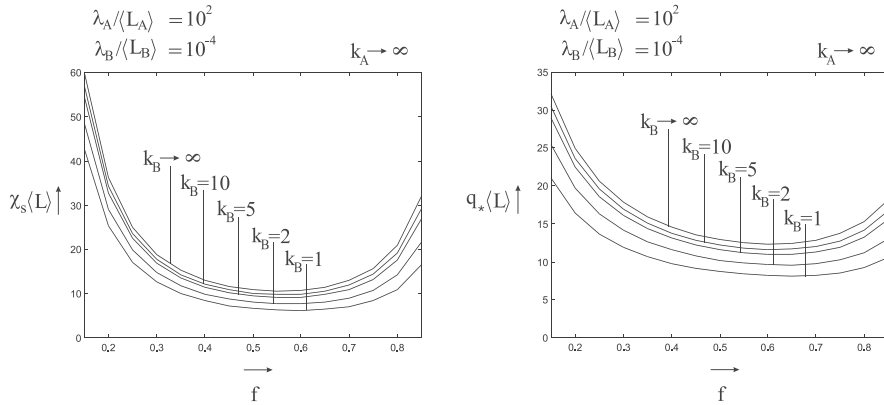
Figure 4.13: The spinodal $\chi_s \langle L \rangle$ and the corresponding wave number $q_* \langle L \rangle$ as a function of f calculated for different k_B in system (c).
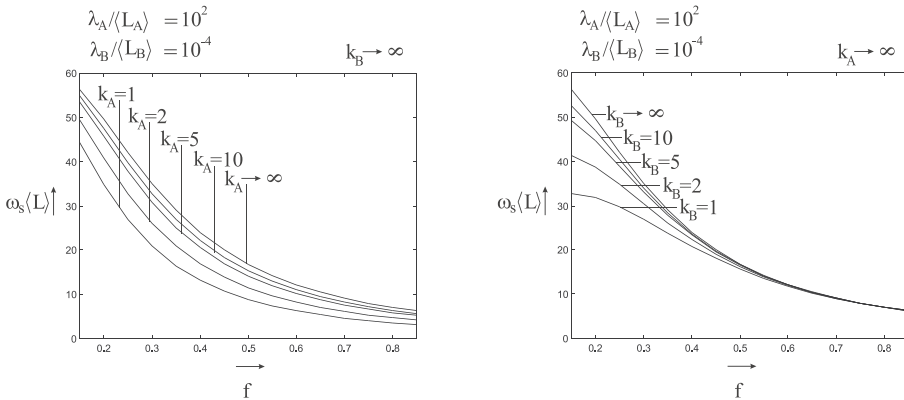
Figure 4.14: The spinodal $\omega_s \langle L \rangle$ as a function of f calculated for different k_A in system (c).

Figure 4.15: The spinodal $\omega_s \langle L \rangle$ as a function of f calculated for different k_B in system (c).

of a melt of monodisperse semi-flexible diblock copolymers has been investigated. It has been verified that the effects observed in the numerical results in chapter 3 also occur in the spinodals $\chi_s \langle L \rangle$ and $\omega_s \langle L \rangle$ of a polydisperse melt. However, in the results of this chapter the influence of the bending stiffness $\lambda_A / \langle L_A \rangle$ and $\lambda_B / \langle L_B \rangle$ is
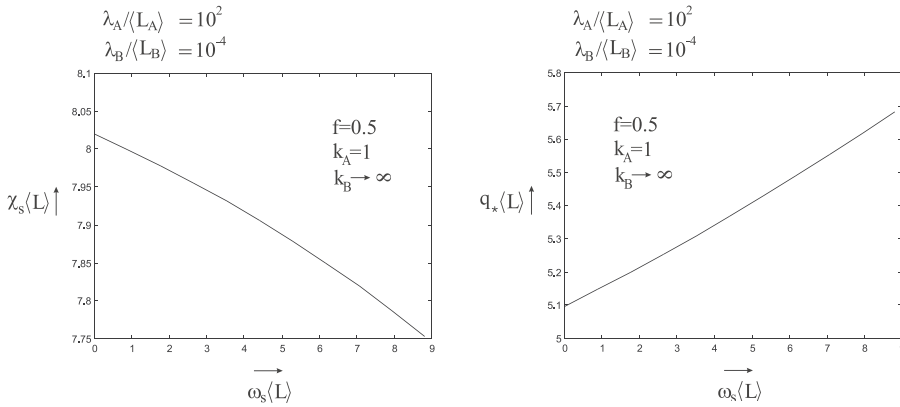
Figure 4.16: The spinodal $\chi_s \langle L \rangle$ and the corresponding wave number $q_* \langle L \rangle$ as a function of $\omega \langle L \rangle = \omega_s \langle L \rangle$ calculated for $f = 0.5$, $k_A = 1$ and $k_B \rightarrow \infty$ in system (c).
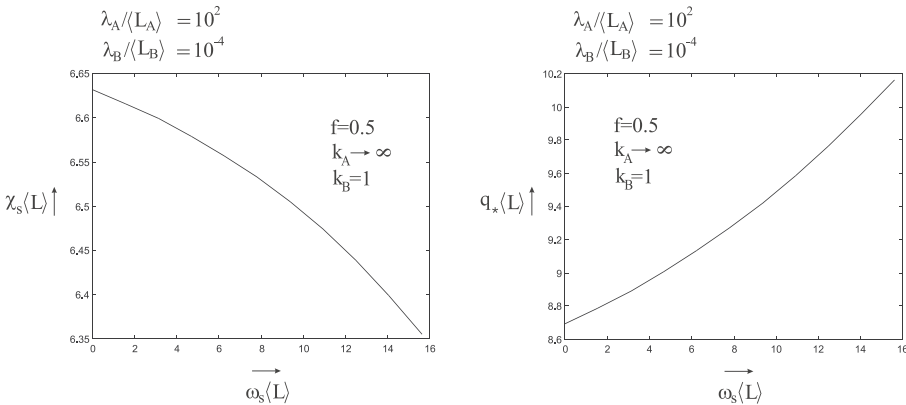
Figure 4.17: The spinodal $\chi_s \langle L \rangle$ and the corresponding wave number $q_* \langle L \rangle$ as a function of $\omega \langle L \rangle = \omega_s \langle L \rangle$ calculated for $f = 0.5$, $k_A \rightarrow \infty$ and $k_B = 1$ in system (c).

relatively small and cannot always be observed clearly. Furthermore, the wave number $q_* \langle L \rangle$ is lowered by the bending stiffness in both monodisperse and polydisperse systems. A more flexible A- or B-block makes it possible to form smaller domains in a microphase structure which yields an entropy gain. If the stiffness is increased

small domains are energetically unfavourable so that $q_* \langle L \rangle$ will decrease.

In the results some remarkable phenomena are observed. First the bending stiffness does not always lower the wave number $q_* \langle L \rangle$ if we look for instance in Fig. (4.1) and (4.2). In Fig. (4.1) macrophase separation is predicted at $f = 0.5$ in the line at which $k = 1$, but not in Fig. (4.2). This could be explained by means of intrinsic mixing entropy within one diblock. In the disordered phase a totally flexible diblock behaves as a random walk such that within one coil the A- and B-block are mixed homogeneously. To form a microphase structure the A-block and B-block within one chain must be separated from each other. This is unfavourable, because this reduces the intrinsic mixing entropy within one chain. However, to form a macrophase structure it is not necessary to separate the A- and B-block within one chain. This could explain why a coil-coil diblock melt prefers macrophase separation. If the diblock is semi-flexible it is energetically unfavourable to fold the chain into a coil. Therefore a semi-flexible diblock is much straighter so that the A- and B-block are already separated within one chain. This could make it easier to form a microphase structure.

Secondly if $k = 1$ we see that $q_* \langle L \rangle = 0$ in Fig. (4.3) and (4.4) at lower values of f, while in Fig. (4.1) and (4.2) a microphase structure is predicted. Comparing these figures at $k = 1$ it again appears that the bending stiffness does not always lower the wave number $q_* \langle L \rangle$. Fig. (4.3) and (4.4) corresponds to asymmetric diblocks in which $\lambda_A / \langle L_A \rangle \gg \lambda_B / \langle L_B \rangle$. In Fig. (4.3) and (4.4) the stiffer A-block is shorter than the totally flexible B-block at lower values of f. To form a microphase structure the stiffer part must be separated from the coil within one chain. If the stiffer part is much longer than the radius of the coil, the A- and B-block are separated sufficiently. However, if the stiffer part is very short it is mixed inside the coil part. This could make it entropically less favourable to form a microphase structure. Maybe therefore the melt prefers macrophase separation if $k = 1$ at a lower f in Fig. (4.3) and (4.4). However, in Fig. (4.1) we see that microphase separation takes place instead of macrophase separation if $k = 1$ at a lower f. This figure corresponds to a melt of totally flexible diblocks. In Fig. (4.1) the wave number $q_* \langle L \rangle$ is much greater than $q_* \langle L \rangle$ calculated in Fig. (4.3) and (4.4). So in a melt of totally flexible diblocks it is possible to form A- and B-rich domains with a small size. The size is much smaller than the average chain length $\langle L \rangle$. Maybe therefore an microphase structure is entropically more favourable. If the coil-like A- or B-block is replaced by a much stiffer block it is not possible to form such small A- and B-rich domains. Therefore the wave length $2\pi / q_*$ is much greater according to Fig. (4.3) and (4.4). Then within each chain a greater separation between the stiffer A-block and the coil-like B-block

is necessary. This could be difficult if the stiffer part is short with respect to the radius of the coil part. So maybe therefore the melt prefers a macrophase structure at lower values of f.

A third remarkable effect is observed in Fig. (4.12). At a smaller rod fraction f the wave number $q_* \langle L \rangle$ is small, but when f is increased further and further at a certain f the wave number $q_* \langle L \rangle$ jumps to a much greater value. The corresponding wave length $\lambda = \frac{2\pi}{q_*}$ has the same order of magnitude as the radius r of the coil which is $r = \sqrt{\langle L_B \rangle}$. In that part of the figure the coils are forming domains which are embedded by a rod-rich matrix. In the other part a macrophase-like structure is formed in which λ is greater than the chain length $\langle L \rangle$. Here A-rich domains are formed by collecting diblocks with an A-block fraction greater than average. At the same time B-rich domains arise. A sharp boundary between A- and B-rich domains cannot be created, so that only a weak separation is possible. This is not favourable because of enthalpy. The separation becomes even weaker when the A- or B-block fraction of the melt is made smaller. Maybe therefore the melt prefers to form small coil-rich domains embedded by a rod rich matrix in the right part of Fig. (4.12). A coil-rich domain is formed by separating a coil from a rod within one chain. Then a sharper separation is possible. Additionally, due to the polydispersity of the rods it is easier to form a rod rich matrix. In the left part the rod-rich domains are embedded by a coil-rich matrix. However, small rod-rich domains with a size in the order of magnitude of $\langle L_A \rangle$ are not formed. Due to polydispersity of rods such a phase could not be favourable.

In the domain in Fig. (4.12) in which $q_* \langle L \rangle$ is much greater it has been verified that $\chi_s \langle L \rangle$ and $q_* \langle L \rangle$ do not change hardly anything when $\omega \langle L \rangle$ is varied. Here the eigenvector $\widehat{x}_1$ belonging to the smallest eigenvalue $\lambda_1 = 0$ is approximately $\widehat{x}_1 = (\widehat{\Psi}_1, \widehat{\Upsilon}_i^A, \widehat{\Upsilon}_i^B) \approx (1, 0, 0)$. This follows from the fact that in the first matrix in Eq. (4.6) the coefficients $\widetilde{\Gamma}_A^{(2)}$ and $\widetilde{\Gamma}_B^{(2)}$ are negligibly small. So in this microphase structure there is hardly any orientation of rods.

In Fig. (4.13) $q_* \langle L \rangle$ does not jump to a greater value at a certain A-block fraction f, so that only a macrophase-like structure is formed. The polydispersity of coils could make it difficult to form a microphase structure of small coils-rich domains embedded by a matrix of rods. Furthermore in the left part of Fig. (4.13) $q_* \langle L \rangle$ is greater than $q_* \langle L \rangle$ in Fig. (4.12). Here a microphase structure is formed in which rod-rich domains are embedded by a matrix of coils. In Fig. (4.13) the rod-rich domains are smaller which is possible due to the monodispersity of rods.

4.4 Concluding remarks

In this chapter the influence of polydispersity on the order-disorder phase transition is investigated in different systems. As expected, the polydispersity promotes a phase transition: in each system the spinodals $\chi_s \langle L \rangle$ and $\omega_s \langle L \rangle$ are lowered when the polydispersity becomes stronger. This effect is also observed in [22] and [35], but from the results in [23] the contrary effect follows. This could be a consequence of the different way of averaging over the block length distribution which describes the polydispersity.

The influence of the bending stiffness on the spinodals $\chi_s \langle L \rangle$ and $\omega_s \langle L \rangle$ of a polydisperse melt appeared to be the same as the effects observed in section 3.5 in which the spinodals $\chi_s L$ and $\omega_s L$ of a melt of monodisperse semi-flexible diblock copolymers are calculated. In a microphase structure the wave number $q_* \langle L \rangle$ is lowered by the bending stiffness in both monodisperse and polydisperse systems.

Furthermore, we observed that the wave number $q_* \langle L \rangle$ is also lowered when the polydispersity becomes stronger. If the polydispersity is strong enough, $q_* \langle L \rangle$ becomes zero which corresponds to macrophase separation. In a macrophase it has appeared that the orientation tensors are zero so that there is only a nonzero scalar order-parameter. Reversibly, in a nematic phase there is only a global orientation. A nonzero scalar order-parameter is not induced. Only in a spatially inhomogeneous structure the density and orientation tensors are related to each other.

Chapter 5

Phase behaviour of a melt of monodisperse semi-flexible triblock copolymers

5.1 Introduction

In chapter 3 and 4 the phase behaviour of a melt of diblock copolymers has been investigated. In the general theory of multi-block copolymers in chapter 2 an arbitrary bending stiffness is added to the chains to make the description more realistic. The general theory is applied to a monodisperse melt of diblock copolymers in chapter 3. To approach reality closer, polydispersity is taken into account in chapter 4 which is described by the Schultz-Zimm distribution.

   In this chapter the phase behaviour of a melt of monodisperse semi-flexible triblock copolymers is investigated. The triblock is an ABA-triblock in which a block of kind B is connected at both sides to an A-block. The expression of the Landau free energy which is derived in section 3.2 for a melt of diblocks copolymers can also be applied to a melt of ABA-triblocks. The results in this chapter are compared to the results obtained from a diblock copolymer melt to see the effect of adding a third block to the diblock chain. In the same way as in section 3.6 in several phase diagrams the influence of the bending stiffness and Maier-Saupe interaction has been investigated. Furthermore, the spinodals $\chi_s L$ and $\omega_s L$ together with the corresponding wave number $q_* L$ are calculated as a function of chain composition and bending stiffness.

In other papers in the literature only Gaussian triblocks are considered. For example, in [47] the stability limit χ_{AB} is calculated in the random phase approximation for linear ABC-triblocks as a function of χ_{AC} and χ_{BC}. These results are compared to the results of random and statistical comb copolymers.

In [50] the phase diagram of different gradient copolymers has been calculated by means of the Landau theory. The gradient copolymers contains two kinds of monomers A and B. The monomer distribution function $g(x)$ is the probability to find a monomer of kind A at a distance xN from the first monomer in which N is the chain length and x is a parameter ranging from zero to one. Different systems with different distribution functions have been considered, for example systems in which the distribution function is given by

$$g(x) = \exp(-(c_3\pi(x - x_0))^4). \tag{5.1}$$

The corresponding chains are similar to BAB-triblock copolymers. In Eq. (5.1) c_3 determines the length of the A-block which is centered at $x = x_0$.

In [3] the self-consistent field theory is applied to investigate the phase behaviour of ABA-triblock copolymers in which the two A-blocks have the same length. In the phase diagram the gyroid phase has been observed besides the classical phases which are the lamellar, hexagonal and bcc structure. This gyroid phase has also been found in [50]. In this chapter and chapter 3 the possibility of complex phases has not been investigated.

5.2   Theory

In the same way as in chapter 3 and 4 the phase behaviour of a melt of monodisperse semi-flexible triblock copolymers is described by means of the Landau theory in the weak segregation regime. In section 3.2 an expression of the Landau free energy has been derived for a melt of monodisperse diblock copolymers. However, this expression is not restricted to diblock copolymers. It can be also be applied to a melt of monodisperse ABA-triblocks, ABAB-tetrablocks and other multi-block copolymers in which two kinds of blocks A and B are connected alternatingly.

This can be explained by means of the expression of the Landau free energy which has been derived in chapter 2 for a very general melt of multi-block copolymers. It is a power series expansion up to the fourth order in Fourier transform of the coarse grained density and orientational order-parameters Ψ^a and $\Upsilon^{\overline{a}}$, respectively.

The microscopic order-parameters are defined in detail by Eq. (2.3) till (2.9). The final form of this expression is given by,

$$
\begin{aligned}
\frac{F_L}{V} = \min_{\underline{\Psi}, \underline{\Upsilon}} \{ & (\Gamma^{(2)}_{ab} - \widetilde{\chi}_{ab})\Psi^a\Psi^b + 2\Gamma^{(2)}_{a\overline{b}}\Psi^a\Upsilon^{\overline{b}} + \\
& (\Gamma^{(2)}_{\overline{ab}} - \frac{1}{2}\omega_{\overline{ab}})\Upsilon^{\overline{a}}\Upsilon^{\overline{b}} - \frac{1}{3}\omega_{ab}\Upsilon^{a,ij}\delta_{ij}(\Psi^b + f^b) + \\
& \Gamma^{(3)}_{abc}\Psi^a\Psi^b\Psi^c + 3\Gamma^{(3)}_{ab\overline{c}}\Psi^a\Psi^b\Upsilon^{\overline{c}} + 3\Gamma^{(3)}_{a\overline{bc}}\Psi^a\Upsilon^{\overline{b}}\Upsilon^{\overline{c}} + \Gamma^{(3)}_{\overline{abc}}\Upsilon^{\overline{a}}\Upsilon^{\overline{b}}\Upsilon^{\overline{c}} + \\
& \Gamma^{(4)}_{abcd}\Psi^a\Psi^b\Psi^c\Psi^d + 4\Gamma^{(4)}_{abc\overline{d}}\Psi^a\Psi^b\Psi^c\Upsilon^{\overline{d}} + 6\Gamma^{(4)}_{ab\overline{cd}}\Psi^a\Psi^b\Upsilon^{\overline{c}}\Upsilon^{\overline{d}} + \\
& 4\Gamma^{(4)}_{a\overline{bcd}}\Psi^a\Upsilon^{\overline{b}}\Upsilon^{\overline{c}}\Upsilon^{\overline{d}} + \Gamma^{(4)}_{\overline{abcd}}\Upsilon^{\overline{a}}\Upsilon^{\overline{b}}\Upsilon^{\overline{c}}\Upsilon^{\overline{d}} \}.
\end{aligned}
\tag{5.2}
$$

In this expression the Γ's are related to single-chain correlation functions in a quite complicated way which is written down in detail in section 2.2. For a monodisperse melt only the single-chain correlation functions of one kind of chain has to be calculated. This has been done in the numerical calculation of the phase diagram of a melt of monodisperse semi-flexible diblock copolymers in chapter 3. In the same way the single-chain correlation functions can be calculated for a multi-block copolymer in which more than two blocks of kind A and B are connected alternatingly, for example an ABA-triblock.

The first harmonics approximation defined in chapter 3 can be applied for a general melt of alternating multi-block copolymers,

$$
\Psi^a = \Psi^A(\underline{q}) = -\Psi^B(\underline{q}) = \Psi(\underline{q}) \equiv \Psi \sum_{\underline{q}' \in H} \exp(i\varphi_{\underline{q}'})\delta(\underline{q} - \underline{q}')
\tag{5.3}
$$

and

$$
\begin{aligned}
\Upsilon^{\overline{a}} = \Upsilon^{\mu\nu}_\alpha(\underline{q}) \equiv & \Upsilon_\alpha(n^\mu_\alpha n^\nu_\alpha - \frac{1}{3}\delta^{\mu\nu}) \sum_{\underline{q}' \in H} \exp(i\varphi_{\underline{q}'})\delta(\underline{q} - \underline{q}') + \\
& \Upsilon^0_\alpha(n^\mu_\alpha n^\nu_\alpha - \frac{1}{3}\delta^{\mu\nu})\delta(\underline{q}),
\end{aligned}
\tag{5.4}
$$

and is inserted in Eq. (5.2). The set H in Eq. (5.3) and (5.4) is a set of wave vectors with equal length q_* describing a certain symmetrical structure, for example the smectic-A or -C phase in which $H = \{-\underline{q}, \underline{q}\}$. According to the Landau theory q_* is the wave number at which the disordered phase is instable and is converted into an ordered structure. The vector $\underline{n}^\mu$ is the director of the orientation of A- or B-blocks.

In chapter 3 it has been explained that it is justified to assume that $\underline{n}_A^\mu = \underline{n}_B^\mu = \underline{n}^\mu$ in a diblock melt. For the same reason it can be assumed that $\underline{n}_A^\mu = \underline{n}_B^\mu = \underline{n}^\mu$ in a melt of alternating multi-block copolymers. In the nematic, smectic-A and smectic-C phase the director $\underline{n}^\mu$ is spatially independent, but in more complicated structures such as the bcc and hexagonal phase a spatially dependent director $\underline{n}^\mu(\underline{x})$ is necessary to describe the orientational structure. In the same way as in chapter 3 the director $\underline{n}^\mu(\underline{x})$ is chosen such that the bcc and hexagonal phase can be expressed as a linear combination of smectic-A phases.

In this way the second order term of the Landau free energy according to Eq. (5.2) can always be written in the following matrix form,

$$
\frac{F_L^{(2)}}{V} = \begin{bmatrix} \Psi & \Upsilon_A & \Upsilon_B \end{bmatrix} \begin{bmatrix} \widetilde{\Gamma}^{(2)} - \chi & \widetilde{\Gamma}_A^{(2)} & \widetilde{\Gamma}_B^{(2)} \\ \widetilde{\Gamma}_A^{(2)} & \widetilde{\Gamma}_{AA}^{(2)} - \frac{1}{3}\omega_{AA} & \widetilde{\Gamma}_{AB}^{(2)} - \frac{1}{3}\omega_{AB} \\ \widetilde{\Gamma}_B^{(2)} & \widetilde{\Gamma}_{AB}^{(2)} - \frac{1}{3}\omega_{AB} & \widetilde{\Gamma}_{BB}^{(2)} - \frac{1}{3}\omega_{BB} \end{bmatrix} \begin{bmatrix} \Psi \\ \Upsilon_A \\ \Upsilon_B \end{bmatrix} +
$$

$$
\begin{bmatrix} \Upsilon_A^0 & \Upsilon_B^0 \end{bmatrix} \begin{bmatrix} \widetilde{\Gamma}_{AA,00}^{(2)} - \frac{1}{3}\omega_{AA} & \widetilde{\Gamma}_{AB,00}^{(2)} - \frac{1}{3}\omega_{AB} \\ \widetilde{\Gamma}_{AB,00}^{(2)} - \frac{1}{3}\omega_{AB} & \widetilde{\Gamma}_{BB,00}^{(2)} - \frac{1}{3}\omega_{BB} \end{bmatrix} \begin{bmatrix} \Upsilon_A^0 \\ \Upsilon_B^0 \end{bmatrix}, \tag{5.5}
$$

after inserting the first harmonics approximation. For simplicity in Eq. (5.5) the three parameters ω_{AA}, ω_{AB} and ω_{BB} have been taken equal, $\omega_{AA} = \omega_{AB} = \omega_{BB} = \omega$. In the first matrix the length q_* of the set H of wave vectors has a nonzero value and in the second matrix q_* is zero. The $\widetilde{\Gamma}$'s in the first matrix are given by

$$
\widetilde{\Gamma}^{(2)} = \Gamma_{ab}^{(2)} S^a S^b, \quad \widetilde{\Gamma}_\alpha^{(2)} = \Gamma_{a\bar{b}}^{(2)} S^a d_\alpha^{\bar{b}} \text{ and } \widetilde{\Gamma}_{\alpha\beta}^{(2)} = \Gamma_{\bar{a}\bar{b}}^{(2)} d_\alpha^{\bar{a}} d_\beta^{\bar{b}} \text{ in which } \alpha, \beta = A, B, \tag{5.6}
$$

and S^a and $d_\alpha^{\bar{b}}$ are defined as,

$$
S^a \equiv (1 - 2\delta_{\alpha B}) \exp(i\varphi_{\underline{q}}) = \pm \exp(i\varphi_{\underline{q}}) \text{ in which } a = \underline{q}, \alpha \tag{5.7}
$$

and

$$
d_\alpha^{\bar{b}} \equiv (n_\beta^{\mu_2} n_\beta^{\nu_2} - \frac{1}{3}\delta^{\mu_2\nu_2}) \exp(i\varphi_{\underline{q}}) \delta_{\alpha\beta} \text{ in which } \bar{b} = \underline{q}, \beta, \mu_2\nu_2. \tag{5.8}
$$

The $\widetilde{\Gamma}$'s in the second matrix in Eq. (5.5) can be written in the same way. The eigenvalues of the first matrix in Eq. (5.5) are denoted as λ_1, λ_2 and λ_3 and in the second matrix these are written as λ_{10} and λ_{20}. The corresponding eigenvectors are $\underline{x}_1, \underline{x}_2, \underline{x}_3, \underline{x}_{10}$ and $\underline{x}_{20}$. If the Flory-Huggins parameter χ and Maier-Saupe parameter ω are low enough the melt is in the disordered state. In that case all eigenvalues λ_1,

λ_2, λ_3, λ_{10} and λ_{20} are positive. At the spinodals $\chi = \chi_s$ or $\omega = \omega_s$ at least one of the eigenvalues is zero and becomes negative if χ or ω is further increased. In this way the expressions of χ_s and ω_s are determined which are,

$$\chi_s = \min_{\{q_*, n^\mu\}} \{\widetilde{\Gamma}^{(2)} - \frac{(\widetilde{\Gamma}^{(2)}_B)^2(\widetilde{\Gamma}^{(2)}_{AA} - \frac{1}{3}\omega) + (\widetilde{\Gamma}^{(2)}_A)^2(\widetilde{\Gamma}^{(2)}_{BB} - \frac{1}{3}\omega) - 2\widetilde{\Gamma}^{(2)}_A\widetilde{\Gamma}^{(2)}_B(\widetilde{\Gamma}^{(2)}_{AB} - \frac{1}{3}\omega)}{(\widetilde{\Gamma}^{(2)}_{AA} - \frac{1}{3}\omega)(\widetilde{\Gamma}^{(2)}_{BB} - \frac{1}{3}\omega) - (\widetilde{\Gamma}^{(2)}_{AB} - \frac{1}{3}\omega)^2}\}$$

(5.9)

and

$$\omega_s = 3 \min_{\{q_*, n^\mu\}} \{\frac{(\widetilde{\Gamma}^{(2)} - \chi)(\widetilde{\Gamma}^{(2)}_{AA}\widetilde{\Gamma}^{(2)}_{BB} - (\widetilde{\Gamma}^{(2)}_{AB})^2) - (\widetilde{\Gamma}^{(2)}_A)^2\widetilde{\Gamma}^{(2)}_{BB} + 2\widetilde{\Gamma}^{(2)}_A\widetilde{\Gamma}^{(2)}_B\widetilde{\Gamma}^{(2)}_{AB} - (\widetilde{\Gamma}^{(2)}_B)^2\widetilde{\Gamma}^{(2)}_{AA}}{(\widetilde{\Gamma}^{(2)} - \chi)(\widetilde{\Gamma}^{(2)}_{AA} + \widetilde{\Gamma}^{(2)}_{BB} - 2\widetilde{\Gamma}^{(2)}_{AB}) - (\widetilde{\Gamma}^{(2)}_A - \widetilde{\Gamma}^{(2)}_B)^2}\},$$

(5.10)

in which a minimization is carried out over q_* and the director vector $\underline{n}^\mu$. These expressions can be applied for both $q_* = 0$ and $q_* \neq 0$.

In general the eigenvalues λ_1, λ_2, λ_3, λ_{10} and λ_{20} are different. In section 3.2 the free energy of a microphase structure is derived in which λ_1 is negative and the other eigenvalues are still positive. It has appeared that this free energy can be written as a power series expansion of only one parameter $x_1 = \pm|\underline{x}_1|$ and is given by

$$\frac{F_L}{V} = \min_{x_1}\{\lambda_1 x_1^2 + C^{(3)}_{111}x_1^3 + (C^{(4)}_{1111} - \sum_{n\neq 1}\frac{(C^{(3)}_{11n})^2}{4\lambda_n})x_1^4\} =$$
$$\min_{x_1}\{\lambda_1 x_1^2 + C^{(3)}_{111}x_1^3 + \widetilde{C}^{(4)}_{1111}x_1^4\}.$$

(5.11)

At the minimum x_1 is

$$x_1 = \frac{-3C^{(3)}_{111} \pm \sqrt{9(C^{(3)}_{111})^2 - 32\lambda_1\widetilde{C}^{(4)}_{1111}}}{8\widetilde{C}^{(4)}_{1111}}.$$

(5.12)

In this final form of the Landau free energy the $C-$coefficients are expressed in detail in section 3.2. Such a form can also be derived for a general melt of alternating multi-block copolymers.

5.3 Results and discussion

In the results of this section a melt of monodisperse semi-flexible triblock copolymers is considered. In the triblock the length of the first and second A-block are denoted

as L_{A1} and L_{A2}. The parameter f is the A-block fraction which is defined by $f \equiv (L_{A1} + L_{A2})/L = L_A/L$. For a triblock melt another parameter τ is necessary to determine the chain composition which is the ratio between the length of the first and second A-block, $\tau \equiv L_{A1}/L_{A2}$. The influence of these composition parameters f and τ on the phase behaviour is investigated in the following systems: (a) coil-coil-coil $(\lambda_A/L_A = 10^{-4} = \lambda_B/L_B)$; (b) semi-semi-semi $(\lambda_A/L_A = 10^{-1} = \lambda_B/L_B)$; (c) coil-rod-coil $(\lambda_A/L_A = 10^{-4} \ll \lambda_B/L_B = 10^2)$; (d) rod-coil-rod $(\lambda_A/L_A = 10^2 \gg \lambda_B/L_B = 10^{-4})$.

First the spinodals $\chi_s L$ and $\omega_s L$ are calculated together with the corresponding wave number $q_* L$. $\chi_s L$ is a function of the parameters f, τ, ω and λ_α/L_α,

$$\chi_s L = \chi_s L(f, \tau, \omega, \lambda_\alpha/L_\alpha) \text{ with } \alpha = A, B. \tag{5.13}$$

The corresponding wave number $q_* L$ depends on the same set of parameters. In the same way the spinodal $\omega_s L$ and corresponding $q_* L$ are both functions of f, τ, χ and λ_α/L_α.

In Eq. (5.9) and (5.10) a minimalization is carried out over the director vector $\underline{n} = (\cos\theta, \sin\theta, 0)$. It has been verified that the angle θ is always zero. So if a microphase structure is found at the spinodal $\chi_s L$ or $\omega_s L$, it is always a smectic-A phase or a superposition of smectic-A phases in different directions.

In Fig. (5.1) till (5.4) $\chi_s L$ and the corresponding wave number $q_* L$ are calculated as a function of f for system (a), (b), (c) and (d). In each figure the lines belonging to $\tau = 0, 1/8, 1/4, 1/2$ and 1 are displayed and $\omega = 0$. In the same way $\omega_s L$ is calculated as a function of f in Fig. (5.5) for system (b), (c) and (d). In these figures $\chi = 0$ and the corresponding wave number $q_* L$ is always zero when Eq. (5.10) is minimized with respect to $q_* L$. Hence, above ω_s the system always becomes unstable against nematic ordering if the Flory-Huggins parameter is chosen to be negligibly small. In Fig. (5.6) $\chi_s L$ and $q_* L$ are calculated as a function of $\omega L = \omega_s L$ for system (c) and (d). The composition parameters are $f = 0.5$ and $\tau = 1$. The line is truncated at the spinodal $\omega_s L = \omega_{s,nem} L$ at which ωL is great enough to form a nematic phase.

In Fig. (5.7) till (5.9) the complete phase diagram has been calculated for system (a), (c) and (d). In system (a) the orientations of the A- and B-block are neglected, $\Upsilon_A \approx 0$ and $\Upsilon_B \approx 0$, because the triblock is regarded as totally flexible. For the same reason in system (c) and (d) only the orientation of the stiff blocks is taken into account. Therefore only the Maier-Saupe interaction ω between stiff blocks may influence the phase behaviour. The ratio $r = \frac{\omega}{\chi}$ has been varied in Fig. (5.8) and (5.9).

In general in Fig. (5.1) till (5.4) the spinodal $\chi_s L$ and corresponding wave number $q_* L$ are decreasing when τ becomes smaller. This could be explained in the following
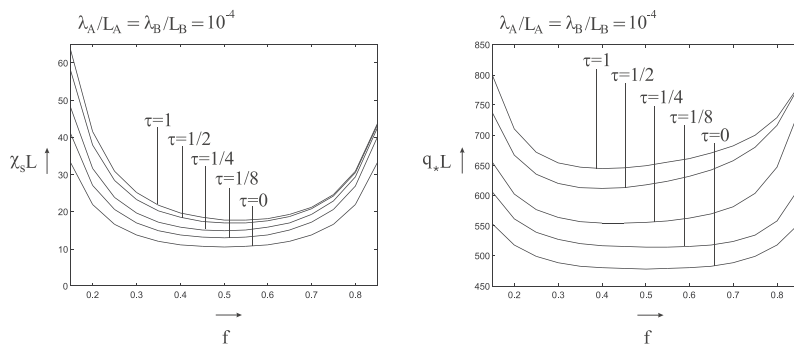
Figure 5.1: The spinodal $\chi_s L$ and the corresponding wave number $q_* L$ as a function of f calculated for different τ in system (a).
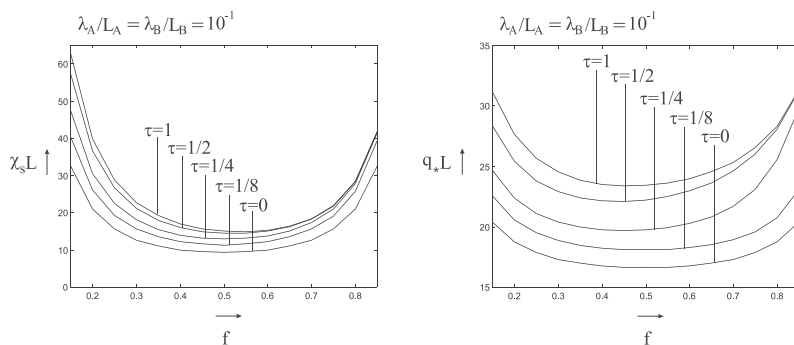
Figure 5.2: The spinodal $\chi_s L$ and the corresponding wave number $q_* L$ as a function of f calculated for different τ in system (b).

way. At $\tau = 0$ the chain is a diblock and so if τ is close to zero the triblock can be regarded as a diblock-like chain. In a melt of ABA-triblocks it could be more difficult to form a microphase structure, because each B-block is connected at both sides to an A-block. This restricts the configurational freedom of a B-block in a B-rich domain. If the chain is a diblock the B-block has one free. The other chain end prefers to be removed further from the centre of a B-rich domain to stimulate microphase separation. In a triblock both ends avoid the centre of a B-rich domain. In that case fewer chain configurations are possible. Consequently in a triblock melt the entropy loss is greater when a microphase structure is formed. The entropy loss
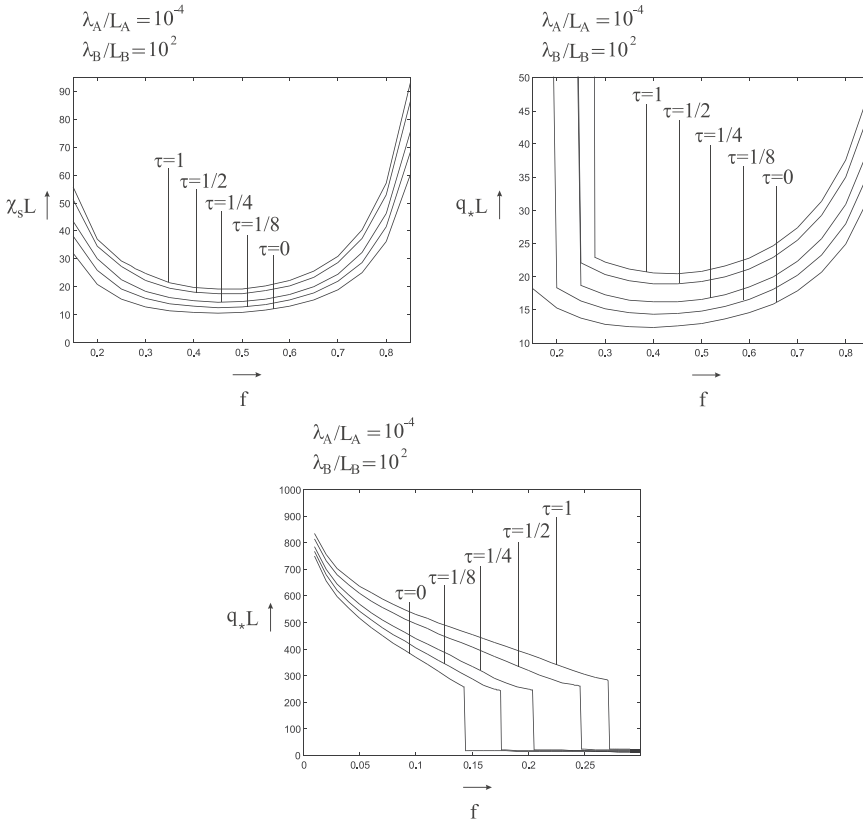
Figure 5.3: The spinodal $\chi_s L$ and the corresponding wave number $q_* L$ as a function of f calculated for different τ in system (c).

must be compensated by a stronger repulsion χ. This effect is weakened when the triblock becomes a diblock-like chain which could explain why the spinodal $\chi_s L$ is lower at a smaller τ.

At the same time the corresponding wave number $q_* L$ is decreasing. So at a smaller τ the size of the domains in the microphase structure becomes greater. This follows from the fact that at a constant f the longest A-block in the ABA-triblock becomes longer when τ decreases. In that case greater A-rich domains are possible which leads to a smaller $q_* L$. This may also explain why $\chi_s L$ is lower at a smaller τ. In a triblock melt the domains are smaller so that an A-block has to travel a shorter
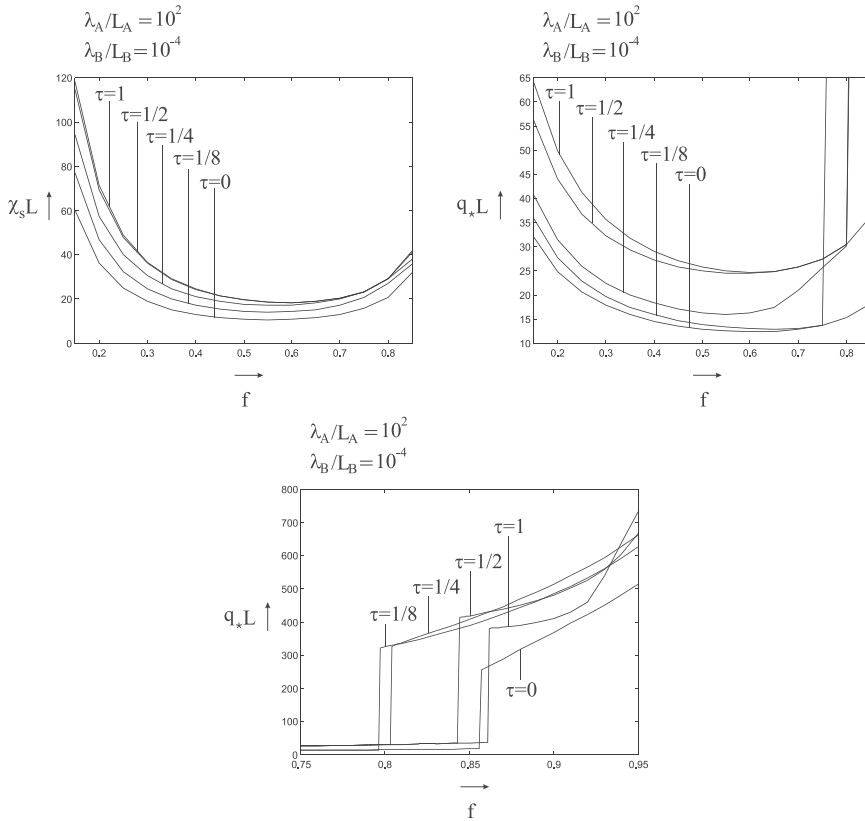
Figure 5.4: The spinodal $\chi_s L$ and the corresponding wave number $q_* L$ as a function of f calculated for different τ in system (d).

distance to reach a B-rich domain. This will make it easier to mix A- and B-blocks so that a stronger χ is necessary to keep the A- and B-blocks separated from each other. In a melt of diblocks mixing is less easier which could also make microphase separation possible at a lower χ.

In Fig. (5.5) the spinodal $\omega_s L$ is calculated which is again lowered when τ becomes smaller. This could be explained by the following two reasons. First in a triblock the B-block is connected at both sides to an A-block but in a diblock the B-block has one free end. Maybe therefore in a triblock melt the B-blocks could be hindered in a greater degree to be aligned along the same direction. Secondly within
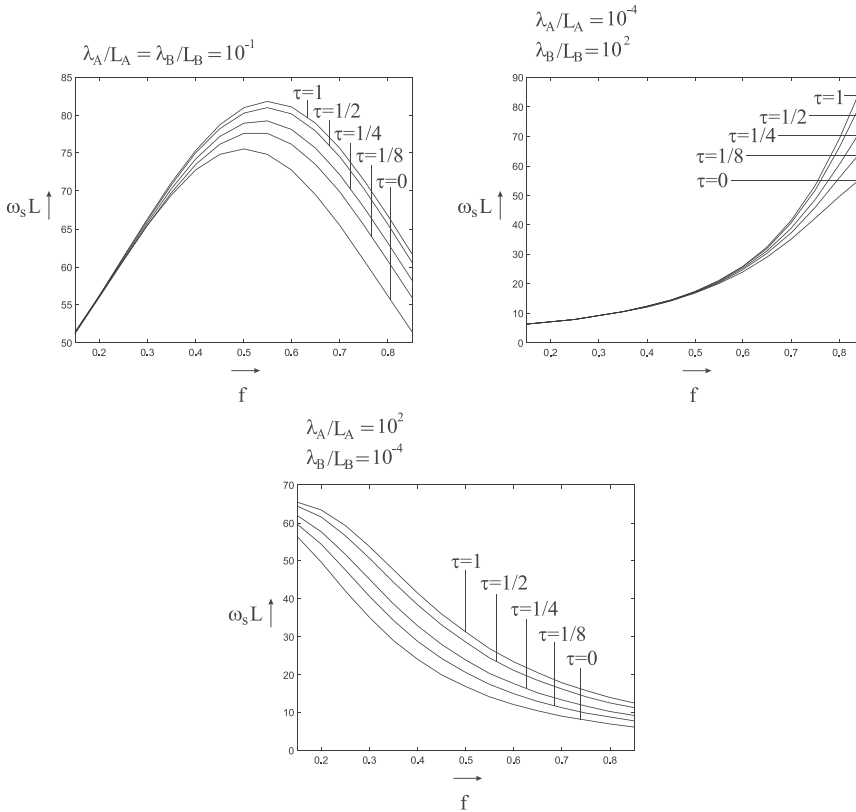
Figure 5.5: The spinodal $\omega_s L$ as a function of f calculated for different τ in system (b), (c) and (d).

each triblock two A-blocks prefer to be directed in the same direction in the nematic phase. However, if the chain is a diblock there is only one A-block which has to be aligned. Maybe therefore in a diblock melt the entropy loss could be smaller when a nematic phase is formed. To system (c) only the first reason is applicable and to system (d) only the second one. To system (b) both reasons can be applied.

In Fig. (5.6) $\chi_s L$ is lowered and $q_* L$ is increased by $\omega_s L$ at $f = 0.5$ and $\tau = 1$ in both system (c) and (d). This has also been observed and explained in chapter 3 and 4 for a diblock melt. The same explanation can be applied to a triblock melt. In Fig. (5.3) in the region $f < 0.3$ the wave number $q_* L$ jumps to a much greater value in each line at a certain point when f is made smaller. The same effect is
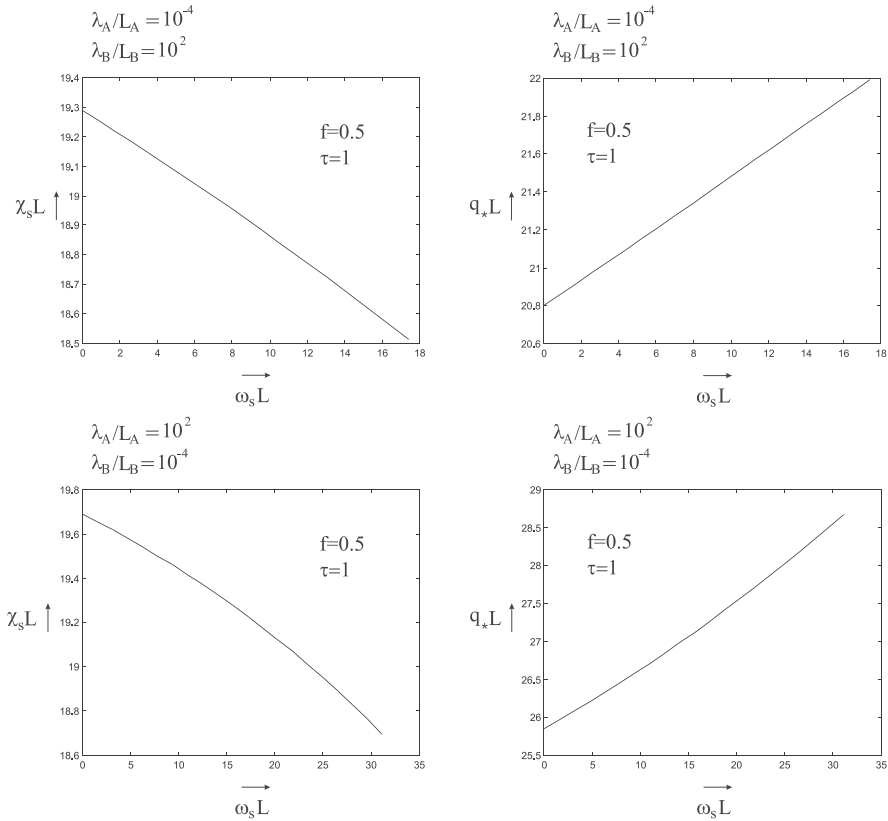
Figure 5.6: The spinodal $\chi_s L$ and corresponding wave number $q_* L$ as a function of $\omega_s L$ calculated in system (c) and (d) at $f = 0.5$ and $\tau = 1$.

observed in the region $f > 0.75$ in Fig. (5.4) when f is made greater. In both figures it has been verified that at such a great wave number the spinodal $\chi_s L$ and corresponding wave number $q_* L$ do not change hardly anything when ωL is varied. Here the eigenvector $\widehat{x}_1$ belonging to the smallest eigenvalue $\lambda_1 = 0$ is approximately $\widehat{x}_1 = (\widehat{\Psi}_1, \widehat{\Upsilon}_i^A, \widehat{\Upsilon}_i^B) \approx (1, 0, 0)$. This follows from the fact that in the first matrix in Eq. (5.5) the coefficients $\widetilde{\Gamma}_A^{(2)}$ and $\widetilde{\Gamma}_B^{(2)}$ are negligibly small. So in this microphase structure there is hardly any orientation of rods. This phase behaviour has also been observed in chapter 4 in which a melt of polydisperse diblock copolymers is investigated.

In Fig. (5.7) at $\tau = 0$ the phase diagram is exactly in agreement with the phase
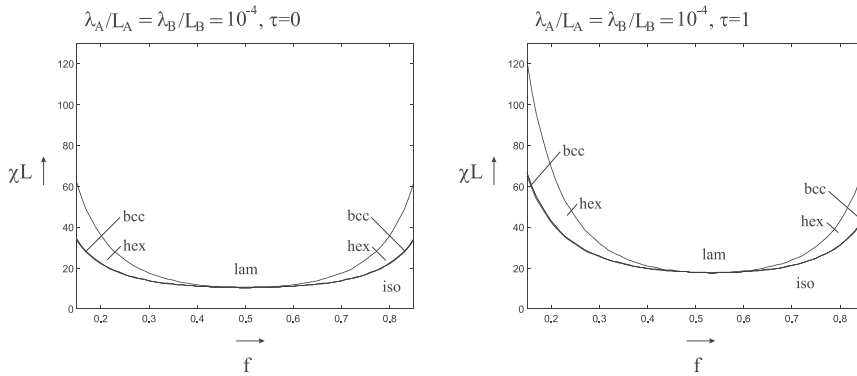
Figure 5.7: Phase diagram calculated for $\tau = 0$ and $\tau = 1$ in system (a).

diagram calculated by Leibler in [5]. Here the phase transition point is reached at $f = 0.5$ but at $\tau = 1$ the phase transition point is shifted to $f = 0.524$. So at $\tau = 1$ the phase diagram is asymmetric. In the left side the domain of the hexagonal phase is greater than in the right side. In the left side the A-block is short enough so that in the hexagonal phase the A-blocks can form cylinders embedded by a B-rich matrix. Within one chain two A-blocks can be positioned in the same cylinder or in two different neighbouring cylinders. This increases the number of possible chain configurations which could explain why the melt prefers the hexagonal phase more than the lamellar phase. In the right side of the phase transition point the reverse hexagonal and bcc phase is formed in which B-rich domains are formed in an A-rich environment. In these phases less chain configurations are possible which makes these phases entropically less favourable. Maybe therefore the phase transition point is reached at $f > 0.5$ and the hexagonal domain is smaller at the right side of the phase diagram.

The phase bevaviour of system (c) observed in Fig. (5.8) is similar to the behaviour of a rod-coil diblock melt investigated in section 3.6. The phase transition point is reached at $f = 0.326$ at which a smectic-A phase is found just above the spinodal $\chi_s L$. The size of the domain of the bcc, hexagonal and smectic-A phase increases when the Maier-Saupe interaction becomes stronger. The smectic-C domain is shifted to a greater χL. This has also been observed in section 3.6 in a rod-coil diblock melt and can be explained in the same way. When $f < 0.272$ the wave number $q_* L$ jumps to a much greater value according to Fig. (5.3). In that region it was
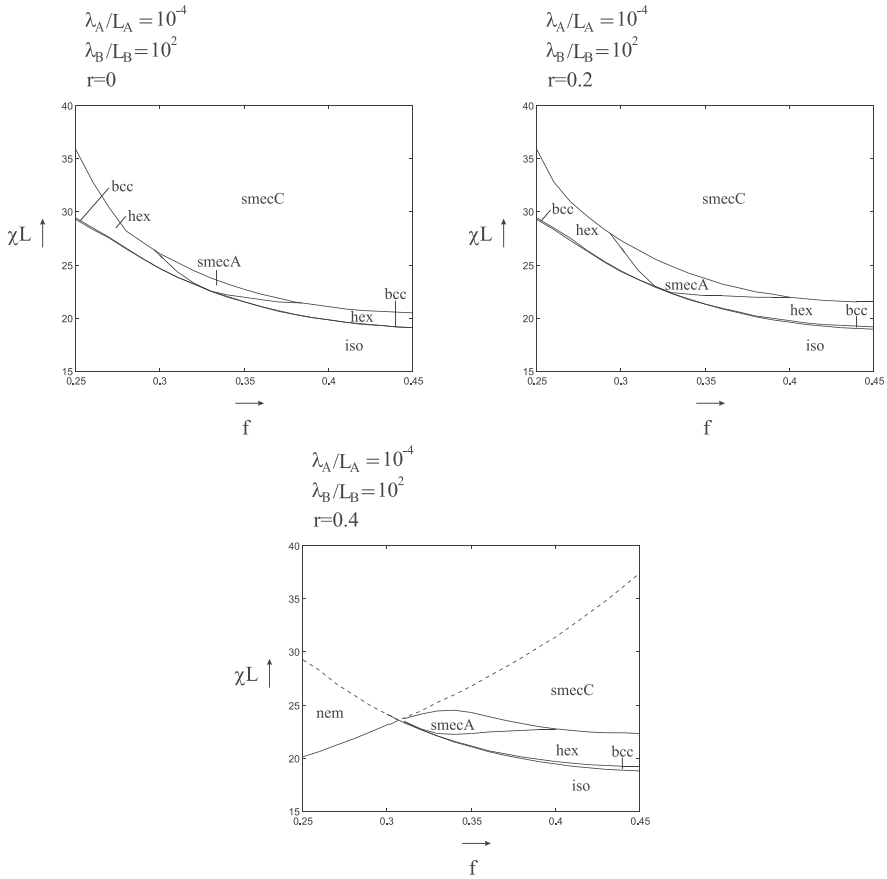
Figure 5.8: Phase diagram calculated for $r = 0$, $r = 0.2$ and $r = 0.4$ in system (c) in which $\tau = 1$.

earlier explained that in the eigenvector $\widehat{x}_1$ belonging to the lowest eigenvalue λ_1 the orientational components are negligible, $\widehat{x}_1 = (\widetilde{\Psi}_1, \widehat{\Upsilon}_i^A, \widehat{\Upsilon}_i^B) \approx (1, 0, 0)$. Because this eigenvector is very dominating, the influence of the Maier-Saupe interaction on the phase behaviour is also negligible. This can be clearly observed in Fig. (5.8) in the part at which $f < 0.272$.

In general the phase behaviour in Fig. (5.9) does not differ very much from the behaviour in Fig. (5.8). The phase transition point is found at $f = 0.742$ at which a smectic-A phase is found just above the spinodal $\chi_s L$. However, if we compare

$\lambda_A/L_A = 10^2$
$\lambda_B/L_B = 10^{-4}$
r=0

$\lambda_A/L_A = 10^2$
$\lambda_B/L_B = 10^{-4}$
r=0.25

$\lambda_A/L_A = 10^2$
$\lambda_B/L_B = 10^{-4}$
r=0.5
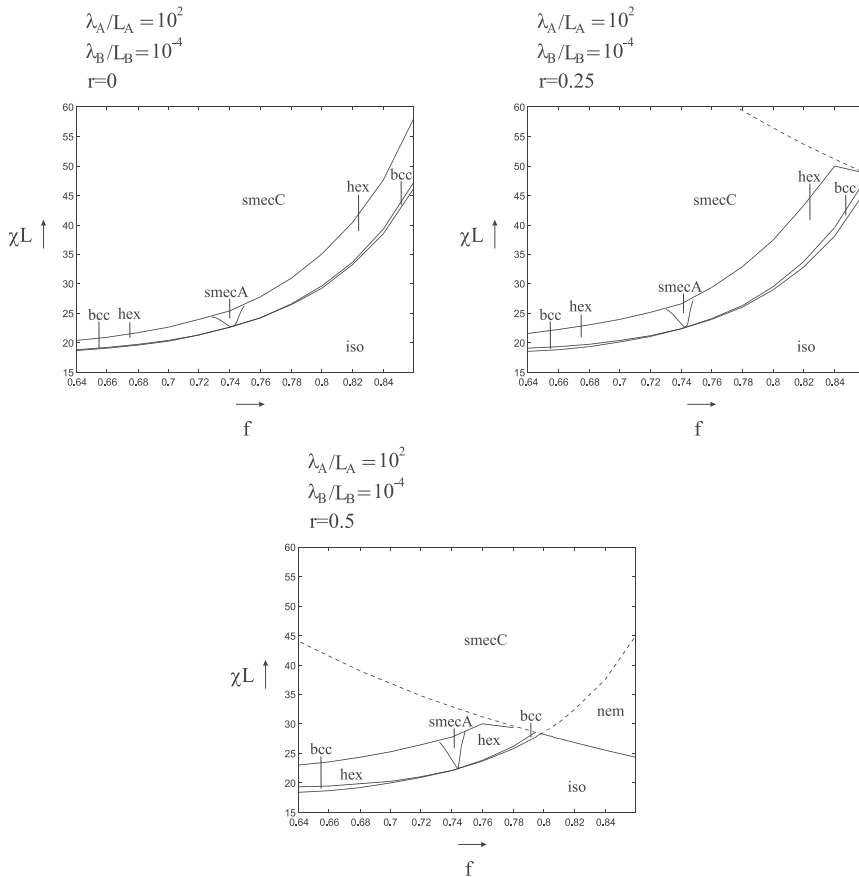
Figure 5.9: Phase diagram calculated for $r = 0$, $r = 0.25$ and $r = 0.5$ in system (d) in which $\tau = 1$.

Fig. (5.8) and (5.9) we see that in Fig. (5.9) the broad of the domain of the smectic-A phase is much smaller and the vertical length of the bcc and hexagonal part is greater. So in system (d) the melt prefers to form a micellar phase above a layered structure. In system (d) in each chain the two rods are connected by flexible coil so that the two rods can be rotated independently of each other. In such a chain there is a greater flexibility to form different chain configurations which makes it easier to form a micellar phase. In system (c) in each chain two coils are connected by a rod. Due to the rod in the middle it is more difficult to form different chain configurations

so that system (c) prefers a layered structure.

In Fig. (5.8) above the phase transition point at $f = 0.326$ the smectic-A phase is converted into the smectic-C phase when χL is increased. Exactly at the transition in the smectic-C phase the orientation θ is $\theta = 8.9°$, $9°$ and $10.8°$ at $r = 0, 0.2$ and 0.4, respectively. If χL is further increased, θ increases and converges to a constant value. At an even greater χL the coefficient $\widetilde{C}_{1111}^{(4)}$ in Eq. (5.11) becomes negative so that higher order terms are necessary to determine θ. In Fig. (5.9) the phase transition point is reached at $f = 0.742$ at which the smectic-A phase is found again which is converted into the smectic-C phase at a greater χL. Here θ jumps from $\theta = 0°$ to $\theta = 8.1°$, $6.8°$ and $7°$ at $r = 0, 0.25$ and 0.5, respectively, and converges to a constant value when χL is increasing. If χL becomes too great the coefficient $\widetilde{C}_{1111}^{(4)}$ in Eq. (5.11) becomes negative again. In general in the smectic-C domain in both Fig. (5.8) and (5.9) $\widetilde{C}_{1111}^{(4)}$ is closer to zero and χL is further away from the spinodal $\chi_s L$. Consequently the magnitude of the order-parameters is greater at the minimum of the Landau free energy, which makes the power series approximation less reliable. Only in the neighbourhood of the phase transition point it is allowed to draw conclusions from the results. In system (c) and (d) the relation between θ and χL is similar to Fig. (3.22) in section 3.6 which corresponds to a rod-coil diblock melt. In this figure each line is truncated at the point at which $\widetilde{C}_{1111}^{(4)}$ becomes negative when χL is further increased.

In the nematic phase the coefficient $\widetilde{C}_{1111}^{(4)}$ in Eq. (5.11) is negative when $\omega L > \omega_s L$ in the neighbourhood of the phase transition point in both system (c) and (d). So fifth and higher order terms would be necessary to calculate the minimum of the free energy. This problem has also occurred in section 3.6. It was assumed that the nematic phase has always the lowest free energy when $\omega L > \omega_s L$. This assumption is again made in this section.

5.4   Concluding remarks

In this chapter the influence of the composition parameter τ on the order-disorder phase transition is investigated in different systems. In each system the spinodal $\chi_s L$ and corresponding wave number $q_* L$ are lowered when τ becomes smaller. The same effect has been observed in the calculations of the spinodal $\omega_s L$.

Furthermore, in different systems the phase diagram has been determined. From the results it has appeared that the phase behaviour of triblock copolymers does not differ very much from diblock copolymers. Around the phase transition point the

same phases are formed in the same sequence. The influence of the Maier-Saupe interaction on the phase behaviour is qualitatively the same. However, in the phase diagram of a melt of rod-coil-rod triblock copolymers the broad of the domain of the smectic-A phase is much smaller.

Appendix A

In this appendix the second, third and fourth order correlation functions as introduced in chapter 2 are calculated. All second order correlation functions can be derived from the following generalised second order correlation function,

$$
\begin{aligned}
A^{\alpha\beta}(\underline{q}_1, \underline{q}_2) \ \equiv\ & \sum_{l_1, l_2} \sigma_{l_1}^{\alpha} \sigma_{l_2}^{\beta} \left\langle \exp\left(-i\underline{q}_1 \cdot \underline{R}(l_1) - i\underline{q}_2 \cdot \underline{R}(l_2) + \int_0^L dl\underline{\eta}(l) \cdot \underline{\dot{R}}(l) \right) \right\rangle_0 = \\
& \sum_{l_1, l_2} \sigma_{l_1}^{\alpha} \sigma_{l_2}^{\beta} \int d\widetilde{\underline{U}} \int d\underline{U} \int D\underline{R} \int D\underline{u} \ \delta(\underline{u}(l) - \underline{\dot{R}}(l)) \times \\
& \delta(\underline{\dot{R}}(0) - \widetilde{\underline{U}})\delta((\underline{\dot{R}}(L) - \underline{U}) \exp(-H_0) \times \\
& \exp\left(-i\underline{q}_1 \cdot \underline{R}(l_1) - i\underline{q}_2 \cdot \underline{R}(l_2) + \int_0^L dl\underline{\eta}(l) \cdot \underline{u}L) \right).
\end{aligned} \tag{A.1}
$$

$\underline{R}(l)$ is the position vector of a certain segment labelled by l. $\widetilde{\underline{U}}$ and $\underline{U}$ are the the tangent vectors of the first and last segment, respectively. H_0 is the Hamiltonian of an unperturbed semi-flexible chain. For a semi-flexible homopolymer H_0 is equal to

$$
H_0 = \frac{3}{4}\widetilde{U}^2 + \frac{3}{4}U^2 + \frac{3}{4}\int_0^L dl[\lambda \underline{\ddot{R}}^2(l) + \frac{1}{\lambda}\underline{\dot{R}}^2(l)], \tag{A.2}
$$

which is the Hamiltonian corresponding to the Bawendi-Freed model [16]. In the Bawendi-Freed model [16] the segments are connected to each other by springs with a spring constant equal to $\frac{3}{2\lambda}$. On a coarse grained level $\underline{u}(l)$ is the tangent vector, but on the microscopic level $\underline{u}(l)$ is the connection vector between two segments. So

the fourth term of H_0 can be regarded as the total spring energy. If we consider $\frac{3\lambda}{2}$ as the mass of a segment, then the third term becomes the total kinetic energy. In this way H_0 can be regarded as the Hamiltonian of a chain of connected harmonic oscillators. $\underline{u}(l)$ is on average equal to a unit vector. Another possible model to describe a semi-flexible chain is the Saitô model [18]. In that model the segments are not connected by springs. The connection vector $\underline{u}(l)$ between two segments has a constant unit length so that only the third term of H_0 remains. So in Eq. (A.1) the delta function $\delta(u^2 - 1)$ has to be added in the functional integration over $\underline{u}$. This restriction makes the calculation of the correlation function analytically impossible. Therefore we choose the Bawendi-Freed model [16] in which $\underline{u}(l)$ is only on average equal to a unit vector. The first and second term in H_0 are local potential energies at the ends of the homopolymer. These terms are added to the free Hamiltonian so that $\left\langle u(l)^2 \right\rangle_0 = 1$ everywhere along the chain. If these terms are omitted, then $\left\langle u(l)^2 \right\rangle_0 \neq 1$ close to the ends of the homopolymer. The local potential energies are necessary to describe a homogeneous chain according to [14]. Eq. (A.2) is the free Hamiltonian of a semi-flexible homopolymer with a constant persistent length λ. It can be proven that in Eq. (A.2) it is allowed to replace the constant λ by an l-dependent persistent length $\lambda(l)$. Then Eq. (A.2) can also be applied to a multiblock copolymer.

In Eq. (A.1) $\underline{\eta}(l)$ is an arbitrary path which is used to calculate the tensorial correlation functions $\left\langle \widehat{S}^{\alpha}_{\mu_1\nu_1}(\underline{q}_1)\rho^{\beta}(\underline{q}_2) \right\rangle_0$ and $\left\langle \widehat{S}^{\alpha}_{\mu_1\nu_1}(\underline{q}_1)\widehat{S}^{\beta}_{\mu_2\nu_2}(\underline{q}_2) \right\rangle_0$. However, in Eq. (2.51) and (2.52) in chapter 2 the tensor $\underline{\underline{\hat{Q}}}^{\alpha}(\underline{x})$ is applied instead of $\underline{\underline{\hat{S}}}^{\alpha}(\underline{x})$ which is defined by,

$$\underline{\underline{\hat{Q}}}^{\alpha}(\underline{x}) \equiv \underline{\underline{\hat{S}}}^{\alpha}(\underline{x}) - \frac{1}{3}\hat{\rho}^{\alpha}(\underline{x})\underline{\underline{I}} \qquad (\alpha = 1, ..., M). \qquad (A.3)$$

By means of this definition $\left\langle \widehat{Q}^{\alpha}_{\mu_1\nu_1}(\underline{q}_1)\rho^{\beta}(\underline{q}_2) \right\rangle_0$ and $\left\langle \widehat{Q}^{\alpha}_{\mu_1\nu_1}(\underline{q}_1)\widehat{Q}^{\beta}_{\mu_2\nu_2}(\underline{q}_2) \right\rangle_0$ can be expressed as,

$$\left\langle \widehat{Q}^{\alpha}_{\mu_1\nu_1}(\underline{q}_1)\rho^{\beta}(\underline{q}_2) \right\rangle_0 = \left\langle \widehat{S}^{\alpha}_{\mu_1\nu_1}(\underline{q}_1)\rho^{\beta}(\underline{q}_2) \right\rangle_0 - \frac{1}{3}\delta_{\mu_1\nu_1}\left\langle \rho^{\alpha}(\underline{q}_1)\rho^{\beta}(\underline{q}_2) \right\rangle_0 \qquad (A.4a)$$

and

$$\left\langle \widehat{Q}^{\alpha}_{\mu_1\nu_1}(\underline{q}_1)\widehat{Q}^{\beta}_{\mu_2\nu_2}(\underline{q}_2) \right\rangle_0 = \left\langle \widehat{S}^{\alpha}_{\mu_1\nu_1}(\underline{q}_1)\widehat{S}^{\beta}_{\mu_2\nu_2}(\underline{q}_2) \right\rangle_0 - \frac{1}{3}\delta_{\mu_1\nu_1}\left\langle \rho^{\alpha}(\underline{q}_1)\widehat{S}^{\beta}_{\mu_2\nu_2}(\underline{q}_2) \right\rangle_0 +$$
$$-\frac{1}{3}\delta_{\mu_2\nu_2}\left\langle \widehat{S}^{\alpha}_{\mu_1\nu_1}(\underline{q}_1)\rho^{\beta}(\underline{q}_2) \right\rangle_0 + \frac{1}{9}\delta_{\mu_1\nu_1}\delta_{\mu_2\nu_2}\left\langle \rho^{\alpha}(\underline{q}_1)\rho^{\beta}(\underline{q}_2) \right\rangle_0. \qquad (A.4b)$$

Third and fourth order tensorial correlation functions are determined in a similar way.

The physical meaning of these single chain correlation functions can be explained by Fourier transforming them back into real space. $\left\langle \rho^\alpha(\underline{x}_1)\rho^\beta(\underline{x}_2) \right\rangle_0$ is the probability that x_1 is in the α-block and x_2 is in the β-block of a certain chain. The average is taken over all possible chain configurations which is denoted by $\langle \rangle_0$. $\left\langle \widehat{S}^\alpha_{\mu_1 \nu_1}(\underline{x}_1)\rho^\beta(\underline{x}_2) \right\rangle_0$ and $\left\langle \widehat{S}^\alpha_{\mu_1 \nu_1}(\underline{x}_1)\widehat{S}^\beta_{\mu_2 \nu_2}(\underline{x}_2) \right\rangle_0$ can be regarded as the expectation value of $u^{\mu_1}u^{\nu_1}$ and $u^{\mu_1}u^{\nu_1}u^{\mu_2}u^{\nu_2}$, respectively. In both cases x_1 must be in the α-block and x_2 in the β-block. The meaning of the higher order correlation functions can be explained in the same way.

According to Eq. (A.1),

$$\left\langle \rho^\alpha(\underline{q}_1)\rho^\beta(\underline{q}_2) \right\rangle_0 \;=\; \lim_{\underline{\eta}\to\underline{0}} A^{\alpha\beta}(\underline{q}_1,\underline{q}_2), \tag{A.5a}$$

$$\left\langle \widehat{S}^\alpha_{\mu_1 \nu_1}(\underline{q}_1)\rho^\beta(\underline{q}_2) \right\rangle_0 \;=\; \lim_{\underline{\eta}\to\underline{0}} \frac{\delta^2}{\delta\eta_{\mu_1}(l_1)\delta\eta_{\nu_1}(l_1)} A^{\alpha\beta}(\underline{q}_1,\underline{q}_2) \tag{A.5b}$$

and

$$\left\langle \widehat{S}^\alpha_{\mu_1 \nu_1}(\underline{q}_1)\widehat{S}^\beta_{\mu_2 \nu_2}(\underline{q}_2) \right\rangle_0 \;=\; \lim_{\underline{\eta}\to\underline{0}} \frac{\delta^4}{\delta\eta_{\mu_1}(l_1)\delta\eta_{\nu_1}(l_1)\delta\eta_{\mu_2}(l_2)\delta\eta_{\nu_2}(l_2)} A^{\alpha\beta}(\underline{q}_1,\underline{q}_2). \tag{A.5c}$$

When the path integral over $\underline{R}(l)$ in Eq. (A.1) is carried out, $\underline{R}(l)$ must be replaced by

$$\underline{R}(l) = \underline{R}(0) + \int_0^l dl'\,\underline{u}(l'), \tag{A.6}$$

because of the delta function $\delta(\underline{u}(l) - \dot{\underline{R}}(l))$. The path integral over $\underline{u}(l)$ remains together with an integral over the initial position $\underline{R}(0)$. Then Eq. (A.1) becomes

$$A^{\alpha\beta}(\underline{q}_1, \underline{q}_2) = \sum_{l_1, l_2} \sigma_{l_1}^{\alpha} \sigma_{l_2}^{\beta} \int d\underline{\widetilde{U}} \int d\underline{U} \int d\underline{R}(0) \int D\underline{u}\, \delta(\underline{u}(0) - \underline{\widetilde{U}})\, \delta(\underline{u}(L) - \underline{U}) \times$$

$$\exp\left(-H_0\right) \exp\left(-i\underline{q}_1 \cdot \underline{R}(0) - i\underline{q}_2 \cdot \underline{R}(0)\right) \times$$

$$\exp\left(-i\underline{q}_1 \cdot \int_0^{l_1} dl\underline{u}(l) - i\underline{q}_2 \cdot \int_0^{l_2} dl\underline{u}(l) + \int_0^L dl\underline{\eta}(l) \cdot \underline{u}(l)\right) =$$

$$\int d\underline{R}(0) \exp\left(-i\underline{q}_1 \cdot \underline{R}(0) - i\underline{q}_2 \cdot \underline{R}(0)\right) \times$$

$$\sum_{l_1, l_2} \sigma_{l_1}^{\alpha} \sigma_{l_2}^{\beta} \int d\underline{\widetilde{U}} \int d\underline{U} \int D\underline{u}\, \delta(\underline{u}(0) - \underline{\widetilde{U}})\, \delta(\underline{u}(L) - \underline{U}) \exp\left(-H_0\right) \times$$

$$\exp\left(-i\underline{q}_1 \cdot \int_0^L \underline{u}(l)\theta(l_1 - l) - i\underline{q}_2 \cdot \int_0^L \underline{u}(l)\theta(l_2 - l) + \int_0^L dl\underline{\eta}(l) \cdot \underline{u}(l)\right) =$$

$$V\delta\left(\underline{q}_1 + \underline{q}_2\right) \sum_{l_1, l_2} \sigma_{l_1}^{\alpha} \sigma_{l_2}^{\beta} \int d\underline{\widetilde{U}} \int d\underline{U} \int D\underline{u}\, \delta(\underline{u}(0) - \underline{\widetilde{U}})\, \delta(\underline{u}(L) - \underline{U}) \exp\left(-H_0\right).$$

$$\text{(A.7)}$$

In Eq. (A.7) $\underline{Q} = \underline{Q}(l)$ is given by,

$$\underline{Q}(l) = -\underline{q}_1 \theta(l_1 - l) - \underline{q}_2 \theta(l_2 - l) - i\underline{\eta}(l). \qquad \text{(A.8)}$$

In a certain interval of l, $\underline{Q}$ takes a constant value if $\underline{\eta}(l) \to \underline{0}$. $\underline{Q} = -\underline{q}_1 - \underline{q}_2$ if l is smaller than both l_1 and l_2. $\underline{Q} = -\underline{q}_1$ or $\underline{Q} = -\underline{q}_2$ if $l_2 < l < l_1$ or $l_1 < l < l_2$, respectively. The persistence length λ takes also constant values in certain intervals of l, because the persistence length in every block is constant. To simplify the calculations the interval $(0, L)$ of the parameter l is divided into smaller parts. In every subinterval $\left(L_{p-1}, L_p\right)$ both $\underline{Q}$ and λ must be constant, which will be denoted as $\underline{Q}_p$ and λ_p. $\underline{Q}_p$ is constant in $\left(L_{p-1}, L_p\right)$ if $\underline{\eta}(l)$ is constant. $\underline{\eta}(l)$ is taken equal to zero everywhere except in $(l_1 - \Delta L, l_1)$ and $(l_2 - \Delta L, l_2)$. In these intervals $\underline{\eta}(l)$ is constant and equal to $\underline{\eta}(l_1)$ and $\underline{\eta}(l_2)$, respectively. ΔL is very small and goes to zero. In this way it is possible to calculate the functional derivatives in Eq. (A.5a), (A.5b) and (A.5c). For a certain $p = p_1$ or p_2, $L_p = l_1$ or l_2, respectively. Then in $\left(L_{p-1}, L_p\right)$, $\underline{Q}_p$ becomes

$$\underline{Q}_p = -\underline{q}_1 \theta(l_1 - L_p) - \underline{q}_2 \theta(l_2 - L_p) - i\delta_{pp_1}\underline{\eta}(l_1) - i\delta_{pp_2}\underline{\eta}(l_2). \qquad \text{(A.9)}$$

According to Eq. (A.2) the free Hamiltonian of each interval is

$$H_0^{(p)} = \frac{3}{4}u_0^2\delta_{p1} + \frac{3}{4}u_{p'}^2\delta_{pp'} + \frac{3}{4}\int\limits_{L_{p-1}}^{L_p} dl[\lambda_p\dot{u}^2(l) + \frac{1}{\lambda_p}u^2(l)]. \qquad (A.10)$$

So Eq. (A.7) can be written as

$$\begin{aligned}
A^{\alpha\beta}(\underline{q}_1, \underline{q}_2) &= V\delta\left(\underline{q}_1 + \underline{q}_2\right)\sum_{l_1,l_2}\sigma_{l_1}^\alpha\sigma_{l_2}^\beta \int d\underline{\widetilde{U}} \int d\underline{U} \times \\
&\int D\underline{u}\,\delta(\underline{u}(0) - \underline{\widetilde{U}})\,\delta(\underline{u}(L) - \underline{U})\exp\left(-\frac{3}{4}u_0^2 - \frac{3}{4}u_{p'}^2\right)\times \\
&\exp\left(-\sum_{p=1}^{p'}\int\limits_{L_{p-1}}^{L_p} dl[\frac{3\lambda_p}{4}\dot{u}^2(l) + \frac{3}{4\lambda_p}u^2(l) - i\underline{Q}_p \cdot \underline{u}(l)]\right).
\end{aligned}$$

$$(A.11)$$

In Eq. (A.11) the last interval p is denoted as p'. Instead of integrating over the whole contour, one can integrate over $\underline{u}(l)$ separately for each interval (L_{p-1}, L_p). This is only allowed when the begin and end points of two subsequent pieces have the same tangent vector. Then along the whole contour $\underline{u}(l)$ is continuous. This is done in Eq. (A.12),

$$A^{\alpha\beta}(\underline{q}_1, \underline{q}_2) = V\delta\left(\underline{q}_1 + \underline{q}_2\right)\sum_{l_1,l_2}\sigma_{l_1}^\alpha\sigma_{l_2}^\beta \left\langle\exp\left(-\sum_{p=1}^{p'}\int\limits_{L_{p-1}}^{L_p} dl[-i\underline{Q}_p \cdot \underline{u}(l)]\right)\right\rangle_0 =$$

$$V\delta\left(\underline{q}_1 + \underline{q}_2\right)\sum_{l_1,l_2}\sigma_{l_1}^\alpha\sigma_{l_2}^\beta \int\prod_{n=0}^{p'}d\underline{u}_n\times$$

$$\exp\left(-\frac{3}{4}u_0^2 - \frac{3}{4}u_{p'}^2\right)\prod_{p=1}^{p'}\int\limits_{\underline{u}_{p-1}}^{\underline{u}_p}D\underline{u}\exp\left(-\int\limits_{L_{p-1}}^{L_p} dl[\frac{3\lambda_p}{4}\dot{u}^2(l) + \frac{3}{4\lambda_p}u^2(l) - i\underline{Q}_p \cdot \underline{u}(l)]\right).$$

$$(A.12)$$

In this equation $\underline{u}_{p-1}$ and $\underline{u}_p$ are the tangent vectors at the end points of (L_{p-1}, L_p). In this notation $\underline{\widetilde{U}} = \underline{u}_0$ and $\underline{U} = \underline{u}_{p'}$. In the functional integration over $\underline{u}(l)$ in the interval

(L_{p-1}, L_p) the tangent vectors $\underline{u}_{p-1}$ and $\underline{u}_p$ are fixed. After the functional integration over $\underline{u}(l)$ integrations over the tangent vectors $\underline{u}_p$ are carried out. In Eq. (A.12) the integral I_p,

$$I_p = \int_{\underline{u}_{p-1}}^{\underline{u}_p} D\underline{u} \exp\left(-\int_{L_{p-1}}^{L_p} dl[\frac{3\lambda_p}{4}\dot{u}^2(l) + \frac{3}{4\lambda_p}u^2(l) - i\underline{Q}_p \cdot \underline{u}(l)]\right), \tag{A.13}$$

has the same form as Eq. (5.21) in [19]. If l is replaced by it and $\hbar = 1$, then I_p is the Feynman path integral representation of a quantum mechanical harmonic oscillator with a constant external force $\underline{Q}_p$ on each segment. Because the force $\underline{Q}_p$ is constant, I_p can be written in terms of a representation of a quantum mechanical harmonic oscillator without external force, which is given by Eq. (5.31) in [19],

$$I_p(\underline{u}_p, \underline{u}_{p-1}) = \exp\left(-\frac{Q_p^2 \Delta L_p \lambda_p}{3}\right) \int_{\underline{u}_{p-1} - \frac{2}{3}i\lambda_p \underline{Q}_p}^{\underline{u}_p - \frac{2}{3}i\lambda_p \underline{Q}_p} D\underline{u} \exp\left(-\int_{L_{p-1}}^{L_p} dl[\frac{3\lambda_p}{4}\dot{u}^2(l) + \frac{3}{4\lambda_p}u^2(l)]\right) =$$

$$\exp\left(-\frac{Q_p^2 \Delta L_p \lambda_p}{3}\right) G(\underline{u}_p - \frac{2}{3}i\lambda_p \underline{Q}_p, \underline{u}_{p-1} - \frac{2}{3}i\lambda_p \underline{Q}_p, \Delta L_p, 0). \tag{A.14}$$

In Eq. (A.14) the propagator G is given by Eq. (A.15). Quantum mechanically the propagator $G(\underline{u}_p, \underline{u}_{p-1}, \Delta L_p, 0)$ is the probability that a particle at $t = 0$ and $\underline{x} = \underline{u}_{p-1}$ travels to $\underline{x} = \underline{u}_p$ after a time $\Delta t = -i\Delta L_p$. In our case it is regarded as the probability that a semi-flexible chain of length ΔL_p has a tangent vector $\underline{u}_p$ along the end point, if $\underline{u}_{p-1}$ is the tangent vector along the begin point. The result is well known in quantum mechanics and given by Eq. (5.32) in [19],

$$G(\underline{u}_p, \underline{u}_{p-1}, \Delta L_p, 0) = \left(\frac{b^{(p)}}{\pi \sinh a^{(p)}}\right)^{\frac{3}{2}} \exp\left(-\frac{b^{(p)}}{\sinh a^{(p)}}\left[(u_p^2 + u_{p-1}^2)\cosh a^{(p)} - 2\underline{u}_p \cdot \underline{u}_{p-1}\right]\right), \tag{A.15}$$

in which $a^{(p)}$ and $b^{(p)}$ are given by

$$a^{(p)} = \frac{\Delta L_p}{\lambda_p} \tag{A.16a}$$

and

$$b^{(p)} = \frac{3}{4}. \tag{A.16b}$$

Applying Eq. (A.15) in Eq. (A.14) yields

$$I_p(\underline{u}_p, \underline{u}_{p-1}) = \exp\left(-\frac{Q_p^2 \Delta L_p \lambda_p}{3}\right)\left(\frac{b^{(p)}}{\pi \sinh a^{(p)}}\right)^{\frac{3}{2}} \times$$

$$\exp\left(-\frac{b^{(p)}}{\sinh a^{(p)}}\left[\left(u_p^2 + u_{p-1}^2 - \frac{4i\lambda_p}{3}\underline{Q}_p \cdot (\underline{u}_p + \underline{u}_{p-1}) - \frac{8\lambda_p^2 Q_p^2}{9}\right)\cosh a^{(p)}\right]\right) \times$$

$$\exp\left(-\frac{b^{(p)}}{\sinh a^{(p)}}\left[-2\underline{u}_p \cdot \underline{u}_{p-1} + \frac{4i\lambda_p}{3}\underline{Q}_p \cdot (\underline{u}_p + \underline{u}_{p-1}) + \frac{8\lambda_p^2 Q_p^2}{9}\right]\right). \qquad (A.17)$$

$I_p(\underline{u}_p, \underline{u}_{p-1})$ can be written in the following form

$$\begin{aligned} I_p(\underline{u}_p, \underline{u}_{p-1}) &= E_p \exp\left(-\frac{1}{2}A_p(u_{p-1}^2 + u_p^2) + B_p\underline{u}_{p-1} \cdot \underline{u}_p\right) \times \\ &\quad \exp\left(C_p\underline{Q}_p \cdot (\underline{u}_{p-1} + \underline{u}_p) - \frac{1}{2}D_pQ_p^2\right), \end{aligned} \qquad (A.18)$$

in which A_p, B_p, C_p, D_p and E_p are given by

$$A_p = 2b^{(p)}\coth a^{(p)} = \frac{3}{2}\coth(\frac{\Delta L_p}{\lambda_p}), \qquad (A.19a)$$

$$B_p = \frac{2b^{(p)}}{\sinh a^{(p)}} = \frac{3}{2\sinh(\frac{\Delta L_p}{\lambda_p})}, \qquad (A.19b)$$

$$C_p = \frac{-4i\lambda_p b^{(p)}(1 - \cosh(a^{(p)}))}{3\sinh a^{(p)}} = \frac{-i\lambda_p\left(1 - \cosh(\frac{\Delta L_p}{\lambda_p})\right)}{\sinh(\frac{\Delta L_p}{\lambda_p})}, \qquad (A.19c)$$

$$D_p = \frac{2\Delta L_p\lambda_p}{3} + \frac{16\lambda_p^2 b^{(p)}(1 - \cosh a^{(p)})}{9\sinh a^{(p)}} = \frac{2\Delta L_p\lambda_p}{3} + \frac{4\lambda_p^2\left(1 - \cosh(\frac{\Delta L_p}{\lambda_p})\right)}{3\sinh(\frac{\Delta L_p}{\lambda_p})} \qquad (A.19d)$$

and

$$E_p = \left(\frac{b^{(p)}}{\pi \sinh a^{(p)}}\right)^{\frac{3}{2}} = \left(\frac{3}{4\pi \sinh(\frac{\Delta L_p}{\lambda_p})}\right)^{\frac{3}{2}}. \qquad (A.19e)$$

To calculate the second order correlation function we have to perform in Eq. (A.12) the integral

$$\int d\underline{u}_{p'} \prod_{p=1}^{p'} \int d\underline{u}_{p-1} I_p(\underline{u}_p, \underline{u}_{p-1}) \exp\left(-\frac{3}{4}u_0^2 - \frac{3}{4}u_{p'}^2\right)$$

$$= \int d\underline{u}_{p'} \prod_{p=1}^{p'} \int d\underline{u}_{p-1} E_p \exp\left(-\frac{3}{4}u_0^2 - \frac{3}{4}u_{p'}^2\right) \times$$

$$\exp\left(-\frac{1}{2}A_p(u_{p-1}^2 + u_p^2) + B_p \underline{u}_{p-1} \cdot \underline{u}_p\right) \times$$

$$\exp\left(C_p \underline{Q}_p \cdot (\underline{u}_{p-1} + \underline{u}_p) - \frac{1}{2}D_p Q_p^2\right). \tag{A.20}$$

The integral over $\underline{u}_{p-1}$ is also a Gaussian integral of the form,

$$\int d\underline{x} \exp(-\frac{1}{2}Cx^2 + \underline{\eta} \cdot \underline{x}) = \left(\frac{2\pi}{C}\right)^{\frac{3}{2}} \exp\left(\frac{\eta^2}{2C}\right). \tag{A.21}$$

First we evaluate the integral over $\underline{u}_0$,

$$\int d\underline{u}_0 I_1(\underline{u}_0, \underline{u}_1) \exp(-\frac{3}{4}u_0^2)$$

$$= \int d\underline{u}_0 E_1 \exp\left(-\frac{1}{2}(A_1 + \frac{3}{2})u_0^2 - \frac{1}{2}A_1 u_1^2 + B_1 \underline{u}_0 \cdot \underline{u}_1\right) \times$$

$$\exp\left(C_1 \underline{Q}_1 \cdot (\underline{u}_0 + \underline{u}_1) - \frac{1}{2}D_1 Q_1^2\right)$$

$$= E_1 \left(\frac{2\pi}{A_1 + \frac{3}{2}}\right)^{\frac{3}{2}} \exp\left(\frac{B_1^2}{2(A_1 + \frac{3}{2})}u_1^2 + \frac{B_1 C_1 \underline{Q}_1}{A_1 + \frac{3}{2}} \cdot \underline{u}_1 + \frac{C_1^2 Q_1^2}{2(A_1 + \frac{3}{2})}\right) \times$$

$$\exp\left(-\frac{1}{2}A_1 u_1^2 + C_1 \underline{Q}_1 \cdot \underline{u}_1 - \frac{1}{2}D_1 Q_1^2\right). \tag{A.22}$$

Using Eq. (A.20) and (A.22) the integration over $\underline{u}_1$ can be written in the following form

$$\int d\underline{u}_1 \widetilde{E}_2 \exp\left(-\frac{1}{2}\widetilde{A}_2 u_1^2 - \frac{1}{2}A_2 u_2^2 + B_2 \underline{u}_1 \cdot \underline{u}_2\right) \times$$

$$\exp\left(\widetilde{\underline{C}}_2 \cdot \underline{u}_1 + C_2 \underline{Q}_2 \cdot \underline{u}_2 - \frac{1}{2}\widetilde{D}_2\right), \tag{A.23}$$

which is a similar form as Eq. (A.20). $\widetilde{A}_2$, $\underline{\widetilde{C}}_2$, $\widetilde{D}_2$ and $\widetilde{E}_2$ are given by

$$\widetilde{A}_2 \;=\; A_2 + A_1 - \frac{B_1^2}{A_1 + \frac{3}{2}}, \tag{A.24a}$$

$$\underline{\widetilde{C}}_2 \;=\; C_2 \underline{Q}_2 + \left(\frac{B_1}{A_1 + \frac{3}{2}} + 1 \right) C_1 \underline{Q}_1, \tag{A.24b}$$

$$\widetilde{D}_2 \;=\; D_2 Q_2^2 + D_1 Q_1^2 - \frac{C_1^2 Q_1^2}{A_1 + \frac{3}{2}} \tag{A.24c}$$

and

$$\widetilde{E}_2 \;=\; E_2 E_1 \left(\frac{2\pi}{A_1 + \frac{3}{2}} \right)^{\frac{3}{2}}. \tag{A.24d}$$

In Eq. (A.23) we can again carry out the integral over $\underline{u}_1$. By means of Eq. (A.20) an integral over $\underline{u}_2$ and next tangent vectors can be derived in the same form as Eq. (A.23). This can be done in the same way for $\underline{u}_3$ and next tangent vectors. After the integration over $\underline{u}_{p'-2}$ and previous tangent vectors we have to carry out the integration over $\underline{u}_{p'-1}$ and $\underline{u}_{p'}$,

$$
\begin{aligned}
& \int d\underline{u}_{p'} \exp(-\frac{3}{4} u_{p'}^2) \int d\underline{u}_{p'-1} \widetilde{E}_{p'} \times \\
& \exp\left(-\frac{1}{2}\widetilde{A}_{p'} u_{p'-1}^2 - \frac{1}{2} A_{p'} u_{p'}^2 + B_{p'}\underline{u}_{p'-1} \cdot \underline{u}_{p'} \right) \times \\
& \exp\left(\underline{\widetilde{C}}_{p'} \cdot \underline{u}_{p'-1} + C_{p'} \underline{Q}_{p'} \cdot \underline{u}_{p'} - \frac{1}{2}\widetilde{D}_{p'} \right) \\
=\;\; & \int d\underline{u}_{p'} \widetilde{E}_{p'+1} \exp\left(-\frac{1}{2}\widetilde{A}_{p'+1} u_{p'}^2 + \underline{\widetilde{C}}_{p'+1} \cdot \underline{u}_{p'} - \frac{1}{2}\widetilde{D}_{p'+1} \right) \\
=\;\; & \widetilde{E}_{p'+2} \exp\left(-\frac{1}{2}\widetilde{D}_{p'+2} \right). \tag{A.25}
\end{aligned}
$$

For $p = 1, 2, ..., p'$, the coefficients $\widetilde{A}_p$, $\underline{\widetilde{C}}_p$, $\widetilde{D}_p$ and $\widetilde{E}_p$ are equal to

$$\widetilde{A}_p \;=\; A_p + A_{p-1} - \frac{B_{p-1}^2}{\widetilde{A}_{p-1}}, \tag{A.26a}$$

$$\underline{\widetilde{C}}_p \;=\; C_p \underline{Q}_p + C_{p-1} \underline{Q}_{p-1} + \frac{B_{p-1}\underline{\widetilde{C}}_{p-1}}{\widetilde{A}_{p-1}}, \tag{A.26b}$$

$$\widetilde{D}_p \;=\; D_p Q_p^2 + \widetilde{D}_{p-1} - \frac{\widetilde{C}_{p-1}^2}{\widetilde{A}_{p-1}}, \tag{A.26c}$$

and

$$\widetilde{E}_p \;=\; E_p \widetilde{E}_{p-1} \left(\frac{2\pi}{\widetilde{A}_{p-1}} \right)^{\frac{3}{2}}. \tag{A.26d}$$

However, $p = p' + 1$ and $p = p' + 2$ give different coefficients,

$$\widetilde{A}_{p'+1} \;=\; A_{p'} - \frac{B_{p'}^2}{\widetilde{A}_{p'}} + \frac{3}{2}, \tag{A.27a}$$

$$\underline{\widetilde{C}}_{p'+1} \;=\; C_{p'} \underline{Q}_{p'} + \frac{B_{p'}\underline{\widetilde{C}}_{p'}}{\widetilde{A}_{p'}}, \tag{A.27b}$$

$$\widetilde{D}_{p'+1} \;=\; \widetilde{D}_{p'} - \frac{\widetilde{C}_{p'}^2}{\widetilde{A}_{p'}}, \tag{A.27c}$$

$$\widetilde{E}_{p'+1} \;=\; \widetilde{E}_{p'} \left(\frac{2\pi}{\widetilde{A}_{p'}} \right)^{\frac{3}{2}}, \tag{A.27d}$$

$$\widetilde{D}_{p'+2} \;=\; \widetilde{D}_{p'+1} - \frac{\widetilde{C}_{p'+1}^2}{\widetilde{A}_{p'+1}}, \tag{A.27e}$$

and

$$\widetilde{E}_{p'+2} \;=\; \widetilde{E}_{p'+1} \left(\frac{2\pi}{\widetilde{A}_{p'+1}} \right)^{\frac{3}{2}}. \tag{A.27f}$$

The factor $\widetilde{E}_{p'+2}$ in Eq. (A.25) must be omitted to normalize the average $\langle\rangle_0$ in Eq. (A.12) over all possible chain configurations, because $\langle 1 \rangle_0 \equiv 1$. Then the second

order correlation function given by Eq. (A.12) becomes,

$$A^{\alpha\beta}(\underline{q}_1,\underline{q}_2) = V\delta\left(\underline{q}_1 + \underline{q}_2\right)\widetilde{E}_{p'+2}\sum_{l_1,l_2}\sigma^{\alpha}_{l_1}\sigma^{\beta}_{l_2}\exp\left(-\frac{1}{2}\widetilde{D}_{p'+2}\right). \tag{A.28}$$

The third and fourth order correlation functions can be obtained by adding $-\underline{q}_3\theta(l_3 - L_p) - i\delta_{pp_3}\underline{\eta}(l_3)$ and $-\underline{q}_3\theta(l_3 - L_p) - \underline{q}_4\theta(l_4 - L_p) - i\delta_{pp_3}\underline{\eta}(l_3) - i\delta_{pp_4}\underline{\eta}(l_4)$ to $\underline{Q}_p$. $\delta\left(\underline{q}_1 + \underline{q}_2\right)$ must be replaced by $\delta\left(\underline{q}_1 + \underline{q}_2 + \underline{q}_3\right)$ and $\delta\left(\underline{q}_1 + \underline{q}_2 + \underline{q}_3 + \underline{q}_4\right)$. In Eq. (A.5b) and (A.5c) functional differentiations are to be carried out. These are operating on $\widetilde{D}_{p'+2}$ in Eq. (A.28). First we carry out the functional differentiations of $A^{\alpha\beta}(\underline{q}_1,\underline{q}_2)$. In appendix B the functional derivatives of $\widetilde{D}_{p'+2}$ are calculated. The first order derivative of $A^{\alpha\beta}(\underline{q}_1,\underline{q}_2)$ is

$$
\begin{aligned}
\frac{\delta A^{\alpha\beta}(\underline{q}_1,\underline{q}_2)}{\delta\eta_{\mu_1}(l_1)} &= -\frac{1}{2}V\delta\left(\underline{q}_1 + \underline{q}_2\right)\widetilde{E}_{p'+2}\sum_{l_1,l_2}\sigma^{\alpha}_{l_1}\sigma^{\beta}_{l_2}\frac{\delta\widetilde{D}_{p'+2}}{\delta\eta_{\mu_1}(l_1)}\exp\left(-\frac{1}{2}\widetilde{D}_{p'+2}\right) \\
&= V\delta\left(\underline{q}_1 + \underline{q}_2\right)\widetilde{E}_{p'+2}\sum_{l_1,l_2}\sigma^{\alpha}_{l_1}\sigma^{\beta}_{l_2}G_1\exp\left(-\frac{1}{2}\widetilde{D}_{p'+2}\right). \tag{A.29}
\end{aligned}
$$

In Eq. (A.29) the differentiation is replaced by a multiplication by G_1. This can also be done for the higher order derivatives. In the second order derivative the multiplication factor is denoted as G_2. G_1 and G_2 are equal to

$$
\begin{aligned}
G_1 &= -\frac{1}{2}\frac{\delta\widetilde{D}_{p'+2}}{\delta\eta_{\mu_1}(l_1)} \tag{A.30a} \\
&\text{and} \\
G_2 &= \left(\frac{\delta}{\delta\eta_{\nu_1}(l_1)} - \frac{1}{2}\frac{\delta\widetilde{D}_{p'+2}}{\delta\eta_{\nu_1}(l_1)}\right)G_1 \\
&= -\frac{1}{2}\frac{\delta^2\widetilde{D}_{p'+2}}{\delta\eta_{\mu_1}(l_1)\delta\eta_{\nu_1}(l_1)} + \frac{1}{4}\frac{\delta\widetilde{D}_{p'+2}}{\delta\eta_{\mu_1}(l_1)}\frac{\delta\widetilde{D}_{p'+2}}{\delta\eta_{\nu_1}(l_1)}. \tag{A.30b}
\end{aligned}
$$

In the second, third and fourth order correlation function it is necessary to calculate

G_4, G_6 and G_8 which are given by

$$G_4 = \left(\frac{\delta}{\delta \eta_{\nu_2}(l_2)} - \frac{1}{2} \frac{\delta \widetilde{D}_{p'+2}}{\delta \eta_{\nu_2}(l_2)} \right) \left(\frac{\delta}{\delta \eta_{\mu_2}(l_2)} - \frac{1}{2} \frac{\delta \widetilde{D}_{p'+2}}{\delta \eta_{\mu_2}(l_2)} \right) G_2, \qquad \text{(A.31a)}$$

$$G_6 = \left(\frac{\delta}{\delta \eta_{\mu_3}(l_3)} - \frac{1}{2} \frac{\delta \widetilde{D}_{p'+2}}{\delta \eta_{\mu_3}(l_3)} \right) \left(\frac{\delta}{\delta \eta_{\nu_3}(l_3)} - \frac{1}{2} \frac{\delta \widetilde{D}_{p'+2}}{\delta \eta_{\nu_3}(l_3)} \right) G_4 \qquad \text{(A.31b)}$$

and

$$G_8 = \left(\frac{\delta}{\delta \eta_{\mu_4}(l_4)} - \frac{1}{2} \frac{\delta \widetilde{D}_{p'+2}}{\delta \eta_{\mu_4}(l_4)} \right) \left(\frac{\delta}{\delta \eta_{\nu_4}(l_4)} - \frac{1}{2} \frac{\delta \widetilde{D}_{p'+2}}{\delta \eta_{\nu_4}(l_4)} \right) G_6. \qquad \text{(A.31c)}$$

So from Eq. (A.31a), (A.31b) and (A.31c) it is clear that G_4 has to be calculated first,

$$
\begin{aligned}
G_4 &= \left(\frac{\delta}{\delta \eta_{\nu_2}(l_2)} - \frac{1}{2} \frac{\delta \widetilde{D}_{p'+2}}{\delta \eta_{\nu_2}(l_2)} \right) \left(\frac{\delta}{\delta \eta_{\mu_2}(l_2)} - \frac{1}{2} \frac{\delta \widetilde{D}_{p'+2}}{\delta \eta_{\mu_2}(l_2)} \right) G_2 \\
&= \left(\frac{\delta}{\delta \eta_{\nu_2}(l_2)} - \frac{1}{2} \frac{\delta \widetilde{D}_{p'+2}}{\delta \eta_{\nu_2}(l_2)} \right) \left(\frac{\delta}{\delta \eta_{\mu_2}(l_2)} - \frac{1}{2} \frac{\delta \widetilde{D}_{p'+2}}{\delta \eta_{\mu_2}(l_2)} \right) \times \\
&\quad \left(-\frac{1}{2} \frac{\delta^2 \widetilde{D}_{p'+2}}{\delta \eta_{\mu_1}(l_1) \delta \eta_{\nu_1}(l_1)} + \frac{1}{4} \frac{\delta \widetilde{D}_{p'+2}}{\delta \eta_{\mu_1}(l_1)} \frac{\delta \widetilde{D}_{p'+2}}{\delta \eta_{\nu_1}(l_1)} \right).
\end{aligned} \qquad \text{(A.32)}
$$

In appendix B the second order derivative of $\widetilde{D}_{p'+2}$ is calculated. It appears that the second order derivative does not depend on $\underline{Q}_p$. Therefore the third and higher order derivatives of $\widetilde{D}_{p'+2}$ are zero. This will reduce the number of terms in Eq. (A.32)

when the product is evaluated,

$$
G_4 = \left(\frac{\delta}{\delta\eta_{\nu_2}(l_2)} - \frac{1}{2} \frac{\delta\widetilde{D}_{p'+2}}{\delta\eta_{\nu_2}(l_2)} \right) \left(\frac{\delta}{\delta\eta_{\mu_2}(l_2)} - \frac{1}{2} \frac{\delta\widetilde{D}_{p'+2}}{\delta\eta_{\mu_2}(l_2)} \right) \times
$$

$$
\left(-\frac{1}{2} \frac{\delta^2\widetilde{D}_{p'+2}}{\delta\eta_{\mu_1}(l_1)\delta\eta_{\nu_1}(l_1)} + \frac{1}{4} \frac{\delta\widetilde{D}_{p'+2}}{\delta\eta_{\mu_1}(l_1)} \frac{\delta\widetilde{D}_{p'+2}}{\delta\eta_{\nu_1}(l_1)} \right)
$$

$$
= (\frac{\delta^2}{\delta\eta_{\mu_2}(l_2)\delta\eta_{\nu_2}(l_2)} - \frac{1}{2} \frac{\delta^2\widetilde{D}_{p'+2}}{\delta\eta_{\mu_2}(l_2)\delta\eta_{\nu_2}(l_2)}
$$

$$
- \frac{1}{2} \frac{\delta\widetilde{D}_{p'+2}}{\delta\eta_{\mu_2}(l_2)} \frac{\delta}{\delta\eta_{\nu_2}(l_2)} - \frac{1}{2} \frac{\delta\widetilde{D}_{p'+2}}{\delta\eta_{\nu_2}(l_2)} \frac{\delta}{\delta\eta_{\mu_2}(l_2)} + \frac{1}{4} \frac{\delta\widetilde{D}_{p'+2}}{\delta\eta_{\mu_2}(l_2)} \frac{\delta\widetilde{D}_{p'+2}}{\delta\eta_{\nu_2}(l_2)}) \times
$$

$$
(-\frac{1}{2} \frac{\delta^2\widetilde{D}_{p'+2}}{\delta\eta_{\mu_1}(l_1)\delta\eta_{\nu_1}(l_1)} + \frac{1}{4} \frac{\delta\widetilde{D}_{p'+2}}{\delta\eta_{\mu_1}(l_1)} \frac{\delta\widetilde{D}_{p'+2}}{\delta\eta_{\nu_1}(l_1)})
$$

$$
= \frac{\delta^2}{\delta\eta_{\mu_2}(l_2)\delta\eta_{\nu_2}(l_2)} \left(\frac{1}{4} \frac{\delta\widetilde{D}_{p'+2}}{\delta\eta_{\mu_1}(l_1)} \frac{\delta\widetilde{D}_{p'+2}}{\delta\eta_{\nu_1}(l_1)} \right)
$$

$$
- \frac{1}{2} \frac{\delta^2\widetilde{D}_{p'+2}}{\delta\eta_{\mu_2}(l_2)\delta\eta_{\nu_2}(l_2)} \left(-\frac{1}{2} \frac{\delta^2\widetilde{D}_{p'+2}}{\delta\eta_{\mu_1}(l_1)\delta\eta_{\nu_1}(l_1)} + \frac{1}{4} \frac{\delta\widetilde{D}_{p'+2}}{\delta\eta_{\mu_1}(l_1)} \frac{\delta\widetilde{D}_{p'+2}}{\delta\eta_{\nu_1}(l_1)} \right) +
$$

$$
- \frac{1}{2} \frac{\delta\widetilde{D}_{p'+2}}{\delta\eta_{\mu_2}(l_2)} \frac{\delta}{\delta\eta_{\nu_2}(l_2)} \left(\frac{1}{4} \frac{\delta\widetilde{D}_{p'+2}}{\delta\eta_{\mu_1}(l_1)} \frac{\delta\widetilde{D}_{p'+2}}{\delta\eta_{\nu_1}(l_1)} \right) +
$$

$$
- \frac{1}{2} \frac{\delta\widetilde{D}_{p'+2}}{\delta\eta_{\nu_2}(l_2)} \frac{\delta}{\delta\eta_{\mu_2}(l_2)} \left(\frac{1}{4} \frac{\delta\widetilde{D}_{p'+2}}{\delta\eta_{\mu_1}(l_1)} \frac{\delta\widetilde{D}_{p'+2}}{\delta\eta_{\nu_1}(l_1)} \right) +
$$

$$
\frac{1}{4} \frac{\delta\widetilde{D}_{p'+2}}{\delta\eta_{\mu_2}(l_2)} \frac{\delta\widetilde{D}_{p'+2}}{\delta\eta_{\nu_2}(l_2)} \left(-\frac{1}{2} \frac{\delta^2\widetilde{D}_{p'+2}}{\delta\eta_{\mu_1}(l_1)\delta\eta_{\nu_1}(l_1)} + \frac{1}{4} \frac{\delta\widetilde{D}_{p'+2}}{\delta\eta_{\mu_1}(l_1)} \frac{\delta\widetilde{D}_{p'+2}}{\delta\eta_{\nu_1}(l_1)} \right)
$$

$$
= \frac{1}{4} \frac{\delta^2\widetilde{D}_{p'+2}}{\delta\eta_{\mu_1}(l_1)\delta\eta_{\mu_2}(l_2)} \frac{\delta^2\widetilde{D}_{p'+2}}{\delta\eta_{\nu_1}(l_1)\delta\eta_{\nu_2}(l_2)} + \frac{1}{4} \frac{\delta^2\widetilde{D}_{p'+2}}{\delta\eta_{\mu_1}(l_1)\delta\eta_{\nu_2}(l_2)} \frac{\delta^2\widetilde{D}_{p'+2}}{\delta\eta_{\mu_2}(l_2)\delta\eta_{\nu_1}(l_1)} +
$$

$$
\frac{1}{4} \frac{\delta^2\widetilde{D}_{p'+2}}{\delta\eta_{\mu_1}(l_1)\delta\eta_{\nu_1}(l_1)} \frac{\delta^2\widetilde{D}_{p'+2}}{\delta\eta_{\mu_2}(l_2)\delta\eta_{\nu_2}(l_2)} - \frac{1}{8} \frac{\delta^2\widetilde{D}_{p'+2}}{\delta\eta_{\mu_2}(l_2)\delta\eta_{\nu_2}(l_2)} \frac{\delta\widetilde{D}_{p'+2}}{\delta\eta_{\mu_1}(l_1)} \frac{\delta\widetilde{D}_{p'+2}}{\delta\eta_{\nu_1}(l_1)} +
$$

$$
- \frac{1}{8} \frac{\delta^2\widetilde{D}_{p'+2}}{\delta\eta_{\mu_1}(l_1)\delta\eta_{\nu_2}(l_2)} \frac{\delta\widetilde{D}_{p'+2}}{\delta\eta_{\mu_2}(l_2)} \frac{\delta\widetilde{D}_{p'+2}}{\delta\eta_{\nu_1}(l_1)} - \frac{1}{8} \frac{\delta^2\widetilde{D}_{p'+2}}{\delta\eta_{\nu_1}(l_1)\delta\eta_{\nu_2}(l_2)} \frac{\delta\widetilde{D}_{p'+2}}{\delta\eta_{\mu_1}(l_1)} \frac{\delta\widetilde{D}_{p'+2}}{\delta\eta_{\mu_2}(l_2)} +
$$

$$
- \frac{1}{8} \frac{\delta^2\widetilde{D}_{p'+2}}{\delta\eta_{\mu_1}(l_1)\delta\eta_{\mu_2}(l_2)} \frac{\delta\widetilde{D}_{p'+2}}{\delta\eta_{\nu_1}(l_1)} \frac{\delta\widetilde{D}_{p'+2}}{\delta\eta_{\nu_2}(l_2)} - \frac{1}{8} \frac{\delta^2\widetilde{D}_{p'+2}}{\delta\eta_{\mu_2}(l_2)\delta\eta_{\nu_1}(l_1)} \frac{\delta\widetilde{D}_{p'+2}}{\delta\eta_{\mu_1}(l_1)} \frac{\delta\widetilde{D}_{p'+2}}{\delta\eta_{\nu_2}(l_2)} +
$$

$$
- \frac{1}{8} \frac{\delta^2\widetilde{D}_{p'+2}}{\delta\eta_{\mu_1}(l_1)\delta\eta_{\nu_1}(l_1)} \frac{\delta\widetilde{D}_{p'+2}}{\delta\eta_{\mu_2}(l_2)} \frac{\delta\widetilde{D}_{p'+2}}{\delta\eta_{\nu_2}(l_2)} + \frac{1}{16} \frac{\delta\widetilde{D}_{p'+2}}{\delta\eta_{\mu_1}(l_1)} \frac{\delta\widetilde{D}_{p'+2}}{\delta\eta_{\nu_1}(l_1)} \frac{\delta\widetilde{D}_{p'+2}}{\delta\eta_{\mu_2}(l_2)} \frac{\delta\widetilde{D}_{p'+2}}{\delta\eta_{\nu_2}(l_2)}. \quad \text{(A.33)}
$$

This expression of G_4 can be written in a more compact form. In Eq. (A.34) a summation is carried out over all possible permutations of μ_1, μ_2, ν_1 and ν_2. $\eta_{\mu_1}(l_1)$ is denoted as η_{μ_1}. The same is done for the other η's. Then Eq. (A.33) becomes,

$$
\begin{aligned}
G_4 = {} & \frac{1}{32} \sum_{perm(\mu_1,\nu_1,\mu_2,\nu_2)} \frac{\delta^2 \widetilde{D}_{p'+2}}{\delta\eta_{\mu_1}\delta\eta_{\nu_1}} \frac{\delta^2 \widetilde{D}_{p'+2}}{\delta\eta_{\mu_2}\delta\eta_{\nu_2}} + \\
& -\frac{1}{32} \sum_{perm(\mu_1,\nu_1,\mu_2,\nu_2)} \frac{\delta^2 \widetilde{D}_{p'+2}}{\delta\eta_{\mu_1}\delta\eta_{\nu_1}} \frac{\delta \widetilde{D}_{p'+2}}{\delta\eta_{\mu_2}} \frac{\delta \widetilde{D}_{p'+2}}{\delta\eta_{\nu_2}} + \\
& \frac{1}{4!16} \sum_{perm(\mu_1,\nu_1,\mu_2,\nu_2)} \frac{\delta \widetilde{D}_{p'+2}}{\delta\eta_{\mu_1}} \frac{\delta \widetilde{D}_{p'+2}}{\delta\eta_{\nu_1}} \frac{\delta \widetilde{D}_{p'+2}}{\delta\eta_{\mu_2}} \frac{\delta \widetilde{D}_{p'+2}}{\delta\eta_{\nu_2}}.
\end{aligned}
\tag{A.34}
$$

This expression of G_4 can be used to calculate G_6,

$$
\begin{aligned}
G_6 = {} & \left(\frac{\delta}{\delta\eta_{\mu_3}} - \frac{1}{2} \frac{\delta \widetilde{D}_{p'+2}}{\delta\eta_{\mu_3}} \right) \left(\frac{\delta}{\delta\eta_{\nu_3}} - \frac{1}{2} \frac{\delta \widetilde{D}_{p'+2}}{\delta\eta_{\nu_3}} \right) G_4 \\
= {} & \Big(\frac{\delta^2}{\delta\eta_{\mu_3}\delta\eta_{\nu_3}} - \frac{1}{2} \frac{\delta^2 \widetilde{D}_{p'+2}}{\delta\eta_{\mu_3}\delta\eta_{\nu_3}} - \frac{1}{2} \frac{\delta \widetilde{D}_{p'+2}}{\delta\eta_{\mu_3}} \frac{\delta}{\delta\eta_{\nu_3}} + \\
& -\frac{1}{2} \frac{\delta \widetilde{D}_{p'+2}}{\delta\eta_{\nu_3}} \frac{\delta}{\delta\eta_{\mu_3}} + \frac{1}{4} \frac{\delta \widetilde{D}_{p'+2}}{\delta\eta_{\mu_3}} \frac{\delta \widetilde{D}_{p'+2}}{\delta\eta_{\nu_3}} \Big) \times \\
& \Big(\frac{1}{32} \sum_{perm(\mu_1,\nu_1,\mu_2,\nu_2)} \frac{\delta^2 \widetilde{D}_{p'+2}}{\delta\eta_{\mu_1}\delta\eta_{\nu_1}} \frac{\delta^2 \widetilde{D}_{p'+2}}{\delta\eta_{\mu_2}\delta\eta_{\nu_2}} + \\
& -\frac{1}{32} \sum_{perm(\mu_1,\nu_1,\mu_2,\nu_2)} \frac{\delta^2 \widetilde{D}_{p'+2}}{\delta\eta_{\mu_1}\delta\eta_{\nu_1}} \frac{\delta \widetilde{D}_{p'+2}}{\delta\eta_{\mu_2}} \frac{\delta \widetilde{D}_{p'+2}}{\delta\eta_{\nu_2}} + \\
& \frac{1}{4!16} \sum_{perm(\mu_1,\nu_1,\mu_2,\nu_2)} \frac{\delta \widetilde{D}_{p'+2}}{\delta\eta_{\mu_1}} \frac{\delta \widetilde{D}_{p'+2}}{\delta\eta_{\nu_1}} \frac{\delta \widetilde{D}_{p'+2}}{\delta\eta_{\mu_2}} \frac{\delta \widetilde{D}_{p'+2}}{\delta\eta_{\nu_2}} \Big) \\
= {} & \sum_{perm(\mu_1,\nu_1,\mu_2,\nu_2)} \Big(-\frac{1}{64} \frac{\delta^2 \widetilde{D}_{p'+2}}{\delta\eta_{\mu_1}\delta\eta_{\nu_1}} \frac{\delta^2 \widetilde{D}_{p'+2}}{\delta\eta_{\mu_2}\delta\eta_{\nu_2}} \frac{\delta^2 \widetilde{D}_{p'+2}}{\delta\eta_{\mu_3}\delta\eta_{\nu_3}} +
\end{aligned}
$$

$$-\frac{1}{128}\frac{\delta^2\widetilde{D}_{p'+2}}{\delta\eta_{\mu_1}\delta\eta_{\nu_1}}\frac{\delta^2\widetilde{D}_{p'+2}}{\delta\eta_{\mu_2}\delta\eta_{\nu_2}}\frac{\delta\widetilde{D}_{p'+2}}{\delta\eta_{\mu_3}}\frac{\delta\widetilde{D}_{p'+2}}{\delta\eta_{\nu_3}}-\frac{1}{32}\frac{\delta^2\widetilde{D}_{p'+2}}{\delta\eta_{\mu_1}\delta\eta_{\nu_1}}\frac{\delta^2\widetilde{D}_{p'+2}}{\delta\eta_{\mu_2}\delta\eta_{\mu_3}}\frac{\delta^2\widetilde{D}_{p'+2}}{\delta\eta_{\nu_2}\delta\eta_{\nu_3}}+$$

$$-\frac{1}{32}\frac{\delta^2\widetilde{D}_{p'+2}}{\delta\eta_{\mu_1}\delta\eta_{\nu_1}}\frac{\delta^2\widetilde{D}_{p'+2}}{\delta\eta_{\mu_2}\delta\eta_{\nu_3}}\frac{\delta^2\widetilde{D}_{p'+2}}{\delta\eta_{\mu_3}\delta\eta_{\nu_2}}+\frac{1}{64}\frac{\delta^2\widetilde{D}_{p'+2}}{\delta\eta_{\mu_1}\delta\eta_{\nu_1}}\frac{\delta^2\widetilde{D}_{p'+2}}{\delta\eta_{\mu_3}\delta\eta_{\nu_3}}\frac{\delta\widetilde{D}_{p'+2}}{\delta\eta_{\mu_2}}\frac{\delta\widetilde{D}_{p'+2}}{\delta\eta_{\nu_2}}+$$

$$\frac{1}{64}\frac{\delta^2\widetilde{D}_{p'+2}}{\delta\eta_{\mu_1}\delta\eta_{\nu_1}}\frac{\delta^2\widetilde{D}_{p'+2}}{\delta\eta_{\mu_2}\delta\eta_{\nu_3}}\frac{\delta\widetilde{D}_{p'+2}}{\delta\eta_{\mu_3}}\frac{\delta\widetilde{D}_{p'+2}}{\delta\eta_{\nu_2}}+\frac{1}{64}\frac{\delta^2\widetilde{D}_{p'+2}}{\delta\eta_{\mu_1}\delta\eta_{\nu_1}}\frac{\delta^2\widetilde{D}_{p'+2}}{\delta\eta_{\nu_2}\delta\eta_{\nu_3}}\frac{\delta\widetilde{D}_{p'+2}}{\delta\eta_{\mu_3}}\frac{\delta\widetilde{D}_{p'+2}}{\delta\eta_{\mu_2}}+$$

$$\frac{1}{64}\frac{\delta^2\widetilde{D}_{p'+2}}{\delta\eta_{\mu_1}\delta\eta_{\nu_1}}\frac{\delta^2\widetilde{D}_{p'+2}}{\delta\eta_{\mu_2}\delta\eta_{\mu_3}}\frac{\delta\widetilde{D}_{p'+2}}{\delta\eta_{\nu_2}}\frac{\delta\widetilde{D}_{p'+2}}{\delta\eta_{\nu_3}}+\frac{1}{64}\frac{\delta^2\widetilde{D}_{p'+2}}{\delta\eta_{\mu_1}\delta\eta_{\nu_1}}\frac{\delta^2\widetilde{D}_{p'+2}}{\delta\eta_{\mu_3}\delta\eta_{\nu_2}}\frac{\delta\widetilde{D}_{p'+2}}{\delta\eta_{\mu_2}}\frac{\delta\widetilde{D}_{p'+2}}{\delta\eta_{\nu_3}}+$$

$$-\frac{1}{128}\frac{\delta^2\widetilde{D}_{p'+2}}{\delta\eta_{\mu_1}\delta\eta_{\nu_1}}\frac{\delta\widetilde{D}_{p'+2}}{\delta\eta_{\mu_2}}\frac{\delta\widetilde{D}_{p'+2}}{\delta\eta_{\nu_2}}\frac{\delta\widetilde{D}_{p'+2}}{\delta\eta_{\mu_3}}\frac{\delta\widetilde{D}_{p'+2}}{\delta\eta_{\nu_3}}+$$

$$\frac{1}{32}\frac{\delta^2\widetilde{D}_{p'+2}}{\delta\eta_{\mu_1}\delta\eta_{\mu_3}}\frac{\delta^2\widetilde{D}_{p'+2}}{\delta\eta_{\nu_1}\delta\eta_{\nu_3}}\frac{\delta\widetilde{D}_{p'+2}}{\delta\eta_{\mu_2}}\frac{\delta\widetilde{D}_{p'+2}}{\delta\eta_{\nu_2}}+$$

$$-\frac{1}{4!32}\frac{\delta^2\widetilde{D}_{p'+2}}{\delta\eta_{\mu_3}\delta\eta_{\nu_3}}\frac{\delta\widetilde{D}_{p'+2}}{\delta\eta_{\mu_1}}\frac{\delta\widetilde{D}_{p'+2}}{\delta\eta_{\nu_1}}\frac{\delta\widetilde{D}_{p'+2}}{\delta\eta_{\mu_2}}\frac{\delta\widetilde{D}_{p'+2}}{\delta\eta_{\nu_2}}+$$

$$-\frac{1}{4!8}\frac{\delta^2\widetilde{D}_{p'+2}}{\delta\eta_{\mu_1}\delta\eta_{\nu_3}}\frac{\delta\widetilde{D}_{p'+2}}{\delta\eta_{\nu_1}}\frac{\delta\widetilde{D}_{p'+2}}{\delta\eta_{\mu_2}}\frac{\delta\widetilde{D}_{p'+2}}{\delta\eta_{\nu_2}}\frac{\delta\widetilde{D}_{p'+2}}{\delta\eta_{\mu_3}}+$$

$$-\frac{1}{4!8}\frac{\delta^2\widetilde{D}_{p'+2}}{\delta\eta_{\mu_1}\delta\eta_{\mu_3}}\frac{\delta\widetilde{D}_{p'+2}}{\delta\eta_{\nu_1}}\frac{\delta\widetilde{D}_{p'+2}}{\delta\eta_{\mu_2}}\frac{\delta\widetilde{D}_{p'+2}}{\delta\eta_{\nu_2}}\frac{\delta\widetilde{D}_{p'+2}}{\delta\eta_{\nu_3}}+$$

$$\frac{1}{4!64}\frac{\delta\widetilde{D}_{p'+2}}{\delta\eta_{\mu_1}}\frac{\delta\widetilde{D}_{p'+2}}{\delta\eta_{\nu_1}}\frac{\delta\widetilde{D}_{p'+2}}{\delta\eta_{\mu_2}}\frac{\delta\widetilde{D}_{p'+2}}{\delta\eta_{\nu_2}}\frac{\delta\widetilde{D}_{p'+2}}{\delta\eta_{\mu_3}}\frac{\delta\widetilde{D}_{p'+2}}{\delta\eta_{\nu_3}})$$

$$=\sum_{perm(\mu_1,\nu_1,\mu_2,\nu_2,\mu_3,\nu_3)}(-\frac{1}{4!16}\frac{\delta^2\widetilde{D}_{p'+2}}{\delta\eta_{\mu_1}\delta\eta_{\nu_1}}\frac{\delta^2\widetilde{D}_{p'+2}}{\delta\eta_{\mu_2}\delta\eta_{\nu_2}}\frac{\delta^2\widetilde{D}_{p'+2}}{\delta\eta_{\mu_3}\delta\eta_{\nu_3}}+$$

$$\frac{1}{256}\frac{\delta^2\widetilde{D}_{p'+2}}{\delta\eta_{\mu_1}\delta\eta_{\nu_1}}\frac{\delta^2\widetilde{D}_{p'+2}}{\delta\eta_{\mu_2}\delta\eta_{\nu_2}}\frac{\delta\widetilde{D}_{p'+2}}{\delta\eta_{\mu_3}}\frac{\delta\widetilde{D}_{p'+2}}{\delta\eta_{\nu_3}}+$$

$$-\frac{1}{4!64}\frac{\delta^2\widetilde{D}_{p'+2}}{\delta\eta_{\mu_1}\delta\eta_{\nu_1}}\frac{\delta\widetilde{D}_{p'+2}}{\delta\eta_{\mu_2}}\frac{\delta\widetilde{D}_{p'+2}}{\delta\eta_{\nu_2}}\frac{\delta\widetilde{D}_{p'+2}}{\delta\eta_{\mu_3}}\frac{\delta\widetilde{D}_{p'+2}}{\delta\eta_{\nu_3}}+$$

$$\frac{1}{6!64}\frac{\delta\widetilde{D}_{p'+2}}{\delta\eta_{\mu_1}}\frac{\delta\widetilde{D}_{p'+2}}{\delta\eta_{\nu_1}}\frac{\delta\widetilde{D}_{p'+2}}{\delta\eta_{\mu_2}}\frac{\delta\widetilde{D}_{p'+2}}{\delta\eta_{\nu_2}}\frac{\delta\widetilde{D}_{p'+2}}{\delta\eta_{\mu_3}}\frac{\delta\widetilde{D}_{p'+2}}{\delta\eta_{\nu_3}}).\tag{A.35}$$

For the fourth order correlation functions G_8 has to be calculated using the expression

of G_6,

$$G_8 = \left(\frac{\delta}{\delta\eta_{\mu_4}(l_4)} - \frac{1}{2} \frac{\delta\widetilde{D}_{p'+2}}{\delta\eta_{\mu_4}(l_4)} \right) \left(\frac{\delta}{\delta\eta_{\nu_4}(l_4)} - \frac{1}{2} \frac{\delta\widetilde{D}_{p'+2}}{\delta\eta_{\nu_4}(l_4)} \right) G_6$$

$$= (\frac{\delta^2}{\delta\eta_{\mu_4}\delta\eta_{\nu_4}} - \frac{1}{2} \frac{\delta^2\widetilde{D}_{p'+2}}{\delta\eta_{\mu_4}\delta\eta_{\nu_4}} - \frac{1}{2} \frac{\delta\widetilde{D}_{p'+2}}{\delta\eta_{\mu_4}} \frac{\delta}{\delta\eta_{\nu_4}} +$$

$$-\frac{1}{2} \frac{\delta\widetilde{D}_{p'+2}}{\delta\eta_{\nu_4}} \frac{\delta}{\delta\eta_{\mu_4}} + \frac{1}{4} \frac{\delta\widetilde{D}_{p'+2}}{\delta\eta_{\mu_4}} \frac{\delta\widetilde{D}_{p'+2}}{\delta\eta_{\nu_4}}) \times$$

$$\sum_{perm(\mu_1,\nu_1,\mu_2,\nu_2,\mu_3,\nu_3)} (-\frac{1}{4!16} \frac{\delta^2\widetilde{D}_{p'+2}}{\delta\eta_{\mu_1}\delta\eta_{\nu_1}} \frac{\delta^2\widetilde{D}_{p'+2}}{\delta\eta_{\mu_2}\delta\eta_{\nu_2}} \frac{\delta^2\widetilde{D}_{p'+2}}{\delta\eta_{\mu_3}\delta\eta_{\nu_3}} +$$

$$\frac{1}{256} \frac{\delta^2\widetilde{D}_{p'+2}}{\delta\eta_{\mu_1}\delta\eta_{\nu_1}} \frac{\delta^2\widetilde{D}_{p'+2}}{\delta\eta_{\mu_2}\delta\eta_{\nu_2}} \frac{\delta\widetilde{D}_{p'+2}}{\delta\eta_{\mu_3}} \frac{\delta\widetilde{D}_{p'+2}}{\delta\eta_{\nu_3}} +$$

$$-\frac{1}{4!64} \frac{\delta^2\widetilde{D}_{p'+2}}{\delta\eta_{\mu_1}\delta\eta_{\nu_1}} \frac{\delta\widetilde{D}_{p'+2}}{\delta\eta_{\mu_2}} \frac{\delta\widetilde{D}_{p'+2}}{\delta\eta_{\nu_2}} \frac{\delta\widetilde{D}_{p'+2}}{\delta\eta_{\mu_3}} \frac{\delta\widetilde{D}_{p'+2}}{\delta\eta_{\nu_3}} +$$

$$\frac{1}{6!64} \frac{\delta\widetilde{D}_{p'+2}}{\delta\eta_{\mu_1}} \frac{\delta\widetilde{D}_{p'+2}}{\delta\eta_{\nu_1}} \frac{\delta\widetilde{D}_{p'+2}}{\delta\eta_{\mu_2}} \frac{\delta\widetilde{D}_{p'+2}}{\delta\eta_{\nu_2}} \frac{\delta\widetilde{D}_{p'+2}}{\delta\eta_{\mu_3}} \frac{\delta\widetilde{D}_{p'+2}}{\delta\eta_{\nu_3}})$$

$$= \sum_{perm(\mu_1,\nu_1,\mu_2,\nu_2,\mu_3,\nu_3)} (\frac{1}{4!32} \frac{\delta^2\widetilde{D}_{p'+2}}{\delta\eta_{\mu_1}\delta\eta_{\nu_1}} \frac{\delta^2\widetilde{D}_{p'+2}}{\delta\eta_{\mu_2}\delta\eta_{\nu_2}} \frac{\delta^2\widetilde{D}_{p'+2}}{\delta\eta_{\mu_3}\delta\eta_{\nu_3}} \frac{\delta^2\widetilde{D}_{p'+2}}{\delta\eta_{\mu_4}\delta\eta_{\nu_4}} +$$

$$-\frac{1}{4!64} \frac{\delta^2\widetilde{D}_{p'+2}}{\delta\eta_{\mu_1}\delta\eta_{\nu_1}} \frac{\delta^2\widetilde{D}_{p'+2}}{\delta\eta_{\mu_2}\delta\eta_{\nu_2}} \frac{\delta^2\widetilde{D}_{p'+2}}{\delta\eta_{\mu_3}\delta\eta_{\nu_3}} \frac{\delta\widetilde{D}_{p'+2}}{\delta\eta_{\mu_4}} \frac{\delta\widetilde{D}_{p'+2}}{\delta\eta_{\nu_4}} +$$

$$\frac{1}{256} \frac{\delta^2\widetilde{D}_{p'+2}}{\delta\eta_{\mu_1}\delta\eta_{\nu_1}} \frac{\delta^2\widetilde{D}_{p'+2}}{\delta\eta_{\mu_2}\delta\eta_{\nu_2}} \frac{\delta^2\widetilde{D}_{p'+2}}{\delta\eta_{\mu_3}\delta\eta_{\mu_4}} \frac{\delta^2\widetilde{D}_{p'+2}}{\delta\eta_{\nu_3}\delta\eta_{\nu_4}} +$$

$$\frac{1}{256} \frac{\delta^2\widetilde{D}_{p'+2}}{\delta\eta_{\mu_1}\delta\eta_{\nu_1}} \frac{\delta^2\widetilde{D}_{p'+2}}{\delta\eta_{\mu_2}\delta\eta_{\nu_2}} \frac{\delta^2\widetilde{D}_{p'+2}}{\delta\eta_{\mu_3}\delta\eta_{\nu_4}} \frac{\delta^2\widetilde{D}_{p'+2}}{\delta\eta_{\mu_4}\delta\eta_{\nu_3}} +$$

$$-\frac{1}{512} \frac{\delta^2\widetilde{D}_{p'+2}}{\delta\eta_{\mu_1}\delta\eta_{\nu_1}} \frac{\delta^2\widetilde{D}_{p'+2}}{\delta\eta_{\mu_2}\delta\eta_{\nu_2}} \frac{\delta^2\widetilde{D}_{p'+2}}{\delta\eta_{\mu_4}\delta\eta_{\nu_4}} \frac{\delta\widetilde{D}_{p'+2}}{\delta\eta_{\mu_3}} \frac{\delta\widetilde{D}_{p'+2}}{\delta\eta_{\nu_3}} +$$

$$-\frac{1}{512} \frac{\delta^2\widetilde{D}_{p'+2}}{\delta\eta_{\mu_1}\delta\eta_{\nu_1}} \frac{\delta^2\widetilde{D}_{p'+2}}{\delta\eta_{\mu_2}\delta\eta_{\nu_2}} \frac{\delta^2\widetilde{D}_{p'+2}}{\delta\eta_{\mu_3}\delta\eta_{\nu_4}} \frac{\delta\widetilde{D}_{p'+2}}{\delta\eta_{\mu_4}} \frac{\delta\widetilde{D}_{p'+2}}{\delta\eta_{\nu_3}} +$$

$$-\frac{1}{512} \frac{\delta^2\widetilde{D}_{p'+2}}{\delta\eta_{\mu_1}\delta\eta_{\nu_1}} \frac{\delta^2\widetilde{D}_{p'+2}}{\delta\eta_{\mu_2}\delta\eta_{\nu_2}} \frac{\delta^2\widetilde{D}_{p'+2}}{\delta\eta_{\nu_3}\delta\eta_{\nu_4}} \frac{\delta\widetilde{D}_{p'+2}}{\delta\eta_{\mu_3}} \frac{\delta\widetilde{D}_{p'+2}}{\delta\eta_{\mu_4}} +$$

$$-\frac{1}{512} \frac{\delta^2\widetilde{D}_{p'+2}}{\delta\eta_{\mu_1}\delta\eta_{\nu_1}} \frac{\delta^2\widetilde{D}_{p'+2}}{\delta\eta_{\mu_2}\delta\eta_{\nu_2}} \frac{\delta^2\widetilde{D}_{p'+2}}{\delta\eta_{\mu_3}\delta\eta_{\mu_4}} \frac{\delta\widetilde{D}_{p'+2}}{\delta\eta_{\nu_3}} \frac{\delta\widetilde{D}_{p'+2}}{\delta\eta_{\nu_4}} +$$

$$-\frac{1}{512}\frac{\delta^2\widetilde{D}_{p'+2}}{\delta\eta_{\mu_1}\delta\eta_{\nu_1}}\frac{\delta^2\widetilde{D}_{p'+2}}{\delta\eta_{\mu_2}\delta\eta_{\nu_2}}\frac{\delta^2\widetilde{D}_{p'+2}}{\delta\eta_{\mu_4}\delta\eta_{\nu_3}}\frac{\delta\widetilde{D}_{p'+2}}{\delta\eta_{\mu_3}}\frac{\delta\widetilde{D}_{p'+2}}{\delta\eta_{\nu_4}}+$$

$$\frac{1}{1024}\frac{\delta^2\widetilde{D}_{p'+2}}{\delta\eta_{\mu_1}\delta\eta_{\nu_1}}\frac{\delta^2\widetilde{D}_{p'+2}}{\delta\eta_{\mu_2}\delta\eta_{\nu_2}}\frac{\delta\widetilde{D}_{p'+2}}{\delta\eta_{\mu_3}}\frac{\delta\widetilde{D}_{p'+2}}{\delta\eta_{\nu_3}}\frac{\delta\widetilde{D}_{p'+2}}{\delta\eta_{\mu_4}}\frac{\delta\widetilde{D}_{p'+2}}{\delta\eta_{\nu_4}}+$$

$$-\frac{1}{128}\frac{\delta^2\widetilde{D}_{p'+2}}{\delta\eta_{\mu_1}\delta\eta_{\nu_1}}\frac{\delta^2\widetilde{D}_{p'+2}}{\delta\eta_{\mu_2}\delta\eta_{\mu_4}}\frac{\delta^2\widetilde{D}_{p'+2}}{\delta\eta_{\nu_2}\delta\eta_{\nu_4}}\frac{\delta\widetilde{D}_{p'+2}}{\delta\eta_{\mu_3}}\frac{\delta\widetilde{D}_{p'+2}}{\delta\eta_{\nu_3}}+$$

$$\frac{1}{4!128}\frac{\delta^2\widetilde{D}_{p'+2}}{\delta\eta_{\mu_1}\delta\eta_{\nu_1}}\frac{\delta^2\widetilde{D}_{p'+2}}{\delta\eta_{\mu_4}\delta\eta_{\nu_4}}\frac{\delta\widetilde{D}_{p'+2}}{\delta\eta_{\mu_2}}\frac{\delta\widetilde{D}_{p'+2}}{\delta\eta_{\nu_2}}\frac{\delta\widetilde{D}_{p'+2}}{\delta\eta_{\mu_3}}\frac{\delta\widetilde{D}_{p'+2}}{\delta\eta_{\nu_3}}+$$

$$\frac{1}{4!32}\frac{\delta^2\widetilde{D}_{p'+2}}{\delta\eta_{\mu_1}\delta\eta_{\nu_1}}\frac{\delta^2\widetilde{D}_{p'+2}}{\delta\eta_{\mu_2}\delta\eta_{\nu_4}}\frac{\delta\widetilde{D}_{p'+2}}{\delta\eta_{\nu_2}}\frac{\delta\widetilde{D}_{p'+2}}{\delta\eta_{\mu_3}}\frac{\delta\widetilde{D}_{p'+2}}{\delta\eta_{\nu_3}}\frac{\delta\widetilde{D}_{p'+2}}{\delta\eta_{\mu_4}}+$$

$$\frac{1}{4!32}\frac{\delta^2\widetilde{D}_{p'+2}}{\delta\eta_{\mu_1}\delta\eta_{\nu_1}}\frac{\delta^2\widetilde{D}_{p'+2}}{\delta\eta_{\mu_2}\delta\eta_{\mu_4}}\frac{\delta\widetilde{D}_{p'+2}}{\delta\eta_{\nu_2}}\frac{\delta\widetilde{D}_{p'+2}}{\delta\eta_{\mu_3}}\frac{\delta\widetilde{D}_{p'+2}}{\delta\eta_{\nu_3}}\frac{\delta\widetilde{D}_{p'+2}}{\delta\eta_{\nu_4}}+$$

$$-\frac{1}{4!256}\frac{\delta^2\widetilde{D}_{p'+2}}{\delta\eta_{\mu_1}\delta\eta_{\nu_1}}\frac{\delta\widetilde{D}_{p'+2}}{\delta\eta_{\mu_2}}\frac{\delta\widetilde{D}_{p'+2}}{\delta\eta_{\nu_2}}\frac{\delta\widetilde{D}_{p'+2}}{\delta\eta_{\mu_3}}\frac{\delta\widetilde{D}_{p'+2}}{\delta\eta_{\nu_3}}\frac{\delta\widetilde{D}_{p'+2}}{\delta\eta_{\mu_4}}\frac{\delta\widetilde{D}_{p'+2}}{\delta\eta_{\nu_4}}+$$

$$\frac{1}{4!64}\frac{\delta^2\widetilde{D}_{p'+2}}{\delta\eta_{\mu_1}\delta\eta_{\mu_4}}\frac{\delta^2\widetilde{D}_{p'+2}}{\delta\eta_{\nu_1}\delta\eta_{\nu_4}}\frac{\delta\widetilde{D}_{p'+2}}{\delta\eta_{\mu_2}}\frac{\delta\widetilde{D}_{p'+2}}{\delta\eta_{\nu_2}}\frac{\delta\widetilde{D}_{p'+2}}{\delta\eta_{\mu_3}}\frac{\delta\widetilde{D}_{p'+2}}{\delta\eta_{\nu_3}}+$$

$$-\frac{1}{6!128}\frac{\delta^2\widetilde{D}_{p'+2}}{\delta\eta_{\mu_4}\delta\eta_{\nu_4}}\frac{\delta\widetilde{D}_{p'+2}}{\delta\eta_{\mu_1}}\frac{\delta\widetilde{D}_{p'+2}}{\delta\eta_{\nu_1}}\frac{\delta\widetilde{D}_{p'+2}}{\delta\eta_{\mu_2}}\frac{\delta\widetilde{D}_{p'+2}}{\delta\eta_{\nu_2}}\frac{\delta\widetilde{D}_{p'+2}}{\delta\eta_{\mu_3}}\frac{\delta\widetilde{D}_{p'+2}}{\delta\eta_{\nu_3}}+$$

$$-\frac{1}{5!128}\frac{\delta^2\widetilde{D}_{p'+2}}{\delta\eta_{\mu_1}\delta\eta_{\nu_4}}\frac{\delta\widetilde{D}_{p'+2}}{\delta\eta_{\nu_1}}\frac{\delta\widetilde{D}_{p'+2}}{\delta\eta_{\mu_2}}\frac{\delta\widetilde{D}_{p'+2}}{\delta\eta_{\nu_2}}\frac{\delta\widetilde{D}_{p'+2}}{\delta\eta_{\mu_3}}\frac{\delta\widetilde{D}_{p'+2}}{\delta\eta_{\nu_3}}\frac{\delta\widetilde{D}_{p'+2}}{\delta\eta_{\mu_4}}+$$

$$-\frac{1}{5!128}\frac{\delta^2\widetilde{D}_{p'+2}}{\delta\eta_{\mu_1}\delta\eta_{\mu_4}}\frac{\delta\widetilde{D}_{p'+2}}{\delta\eta_{\nu_1}}\frac{\delta\widetilde{D}_{p'+2}}{\delta\eta_{\mu_2}}\frac{\delta\widetilde{D}_{p'+2}}{\delta\eta_{\nu_2}}\frac{\delta\widetilde{D}_{p'+2}}{\delta\eta_{\mu_3}}\frac{\delta\widetilde{D}_{p'+2}}{\delta\eta_{\nu_3}}\frac{\delta\widetilde{D}_{p'+2}}{\delta\eta_{\nu_4}}+$$

$$\frac{1}{6!256}\frac{\delta\widetilde{D}_{p'+2}}{\delta\eta_{\mu_1}}\frac{\delta\widetilde{D}_{p'+2}}{\delta\eta_{\nu_1}}\frac{\delta\widetilde{D}_{p'+2}}{\delta\eta_{\mu_2}}\frac{\delta\widetilde{D}_{p'+2}}{\delta\eta_{\nu_2}}\frac{\delta\widetilde{D}_{p'+2}}{\delta\eta_{\mu_3}}\frac{\delta\widetilde{D}_{p'+2}}{\delta\eta_{\nu_3}}\frac{\delta\widetilde{D}_{p'+2}}{\delta\eta_{\mu_4}}\frac{\delta\widetilde{D}_{p'+2}}{\delta\eta_{\nu_4}}$$

$$=\sum_{perm(\mu_1,\nu_1,\mu_2,\nu_2,\mu_3,\nu_3,\mu_4,\nu_4)}\left(\frac{1}{4!256}\frac{\delta^2\widetilde{D}_{p'+2}}{\delta\eta_{\mu_1}\delta\eta_{\nu_1}}\frac{\delta^2\widetilde{D}_{p'+2}}{\delta\eta_{\mu_2}\delta\eta_{\nu_2}}\frac{\delta^2\widetilde{D}_{p'+2}}{\delta\eta_{\mu_3}\delta\eta_{\nu_3}}\frac{\delta^2\widetilde{D}_{p'+2}}{\delta\eta_{\mu_4}\delta\eta_{\nu_4}}+\right.$$

$$-\frac{1}{4!128}\frac{\delta^2\widetilde{D}_{p'+2}}{\delta\eta_{\mu_1}\delta\eta_{\nu_1}}\frac{\delta^2\widetilde{D}_{p'+2}}{\delta\eta_{\mu_2}\delta\eta_{\nu_2}}\frac{\delta^2\widetilde{D}_{p'+2}}{\delta\eta_{\mu_3}\delta\eta_{\nu_3}}\frac{\delta\widetilde{D}_{p'+2}}{\delta\eta_{\mu_4}}\frac{\delta\widetilde{D}_{p'+2}}{\delta\eta_{\nu_4}}+$$

$$\frac{1}{4!512}\frac{\delta^2\widetilde{D}_{p'+2}}{\delta\eta_{\mu_1}\delta\eta_{\nu_1}}\frac{\delta^2\widetilde{D}_{p'+2}}{\delta\eta_{\mu_2}\delta\eta_{\nu_2}}\frac{\delta\widetilde{D}_{p'+2}}{\delta\eta_{\mu_3}}\frac{\delta\widetilde{D}_{p'+2}}{\delta\eta_{\nu_3}}\frac{\delta\widetilde{D}_{p'+2}}{\delta\eta_{\mu_4}}\frac{\delta\widetilde{D}_{p'+2}}{\delta\eta_{\nu_4}}+$$

$$
-\frac{1}{6!256}\frac{\delta^2\widetilde{D}_{p'+2}}{\delta\eta_{\mu_1}\delta\eta_{\nu_1}}\frac{\delta\widetilde{D}_{p'+2}}{\delta\eta_{\mu_2}}\frac{\delta\widetilde{D}_{p'+2}}{\delta\eta_{\nu_2}}\frac{\delta\widetilde{D}_{p'+2}}{\delta\eta_{\mu_3}}\frac{\delta\widetilde{D}_{p'+2}}{\delta\eta_{\nu_3}}\frac{\delta\widetilde{D}_{p'+2}}{\delta\eta_{\mu_4}}\frac{\delta\widetilde{D}_{p'+2}}{\delta\eta_{\nu_4}}+
$$

$$
\frac{1}{8!256}\frac{\delta\widetilde{D}_{p'+2}}{\delta\eta_{\mu_1}}\frac{\delta\widetilde{D}_{p'+2}}{\delta\eta_{\nu_1}}\frac{\delta\widetilde{D}_{p'+2}}{\delta\eta_{\mu_2}}\frac{\delta\widetilde{D}_{p'+2}}{\delta\eta_{\nu_2}}\frac{\delta\widetilde{D}_{p'+2}}{\delta\eta_{\mu_3}}\frac{\delta\widetilde{D}_{p'+2}}{\delta\eta_{\nu_3}}\frac{\delta\widetilde{D}_{p'+2}}{\delta\eta_{\mu_4}}\frac{\delta\widetilde{D}_{p'+2}}{\delta\eta_{\nu_4}}). \tag{A.36}
$$

G_2, G_4, G_6 and G_8 are expressed in first and second order derivatives of $\widetilde{D}_{p'+2}$. These derivatives are calculated in appendix B. The G's are used to calculate correlation functions with one or more orientation tensors $\underline{\underline{S}}$. According to Eq. (A.5b), (A.5c) and (A.29), the following second order correlation functions are equal to

$$
\left\langle\widehat{S}^{\alpha}_{\mu_1\nu_1}(\underline{q}_1)\rho^{\beta}(\underline{q}_2)\right\rangle_0 =
$$

$$
\lim_{\underline{\eta}\to\underline{0}} V\delta\left(\underline{q}_1+\underline{q}_2\right)\sum_{l_1,l_2}\sigma^{\alpha}_{l_1}\sigma^{\beta}_{l_2}G_2\exp\left(-\frac{1}{2}\widetilde{D}_{p'+2}\right) \tag{A.37a}
$$

and

$$
\left\langle\widehat{S}^{\alpha}_{\mu_1\nu_1}(\underline{q}_1)\widehat{S}^{\beta}_{\mu_2\nu_2}(\underline{q}_2)\right\rangle_0 =
$$

$$
\lim_{\underline{\eta}\to\underline{0}} V\delta\left(\underline{q}_1+\underline{q}_2\right)\sum_{l_1,l_2}\sigma^{\alpha}_{l_1}\sigma^{\beta}_{l_2}G_4\exp\left(-\frac{1}{2}\widetilde{D}_{p'+2}\right). \tag{A.37b}
$$

For third and fourth order correlation functions it is necessary to calculate G_6 and G_8 if there are three or four orientation tensors coupled to each other. In Eq. (A.5b) and (A.5c) the summations over l_1 and l_2 can be replaced by an integration over the α- and β-block, respectively.

$$
\left\langle\widehat{S}^{\alpha}_{\mu_1\nu_1}(\underline{q}_1)\rho^{\beta}(\underline{q}_2)\right\rangle_0 =
$$

$$
\lim_{\underline{\eta}\to\underline{0}} V\delta\left(\underline{q}_1+\underline{q}_2\right)\int_{\alpha}dl_1\int_{\beta}dl_2 G_2\exp\left(-\frac{1}{2}\widetilde{D}_{p'+2}\right) \tag{A.38a}
$$

and

$$
\left\langle\widehat{S}^{\alpha}_{\mu_1\nu_1}(\underline{q}_1)\widehat{S}^{\beta}_{\mu_2\nu_2}(\underline{q}_2)\right\rangle_0 =
$$

$$
\lim_{\underline{\eta}\to\underline{0}} V\delta\left(\underline{q}_1+\underline{q}_2\right)\int_{\alpha}dl_1\int_{\beta}dl_2 G_4\exp\left(-\frac{1}{2}\widetilde{D}_{p'+2}\right). \tag{A.38b}
$$

The integrations over l_1 and l_2 can be calculated numerically. The other correlation functions can also be written in a form similar to Eq. (A.38a) and (A.38b). This form is the final result of the whole derivation of the correlation functions. These correlation functions are necessary to calculate the Landau free energy.

Appendix B

In this appendix the first and second order derivatives of $\widetilde{D}_{p'+2}$ are calculated. These can be used to calculate the factors G_2, G_4, G_6 and G_8 that are given by Eq. (A.30b), (A.34), (A.35) and (A.36). First the limit $\Delta L \to 0$ in the interval $(l_1 - \Delta L, l_1)$ is considered. The index $p = p_1$ corresponds to this interval. It can be derived that in this limit A_{p_1}, B_{p_1} ,C_{p_1} ,D_{p_1} and E_{p_1} become

$$A_{p_1} \quad \to \quad B_{p_1} \to \frac{3\lambda_{p_1}}{2\Delta L}, \tag{B.1a}$$

$$C_{p_1} \quad = \quad \frac{i}{2}\Delta L, \tag{B.1b}$$

$$D_{p_1} \quad \to \quad \frac{-(\Delta L)^3}{18\lambda_{p_1}} \tag{B.1c}$$

$$\text{and}$$

$$E_{p_1} \quad \to \quad \left(\frac{3\lambda_{p_1}}{4\pi\Delta L}\right)^{\frac{3}{2}}. \tag{B.1d}$$

To derive $\widetilde{A}_{p_1+1}, \widetilde{\underline{C}}_{p_1+1}, \widetilde{D}_{p_1+1}$ and $\widetilde{E}_{p_1+1}$, Eq.(A.25) is applied in which p' is replaced by p_1 and the limit $\Delta L \to 0$ is taken,

$$\lim_{\Delta L \to 0} \int d\underline{u}_{p_1} \prod_{p=1}^{p_1} \int d\underline{u}_{p-1} I_p \exp\left(-\frac{3}{4}u_{p-1}^2 - \frac{3}{4}u_p^2\right) =$$

$$\lim_{\Delta L \to 0} \int d\underline{u}_{p_1} \int d\underline{u}_{p_1-1} \widetilde{E}_{p_1} \exp(-\frac{1}{2}\widetilde{A}_{p_1}u_{p_1-1}^2 - \frac{1}{2}A_{p_1}u_{p_1}^2 + B_{p_1}\underline{u}_{p_1-1} \cdot \underline{u}_{p_1}) \times$$

$$\exp(\widetilde{\underline{C}}_{p_1} \cdot \underline{u}_{p_1-1} + C_{p_1}\underline{Q}_{p_1} \cdot \underline{u}_{p_1} - \frac{1}{2}\widetilde{D}_{p_1}). \tag{B.2}$$

For every tangent vector $\underline{u}_p$ the integrand $I_p \exp\left(-\frac{3}{4}u_{p-1}^2 - \frac{3}{4}u_p^2\right)$ in Eq. (B.2) is continuous with respect to $\Delta L \neq 0$. Therefore it is allowed to interchange the limit $\Delta L \to 0$ and the integrals over the tangent vectors $\underline{u}_p$. Then Eq. (A.26a),(A.26b),(A.26c) and (A.26d) can be inserted in Eq. (B.2), which gives,

$$
\int d\underline{u}_{p_1} \prod_{p=1}^{p_1} \int d\underline{u}_{p-1} \lim_{\Delta L \to 0} I_p \exp\left(-\frac{3}{4}u_{p-1}^2 - \frac{3}{4}u_p^2\right) =
$$

$$
\int d\underline{u}_{p_1} \int d\underline{u}_{p_1-1} \lim_{\Delta L \to 0} \widetilde{E}_{p_1-1} \left(\frac{2\pi}{\widetilde{A}_{p_1-1}}\right)^{\frac{3}{2}} \times
$$

$$
E_{p_1} \exp\left(-\frac{1}{2}A_{p_1}u_{p_1-1}^2 - \frac{1}{2}A_{p_1}u_{p_1}^2 + B_{p_1}\underline{u}_{p_1-1} \cdot \underline{u}_{p_1}\right) \times
$$

$$
\exp(-\frac{1}{2}A_{p_1-1}u_{p_1-1}^2 + \frac{B_{p_1-1}^2}{2\widetilde{A}_{p_1-1}}u_{p_1-1}^2) \times
$$

$$
\exp(\widetilde{\underline{C}}_{p_1} \cdot \underline{u}_{p_1-1} + C_{p_1}\underline{Q}_{p_1} \cdot \underline{u}_{p_1} - \frac{1}{2}\widetilde{D}_{p_1}). \tag{B.3}
$$

From Eq.(B.1a) and (B.1d) it follows that in the limit $\Delta L \to 0$,

$$
E_{p_1} \exp\left(-\frac{1}{2}A_{p_1}u_{p_1-1}^2 - \frac{1}{2}A_{p_1}u_{p_1}^2 + B_{p_1}\underline{u}_{p_1-1} \cdot \underline{u}_{p_1}\right) \to \delta(\underline{u}_{p_1} - \underline{u}_{p_1-1}). \tag{B.4}
$$

Then integrating over $\underline{u}_{p_1-1}$ in Eq. (B.3) yields,

$$
\int d\underline{u}_{p_1} \prod_{p=1}^{p_1} \int d\underline{u}_{p-1} \lim_{\Delta L \to 0} I_p \exp\left(-\frac{3}{4}u_{p-1}^2 - \frac{3}{4}u_p^2\right) =
$$

$$
\int d\underline{u}_{p_1} \widetilde{E}_{p_1-1} \left(\frac{2\pi}{\widetilde{A}_{p_1-1}}\right)^{\frac{3}{2}} \times
$$

$$
\exp(-\frac{1}{2}A_{p_1-1}u_{p_1}^2 + \frac{B_{p_1-1}^2}{2\widetilde{A}_{p_1-1}}u_{p_1}^2) \times
$$

$$
\lim_{\Delta L \to 0} \exp(\widetilde{\underline{C}}_{p_1} \cdot \underline{u}_{p_1} + C_{p_1}\underline{Q}_{p_1} \cdot \underline{u}_{p_1} - \frac{1}{2}\widetilde{D}_{p_1}). \tag{B.5}
$$

To derive $\widetilde{A}_{p_1+1}$, $\underline{\widetilde{C}}_{p_1+1}$, $\widetilde{D}_{p_1+1}$ and $\widetilde{E}_{p_1+1}$, Eq. (B.5) can be used in combination with $I_{p_1+1} \exp\left(-\frac{3}{4}u^2_{p_1} - \frac{3}{4}u^2_{p_1+1}\right)$, given by

$$I_{p_1+1} \exp\left(-\frac{3}{4}u^2_{p_1} - \frac{3}{4}u^2_{p_1+1}\right) = E_{p_1+1} \exp(-\frac{1}{2}A_{p_1+1}(u^2_{p_1} + u^2_{p_1+1}) + B_{p_1+1}\underline{u}_{p_1} \cdot \underline{u}_{p_1+1})$$

$$\exp(C_{p_1+1}\underline{Q}_{p_1+1} \cdot (\underline{u}_{p_1} + \underline{u}_{p_1+1}) - \frac{1}{2}D_{p_1+1}Q^2_{p_1+1}). \tag{B.6}$$

It follows that $\widetilde{A}_{p_1+1}$, $\underline{\widetilde{C}}_{p_1+1}$, $\widetilde{D}_{p_1+1}$ and $\widetilde{E}_{p_1+1}$ are equal to

$$\widetilde{A}_{p_1+1} = A_{p_1+1} + A_{p_1-1} - \frac{B^2_{p_1-1}}{\widetilde{A}_{p_1-1}}, \tag{B.7a}$$

$$\underline{\widetilde{C}}_{p_1+1} = \underline{\widetilde{C}}_{p_1} + C_{p_1}\underline{Q}_{p_1} + C_{p_1+1}\underline{Q}_{p_1+1}, \tag{B.7b}$$

$$\widetilde{D}_{p_1+1} = \widetilde{D}_{p_1} + D_{p_1+1}Q^2_{p_1+1}, \tag{B.7c}$$

and

$$\widetilde{E}_{p_1+1} = E_{p_1+1}\widetilde{E}_{p_1-1}\left(\frac{2\pi}{\widetilde{A}_{p_1-1}}\right)^{\frac{3}{2}}. \tag{B.7d}$$

For $p = p_2 + 1$, $p_3 + 1$ and $p_4 + 1$ the same relations can be applied. For other p's we use Eq. (A.26a), (A.26b), (A.26c) and (A.26d). Eq. (B.7a) and (B.7d) have the same form as Eq. (A.26a) and (A.26d). In the limit $\Delta L \to 0$ the contribution of the p_1-th interval has disappeared in $\widetilde{A}_{p_1+1}$ and $\widetilde{E}_{p_1+1}$. In Eq. (B.7b) and (B.7c) the limit $\Delta L \to 0$ has not been taken yet. Taking the limit and applying Eq. (A.26b), (A.26c), (B.1c) and (B.1d), it follows that,

$$\underline{\widetilde{C}}_{p_1+1} = C_{p_1+1}\underline{Q}_{p_1+1} + C_{p_1-1}\underline{Q}_{p_1-1} + \frac{B_{p_1-1}\underline{\widetilde{C}}_{p_1-1}}{\widetilde{A}_{p_1-1}}, \tag{B.8a}$$

and

$$\widetilde{D}_{p_1+1} = D_{p_1+1}Q^2_{p_1+1} + \widetilde{D}_{p_1-1} - \frac{\widetilde{C}^2_{p_1-1}}{\widetilde{A}_{p_1-1}}. \tag{B.8b}$$

These equations have also the same form as Eq. (A.26b) and (A.26c). In this form $\underline{\widetilde{C}}_{p_1+1}$ and $\underline{\widetilde{E}}_{p_1+1}$ do not depend on $\underline{Q}_{p_1}$ any more. So the $\underline{\eta}(l)$-dependence of $\underline{\widetilde{C}}_{p_1+1}$ and $\underline{\widetilde{E}}_{p_1+1}$ is lost. To derive the first and second order functional derivatives of $\underline{\widetilde{C}}_{p_1+1}$

and $\widetilde{D}_{p_1+1}$ with respect to $\eta(l_1)$, $\eta(l_2)$, $\eta(l_3)$ and/or $\eta(l_4)$, Eq. (B.7b) and (B.7c) are used instead of Eq. (B.8a) and (B.8b). In these expressions the limit $\Delta L \to 0$ has not been taken yet and so that the $\eta(l)$-dependence is conserved. The functional derivative is defined by Eq. (B.12). In this definition the limit $\Delta L \to 0$ is included.

The derivatives of $\underline{\widetilde{C}}_{p_1+1}$ and $\widetilde{D}_{p_1+1}$ must be known to calculate the first and second order functional derivatives. According to Eq. (B.7b) the first order functional derivative of $\underline{\widetilde{C}}_{p_1+1}$ is,

$$\frac{\delta \underline{\widetilde{C}}_{p_1+1}}{\delta \eta_{\mu_1}(l_1)} = \frac{\delta \underline{\widetilde{C}}_{p_1}}{\delta \eta_{\mu_1}(l_1)} + C_{p_1} \frac{\delta \underline{Q}_{p_1}}{\delta \eta_{\mu_1}(l_1)} + C_{p_1+1} \frac{\delta \underline{Q}_{p_1+1}}{\delta \eta_{\mu_1}(l_1)}. \tag{B.9}$$

In Eq. (B.9), $\underline{\widetilde{C}}_{p_1}$ is equal to,

$$\underline{\widetilde{C}}_{p_1} = C_{p_1} \underline{Q}_{p_1} + C_{p_1-1} \underline{Q}_{p_1-1} + \frac{B_{p_1-1} \underline{\widetilde{C}}_{p_1-1}}{\widetilde{A}_{p_1-1}}, \tag{B.10}$$

according to Eq. (A.26b). Now Eq. (B.9) can be written as,

$$\frac{\delta \underline{\widetilde{C}}_{p_1+1}}{\delta \eta_{\mu_1}(l_1)} = \frac{B_{p_1-1}}{\widetilde{A}_{p_1-1}} \frac{\delta \underline{\widetilde{C}}_{p_1-1}}{\delta \eta_{\mu_1}(l_1)} + C_{p_1-1} \frac{\delta \underline{Q}_{p_1-1}}{\delta \eta_{\mu_1}(l_1)} +$$
$$2C_{p_1} \frac{\delta \underline{Q}_{p_1}}{\delta \eta_{\mu_1}(l_1)} + C_{p_1+1} \frac{\delta \underline{Q}_{p_1+1}}{\delta \eta_{\mu_1}(l_1)}. \tag{B.11}$$

In Eq.(B.11) the functional derivative of $\underline{Q}_p$ is defined as

$$\frac{\delta \underline{Q}_p}{\delta \eta_{\mu_1}(l_1)} \equiv \lim_{\Delta L \to 0} \frac{1}{\Delta L} \frac{\partial \underline{Q}_p}{\partial \eta_{\mu_1}(l_1)} =$$
$$-i\underline{e}_{\mu_1} \lim_{\Delta L \to 0} \frac{1}{\Delta L} \delta_{pp_1} = -i\underline{e}_{\mu_1} \delta(l_1 - L_p), \tag{B.12}$$

using Eq. (A.9). Therefore in Eq. (B.11) the first, second and fourth terms are zero, because $\underline{\widetilde{C}}_{p_1-1}$, $\underline{Q}_{p_1-1}$ and $\underline{Q}_{p_1+1}$ do not depend on $\eta_{\mu_1}(l_1)$. In the third term Eq. (B.1c) and (B.12) can be inserted which yields,

$$\frac{\delta \underline{\widetilde{C}}_{p_1+1}}{\delta \eta_{\mu_1}(l_1)} = -2 \frac{i^2}{2} \underline{e}_{\mu_1} \lim_{\Delta L \to 0} \Delta L \frac{1}{\Delta L} = \underline{e}_{\mu_1}. \tag{B.13}$$

In the the same way it follows that

$$\frac{\delta \widetilde{\underline{C}}_{p_1}}{\delta \eta_{\mu_1}(l_1)} = \frac{1}{2} \underline{e}_{\mu_1} \tag{B.14a}$$

and

$$\frac{\delta \widetilde{\underline{C}}_p}{\delta \eta_{\mu_1}(l_1)} = 0 \quad \text{for } p < p_1. \tag{B.14b}$$

If $p > p_1 + 1$, then the first order derivative is not zero. For $p \le p'$ Eq. (A.26b) can be applied to calculate this first order derivative,

$$\frac{\delta \widetilde{\underline{C}}_p}{\delta \eta_{\mu_1}(l_1)} = C_p \frac{\delta \underline{Q}_p}{\delta \eta_{\mu_1}(l_1)} + C_{p-1} \frac{\delta \underline{Q}_{p-1}}{\delta \eta_{\mu_1}(l_1)} + \frac{B_{p-1}}{\widetilde{A}_{p-1}} \frac{\delta \widetilde{\underline{C}}_{p-1}}{\delta \eta_{\mu_1}(l_1)}. \tag{B.15}$$

The first and second term cancel out, because $\underline{Q}_p$ and $\underline{Q}_{p-1}$ are independent of $\eta_{\mu_1}(l_1)$. The same terms cancel out in the first order derivative of $\widetilde{\underline{C}}_{p-1}$, $\widetilde{\underline{C}}_{p-2}$, $\widetilde{\underline{C}}_{p-3}$ until $\widetilde{\underline{C}}_{p_1+2}$. Then it follows that,

$$\frac{\delta \widetilde{\underline{C}}_p}{\delta \eta_{\mu_1}(l_1)} = \frac{B_{p-1}}{\widetilde{A}_{p-1}} \frac{B_{p-2}}{\widetilde{A}_{p-2}} ...... \frac{B_{p_1+1}}{\widetilde{A}_{p_1+1}} \frac{\delta \widetilde{\underline{C}}_{p_1+1}}{\delta \eta_{\mu_1}(l_1)} =$$

$$\frac{\delta \widetilde{\underline{C}}_{p_1+1}}{\delta \eta_{\mu_1}(l_1)} \prod_{n=1}^{p-p_1-1} \frac{B_{p-n}}{\widetilde{A}_{p-n}} = \underline{e}_{\mu_1} \prod_{n=1}^{p-p_1-1} \frac{B_{p-n}}{\widetilde{A}_{p-n}}, \tag{B.16}$$

if $p_1 + 1 < p < p_2 + 1$. If $p_2 + 1 < p < p_3 + 1$, then

$$\frac{\delta \widetilde{\underline{C}}_p}{\delta \eta_{\mu_1}(l_1)} = \frac{B_{p-1}}{\widetilde{A}_{p-1}} \frac{B_{p-2}}{\widetilde{A}_{p-2}} ...... \frac{B_{p_2+1}}{\widetilde{A}_{p_2+1}} \frac{\delta \widetilde{\underline{C}}_{p_2+1}}{\delta \eta_{\mu_1}(l_1)}, \tag{B.17}$$

in which the derivative of $\widetilde{\underline{C}}_{p_2+1}$ is the same as Eq. (B.11),

$$\frac{\delta \widetilde{\underline{C}}_{p_2+1}}{\delta \eta_{\mu_1}(l_1)} = \frac{B_{p_2-1}}{\widetilde{A}_{p_2-1}} \frac{\delta \widetilde{\underline{C}}_{p_2-1}}{\delta \eta_{\mu_1}(l_1)} + C_{p_2-1} \frac{\delta \underline{Q}_{p_2-1}}{\delta \eta_{\mu_1}(l_1)} +$$

$$2 C_{p_2} \frac{\delta \underline{Q}_{p_2}}{\delta \eta_{\mu_1}(l_1)} + C_{p_2+1} \frac{\delta \underline{Q}_{p_2+1}}{\delta \eta_{\mu_1}(l_1)}. \tag{B.18}$$

If $l_1 \neq l_2$, then p_1 is not equal to $p_2 - 1$, p_2 and $p_2 + 1$. Therefore the second, third and fourth term are zero and only the first term remains in Eq. (B.18). Combining Eq.(B.16), Eq. (B.17) and Eq. (B.18) yields,

$$\frac{\delta \widetilde{\underline{C}}_p}{\delta \eta_{\mu_1}(l_1)} = \underline{e}_{\mu_1} \prod_{n=1}^{p-p_2-1} \frac{B_{p-n}}{\widetilde{A}_{p-n}} \prod_{n=1}^{p_2-p_1-1} \frac{B_{p_2-n}}{\widetilde{A}_{p_2-n}} = \underline{e}_{\mu_1} \prod_{\substack{n=1, \\ n \neq p-p_2}}^{p-p_1-1} \frac{B_{p-n}}{\widetilde{A}_{p-n}}, \qquad (B.19)$$

In this form Eq. (B.19) has the same form as Eq. (B.16). The factor in which $n \neq p - p_2$ has been omitted. If $p > p_3 + 1, p_4 + 1, ...$etc., then factors with $n \neq p - p_3$, $p - p_4, ...$etc are also removed from the multiplication. If $p = p' + 1$, then Eq. (B.19) can also be applied. This follows from Eq.(A.27b). For every p the second order derivative is always zero,

$$\frac{\delta^2 \widetilde{\underline{C}}_p}{\delta \eta_{\mu_1}(l_1) \delta \eta_{\nu_1}(l_1)} = 0, \quad \forall p. \qquad (B.20)$$

The first and second order derivatives of $\widetilde{C}$ are used to calculate and simplify the derivatives of $\widetilde{D}$ for every p. If $p = p_1 + 1$, the first order functional derivative of $\widetilde{D}_{p_1+1}$ is,

$$\frac{\delta \widetilde{D}_{p_1+1}}{\delta \eta_{\mu_1}(l_1)} = \frac{\delta \widetilde{D}_{p_1}}{\delta \eta_{\mu_1}(l_1)} + 2 D_{p_1+1} \underline{Q}_{p_1+1} \cdot \frac{\delta \underline{Q}_{p_1+1}}{\delta \eta_{\mu_1}(l_1)}, \qquad (B.21)$$

using Eq. (B.7c). Because $\underline{Q}_{p_1+1}$ does not depend on $\eta_{\mu_1}(l_1)$, Eq. (B.21) becomes,

$$\frac{\delta \widetilde{D}_{p_1+1}}{\delta \eta_{\mu_1}(l_1)} = \frac{\delta \widetilde{D}_{p_1}}{\delta \eta_{\mu_1}(l_1)}. \qquad (B.22)$$

Using Eq. (A.26c), Eq. (B.22) becomes

$$\frac{\delta \widetilde{D}_{p_1+1}}{\delta \eta_{\mu_1}(l_1)} = 2 D_{p_1} \underline{Q}_{p_1} \cdot \frac{\delta \underline{Q}_{p_1}}{\delta \eta_{\mu_1}(l_1)} + \frac{\delta \widetilde{D}_{p_1-1}}{\delta \eta_{\mu_1}(l_1)} - \frac{2 \widetilde{C}_{p_1-1}}{\widetilde{A}_{p_1-1}} \cdot \frac{\delta \widetilde{C}_{p_1-1}}{\delta \eta_{\mu_1}(l_1)}. \qquad (B.23)$$

The derivatives of $\widetilde{D}_{p_1-1}$ and $\widetilde{C}_{p_1-1}$ are zero, so only the first term of Eq. (B.23) remains. In the first term Eq. (B.1d) and (B.12) can be inserted so that

$$\frac{\delta \widetilde{D}_{p_1+1}}{\delta \eta_{\mu_1}(l_1)} = \lim_{\Delta L \to 0} 2 \left(-\frac{1}{18} \frac{(\Delta L)^3}{\lambda_{p_1}} \right) \underline{Q}_{p_1} \cdot \left(-i\underline{e}_{\mu_1} \frac{1}{\Delta L} \right) = \lim_{\Delta L \to 0} \frac{i(\Delta L)^2}{9 \lambda_{p_1}} \underline{e}_{\mu_1} \cdot \underline{Q}_{p_1}. \qquad (B.24)$$

If we take the limit $\Delta L \to 0$, then the first order derivative of $\widetilde{D}_{p_1+1}$ goes to zero. The second order derivative of $\widetilde{D}_{p_1+1}$ becomes,

$$\frac{\delta^2 \widetilde{D}_{p_1+1}}{\delta\eta_{\mu_1}(l_1)\delta\eta_{\nu_1}(l_1)} = \lim_{\Delta L \to 0} \frac{\delta}{\delta\eta_{\nu_1}(l_1)}\left(\frac{i(\Delta L)^2}{9\lambda_{p_1}}\underline{e}_{\mu_1} \cdot \underline{Q}_{p_1}\right) =$$

$$\lim_{\Delta L \to 0}\left(\frac{i(\Delta L)^2}{9\lambda_{p_1}}\underline{e}_{\mu_1}\right) \cdot \left(-i\underline{e}_{\nu_1}\frac{1}{\Delta L}\right) = \lim_{\Delta L \to 0}\frac{\Delta L}{9\lambda_{p_1}}\delta_{\mu_1\nu_1}, \tag{B.25}$$

which is also going to zero. In general if $p \le p_1 + 1$, then the first and second order derivatives of $\widetilde{D}_p$ are zero,

$$\frac{\delta\widetilde{D}_p}{\delta\eta_{\mu_1}(l_1)} = 0, \tag{B.26a}$$

and

$$\frac{\delta^2 \widetilde{D}_p}{\delta\eta_{\mu_1}(l_1)\delta\eta_{\nu_1}(l_1)} = 0, \quad \text{for } p \le p_1 + 1. \tag{B.26b}$$

However, these derivatives are in general nonzero for $p > p_1 + 1$. From Eq. (A.26c) it follows that,

$$\frac{\delta\widetilde{D}_p}{\delta\eta_{\mu_1}(l_1)} = 2D_p\underline{Q}_p \cdot \frac{\delta\underline{Q}_p}{\delta\eta_{\mu_1}(l_1)} - \frac{2\widetilde{C}_{p-1}}{\widetilde{A}_{p-1}} \cdot \frac{\delta\widetilde{C}_{p-1}}{\delta\eta_{\mu_1}(l_1)} + \frac{\delta\widetilde{D}_{p-1}}{\delta\eta_{\mu_1}(l_1)}. \tag{B.27}$$

If $p > p_1 + 1$, then the first term cancels out. In the second term Eq. (B.16) can be applied if $p > p_1 + 2$.

$$\frac{\delta\widetilde{D}_p}{\delta\eta_{\mu_1}(l_1)} = \frac{\delta\widetilde{D}_{p-1}}{\delta\eta_{\mu_1}(l_1)} - \frac{2\widetilde{C}_{p-1}}{\widetilde{A}_{p-1}} \cdot \underline{e}_{\mu_1}\prod_{n=2}^{p-p_1-1}\frac{B_{p-n}}{\widetilde{A}_{p-n}}. \tag{B.28}$$

If $p = p_1 + 2$, then the first order derivative of $\widetilde{D}_p$ is,

$$\begin{aligned}\frac{\delta\widetilde{D}_{p_1+2}}{\delta\eta_{\mu_1}(l_1)} &= \frac{\delta\widetilde{D}_{p_1+1}}{\delta\eta_{\mu_1}(l_1)} - \frac{2\widetilde{C}_{p_1+1}}{\widetilde{A}_{p_1+1}} \cdot \underline{e}_{\mu_1}\\[2mm] &= \frac{\delta\widetilde{D}_{p_1}}{\delta\eta_{\mu_1}(l_1)} - \frac{2\widetilde{C}_{p_1+1}}{\widetilde{A}_{p_1+1}} \cdot \underline{e}_{\mu_1} \to\\[2mm] &\quad -\frac{2\widetilde{C}_{p_1+1}}{\widetilde{A}_{p_1+1}} \cdot \underline{e}_{\mu_1},\end{aligned} \tag{B.29}$$

using Eq. (B.22). If $p = p' + 1$ or $p' + 2$ it becomes more difficult to calculate the first order derivative of $\widetilde{D}_p$. The following equations can be derived,

$$\frac{\delta \widetilde{D}_{p'+1}}{\delta \eta_{\mu_1}(l_1)} = \frac{\delta \widetilde{D}_{p'-1}}{\delta \eta_{\mu_1}(l_1)} - \frac{2\widetilde{\underline{C}}_{p'-1}}{\widetilde{A}_{p'-1}} \cdot \underline{e}_{\mu_1} \prod_{n=2}^{p'-p_1-1} \frac{B_{p'-n}}{\widetilde{A}_{p'-n}},$$
$$\text{if } p_2 = p' > p_1 + 2, \tag{B.30a}$$

$$\frac{\delta \widetilde{D}_{p'+1}}{\delta \eta_{\mu_1}(l_1)} = -\frac{2\widetilde{\underline{C}}_{p'-1}}{\widetilde{A}_{p'-1}} \cdot \underline{e}_{\mu_1}, \text{ if } p_2 = p' = p_1 + 2 \tag{B.30b}$$

$$\frac{\delta \widetilde{D}_{p'+1}}{\delta \eta_{\mu_1}(l_1)} = 0, \text{if } p_2 = p' = p_1, \tag{B.30c}$$

$$\frac{\delta \widetilde{D}_{p'+1}}{\delta \eta_{\mu_1}(l_1)} = \frac{2\widetilde{\underline{C}}_{p'}}{\widetilde{A}_{p'}} \cdot \underline{e}_{\mu_1}, \text{if } p_2 = p' - 1 = p_1, \tag{B.30d}$$

$$\frac{\delta \widetilde{D}_{p'+1}}{\delta \eta_{\mu_1}(l_1)} = \frac{\delta \widetilde{D}_{p'}}{\delta \eta_{\mu_1}(l_1)} - \frac{2\widetilde{\underline{C}}_{p'}}{\widetilde{A}_{p'}} \cdot \underline{e}_{\mu_1} \prod_{n=2}^{p'-p_1-1} \frac{B_{p'-n}}{\widetilde{A}_{p'-n}},$$
$$\text{if } p_2 = p' - 1, p_2 > p_1, \tag{B.30e}$$

$$\frac{\delta \widetilde{D}_{p'+1}}{\delta \eta_{\mu_1}(l_1)} = \frac{\delta \widetilde{D}_{p'}}{\delta \eta_{\mu_1}(l_1)} - \frac{2\widetilde{\underline{C}}_{p'}}{\widetilde{A}_{p'}} \cdot \underline{e}_{\mu_1} \prod_{n=1}^{p'-p_1-1} \frac{B_{p'-n}}{\widetilde{A}_{p'-n}},$$
$$\text{if } p' > p_2 + 1, \tag{B.30f}$$

$$\frac{\delta \widetilde{D}_{p'+2}}{\delta \eta_{\mu_1}(l_1)} = -\frac{2\widetilde{\underline{C}}_{p'}}{\widetilde{A}_{p'+1}} \cdot \underline{e}_{\mu_1}, \text{ if } p_2 = p' = p_1, \tag{B.30g}$$

$$\frac{\delta \widetilde{D}_{p'+2}}{\delta \eta_{\mu_1}(l_1)} = -\frac{2\widetilde{\underline{C}}_{p'}}{\widetilde{A}_{p'+1}} \cdot \underline{e}_{\mu_1} \prod_{n=1}^{p'-p_1-1} \frac{B_{p'-n}}{\widetilde{A}_{p'-n}},$$
$$\text{if } p_2 = p' > p_1 \text{ and} \tag{B.30h}$$

$$\frac{\delta \widetilde{D}_{p'+2}}{\delta \eta_{\mu_1}(l_1)} = \frac{\delta \widetilde{D}_{p'+1}}{\delta \eta_{\mu_1}(l_1)} - \frac{2\widetilde{\underline{C}}_{p'+1}}{\widetilde{A}_{p'+1}} \cdot \underline{e}_{\mu_1} \prod_{n=1}^{p'-p_2} \frac{B_{p'+1-n}}{\widetilde{A}_{p'+1-n}},$$
$$\text{if } p' > p_2. \tag{B.30i}$$

In Eq. (B.30g) and (B.30h) $\widetilde{\underline{C}}_{p'} \to C_{p'-1}\underline{Q}_{p'-1} + \dfrac{B_{p'-1}\widetilde{\underline{C}}_{p'-1}}{\widetilde{A}_{p'-1}}$ in the limit $\Delta L \to 0$. In

Eq. (B.28) a differentiation can be carried out a second time with respect to $\eta_{\nu_1}(l_1)$, which leads to

$$\frac{\delta^2 \widetilde{D}_p}{\delta \eta_{\mu_1}(l_1) \delta \eta_{\nu_1}(l_1)} =$$

$$\frac{\delta^2 \widetilde{D}_{p-1}}{\delta \eta_{\mu_1}(l_1) \delta \eta_{\nu_1}(l_1)} - \frac{2}{\widetilde{A}_{p-1}} \delta_{\mu_1 \nu_1} \prod_{n=2}^{p-p_1-1} \left(\frac{B_{p-n}}{\widetilde{A}_{p-n}} \right)^2, \text{ if } p > p_1 + 2, \tag{B.31a}$$

$$\text{and}$$

$$\frac{\delta^2 \widetilde{D}_p}{\delta \eta_{\mu_1}(l_1) \delta \eta_{\nu_1}(l_1)} = \frac{\delta^2 \widetilde{D}_{p-1}}{\delta \eta_{\mu_1}(l_1) \delta \eta_{\nu_1}(l_1)} - \frac{2}{\widetilde{A}_{p-1}} \delta_{\mu_1 \nu_1}, \text{ if } p = p_1 + 2. \tag{B.31b}$$

If Eq. (B.28) is differentiated with respect to $\eta_{\nu_2}(l_2)$, then there are several possibilities,

$$\frac{\delta^2 \widetilde{D}_p}{\delta \eta_{\mu_1}(l_1) \delta \eta_{\nu_2}(l_2)} = 0, \text{ if } p \leq p_2 + 1 \tag{B.32a}$$

$$\frac{\delta^2 \widetilde{D}_{p_2+2}}{\delta \eta_{\mu_1}(l_1) \delta \eta_{\nu_2}(l_2)} = - \frac{2}{\widetilde{A}_{p_2+1}} \delta_{\mu_1 \nu_2} \prod_{n=2}^{p_2-p_1} \frac{B_{p_2+1-n}}{\widetilde{A}_{p_2+1-n}},$$

$$\text{if } p = p_2 + 2 \text{ and } p_1 < p_2 - 1 \tag{B.32b}$$

$$\frac{\delta^2 \widetilde{D}_{p_2+2}}{\delta \eta_{\mu_1}(l_1) \delta \eta_{\nu_2}(l_2)} = - \frac{2}{\widetilde{A}_{p_2+1}} \delta_{\mu_1 \nu_2}, \text{ if } p = p_2 + 2 \text{ and } p_1 = p_2 \tag{B.32c}$$

$$\frac{\delta^2 \widetilde{D}_p}{\delta \eta_{\mu_1}(l_1) \delta \eta_{\nu_2}(l_2)} = \frac{\delta^2 \widetilde{D}_{p-1}}{\delta \eta_{\mu_1}(l_1) \delta \eta_{\nu_2}(l_2)} +$$

$$- \frac{2}{\widetilde{A}_{p-1}} \delta_{\mu_1 \nu_2} \prod_{n=2}^{p-p_1-1} \frac{B_{p-n}}{\widetilde{A}_{p-n}} \times$$

$$\prod_{n=2}^{p-p_2-1} \frac{B_{p-n}}{\widetilde{A}_{p-n}}, \text{ if } p > p_2 + 2. \tag{B.32d}$$

It can be verified that Eq. (B.31a), (B.31b), (B.32a), (B.32b), (B.32c) and (B.32d) are the same if $p = p' + 1$ or $p' + 2$. So now we also have found the second order derivatives of $\widetilde{D}_{p'+2}$. The first order derivatives are given by Eq. (B.30g), (B.30h) and (B.30i). These can be used to calculate the factors G_2, G_4, G_6 and G_8 given by

Eq. (A.30b), (A.34), (A.35) and (A.36). The second order derivatives do not depend on $\underline{Q}_p$ any more. So third and higher order derivatives are zero.

Appendix C

In Eq. (3.26) the integral,

$$I_j = \frac{1}{V} \sum_k \int_{V_{jk}} d^3x \exp(i(\underline{q} + \underline{q}') \cdot \underline{x}) = \sum_k I_{jk}, \qquad \text{(C.1)}$$

is restricted to the domains V_{jk} belonging to the same director index j. If all domains are translated by a certain vector $\underline{x}_t$ then the integral I'_j over the shifted space differs only by a complex factor with respect to I_j,

$$I'_j = \frac{1}{V} \sum_k \int_{V_{jk}} d^3x \exp(i(\underline{q} + \underline{q}') \cdot (\underline{x} + \underline{x}_t)) = I_j \exp(i(\underline{q} + \underline{q}') \cdot \underline{x}_t). \qquad \text{(C.2)}$$

By means of this translation property and the translation vectors $\underline{x}_l = \underline{x}_1$, $\underline{x}_2$ and $\underline{x}_3$ given by

$$\underline{x}_1 = \frac{2\pi}{3q_*}(\underline{n}_1 + \underline{n}_3) = \frac{2\pi}{q_*} \frac{1}{\sqrt{3}}[1,0,0], \qquad \text{(C.3a)}$$

$$\underline{x}_2 = \frac{2\pi}{3q_*}(\underline{n}_2 + \underline{n}_1) = \frac{2\pi}{q_*} \frac{1}{\sqrt{3}}[\frac{1}{2}, \frac{1}{2}\sqrt{3}, 0], \qquad \text{(C.3b)}$$

and

$$\underline{x}_3 = \frac{2\pi}{3q_*}(\underline{n}_3 - \underline{n}_2) = \frac{2\pi}{q_*} \frac{1}{\sqrt{3}}[\frac{1}{2}, -\frac{1}{2}\sqrt{3}, 0], \qquad \text{(C.3c)}$$

the integral over the whole space can be written as

$$\frac{1}{V} \int d^3x \exp(i(\underline{q} + \underline{q}') \cdot \underline{x}) = \delta(\underline{q} + \underline{q}') =$$
$$I_j + I_j \exp(i(\underline{q} + \underline{q}') \cdot \underline{x}_l) + I_j \exp(i(\underline{q} + \underline{q}') \cdot 2\underline{x}_l). \qquad \text{(C.4)}$$

This becomes clear if we look at Fig. (3.1) in which the translation vectors $\underline{x}_1$, $\underline{x}_2$ and $\underline{x}_3$ are drawn. For example consider the domains in which $\underline{n}(\underline{x}) = \underline{n}_2$. These $\underline{n}_2$-domains occupy $\frac{1}{3}$ of the whole space. The remaining space can be covered by the same $\underline{n}_2$-domains if we shift these domains by $\underline{x}_1$ and $2\underline{x}_1$. Instead of $\underline{x}_1$ other translation vectors $\underline{x}_2$ and $\underline{x}_3$ can also be used to cover the remaining space. In the same way the whole space can be covered by domains in which $\underline{n}(\underline{x}) = \underline{n}_1$ or $\underline{n}_3$. Therefore in Eq. (C.4) the integral over the whole space can be split up in three integrals over $\underline{n}_1$-, $\underline{n}_2$- and $\underline{n}_3$-domains which are shifted from each other by a translation $\underline{x}_1$, $\underline{x}_2$ or $\underline{x}_3$. According to Eq. (C.4) the integral I_j is equal to

$$I_j = \frac{\delta(\underline{q} + \underline{q}')}{1 + \exp(i(\underline{q} + \underline{q}') \cdot \underline{x}_l) + \exp(i(\underline{q} + \underline{q}') \cdot 2\underline{x}_l)}. \tag{C.5}$$

If in Eq. (C.5) the denominator is nonzero for every l the integral I_j may also be written as,

$$I_j = \frac{1}{3}\delta(\underline{q} + \underline{q}'). \tag{C.6}$$

Eq. (C.5) has singularities at the wave vectors $\underline{q}$ and $\underline{q}'$ for which,

$$(\underline{q} + \underline{q}') \cdot \underline{x}_l = \pm\frac{2\pi}{3} + 2\pi k_l \text{ with } k_l = 0, \pm 1, \pm 2, ... \tag{C.7}$$

If Eq. (C.7) is satisfied for both $\underline{x}_1$, $\underline{x}_2$ and $\underline{x}_3$ then the integral I_j cannot be determined by Eq. (C.5). This does not occur if the wave vectors $\underline{q}$ and $\underline{q}'$ are restricted to the set $H = H_{hex} \cup H_{nem}$ in which $H_{hex} = \{\pm q_*\underline{n}_1, \pm q_*\underline{n}_2, \pm q_*\underline{n}_3\}$ and $H_{nem} = \{0\}$. Then it is allowed to express the integral I_j by Eq. (C.6).

Appendix D

The vertices $\Gamma^{(2)}_{\widetilde{ab}}$, $\Gamma^{(3)}_{\widetilde{abc}}$ and $\Gamma^{(4)}_{\widetilde{abcd}}$ in the final form of the Landau free energy in chapter 2 depend only on the single-chain correlation functions $A_{\widetilde{ab}}$, $B_{\widetilde{abc}}$ and $C_{\widetilde{abcd}}$ in a quite complicated way. So first the single-chain correlation functions must be calculated to determine the vertices. The n-th order single-chain correlation function is an integral over the chain positions l_1, l_2 and l_n. From the expressions of the correlation functions it is clear that it is not possible to work out the integral analytically.

The multidimensional integral is calculated by means of repeated integration which is described in section 4.6 in [55]. In this method the multidimensional integral is written as a one dimensional integral over l_n,

$$\int dl_n f_n(l_n). \tag{D.1}$$

The integrand f_n is given by,

$$f_n(l_n) = \int dl_1 \int dl_2 ... \int dl_{n-2} \int dl_{n-1} C(l_1, l_2, ..., l_n). = \int dl_{n-1} f_{n-l}(l_{n-1}, l_n). \tag{D.2}$$

$C(l_1, l_2, ..., l_n)$ is the correlation between the points l_1, l_2 and l_n on the chain. $f_n(l_n)$ and $f_{n-l}(l_{n-1}, l_n)$ are lower multidimensional integrals which can be written as one dimensional integrals in the same way. The Romberg method, which is described on page 140 in [55], was first applied to calculate the one dimensional integrals numerically. The speed of the integration becomes slower when the dimension of the multidimensional integral becomes larger. The calculation time of the integration becomes also larger when the persistent length of the chain is very small such that the chain can be regarded as flexible. The integrand $C(l_1, l_2, ..., l_n)$ is the correlation between l_1, l_2 and l_n. So in a flexible chain the integrand becomes small or even negligible when l_1, l_2 and l_n are far away from each other. Only when l_1, l_2 and l_n are close enough to each

other the integrand gives a great contribution to the integral. In the Romberg method the whole interval is used to calculate the integral so that the integral is converging slowly for a flexible chain. However, the Monte Carlo method appeared to be even slower. In the Monte Carlo method repeated integration is not applied. The integrand is calculated at random points $(l_1, l_2, ..., l_n)$ in the n-dimensional space, but such that the distance among l_1, l_2 and l_n is not too great. For some correlations functions it is still necessary to take the whole interval into account.

In both the Romberg and Monte Carlo method the calculation speed gives problems especially when the fourth order single-chain correlations functions are calculated to determine the phase diagram. Each of these correlation functions are converging much slower and there are much more combinations which have to be calculated separately. Finally to calculate the spinodal and phase diagram Gauss-Jacobi integration has been applied which gives an acceptable calculation time. This method is described on page 147-161 in [55].

$C(l_1, l_2, ..., l_n)$ is the integrand of the single-chain correlation function which has been expressed in Appendix A and B. In this integrand $\widetilde{D}_{p'+2}$ is calculated by recurrence relations. These relations depend on the interval length ΔL_p which can become zero or very small. This causes problems in the numerical calculation of $C(l_1, l_2, ..., l_n)$. To solve this problem ΔL_p is taken equal to $10^{-9} \times L$, when $\Delta L_p \leq 10^{-9} \times L$. This has a negligible effect on the final result.

In the tensorial correlation functions G_2, G_4, G_6 and G_8 must be calculated. These G's depend on the first and second functional derivatives of $\widetilde{D}_{p'+2}$ with respect to $\lambda_{\mu_m}(l_m)$. These derivatives are expressed in Appendix B in a rather compact form which has to be worked out further to implement it in an algorithm. It follows that if l_m is the starting point of the m-the interval, then the first and second derivative of $\widetilde{D}_{p'+2}$ with respect to $\lambda_{\mu_m}(l_m)$ are,

$$\frac{\delta \widetilde{D}_{p'+2}}{\delta \lambda_{\mu_m}} = -2e_{\mu_m} \cdot \left[\frac{\widetilde{C}_{p'+1}}{\widetilde{A}_{p'+1}} \frac{B_{p'}}{\widetilde{A}_{p'}} ... \frac{B_m}{\widetilde{A}_m} + \frac{\widetilde{C}_{p'}}{\widetilde{A}_{p'}} \frac{B_{p'-1}}{\widetilde{A}_{p'-1}} ... \frac{B_m}{\widetilde{A}_m} + ... \frac{\widetilde{C}_m}{\widetilde{A}_m} \right] \tag{D.3a}$$

and

$$\frac{\delta^2 \widetilde{D}_{p'+2}}{\delta \lambda_{\mu_m} \delta \lambda_{\nu_m}} = \frac{-2\delta_{\mu_m \nu_m}}{\widetilde{A}_{p'+1}} \left[\frac{B_{p'}}{\widetilde{A}_{p'}} ... \frac{B_m}{\widetilde{A}_m} \right]^2 + \frac{-2\delta_{\mu_m \nu_m}}{\widetilde{A}_{p'}} \left[\frac{B_{p'-1}}{\widetilde{A}_{p'-1}} ... \frac{B_m}{\widetilde{A}_m} \right]^2 + ... \frac{-2\delta_{\mu_m \nu_m}}{\widetilde{A}_m}. \tag{D.3b}$$

If l_n is the starting point of the n-th interval and $l_n > l_m$, then

$$
\begin{aligned}
\frac{\delta^2 \widetilde{D}_{p'+2}}{\delta \lambda_{\mu_m} \delta \lambda_{\nu_n}} &= \frac{-2\delta_{\mu_m \nu_n}}{\widetilde{A}_{p'+1}} \left[\frac{B_{p'}}{\widetilde{A}_{p'}} \cdots \frac{B_m}{\widetilde{A}_m} \right] \left[\frac{B_{p'}}{\widetilde{A}_{p'}} \cdots \frac{B_n}{\widetilde{A}_n} \right] + \\
&\quad \frac{-2\delta_{\mu_m \nu_n}}{\widetilde{A}_{p'}} \left[\frac{B_{p'-1}}{\widetilde{A}_{p'-1}} \cdots \frac{B_m}{\widetilde{A}_m} \right] \left[\frac{B_{p'-1}}{\widetilde{A}_{p'-1}} \cdots \frac{B_n}{\widetilde{A}_n} \right] + \cdots + \\
&\quad \frac{-2\delta_{\mu_m \nu_n}}{\widetilde{A}_n} \left[\frac{B_{n-1}}{\widetilde{A}_{n-1}} \cdots \frac{B_m}{\widetilde{A}_m} \right].
\end{aligned}
\tag{D.4}
$$

In the expressions of G_4, G_6 and G_8 in Appendix A a summation is carried out over the permutations of the indices μ_m of $\lambda_{\mu_m}(l_m)$. In Eq. (D.3a) and (D.4) we see that the second order derivative is nonzero if the indices are equal. So not every permutation gives a contribution. Some permutations give the same nonzero contributions, because it is allowed to interchange the first and second order derivatives in each term and the sequence of differentiation in the second order derivative may also be interchanged. So in G_4, G_6 and G_8 the different groups of the same nonzero contributions has to be found and how many times each one counts in the summation. For example G_4 is given by,

$$
\begin{aligned}
G_4 &= \frac{1}{32} \sum_{perm(\mu_1, \nu_1, \mu_2, \nu_2)} \frac{\delta^2 \widetilde{D}_{p'+2}}{\delta \lambda_{\mu_1} \delta \lambda_{\nu_1}} \frac{\delta^2 \widetilde{D}_{p'+2}}{\delta \lambda_{\mu_2} \delta \lambda_{\nu_2}} + \\
&\quad -\frac{1}{32} \sum_{perm(\mu_1, \nu_1, \mu_2, \nu_2)} \frac{\delta^2 \widetilde{D}_{p'+2}}{\delta \lambda_{\mu_1} \delta \lambda_{\nu_1}} \frac{\delta \widetilde{D}_{p'+2}}{\delta \lambda_{\mu_2}} \frac{\delta \widetilde{D}_{p'+2}}{\delta \lambda_{\nu_2}} + \\
&\quad \frac{1}{4!16} \sum_{perm(\mu_1, \nu_1, \mu_2, \nu_2)} \frac{\delta \widetilde{D}_{p'+2}}{\delta \lambda_{\mu_1}} \frac{\delta \widetilde{D}_{p'+2}}{\delta \lambda_{\nu_1}} \frac{\delta \widetilde{D}_{p'+2}}{\delta \lambda_{\mu_2}} \frac{\delta \widetilde{D}_{p'+2}}{\delta \lambda_{\nu_2}}.
\end{aligned}
\tag{D.5}
$$

In the first term two pairs of equal indices are necessary to be nonzero. If $\mu_1 = \nu_1$ and $\mu_2 = \nu_2$, then

$$
\frac{\delta^2 \widetilde{D}_{p'+2}}{\delta \lambda_{\mu_1} \delta \lambda_{\nu_1}} \frac{\delta^2 \widetilde{D}_{p'+2}}{\delta \lambda_{\mu_2} \delta \lambda_{\nu_2}} \neq 0
\tag{D.6a}
$$

and

$$
\sum_{perm(\mu_1, \nu_1, \mu_2, \nu_2)} \frac{\delta^2 \widetilde{D}_{p'+2}}{\delta \lambda_{\mu_1} \delta \lambda_{\nu_1}} \frac{\delta^2 \widetilde{D}_{p'+2}}{\delta \lambda_{\mu_2} \delta \lambda_{\nu_2}} = 8 \frac{\delta^2 \widetilde{D}_{p'+2}}{\delta \lambda_{\mu_1} \delta \lambda_{\nu_1}} \frac{\delta^2 \widetilde{D}_{p'+2}}{\delta \lambda_{\mu_2} \delta \lambda_{\nu_2}}.
\tag{D.6b}
$$

The group of permutations in which $\mu_1 = \mu_2$ and $\nu_1 = \nu_2$ or $\mu_1 = \nu_2$ and $\mu_2 = \nu_1$ also count 8 times in the summation over the permutations. If $\mu_1 = \nu_1 = \mu_2 = \nu_2$, the permutations belong to both the first, second and third possible group and contribute 3×8 times. In the second term of G_4 one pair of equal indices is necessary to be nonzero. In the set $\{\mu_1, \nu_1, \mu_2, \nu_2\}$ six different pairs can be formed. Each pair counts 4 times in the summation if the indices are equal. The last term contains only first order derivatives, so the summation can be replaced by $4!$. In G_6 and G_8 the groups of nonzero contributions are found in the same way, but the number of possible groups is greater.

Summary

In this thesis the phase behaviour of melts of chain-like molecules, also known as polymers, is studied. Polymers are built from monomers. These monomers are connected consecutively to form chains. If all monomers are of the same kind the chain is called a homopolymer. The polymers studied in this thesis are block copolymers. In a block copolymer different kinds of homopolymers or so-called blocks are connected. For example a diblock copolymer consists of two different kinds of blocks A and B connected to each other.

Chains in a melt are not moving independently of each other. There are different kinds of interactions between the chains. The Flory-Huggins interaction describes the incompatibility between chemically different kinds of blocks. This means that different kinds of blocks generally do not mix very well, as they are repelling each other. At high enough temperatures this interaction has a weak influence. The chains are moving fast such that the arrangement of chains is arbitrary. This is the disordered phase. If the temperature is lowered the chains are moving slower and the Flory-Huggins interaction becomes more dominant. At a certain critical temperature a phase transition takes place. When the temperature becomes lower than the critical temperature the disordered phase is converted into an ordered structure. In the ordered structure blocks avoid each other if they are chemically different. Little domains arise in which the density of a certain kind of block is greater than average. This is called microphase separation. Just below the critical temperature the degree of separation is very weak. When the temperature is further lowered the separation becomes more pronounced. For example in a melt of diblock copolymers A-rich and B-rich domains are formed. Different kinds of microphase structures are possible such as for example the bcc, hexagonal and lamellar structure. In the bcc structure the A-rich domains are spheres arranged on a cubic lattice. Outside the spheres the density of B-blocks is greater than average. In the hexagonal structure a B-rich ma-

trix embeds A-rich cylinders. The cylinders are arranged in a honeycomb structure. In the lamellar phase the A- and B-rich domains are alternating layers.

In the past decades much attention has been paid to block copolymers that are totally flexible. In this thesis the effect of chain stiffness is taken into account. This makes the description of the polymers more general and more realistic. In a chain each block has a certain bending stiffness depending on the kind of monomer. Such block copolymers are called semi-flexible. A certain amount of energy is needed to bend a semi-flexible chain. If the bending stiffness of a block is infinite the block is rigid and hence cannot be bent and when the stiffness is zero the block is totally flexible. Due to this chain stiffness another interaction is important which is the Maier-Saupe interaction. At high enough temperatures this interaction also has a weak influence due to the fast movement of the chains. However, when the temperature becomes lower than a certain critical temperature the disordered phase is converted into the nematic structure by the Maier-Saupe interaction. In the nematic structure the chains prefer to be aligned on average along the same direction. This orientation is very weak just below the critical temperature, but at lower temperatures it becomes stronger. In the nematic phase there is no separation of chemically different blocks. Due to the stiffness other structures may also appear such as the smectic-A and smectic-C structure. In these structures there is both separation and orientation of blocks. For example in a melt of semi-flexible diblock copolymers the A-rich and B-rich domains form alternating layers in the same way as in the lamellar structure belonging to a flexible diblock copolymer melt. In the smectic-A structure the semi-flexible diblocks prefer to be oriented perpendicular to the layers while in the smectic-C structure the orientation direction of the blocks is at a fixed non-zero angle with respect to the normal of the layers. Orientation of semi-flexible blocks also occurs in the bcc and hexagonal structures. In the nematic structure the alignment is along the same direction everywhere in the melt. However, in a microphase structure the orientation is typically spatially dependent.

In this thesis the Landau theory has been applied to predict/calculate the phase structure of block copolymers. This theory is valid if the temperature is close to the critical temperature at which the phase transition takes place from the disordered phase to an ordered structure. In chapter two the Landau theory pertaining to a very general polymer melt is considered. This melt is a mixture of different kinds of block copolymers. The composition of the mixture, number of blocks in a chain, block length and stiffness of a block can be chosen arbitrary.

This general theory is applied to a simple system consisting of monodisperse di-

block copolymers in chapter three. This means that the length of both the A- and B-block is identical for each chain in the melt. For this system several predicted phase diagrams are discussed in which the chain composition, stiffness and strength of the Flory-Huggins and Maier-Saupe interaction are varied. In these phase diagrams the bcc, hexagonal, lamellar, smectic-A, smectic-C and nematic structure are observed. From the results the following conclusions can be drawn. It appears that the order-disorder phase transition takes place at a higher temperature if the stiffness of the A- or B-block is increased. Furthermore the separation of A- and B-blocks in a microphase structure is weakened if the strength of the Maier-Saupe interaction is increased. At the same time the domain size becomes smaller. In a microphase structure a spatially dependent orientation is necessary to separate A- and B-blocks. However, the Maier-Saupe interaction favors a global alignment in one direction to form a nematic phase. This reduces the spatially dependent orientation in a microphase structure so that the separation of A- and B-blocks is also reduced.

The diblock copolymers that are considered in chapter three are monodisperse. In reality it is usually difficult to synthesize such identical diblocks. Usually there is a certain degree of polydispersity in block length present. The effect of this polydispersity is considered in chapter four. In a polydisperse system in some chains the length of the A-block is larger than average and in other chains it is smaller. The length of the B-block is also variable and usually independent of the length of the A-block. Due to polydispersity, instead of microphase separation, macrophase separation is possible. The ultimate macrophase structure is a melt with one big A-rich and one big B-rich domain. The A-rich domain is formed by collecting diblocks with an A-block fraction greater than average. The remaining diblocks form the B-rich domain. The length scale of the A-rich and B-rich domain is much greater than the average length of a diblock chain. If the diblocks are monodisperse only microphase separation is possible with a small domain size. The results in chapter four suggest that the order-disorder phase transition takes place at a higher temperature when the degree of polydispersity becomes larger. At the same time the domain size in a microphase structure increases. In certain systems the domain size may even become infinite which then corresponds to macrophase separation.

In chapter five the phase behaviour of a melt of monodisperse ABA-triblocks copolymers is investigated. In an ABA-triblock copolymer a block of kind B is connected on both sides to an A-block. As in chapter three several predicted phase diagrams are discussed in which the chain composition, stiffness and strength of the Flory-Huggins and Maier-Saupe interaction is varied. The phase behaviour of such

a melt does not differ very much from that of the diblock melt considered in chapter three. In the phase diagrams the same structures are found. The Maier-Saupe interaction is again weakening the separation of A- and B-blocks in a microphase structure if its strength is increased. However, the order-disorder phase transition occurs at a higher temperature if the ABA-triblocks are replaced by diblocks with the same length and the same A-block fraction. In that case the domain size is bigger when a microphase structure is formed at the phase transition.

Samenvatting

In dit proefschrift wordt het fasegedrag van smelten van ketenachtige moleculen, ook bekend als polymeren, bestudeerd. Polymeren zijn opgebouwd uit monomeren. Deze monomeren zijn op een lineaire wijze met elkaar verbonden in lange ketens. Indien alle monomeren van dezelfde soort zijn, wordt de keten een homopolymeer genoemd. De polymeren bestudeerd in dit proefschrift zijn blokcopolymeren. In een blokcopolymeer zijn verschillende soorten homopolymeren of zogeheten blokken met elkaar verbonden. Een diblokcopolymeer bijvoorbeeld bestaat uit twee verschillende soorten blokken A en B die aan elkaar gekoppeld zijn.

Ketens in een smelt bewegen niet onafhankelijk van elkaar. Er zijn verschillende soorten interacties tussen ketens. De Flory-Huggins interactie beschrijft de incompatibiliteit tussen chemisch verschillende soorten blokken. Dit betekent dat chemisch verschillende blokken in het algemeen niet erg goed mengen aangezien ze elkaar afstoten. Bij voldoende hoge temperatuur heeft deze interactie een geringe invloed. De ketens bewegen zo snel dat de rangschikking of conformatie van de ketens willekeurig is. Dit is de wanordelijke fase. Indien de temperatuur verlaagd wordt, bewegen de ketens langzamer en wordt de Flory-Huggins interactie belangrijker. Bij een bepaalde kritische temperatuur vindt een faseovergang plaats. Wanneer de temperatuur beneden de kritische temperatuur daalt wordt de wanordelijke fase omgezet in een geordende structuur. In deze geordende structuur mijden blokken elkaar indien ze chemisch verschillend zijn. Er onstaan kleine gebieden waarin de dichtheid van een bepaald soort blok groter is dan gemiddeld. Dit wordt microfase scheiding genoemd. Net beneden de kritische temperatuur is de mate van scheiding zeer gering. Wanneer de temperatuur verder verlaagd wordt, wordt de scheiding markanter. In een diblokcopolymeersmelt worden zo A-rijke en B-rijke gebieden gevormd. Verschillende soorten microfase structuren zijn mogelijk zoals bijvoorbeeld de body centered cubic (bcc), hexagonale en lamellaire structuur. In de bcc structuur zijn de

A-rijke gebieden bollen gerangschikt op een simpel kubisch rooster. Buiten de bollen is de dichtheid van de B-blokken groter dan gemiddeld. In de hexagonale structuur zijn A-rijke cylinders ingebed in een B-rijke matrix. De cilinders zijn gerangschikt in een honingraat structuur. In de lamellaire fase vormen de A- en B-rijke gebieden alternerende lagen.

In de afgelopen decennia is veel aandacht besteed aan de studie van het fasegedrag van smelten van volledig flexibele blokcopolymeren. In dit proefschrift is het effect van ketenstijfheid hierop bestudeerd. Dit maakt de theoretische beschrijving van polymeren algemener en meer realistisch. In een keten heeft ieder blok een bepaalde buigstijfheid afhankelijk van het soort monomeer waaruit het is opgebouwd. Zulke blokcopolymeren worden semi-flexibel genoemd. Een bepaalde hoeveelheid energie is nodig om een semi-flexibele keten te buigen. Indien de buigstijfheid van een blok oneindig groot is, is het blok star en kan het derhalve niet gebogen worden en wanneer de stijfheid nul is, is het blok volledig flexibel. Vanwege deze ketenstijfheid is nog een andere interactie belangrijk de zogeheten Maier-Saupe interactie. Bij hoge temperaturen heeft deze interactie eveneens een geringe invloed vanwege de snelle beweging van de ketens. Echter wanneer de temperatuur beneden een bepaalde kritische temperatuur komt zorgt de Maier-Saupe interactie ervoor dat de wanordelijke fase over gaat in de zogeheten nematische fase of structuur. In de nematische structuur prefereren de blokken om gemiddeld in dezelfde richting opgelijnd te worden. Deze oriëntatie is zeer zwak net beneden de kritische temperatuur, maar wordt bij lagere temperaturen markanter. In de nematische fase is er geen scheiding van chemisch verschillende blokken. Vanwege de combinatie van ketenstijfheid en blokcopolymeerkarakter kunnen ook andere structuren voorkomen zoals de smectische-A en smectische-C structuur. In deze structuren is er zowel scheiding als oriëntatie van blokken. In een smelt van bijvoorbeeld semi-flexibele diblokcopolymeren vormen de A-rijke en B-rijke gebieden alternerende lagen op dezelfde manier als in de lamellaire structuur behorende bij een flexibele diblokcopolymeersmelt. In de smectische-A structuur prefereren de semi-flexibele diblokken om geörienteerd te zijn loodrecht op de lagen terwijl in de smectische-C structuur de blokken de voorkeur geven om georiënteerd zijn in een richting die een vaste hoek (ongelijk aan nul) maakt met de normaal van de lagen. Oriëntatie van semi-flexibele blokken wordt ook aangetroffen in de bcc - en de hexagonale structuur. In de nematische structuur is er sprake van een globale oriëntatie in de smelt. Echter, in een microfase structuur vertoont de oriëntatie typisch een ruimtelijke afhankelijkheid.

In dit proefschrift is de zogeheten Landau theorie toegepast om de fasestruc-

tuur van blokcopolymeren te voorspellen/berekenen. Deze theorie is geldig indien de temperatuur dichtbij de kritische temperatuur ligt waarop de faseovergang plaatsvindt van de wanordelijke fase naar een geordende structuur. In hoofdstuk twee wordt de Landau theorie betrekking hebbende op een zeer algemene polymeersmelt beschouwd. Deze smelt is een mengsel van verschillende soorten blokcopolymeren. De samenstelling van het mengsel, het aantal blokken in een keten en de lengte en stijfheid van een blok kunnen willekeurig gekozen worden.

Deze algemene theorie wordt toegepast op een eenvoudig systeem bestaande uit een monodisperse diblokcopolymeersmelt in hoofdstuk drie. Dit betekent dat de lengte van zowel het A- als het B-blok identiek gekozen wordt voor iedere keten in de smelt. Van dit systeem worden in dat hoofdstuk verschillende voorspelde fasediagrammen bediscussieerd waarin de ketensamenstelling, stijfheid en sterkte van de Flory-Huggins en Maier-Saupe interactie gevarieerd wordt. In deze fasediagrammen worden de bcc, hexagonale, lamellaire, smectische-A, smectische-C en nematische structuur waargenomen. Uit de resultaten kunnen de volgende conclusies getrokken worden. Het blijkt dat de orde-wanordefaseovergang plaatsvindt bij hogere temperaturen indien de stijfheid van het A- of het B-blok toeneemt. Verder wordt de scheiding van A- en B-blokken in een microfase structuur geringer indien de sterkte van de Maier-Saupe interactie verhoogd wordt. Tegelijkertijd wordt de gebiedsafmeting kleiner. In een microfase structuur is een ruimtelijk afhankelijke oriëntatie noodzakelijk om A- en B-blokken te scheiden. Echter de Maier-Saupe interactie prefereert een globale oriëntatie teneinde de nematische fase te vormen. Dit reduceert de ruimtelijk afhankelijke orientatie in een microfase structuur zodat de scheiding van A- en B-blokken ook daarmee gereduceerd wordt.

De diblokcopolymeren die beschouwd worden in hoofdstuk drie zijn monodispers. In werkelijkheid is het doorgaans moeilijk om zulke identieke diblokcopolymeren te synthetiseren. Doorgaans is er een bepaalde mate van polydispersiteit in bloklengte aanwezig. Het effect van deze polydispersiteit wordt beschouwd in hoofdstuk vier. In een polydispers systeem is in sommige ketens de lengte van het A-blok groter dan gemiddeld en in andere ketens is deze kleiner. De lengte van het B-blok is ook variabel en doorgaans onafhankelijk van de lengte van het A-blok. Vanwege polydispersiteit is, in plaats van microfase scheiding, macrofase scheiding mogelijk. De ultieme macrofase structuur is een smelt met één groot A-rijk gebied en één groot B-rijk gebied. Het A-rijke gebied wordt gevormd door het verzamelen van diblokken met een A-blok fractie groter dan gemiddeld. De resterende diblokken vormen het B-rijke gebied. De lengteschaal van het A-rijke en B-rijke gebied is veel groter dan

de gemiddelde lengte van een diblokcopolymeerketen. Indien de diblokken monodispers zijn, is alleen microfase scheiding mogelijk met een kleine gebiedsafmeting. De resultaten in hoofdstuk vier suggereren dat de orde-wanorde faseovergang plaatsvindt bij een hogere temperatuur wanneer de polydispersiteit groter wordt. Tegelijkertijd neemt de gebiedsafmeting in een microfasestructuur toe. In bepaalde systemen kan de gebiedsafmeting zelfs oneindig groot worden hetgeen dan correspondeert met macrofasescheiding.

In hoofdstuk vijf wordt het fasegedrag van een smelt van monodisperse ABA-triblokcopolymeren onderzocht. In een ABA-triblokcopolymeer is een blok van soort B aan beide kanten verbonden met een A-blok. Op dezelfde manier als in hoofdstuk drie worden verschillende voorspelde fasediagrammen bediscussieerd waarin de ketensamenstelling, stijfheid en sterkte van de Flory-Huggins en Maier-Saupe interactie gevarieerd wordt. Het fasegedrag van zo'n smelt verschilt niet erg veel van dat van de diblokcopolymeersmelt die in hoofdstuk drie bestudeerd wordt. In de fasediagrammen worden dezelfde type structuren gevonden. De Maier-Saupe interactie verzwakt wederom de scheiding van A- en B-blokken in een microfasestructuur indien de sterkte hiervan toeneemt. Echter de orde-wanorde faseovergang vindt plaats bij een hogere temperatuur indien de ABA-triblokken vervangen worden door diblokken met dezelfde lengte en dezelfde A-blok fractie. In dat geval is de gebiedsafmeting groter wanneer een microfasestructuur gevormd wordt bij de faseovergang.

Dankwoord

Graag zou ik een aantal mensen willen bedanken die direct of indirect meegewerkt hebben aan dit proefschrift. Allereerst wil ik mijn promotor Han bedanken die mij de gelegenheid geboden heeft promotie-onderzoek te doen op het gebied van polymeerfysica in de vakgroep Computational Biophysics. Han heeft mij goed op weg geholpen gedurende het onderzoek. Vooral zijn bijdrage in het uitwerken van de theorie is erg belangrijk geweest. De moeilijkheden die we hierbij tegenkwamen, zou ik niet geheel alleen opgelost kunnen hebben. Gedurende het onderzoek heeft hij mij goed gestimuleerd, geënthousiasmeerd en het vertrouwen gegeven dat ik het tot een goed einde kon brengen. Ik dank hem verder voor de vele nuttige discussies en het zorgvuldig doorlezen en corrigeren van mijn proefschrift.

Ook Roman ben ik dankbaar voor de begeleiding gedurende de laatste twee jaar van mijn promotie. Hij stond altijd voor me klaar om te helpen wanneer ik tegen een bepaald probleem aanliep of advies nodig had. Ook was hij altijd geïnteresseerd om nieuw behaalde resultaten nader te bediscussiëren. De hoofdstukken en publicaties die ik voor mijn proefschrift schreef, werden door hem kritisch bestudeerd en gecorrigeerd.

I would like to thank the members of the Computational Biophysics group for giving me a pleasant time during the last two years: Wim, Dick, Marieke, Albert, Adrian, Becky, Marleen, Amol, Wouter, Johan, Sergey, Peter, Wladimir and Yu-Guo.

Before I joined the Computational Biophysics group I did my PhD-project in the Physics of Complex Fluids group. I would like to thank: Niki, Joris, Jorrit, Frieder, Jasper, Jacob, Gerrit, Mariska, Arup, Boris, Ileana, Alexei, Ryan, Renske, Eco, Violeta, Dirk, Michel, Annelies, Martijn, Yuri, Diana, Andrei, Valentin, Zaosheng, Rina, Manuela, Tamara, Helmut, Adrian, etc. It was a nice time. Every day we went to the mensa for lunch. I thank you for the parties and birthdays we celebrated. Furthermore, I liked the evenings when we went to the cinema.

Piet en José Suikerbuyk en Marietje Berendsen wil ik bedanken voor het verhuren van een appartement aan mij in Deurningen en de huishoudelijke hulp. Tenslotte wil ik mijn familie bedanken voor al jullie hulp en steun.

Curriculum Vitae

De schrijver van dit proefschrift is geboren op 14 juni 1976 in Rotterdam. In 1995 rondde hij het VWO af aan het Willem de Zwijgercollege in Bussum en begon hij aan de studie natuurkunde aan de Vrije Universiteit in Amsterdam. Zijn afstudeerstage was op het gebied van supergeleiding in de vakgroep Theoretische Natuurkunde. Hij voltooide zijn studie in 2001 en besloot de wetenschap nog niet te verlaten. In hetzelfde jaar begon hij aan een door het Dutch Polymer Institute gesponsord promotieonderzoek op het gebied van de polymeerfysica in achtereenvolgens de vakgroepen Physics of Complex Fluids en Computational Biophysics van de Universiteit Twente hetgeen geresulteerd heeft in dit proefschrift.

Bibliography

[1] I.W. Hamley, The Physics of Block Copolymers (Oxford University Press, Oxford, 1998).

[2] P.J. Flory, Principles of Polymer Chemistry (Cornell University Press, Ithaca, New York, 1953).

[3] M.W. Matsen and R. B. Thompson, J. Chem. Phys., **111** (15), 7139 (1999).

[4] M.W. Matsen, J. Phys. Cond. Mat., **14**, R21 (2002).

[5] L. Leibler, Macromolecules, **13**, 1602 (1980).

[6] J.J.M. Slot, H. J. Angerman and G. ten Brinke, J. Chem. Phys., **109**, 19, 8677 (1998).

[7] W. Maier and A. Z. Saupe, Z. Naturforsch. A **13A**, 564 (1958).

[8] M.W. Matsen and M. Schick, Phys. Rev. Lett., **72**, 2660 (1994).

[9] M. Reenders and G. ten Brinke, Macromolecules, **35**, 3266 (2002).

[10] P. Friedel, A. John, D. Pospiech, D. Jehnichen and R.R. Netz, Macromol. Theory Simul., **11**,7,785 (2002).

[11] M.W. Matsen, J. Chem. Phys., **104**, 19, 7758 (1996).

[12] C. Singh, M. Goulian, A.J. Liu and G.H. Fredrickson, Macromolecules, **27**, 2974 (1994).

[13] R. Holyst and M. Schick, J. Chem. Phys., **96**, 1, 730 (1992).

[14] J.B. Lagowski and J. Noolandi, J. Chem. Phys., **95**, 2, 1266 (1991)

[15] M. Bixon and R. Zwanzig, J. Chem. Phys., **68** ,4, 1896 (1978).

[16] M.G. Bawendi and K.F. Freed, J. Chem. Phys., **83**, 5, 2491 (1985).

[17] R.A. Harris and J.E. Hearst, J. Chem. Phys., **44**, 7, 2595 (1966).

[18] N. Saitô, K. Takahashi and Y. Yunoki, J. Phys. Soc. of Jap., **22**, 1, 219 (1967).

[19] K.F. Freed, Adv. Chem. Phys., **22**, 1 (1972).

[20] A.M. Gupta and S.F. Edwards, J. Chem. Phys., **98**, 2, 1588 (1993).

[21] I.M. Lifshitz, A. Yu. Grosberg, and A.R. Khokhlov, Rev. Mod. Phys., **50**, 683 (1978).

[22] C. Burger, W. Ruland and A.N. Semenov, Macromolecules, **23**, 3339 (1990).

[23] A. John, P. Friedel, D. Pospiech, D. Jehnichen and C. Kunert, Macromol. Theory Simul., **13**, 8, 702 (2004).

[24] N.G. van Kampen, Stochastic Processes in Physics and Chemistry (North-Holland, Amsterdam, 1981).

[25] P.M. Chaikin and T.C. Lubensky, Principles of Condensed Matter Physics (Cambridge University Press, Cambridge, 1995).

[26] J.C. Toledano and P. Toledano, The Landau Theory of Phase Transitions (World Scientific, Singapore, 1987), Vol. 3.

[27] S.V. Panyukov and S.I. Kuchanov, J. Phys. II (France), **2**, 1973 (1992).

[28] E.I. Shakhnovich and A.M. Gutin, J. Phys. (France), **50**, 1843 (1989).

[29] A.N. Semenov and A.R. Kokhlov, Sov. Phys. Usp., **31**, 988 (1988).

[30] A.R. Kokhlov and A.N. Semenov, Macromolecules, **19**, 373 (1986).

[31] G.H. Fredrickson, S.T. Milner, and L. Leibler, Macromolecules, **25**, 6341 (1992).

[32] G.H. Fredrickson and E. Helfand, J. Chem. Phys., **87**, 1, 697 (1987).

[33] G.H. Fredrickson and L. Leibler, Macromolecules, **23**, 531 (1990).

[34] G.H. Fredrickson and S.W. Sides, Macromolecules, **36**, 5415 (2003).

[35] S.W. Sides and G.H. Fredrickson, J. Chem. Phys., **121**, 10, 4974 (2004).

[36] H.J. Angerman, G. ten Brinke and J.J.M. Slot, Eur. Phys. J. B., **12**, 397 (1999).

[37] H.J. Angerman, G. ten Brinke and I. Erukhimovich, Macromolecules, **29**, 3255 (1996).

[38] H.J. Angerman, PhD-thesis, University of Groningen (1998).

[39] M. Foroutan and M.A. Jafarizadeh, Physica A, **307**, 221 (2002).

[40] M. Foroutan and M.A. Jafarizadeh, Physica A, **329**, 337 (2002).

[41] S. Panyukov and I. Potemkin, Physica A, **249**, 321 (1998).

[42] I. Potemkin and S. Panyukov, Phys. Rev. E, **57**, 6, 6902 (1998).

[43] A.M. Gutin, C.D. Sfatos and E.I. Shakhnovich, J. Phys. A, **27**, 7957 (1994).

[44] A. Nesarikar, M. Olvera de la Cruz and B. Crist, J. Chem. Phys., **98**, 9, 7385 (1993).

[45] A.V. Dobrynin and L. Leibler, Macromolecules, **30**, 4756 (1997).

[46] V. Abetz, R. Stadler and L. Leibler, Polymer Bulletin, **37**, 135 (1996).

[47] A. Werner and G.H. Fredrickson, J. Polym. Science B, **35** (5), 849 (1997).

[48] I. Erukhimovich, V. Abetz and R. Stadler, Macromolecules, **30**, 7435 (1997).

[49] M.W. Matsen, J. Chem. Phys., **108** (2), 785 (1998).

[50] A. Aksimentiev and R. Holyst, J. Chem. Phys., **111** (5), 2329 (1999).

[51] S.M. Mai, W. Mingvanish, S.C. Turner SC, et al, Macromolecules, **33**, 5124 (2000).

[52] X. Ren and J. Wei, Physica D, **178**, 103 (2003).

[53] E.W. Cochran, D.C. Morse and F.S. Bates, Macromolecules, **36**, 782 (2003).

[54] K.M. Jaffer, R.A. Wickham and A. Shi, Macromolecules, **37**, 7042 (2004).

[55] W.H. Press, S.A. Teukolsky, W.T. Vetterling, B.P. Flannery, Numerical Recipes in C, second edition (Cambridge University Press, Cambridge, 1996).